N° d'ordre :

Université du Sud Toulon-Var

ÉCOLE DOCTORALE : de l'Université du Sud Toulon Var

THESE

Présentée par

Aymeric JOUON

Pour obtenir le grade de

DOCTEUR

SPÉCIALITÉ : OCÉANOGRAPHIE PHYSIQUE

HYDRODYNAMIQUE ET TRANSPORT DE PARTICULES EN SUSPENSION DANS LE LAGON SUD-OUEST DE NOUVELLE-CALÉDONIE

Manuscrit soumis aux rapporteurs

Eric DELEERSNIJDER, FNRS Université catholique de Louvain	Rapporteur
Pierre LE HIR, IFREMER, Centre de Brest	Rapporteur
Philippe BONNETON, CNRS, Université Bordeaux I	Rapporteur
Philippe FRAUNIE, Université du Sud Toulon Var	Directeur de thèse
Pascal DOUILLET, IRD, Centre de Nouméa	Responsable scientifique
Sylvain OUILLON, IRD, Centre de Nouméa	Responsable scientifique

Thèse préparée au sein de l'UR 103 CAractérisation Modélisation des Ecosystèmes Lagonnaires sous Influence terrigène et Anthropique au centre IRD de Nouméa

IRD
Institut de recherche pour le développement

ZoNéCo
PROGRAMME D'ÉVALUATION DES RESSOURCES MARINES DE LA ZONE ÉCONOMIQUES DE NOUVELLE-CALÉDONIE

RESUME FRANÇAIS

Cette thèse s'inscrit dans le cadre d'une étude conduite depuis plusieurs années par l'IRD qui vise à mieux connaître les processus de l'hydrodynamique et du transport d'éléments dissous et de particules dans le Lagon Sud-Ouest de Nouvelle Calédonie (SLNC). Les travaux présentés s'appuient sur des mesures de terrain et la modélisation numérique.

Le premier volet de la thèse vise à synthétiser l'abondante information produite par un modèle numérique hydrodynamique (MARS3D). Des indices relatifs au renouvellement des masses d'eau et ayant la dimension d'un temps, communément appelés temps de résidence, sont élaborés à partir d'outils numériques. La signification de ces indices, leur mode de calcul et leur application au SLNC sont exposés. Plusieurs applications mettent en évidence les effets de l'hydrodynamique sur des processus biologiques et biochimiques.

Hors période de crue, les sédiments fraîchement déposés constituent la principale source de particules en suspension. Les tensions de cisaillement provoquées par les effets combinés de la houle et du courant provoquent leur remise en suspension. Pour les calculer en tout point, il est nécessaire de simuler précisément le champ de vagues. La seconde partie de la thèse y est consacrée. Pour cela, le modèle de houle WaveWatchIII est adapté au SLNC et validé par des mesures directionnelles de vagues.

Le troisième et dernier volet de la thèse est focalisé sur la détermination des propriétés physiques des particules en suspension. Ces paramètres (concentration par classe granulométrique, densité, vitesse de chute) sont nécessaires pour modéliser le transport des particules. Ce travail s'appuie sur des mesures *in situ* et des expériences en laboratoire réalisées à l'aide d'un granulomètre laser. Les résultats mettent en évidence l'importance de la bio agrégation en milieu corallien.

ENGLISH ABSTRACT

This thesis participates to a study that has been lead for several years by IRD which aims increased knowledge of hydrodynamics and transport of dissolved substances and particles on the South-West Lagoon of New Caledonia (SLNC). This work stands on field measurements and numerical modelling.

The first step of this thesis is an attempt to synthesise the great amount of data produced by a numerical hydrodynamic model (MARS3D). Indexes having the dimension of time and related to the renewal of water masses were computed from numerical tools applied to the hydrodynamic model. The computation methods, the significance and the application of these indexes to the Southwest Lagoon of New-Caledonia (SLNC) are exposed. Examples of application of these indexes aiming to quantify the influence of hydrodynamics on biological processes are shown.

Out of flooding periods, the re-suspension of freshly deposited sediments is the main source of suspended particles on the SLNC. The combined actions of waves and currents induce a bottom shear stress that is responsible for particle re-suspension. In order to access the wave field characteristics, a wave model (WavewatchIII) was implemented over the SLNC. It was validated by *in situ* directional measurements of the wave field.

The last part of this thesis focuses on the determination of physical properties of suspended particles such as particle size distributions, density, and fall velocity, are compulsory to model particle transport. This work stands on *in situ* measurements and laboratory experiences performed with laser particle size analyser. Results emphasise the importance of bio-aggregation in a coral reef ecosystem.

TABLE DES MATIERES

PREAMBULE

« Quand les mouettes ont pied
il est temps de virer »
(Proverbe Breton)

L'importance croissante accordée aux questions environnementales témoigne d'une prise de conscience collective : l'Homme a un impact non négligeable sur son environnement. La phrase tristement célèbre, prononcée par George W. Bush pour justifier les raisons de la non ratification des accords de Kyoto par les Etats-Unis : « Le mode de vie américain n'est pas négociable » montre que la réduction des effets de l'activité humaine sur l'environnement est encore considérée par beaucoup comme un frein au développement économique. Outre le fait acquis que l'impact de l'activité humaine sur l'environnement puisse anéantir des ressources naturelles dont l'Homme tire profit, le récent rapport de Sir Nicholas Stern (2006) qui chiffre en terme de pertes économiques les effets dévastateurs du réchauffement climatique rappelle à chacun l'importance de l'environnement sur nos modes de vies.

Si le réchauffement climatique s'impose comme le fer de lance d'un débat environnemental, il est nécessaire que celui-ci soit élargi à l'ensemble des impacts de l'activité humaine sur l'environnement. Environ 3,2 milliards de personnes, soit la moitié de population actuelle du globe, vivent sur une côte ou à moins de 200 km d'un littoral (**http://www.unesco.org/csi/wise/wise6f.htm**). Que ce soit par des processus globaux (réchauffement climatique) ou des processus locaux (liés à la pression anthropique locale), les zones côtières sont au premier rang des environnements et écosystèmes impactés par l'activité humaine. Or le mode de vie des populations des zones côtières dépend de l'état du milieu marin côtier. L'équilibre de ces milieux marins côtiers est complexe et de nombreux processus garants de cet équilibre ne sont que partiellement appréhendés. Une meilleure connaissance du fonctionnement de ces environnements et des modifications engendrées par l'activité humaine est nécessaire pour servir de base au débat sur les effets environnementaux de l'activité anthropique et leur gestion.

Les milieux coralliens figurent parmi les environnements côtiers les plus fascinants. Au-delà de l'esthétique produite par la multitude des couleurs, la quantité et la diversité de la faune et de la flore qui en font un outil de sensibilisation médiatique, ces ecosystèmes complexes et fragiles constituent des sites privilégiés pour étudier l'impact de l'activité humaine sur l'environnement marin côtier.

A l'échelle de la planète, l'augmentation anthropique de la teneur en CO_2 dans l'atmosphère provoque des bouleversements (changements de température des eaux marines, acidification des océans, The Royal Society (2005)) qui engendrent le déclin d'une portion alarmante de récifs coralliens (Bryant et al., 1998 ; Hoegh-Guldberg, 1999 ; Kleypas et al., 1999 ; Hugues et al., 2003 ; Pandolfi et al., 2003, DVD « Juan de Nova, l'île de corail »). Or,

les coraux produisent 1 Gt de carbone par année (Field et al 1998). La production récifale de carbonates est une composante importante du cycle du carbone (Vecsei, 2004). La montée du niveau de la mer (Douglas, 1991) est une conséquence du réchauffement climatique (Wigley et Raper, 1987 ; Meehl et al., 2005). L'érosion littorale est favorisée par une montée du niveau de l'eau (Bruun, 1962). Les assauts de la mer sur certaines îles coralliennes du pacifique forcent le retrait de la côte et contraindront les populations à l'exil (Wilkinson, 1996). Le déferlement des puissantes houles océaniques sur les récifs est le processus majeur de dissipation de l'énergie transportée par les vagues. Les récifs constituent ainsi des remparts qui protègent les terres de l'action érosive de la houle.

A l'échelle locale, les îles du Pacifique regroupent une importante part des récifs coralliens du monde (Figure 1). La pression démographique locale y est en augmentation (**http://www.spc.int/demog/fr/index.html**), le développement concomitant des activités accroît la pression anthropique sur les milieux coralliens environnants qui représentent une ressource indispensable pour les populations et les industries de nombreux pays et îles du Pacifique (Spalding et al., 2001).

Il est urgent de se donner les moyens de mieux cerner les impacts de l'activité humaine sur l'environnement. Pour cela, il faut comprendre les processus qui lient les activités à leurs impacts. Cette démarche doit être le préambule à tout projet visant à gérer les effets de l'activité humaine sur l'environnement, pour qu'un développement durable soit possible.

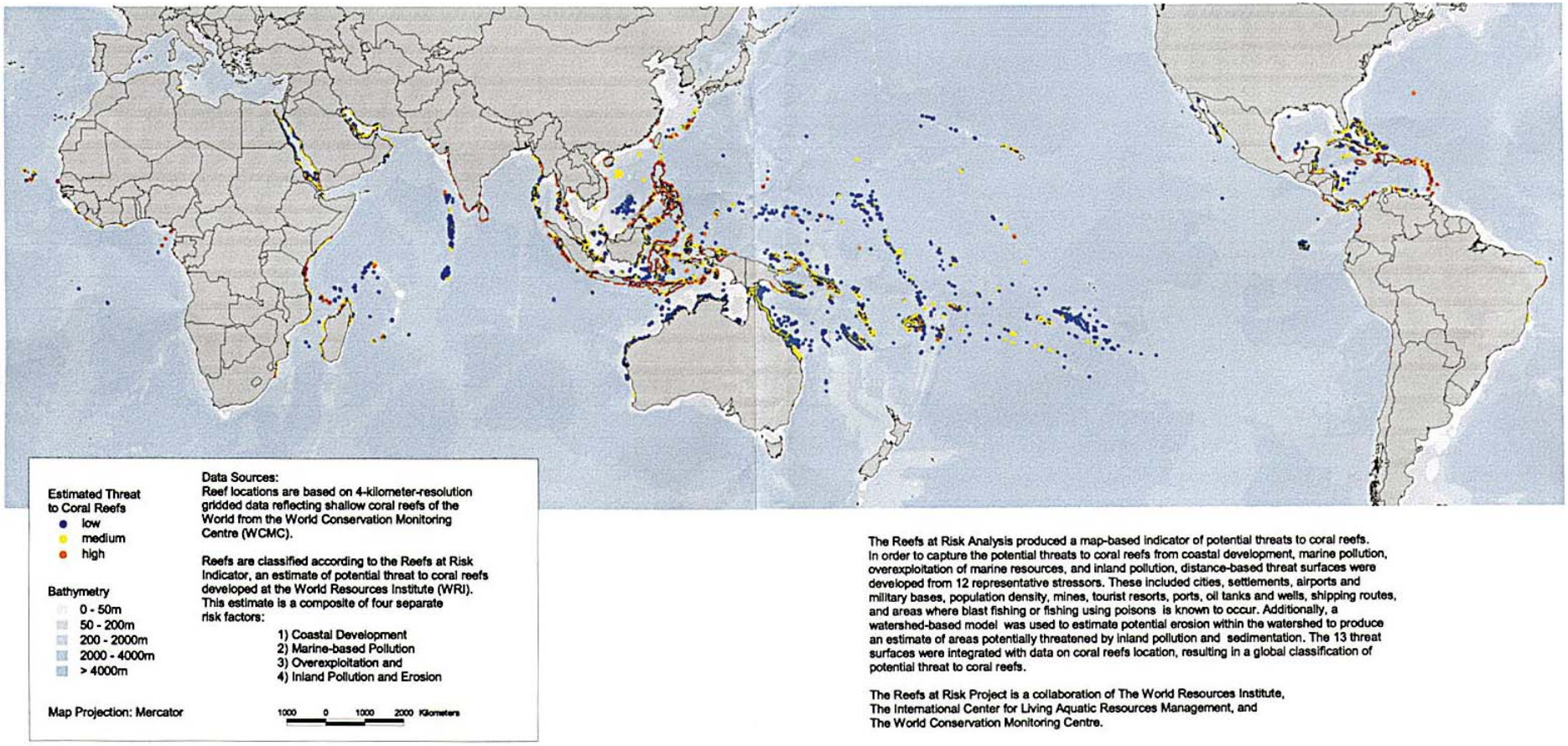

Figure 1 Classification des récifs coralliens du monde par potentiel de menace induite par l'activité humaine (Bryant et al., 1998)

Chapitre I INTRODUCTION

I.1 Pourquoi s'intéresse-t'on à l'hydrodynamique et au transport de particules en suspension ?

Le transport de particules en suspension et de substances dissoutes est contraint par l'hydrodynamique. La quantité de particules en suspension et les concentrations en substances dissoutes sont des paramètres déterminants pour le fonctionnement des écosystèmes marins.

Les nutriments sont présents sous forme particulaire et dissoute. Ils ont une importance fondamentale pour la biologie car ils sont nécessaires à la photosynthèse. L'hydrodynamique, qui les transporte et les disperse, délimite ainsi les zones potentiellement favorables à la photosynthèse ou les zones oligotrophes. L'hydrodynamique joue également un rôle dans l'oxygénation de la colonne d'eau. La consommation d'oxygène dans la colonne d'eau, associée à une insuffisance des apports en oxygène dissous donne lieu à des phénomènes d'anoxie. La circulation, qui advecte et diffuse l'oxygène dissous d'une zone à l'autre, en est un vecteur de régulation.

En transportant les nutriments, l'oxygène dissous, ainsi que d'autres éléments, l'hydrodynamique joue un rôle fondamental dans la régulation de la production primaire d'un écosystème. De manière plus générale la circulation des masses d'eau a un tel impact sur les processus biologiques qu'il est inconcevable d'envisager une modélisation réaliste d'un écosystème côtier sans une reproduction fidèle de son hydrodynamique (Skogen & Moll, 2005 ; Faure, 2006).

La quantité des particules en suspension peut avoir une influence sur les propriétés physiques de l'eau, notamment sur ses propriétés optiques. L'augmentation de la quantité de particules en suspension diminue la visibilité et l'épaisseur de la couche euphotique. La quantité de particules en suspension influence ainsi la photosynthèse. Par ailleurs, à des seuils de concentration élevés, la quantité de particules en suspension modifie la densité de l'eau et fait varier sa viscosité.

A cause de l'activité humaine en mer et/ou à terre, des substances solubles ou particulaires peuvent également être accidentellement introduites dans les milieux marins. Dans certains cas, ces substances modifient les équilibres et perturbent le fonctionnement des écosystèmes. C'est le cas des « marées vertes » en Bretagne produites par de forts apports en nitrates. Dans ce cas, la connaissance de l'hydrodynamique peut participer à l'identification de solutions visant à minimiser l'impact des polluants sur le milieu marin. Dans d'autres cas, les substances introduites dans le milieu marin peuvent être toxiques. La connaissance du comportement de ces substances dans l'eau de mer et l'évaluation de l'étendue de la zone impactée sont fondamentales pour prévenir des problèmes potentiels de santé publique. Or, de

nombreux contaminants chimiques, organiques et métalliques, ont tendance à s'agréger aux particules fines. Le devenir de ces polluants est alors directement lié à celui des particules qui les transportent.

L'étape finale du transport d'une particule en suspension est son dépôt sur le fond. La modification de la localisation et/ou de la quantité de particules déposées modifient également les caractéristiques du substrat sous-marin. Le transport particulaire influe de ce fait sur les caractéristiques de l'habitat sous-marin.

I.2 Quels paramètres faut-il considérer ?

I.2.1 Quelles particules ?

Il existe une grande variété de nature de particules en suspension (Figure I-1). Les particules en suspension faisant partie du vivant ont leur dynamique propre. L'apparition, la prolifération et la disparition de ces organismes vivant obéissent à des règles biologiques. Certaines particules vivantes ont une capacité natatoire, elles participent à leur propre transport. Ce type de particules vivantes, dites « actives », n'est pas abordé dans le cadre de cette thèse.

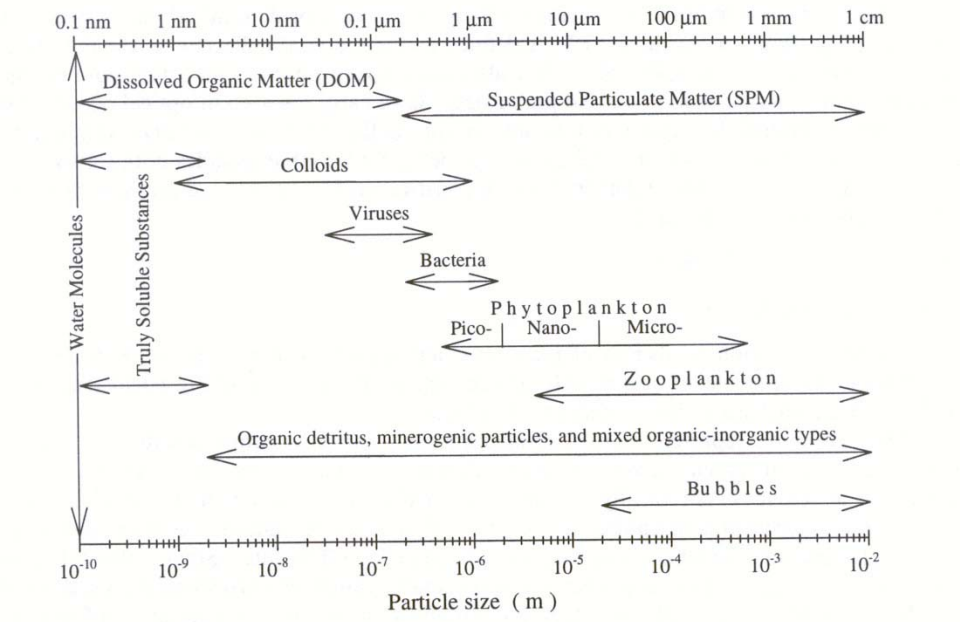

Figure I-1 Principaux constituants dans l'eau de mer (Stramski et al., 2004).

Le transport de particules en suspension fait le plus souvent référence à des particules passives telles que les particules d'origines terrigènes (minérales et/ou organiques) ou bien des particules biogènes (débris coquillés carbonatés et/ou débris coralliens) inertes. La grande majorité des études de transport particulaire a été concentrée sur des milieux côtiers à forts apports particulaires terrigènes.

Le transport de particules procède de deux modes distincts : le transport par charriage et le transport par suspension.

Le transport par charriage concerne les particules dont la vitesse de chute est trop importante pour qu'elles soient maintenues en suspension dans un écoulement donné. Le transport par charriage ne concerne que les particules de sable dont le diamètre est supérieur ou égal à 60 µm (Soulsby, 1997). Les études de transport particulaire qui se focalisent sur le transport par charriage répondent le plus souvent à des problématiques de morphodynamique. Les études morphodynamique en milieu côtier concernent des échelles spatiales plus fine que la présente étude.

Cette thèse est focalisée exclusivement sur le transport de particules en suspension. Le transport par suspension concerne les particules dont la vitesse de chute est suffisamment faible pour qu'elles soient susceptibles de rester en suspension dans la colonne d'eau. En zone côtière, ce mode de transport concerne principalement les particules de petites dimensions : les vases (<60µm Soulsby, 1997). La capacité des vases à adsorber les contaminants explique en partie l'intérêt que l'on porte à étudier leur transport. Ces particules fines ont tendance à adhérer les unes aux autres, ce sont des particules cohésives. Il est nécessaire de tenir compte du processus de floculation encore mal connu dans les simulations de leur transport induit par la circulation.

I.2.2 D'où viennent-elles ?

A l'inverse des particules vivantes, les particules passives n'apparaissent pas spontanément dans la colonne d'eau. On peut donc considérer que la masse de particules en suspension est conservative.

Dans une zone côtière donnée, les apports proviennent généralement des fleuves. Il est donc essentiel de connaître le débit et la charge particulaire des fleuves qui alimentent la zone côtière. En fonction des spécificités de la zone, il peut être nécessaire de considérer d'autres sources d'apport de particules. Ainsi il peut être utile de tenir compte du flux de particules introduit par des rejets urbains ou industriels à proximité d'une agglomération, ou bien de la quantité de matière arrachée au trait de côte dans des cas d'érosion littorale importante, des apports éoliens ou bien du largage en mer de produits de dragages dans une zone de remaniement des fonds.

Les particules en suspension en zone côtière proviennent également du milieu marin. La remise en suspension des particules déposées sur le fond constitue une source de particules. Les premières données à acquérir pour estimer la part de particules remises en suspension concernent les particules déposées sur le fond. La nature et la taille des particules déposées conditionnent leur capacité à être remises en suspension.

Suivant le contexte et les spécificités du milieu étudié, il peut être important de tenir compte de différents processus remettant en suspension des particules du fond tels que le dragage de sédiment ou bien le chalutage benthique. De manière naturelle, la remise en suspension des particules se produit lorsque la tension de cisaillement au fond est suffisamment importante pour arracher les particules du fond. La tension de cisaillement est générée par le mouvement de l'eau au-dessus du fond, induit par le courant et l'oscillation des particules d'eau au passage d'une vague ou induit par le déferlement par petit fond. Pour quantifier la tension de cisaillement au fond, il est nécessaire de définir et quantifier le profil des vitesses et les caractéristiques du champ des vagues.

I.2.3 Comment se déplacent-elles ?

Les particules en suspension sont transportées à l'horizontale par advection et diffusion sous l'effet de la circulation générale. Sur la verticale, elles subissent un mouvement résultant de leur propre vitesse de chute, fonction de leurs caractéristiques physiques (densité, dimension, forme), de l'advection, et de la turbulence.

Dans chaque contexte, l'importance relative de chaque processus est variable. Il est nécessaire d'effectuer des analyses d'échelle afin de cerner l'importance relative des processus les uns par rapport aux autres afin de les hiérarchiser et de concentrer les efforts sur les principaux processus qui caractérisent le transport particulaire sur un site déterminé.

I.3 Le contexte calédonien et l'environnement scientifique

I.3.1 Motivations locales

Le développement que connaît la Nouvelle-Calédonie engendre une augmentation des apports particulaires au lagon depuis plusieurs décennies (Fernandez et al., 2002).

Le premier vecteur apportant davantage de particules dans le lagon est le ruissellement.

L'activité minière est la source principale d'accroissement des apports particulaires au lagon. Les paysages de Nouvelle-Calédonie présentent les stigmates de l'activité minière. De vastes pans de montagne sont de couleur rouge (latérites) suite à leur mise à nu lors de l'exploration et de l'exploitation minière. Celle-ci se fait à ciel ouvert. Les concentrations de nickel dans le minerai étant faible, de l'ordre de 2 à 3 %, les superficies des exploitations sont très importantes. Le couvert végétal de ces surfaces est rasé, les sols sont remaniés, ce qui rend les terrains miniers extrêmement vulnérables à l'érosion. Sur les sites des plus anciennes exploitations sur lesquelles aucune précaution n'était prise, les particules érodées sont transportées par ruissellement jusque dans le lagon. Les sites d'exploration ont une emprise spatiale individuelle plus restreinte. En revanche, les sites d'exploration sont beaucoup plus nombreux et sont également responsable d'importants ravinements dans le paysage

calédonien. L'eau entraîne avec elle d'importants volumes de sols. Lors d'évènements pluvieux, une partie importante de ces particules terrigènes est exportée jusqu'au lagon.

L'activité minière est la première source de revenu du Territoire Calédonien. En 1995, la production du Territoire avoisinait les 120 000 tonnes, pour un montant d'environ 46,5 milliards de francs pacifique, soit 381 millions d'euros. En 1997, avec près de 30% des ressources mondiales de nickel, la Nouvelle-Calédonie se situait au second rang des producteurs mondiaux (**http://nouvellecaledonie.rfo.fr/article12.html**). Le secteur minier est donc un pilier du développement économique de la Calédonie. Au premier trimestre 2005, le secteur minier générait 3421 emplois directs (http://www.info.lnc.nc/nickel /20050705.LNC0153.html?0350). Ce secteur est en pleine expansion. En 2001, le Territoire a reçu plusieurs propositions de développement liées au nickel, dont celui de Koniambo (anciennement Falconbridge-SMSP) en Province Nord et celui de Goro (Inco-Goro Nickel) en Province Sud. Le projet Koniambo prévoit la construction d'une usine pyrométallurgique, la création d'une centrale électrique, d'un barrage et d'un port en eau profonde. Selon les estimations de l'époque, ce projet devait permettre l'extraction annuelle de 60 000 tonnes de nickel sous forme de ferronickel (http://archive.xstrata.com/falconbridge/ www.falconbridge.com/french/growth/growth_initiatives/nickel/koniambo.htm) et de 5 400 tonnes de cobalt. La mise en service de ce complexe industriel minier, initialement prévue en décembre 2005, a été retardée. Le projet Goro concerne la réalisation d'une usine hydrométallurgique. Selon les estimations de l'époque, cette usine doit permettre l'extraction de 54 000 tonnes de nickel et de 5 400 tonnes de cobalt par an. Elle induit la création de 3 500 emplois directs et de 4 000 emplois indirects bénéficiant aux populations de l'archipel (http://www.goronickel.nc /pages/impacts/emplois.htm).

Si en Nouvelle-Calédonie l'activité minière est responsable d'une part importante de l'augmentation des flux de particules terrigènes vers le lagon, cette augmentation a néanmoins d'autres origines liées au développement.

L'accroissement de la population néo-calédonienne impose depuis plusieurs années l'extension de zones de construction. Les surfaces aménagées favorisent le ruissellement des eaux de pluie au détriment de leur infiltration dans le sol. Le ruissellement charrie davantage de particules vers le lagon. Le volume des eaux rejetées, qu'elles soient d'origines urbaines ou industrielles augmente également. Ces rejets n'étant que partiellement traités, ils constituent une autre source de particules injectées directement dans le lagon. Enfin, les feux de brousse causent chaque année des ravages sur la couverture végétale et rendent les sols plus vulnérables à l'érosion.

En contrepoids des menaces que fait peser le développement sur l'environnement, le Gouvernement de la Nouvelle-Calédonie, les trois provinces du Territoire, associées au Ministère de l'écologie et du développement durable et au Ministère de l'Outre mer ont

constitué un dossier de présentation des lagons de Nouvelle-Calédonie en vue de leur inscription sur la liste du Patrimoine Mondial de l'UNESCO au titre d'un bien naturel. Le dossier a été déposé par l'ambassadeur de France auprès de l'UNESCO le 31 janvier 2007. Cette démarche s'inscrit dans un projet de préservation de l'environnement calédonien. Le développement économique de la Nouvelle-Calédonie doit donc tenir compte de la volonté affichée de préserver le patrimoine naturel que représentent les lagons de Nouvelle-Calédonie.

I.3.2 Contexte scientifique et logistique

L'empreinte du contexte dans lequel s'est effectué cette thèse est perceptible tant au niveau de la logistique du projet qu'au niveau de ses orientations scientifiques.

Ce travail de Doctorat a bénéficié d'un financement du programme ZoNéCo. Le programme ZoNéCo (ZONe ECOnomique exclusive de Nouvelle-Calédonie **http://www.zoneco.nc/**) est née de l'association de l'Etat Français, la Nouvelle-Calédonie et ses trois provinces, l'IRD (Institut de Recherche pour le Développement **http://www.ird.fr/**), l'UNC (Université de Nouvelle Calédonie), l'Ifremer (Institut Français de REcherche sur la MER), Météo-France, le SHOM (Service Hydrographique et Océanographique de la Marine nationale). Ce programme sert d'interface entre les décideurs et les instituts de recherches en incitant le transfert des connaissances. Il a pour objectif principal de rassembler et de rendre accessibles les informations nécessaires à l'identification, l'inventaire et la gestion des ressources minérales et vivantes de la Zone Economique Exclusive de la Nouvelle-Calédonie.

Au niveau scientifique, cette étude a été effectuée au sein de l'Unité de Recherche 103, « Caractérisation et Modélisation des Échanges dans des Lagons soumis aux Influences terrigènes et Anthropiques » (CAMELIA **http://www.ird.fr/sais/cgi/Ar?unite=R103**). L'UR 103 est une unité de recherche propre de l'IRD. L'UR Camélia cherche à déterminer l'influence des 3 grands types d'apports (particules, nutriments, métaux) sur certains écosystèmes caractéristiques des environnements côtiers tropicaux.

La compréhension des processus naturels qui régissent les équilibres au sein des écosystèmes passe par le découpage des phénomènes globaux en questions scientifiques propres à chaque discipline. L'océanologie fait appel à de nombreuses disciplines. L'analyse des phénomènes globaux ne peut se passer d'une certaine transdisciplinarité. Dans cette logique, l'UR Camélia regroupe des chercheurs d'horizons disciplinaires différents. Cette pluridisciplinarité a été un des facteurs qui a participé aux orientations scientifiques d'une partie de ce travail de Doctorat.

Au sein de l'UR Camélia, les moyens mis en œuvre pour décrire l'hydrodynamique et le transport particulaire sont de trois types. Les mesures de terrain produisent les données de référence. La variabilité spatiale et temporelle des phénomènes que l'on cherche à décrire requiert l'emploi d'autres méthodes permettant une description plus large qu'à travers les

seules mesures de terrain. La télédétection spatiale est un de ces moyens. Après traitement par des algorithmes spécifiques, et calibration par confrontation à des mesures de terrain, les données satellites peuvent fournir une vision synoptique de grandeurs physiques à la surface du plan d'eau. Le troisième moyen mis en œuvre est celui sur lequel une grande partie de ce travail est focalisé : la modélisation numérique. La modélisation numérique du transport particulaire repose sur une architecture de modules interconnectés (Figure I-2). La démarche de modélisation numérique sera exposée plus en détail par la suite (section II.2.1).

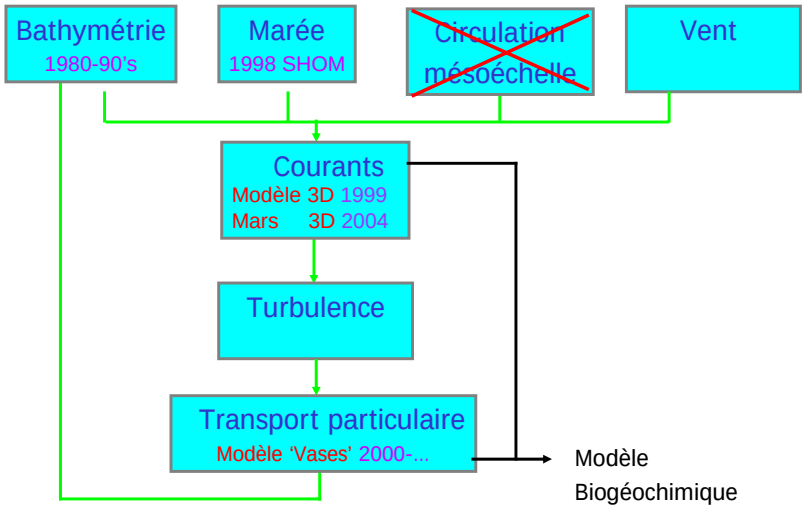

Figure I-2 Architecture de la modélisation numérique du transport de particules

Dans le cadre de ce travail pluridisciplinaire, une part du travail de l'équipe hydrodynamique et transport particulaire de l'Unité Camélia consiste à synthétiser les données produites de manière à les rendre compréhensibles et directement utilisables par les chercheurs d'autres disciplines. Les sites d'études de l'UR Camélia sont répartis suivant deux pôles : Pacifique et Caraïbes. La Nouvelle-Calédonie est le site de recherche principal, les outils et les méthodes développés sur ce site sont ensuite appliqués sur les autres sites d'étude : le lagon de Suva à Fidji (« BULA, ou la caractérisation des eaux d'un lagon » visible sur http://www.canal.ird.fr/sommaires/missions_cp.htm) et la lagune de Cienfuegos à Cuba.

I.3.3 Présentation de la zone d'étude

L'archipel de Nouvelle-Calédonie est situé dans la zone intertropicale, entre 18° et 23° de latitude Sud, et 164° et 167° de longitude Est, approximativement à équidistance entre l'Australie et les îles Fidji (Figure I-3). L'archipel regroupe la Grande Terre, les îles Loyauté, l'île des pins et les îles Belep. La zone d'étude est le Lagon Sud Ouest de Nouvelle-Calédonie

(SLNC) qui entoure la presqu'île de Nouméa, capitale de la Nouvelle-Calédonie situé sur la Grande Terre. Nouméa et ses environs concentrent la moitié de la population de l'archipel.

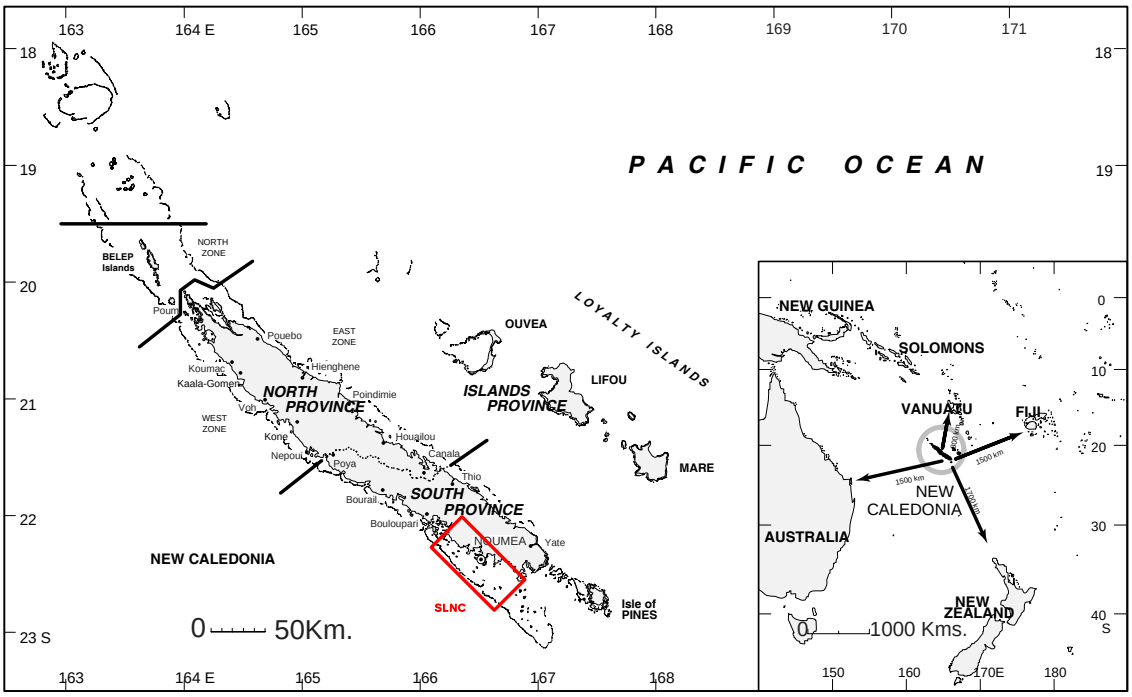

Figure I-3 Carte et situation de la Nouvelle-Calédonie dans l'Océan Pacifique, localisation du Lagon Sud Ouest de Nouvelle-Calédonie (SLNC)

L'archipel est très isolée géographiquement et soumis au régime des alizés (Figure I-3). Il bénéficie d'un climat relativement tempéré que l'on peut qualifier de "tropical océanique". La variation annuelle de la position de la ceinture anticyclonique subtropicale et des basses pressions intertropicales détermine deux saisons principales séparées par deux intersaisons :

La saison chaude et humide, dite "saison des cyclones" dure de mi-novembre à mi-avril. La zone de convergence intertropicale (Z.C.I.T.) se situe alors dans l'hémisphère Sud, sa position moyenne oscillant autour du 15ème parallèle sud. Des dépressions s'y creusent, évoluant parfois en cyclones tropicaux et affectant fréquemment le territoire, y provoquant de fortes pluies et des coups de vents d'Ouest. Cette saison fait place à une période de transition, de mi-avril à mi-mai, pendant laquelle la Z.C.I.T. remonte vers le nord ; les perturbations tropicales sont rares et en général peu actives. La pluviosité diminue et la température de l'air décroît sensiblement (les différences annuelles de température atteignent 8°C). La saison fraîche débute lorsque la zone de convergence intertropicale passe dans l'hémisphère Nord. Des perturbations d'origine polaire traversent alors fréquemment la mer de Tasman et atteignent assez souvent le Territoire, pouvant provoquer des "coups d'Ouest". La température de l'air passe alors par son minimum annuel. Vient ensuite la deuxième intersaison dite sèche, de mi-septembre à mi-novembre. La zone de convergence intertropicale descend vers le sud, franchit l'Equateur, mais son action ne se fait pas encore sentir en Nouvelle-Calédonie. La ceinture anticyclonique subtropicale, qui atteint alors son étendue maximale, protège la région

des perturbations d'origine polaire. La température de l'air augmente progressivement, tandis que la pluviosité est à son minimum annuel. L'alizé souffle en quasi permanence.

L'archipel est par ailleurs soumis à l'influence de l'évènement interannuel ENSO (El Niño Southern Oscillation). Durant El Niño (respectivement La Niña) les précipitations ont tendance à diminuer (respectivement augmenter), l'intensité des vents tend à se renforcer (respectivement faiblir) et la salinité et les températures augmentent (respectivement diminuent) (Nicet et Delcroix, 2000 ; Gouriou et Delcroix, 2002 ; Ouillon et al., 2005).

Le SLNC représente une superficie d'environ 2066 km^2 (Testau et Conand, 1983). La limite Sud-Est du SLNC est définie par une radiale perpendiculaire au récif barrière passant par l'extrémité Sud-Est de l'île Ouen (Figure I-4). La limite Nord Ouest du SLNC correspond à l'étranglement naturel produit par la presqu'île de Uitoé vers le récif barrière. Le SLNC s'étend du récif barrière à la côte. Le récif barrière découvre aux marées basses de vives eaux, il représente donc un obstacle important pour l'hydrodynamique. Le récif barrière est entrecoupé de passes profondes. C'est par ces passes que s'effectue la majeure partie des échanges avec l'océan. La côte qui constitue la limite Nord-Ouest du SLNC est particulièrement découpée. Progressant vers la côte en partant du récif barrière, on rencontre une zone d'arrière récif de faible profondeur (environs 5 à 10 m), puis l'étendue principale du lagon dont la profondeur moyenne est de 17.5 m. L'étendue du lagon est entrecoupée de profonds canyons sous-marins, vestiges d'une évolution fluviatile aérienne en période de bas niveau marin (Chevillotte et al., 2005), qui débouchent au niveau des passes. Le lagon est parsemé de nombreux platiers coralliens. Ces platiers coralliens découvrent partiellement à marée basse et sont parfois surmontés d'un îlot. La côte est une succession de presqu'îles, pointes et de baies au-devant desquelles la profondeur diminue. La ligne de côte est souvent précédée d'un récif frangeant.

L'ensemble des données CTD (*Conductivity-Temperature-Depth*) collectées par l'UR Camélia au cours des 10 dernières années a été intégré dans une base de données. A partir de cet outil, il a été possible d'analyser le comportement de la température et de la salinité dans le SLNC. La salinité varie entre 34.5 à 36.5 psu pour une moyenne d'environ 35 psu (Ouillon et al., 2005). La température de l'eau varie suivant la saison entre 20°C et 29°C. Les données CTD ont également permis de mettre en évidence que le SLNC avait tendance à amplifier les variations saisonnières et interannuelles de température et de salinité par rapport à l'extérieur du lagon (Ouillon et al., 2005). Les mesures de terrain effectuées pendant la thèse ont été intégrées dans cette base de données.

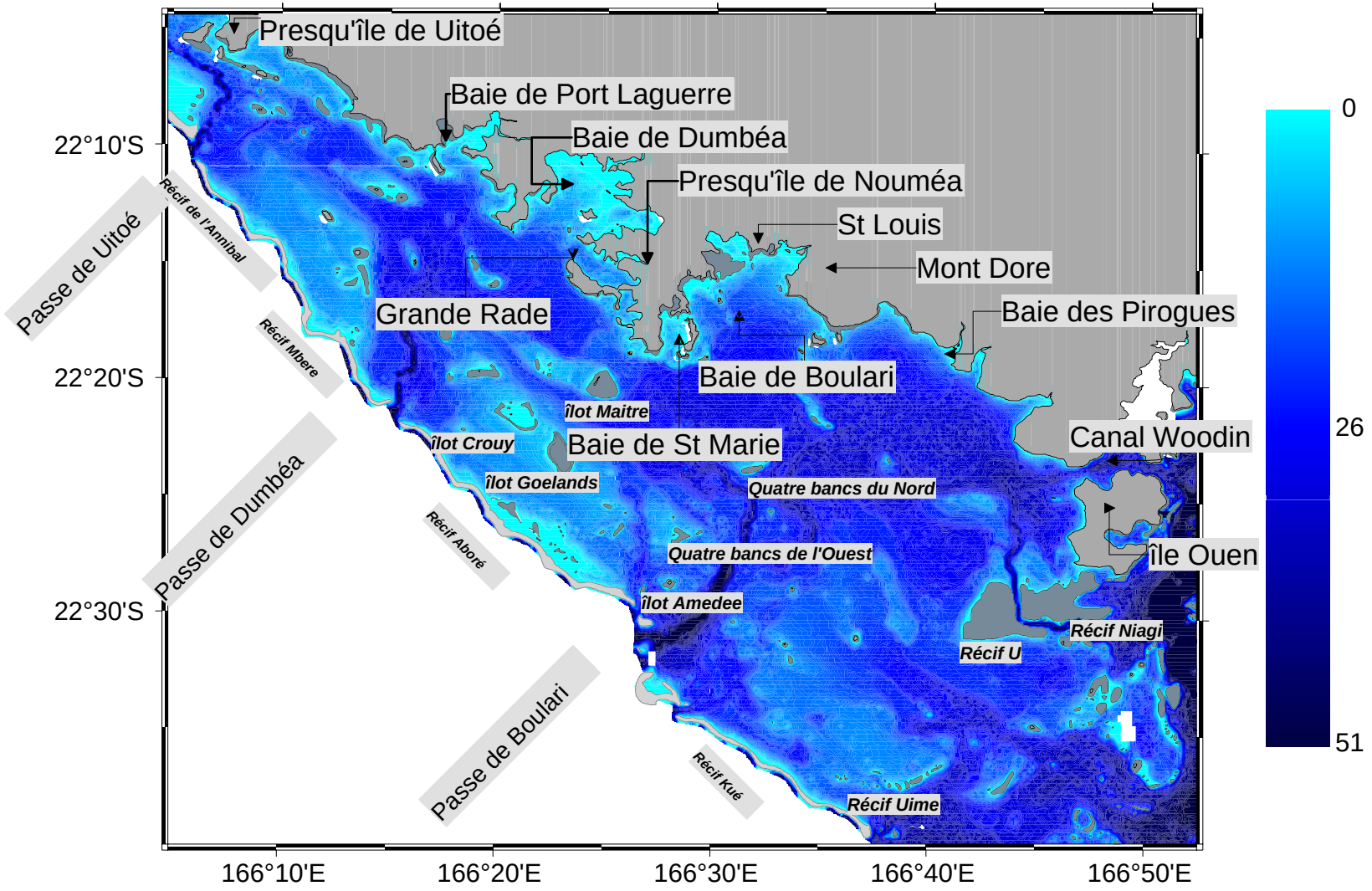

Figure I-4 Repères géographiques et bathymétrie du SLNC

De nombreux cours d'eaux se jettent dans le SLNC. Ils représentent des sources de particules terrigènes pour le SLNC. Les bassins versants qui alimentent les cours d'eaux de Nouvelle-Calédonie sont de faibles étendues. Les débits liquides de ces cours d'eau réagissent étroitement à la pluviométrie. Les débits liquides des fleuves ont une variabilité saisonnière marquée, ainsi qu'une variabilité interannuelle liée aux évènements El Niño (Ouillon et al., 2005). Cette variabilité rend difficile l'estimation des débits solides de ces cours d'eaux.

Depuis que Clavier et al. (1995) ont montré que 80% du dépôt mesuré sur 24 h dans le SLNC avait pour origine la remise en suspension, les efforts de recherche en transport particulaire se sont concentrés sur ce processus en tant que source majeur de particules en suspension sur le SLNC.

La couverture sédimentaire benthique décrite par Chardy et al. (1988) fait référence à trois types de fonds (Figure I-5). Cette description s'appuie sur des critères granulométriques des sédiments déposés ainsi que sur des critères liés à la caractérisation du macro-benthos. Selon cette classification, les fonds envasés sont essentiellement rencontrés dans les baies et les zones les plus profondes du SLNC dont les canyons sous-marins, les fonds de sables blancs sont localisés en zone d'arrière récif barrière, l'espace intermédiaire entre des deux types de fond est occupé par des fonds de sable gris.

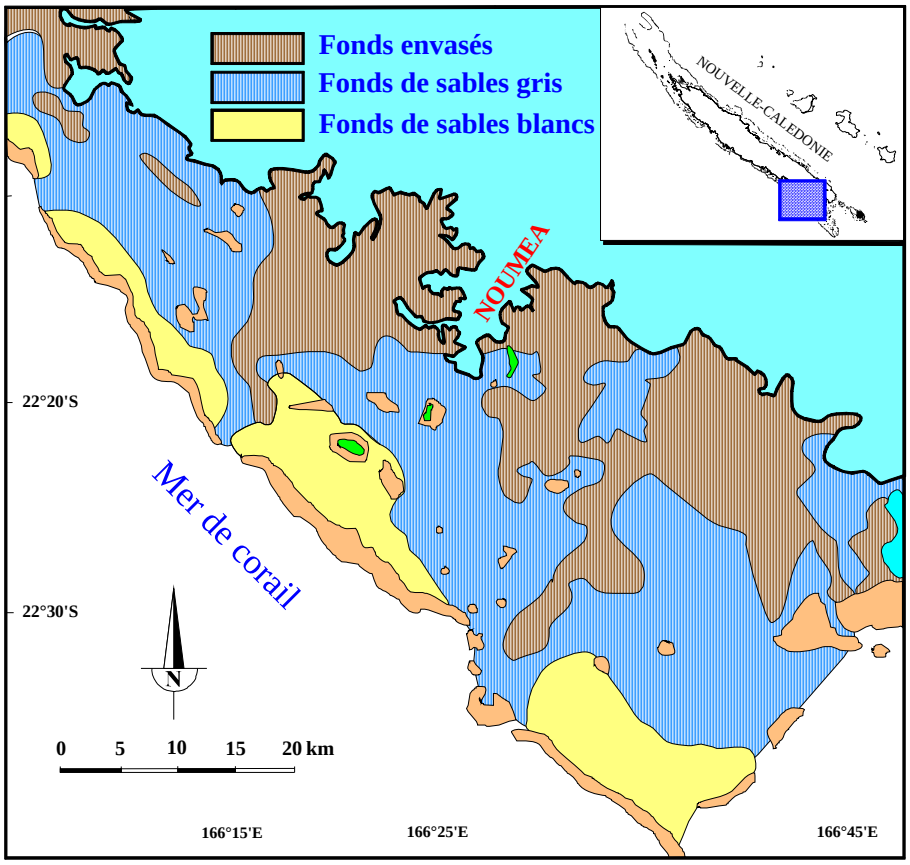

Figure I-5 Types de fonds rencontrés sur le SLNC d'après Chardy et al. (1988)

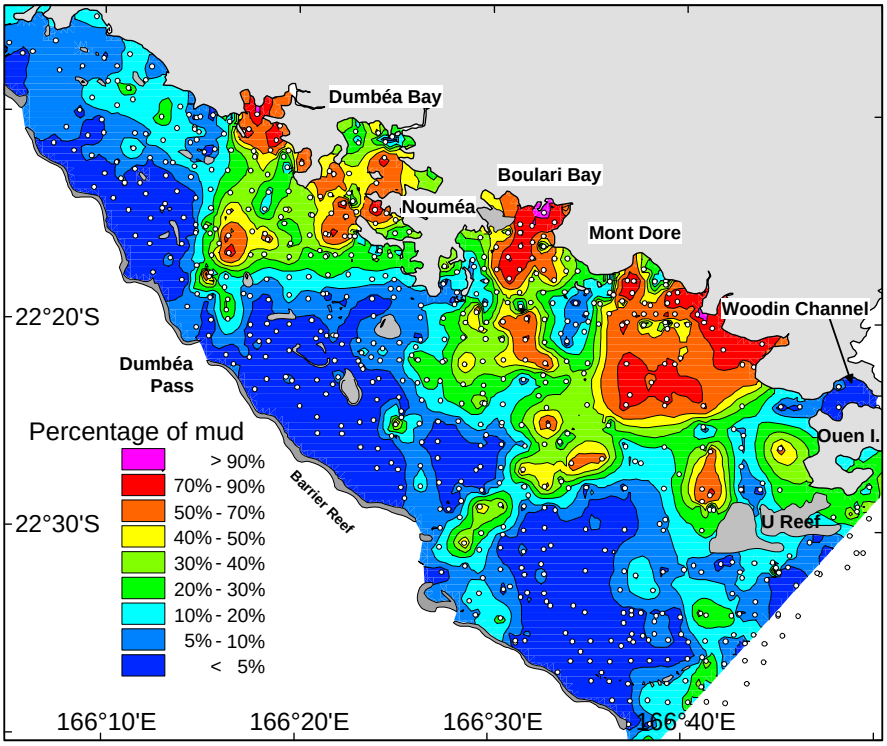

Figure I-6 Couverture sédimentaire benthique en fonction du pourcentage de vases d'après Debenay (1987), Chardy et al. (1988), Chevillon (données non publiées)

Les mesures de sédimentologie réalisées par Debenay (1987) et Chardy et al. (1988) complétées par Chevillon (non publiées) ont été compilées pour obtenir une carte du pourcentage de vase contenu dans les sédiments superficiels (Douillet et al., 2001) (Figure I-6). Les structures générales des cartes des trois types de fond (Figure I-5) et du pourcentage de vase (Figure I-6) sont cohérentes. Si la granulométrie des sédiments superficiels est importante pour quantifier la remise en suspension, la nature des matériaux qui constitue ce sédiment l'est aussi. Les sédiments ont deux types d'origine dans le SLNC, ils sont d'origine terrigène ou biogène. Dans le SLNC, la caractéristique des sédiments biogènes est d'être essentiellement constitués de carbonates. Une carte de la teneur en carbonate des sédiments fins a été établie par Chevillon (non publiée). En faisant l'hypothèse que la partie carbonatée est biogène et que le reste de la matière est terrigène, Chevillon obtient une carte des apports terrigènes sur le SLNC (Figure I-7).

L'hydrodynamique au sein du SLNC a fait l'objet de nombreuses études (Hénin et al., 1984 ; Rougerie, 1985 ; Clavier et Douillet, 1996 ; Douillet, 1998 ; Douillet et al., 2001). De nombreuses mesures de courant et de variation de l'élévation de la surface ont été effectuées pour caractériser l'hydrodynamique sur le SLNC. Un modèle numérique hydrodynamique 3D a progressivement été implanté sur le zone du SLNC (Douillet, 1998 ; Douillet et al., 2001 ; Ouillon et al., 2004). Sa résolution a été affinée à mesure que les moyens de calcul le permettaient. Un modèle 2D (Douillet, 1998), puis un modèle 3D (Douillet, 2001) ont précédé la version du modèle hydrodynamique 3D utilisé pendant ce travail. Les équations résolues et les schémas numériques de ces précédents modèles étaient ceux du code MARS3D de

l'IFREMER. Depuis 2003 et l'établissement d'une convention entre l'IFREMER et Camélia, l'UR Camélia s'est jointe à la communauté des utilisateurs de MARS3D. Cette convention fait bénéficier l'UR des sources de MARS3D qui met les outils développés par Camélia à disposition de l'ensemble des utilisateurs du code.

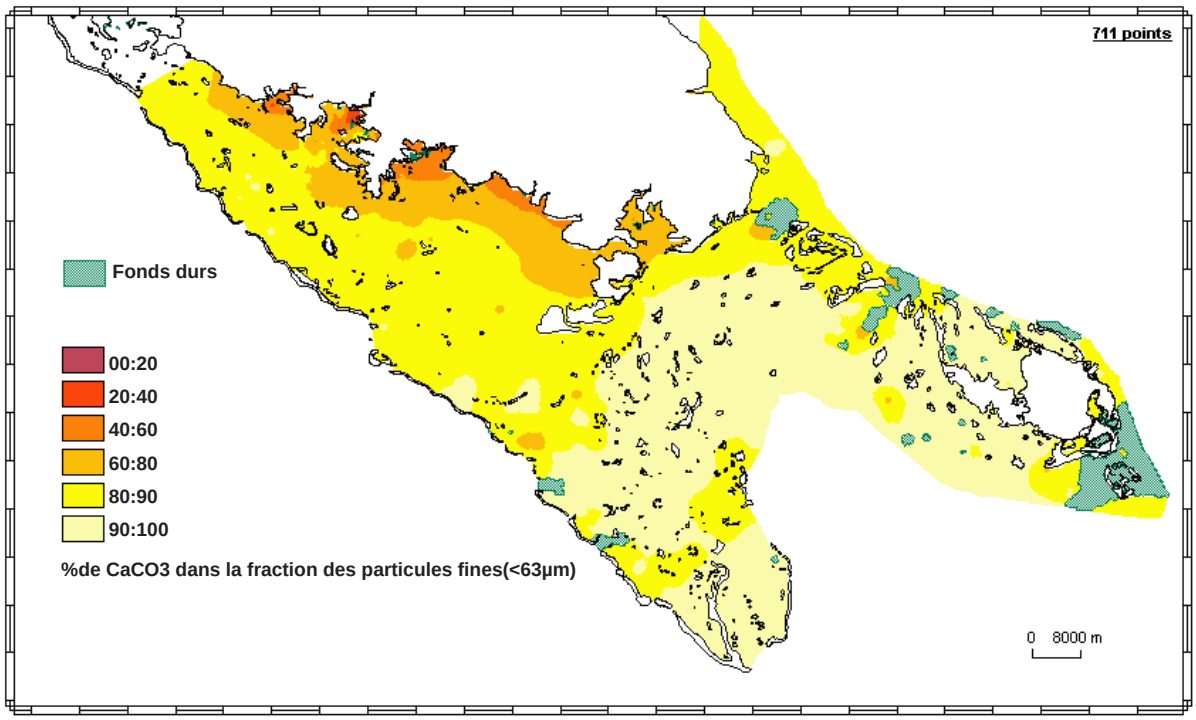

Figure I-7 Répartition des sédiments en fonction de leur teneur en carbonates, apports terrigènes sur le SLNC (Chevillon, communication personnelle)

Des données de terrain (élévation de surface, profils de courant) ont été utilisées pour valider l'implantation du modèle numérique MARS3D sur le SLNC. La dynamique du SLNC est forcée principalement par la marée et le vent. La marée est de type semi-diurne à inégalité diurne, avec une prédominance des ondes M_2 et S_2, l'amplitude maximale est de 1.8 m (Rougerie, 1986 ; Douillet, 1998). Dans le SLNC, le marnage des vives eaux est d'environ 1.4 m contre 0.3 m en mortes eaux. Pendant le flot (Figure I-8A), les masses d'eau pénètrent dans le SLNC principalement entre l'île Ouen et le récif barrière mais aussi par les passes et le canal Woodin (Figure I-4). À l'intérieur du lagon, le courant de flot est globalement orienté vers le Nord-Ouest, et dans les baies le courant est orienté vers le fond des baies. Au jusant, les courants s'inversent. A l'intérieur du lagon, le courant est orienté Sud-Est, il reflue des baies. Au jusant, les masses d'eau sortent principalement entre l'île Ouen et le récif barrière, par les passes, et par le canal Woodin (Figure I-8B).

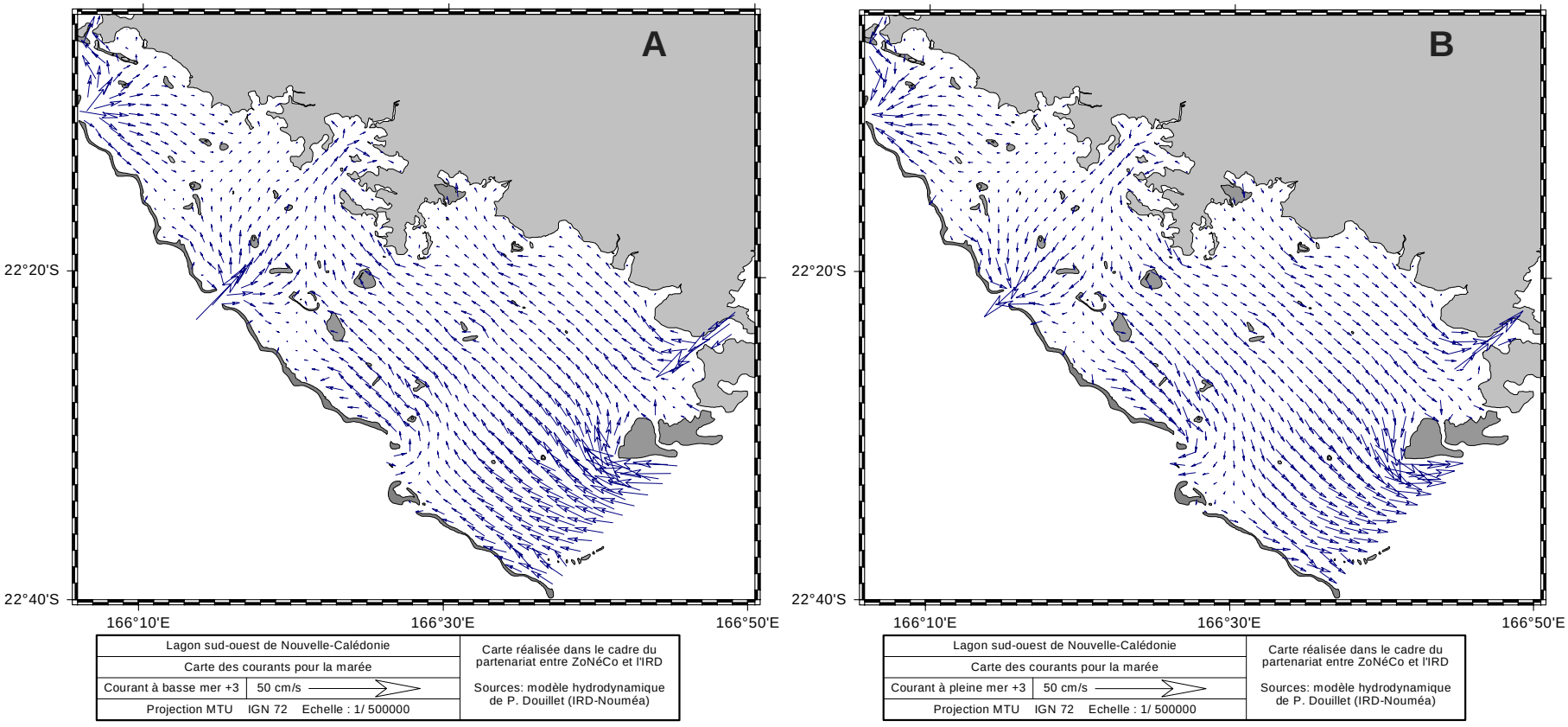

Figure I-8 Cartes des courants de marée, A au plus fort du flot, B au plus fort du jusant. Données issues du modèle MARS3D implanté sur le SLNC.

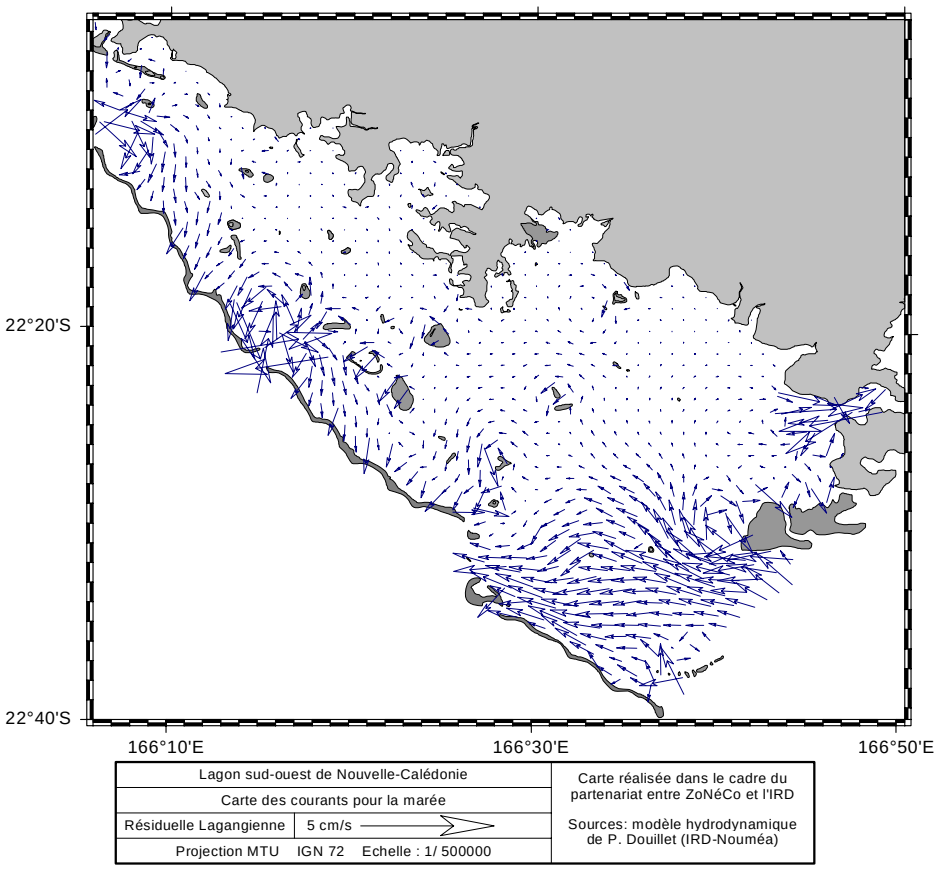

Figure I-9 Carte de résiduelle de marée issue du modèle MARS3D implanté sur le SLNC.

Sur un cycle de marée, les courants de flot et de jusant ont tendance à se compenser, les résiduelles lagrangiennes de marée (Salomon et al., 1988 ; Garreau, 1993 ; Douillet, 1998) sont dix fois moins intenses que les courants de flot ou de jusant (Figure I-9). A la côte, les résiduelles de marée sont quasiment nulles, elles sont plus importantes du côté récif barrière du SLNC (Figure I-9). Les vecteurs de résiduelle de marée entre le récif U et la barrière sont orientés vers la passe de Boulari. A partir de l'analyse des résiduelles lagrangiennes de marée, Douillet (1998) sépare le lagon en deux parties : une partie Sud, dans laquelle les résiduelles lagrangiennes sont orientées de l'extrémité Sud-Est vers les passes de Boulari et de Dumbéa, et une partie Nord, dans laquelle les résiduelles lagrangiennes sont orientées des passes de Uitoé et de St Vincent vers l'intérieur du Lagon. Les résiduelles lagrangiennes convergent à la frontière de ces deux parties du lagon.

Le vent est le second forçage important de l'hydrodynamique sur le SLNC. Une analyse statistique du vent a permis d'identifier deux régimes de vents dominants sur le SLNC : les alizés et les coups d'Ouest (Bujan, 2000). Les alizés, vents d'Est à Sud-est sont prépondérants sur l'année (70% du temps). L'intensité des alizés est souvent renforcée d'une composante thermique, la résultante atteint au moins 15 nœuds, parfois jusqu'à 35 nœuds, et est en moyenne de l'ordre de 20 nœuds quand elle est établie. L'intensité des vents a tendance à être plus soutenue pendant les épisodes El Niño (Ouillon et al. 2005). Les coups d'Ouest sont plus

occasionnels. Ils ont des directions plus variables allant du Nord-Ouest au Sud-Ouest. Les coups d'Ouest sont généralement associés au passage des perturbations (dépressions et cyclones), leurs intensités sont également très variables.

Contrairement à la marée qui génère des courants barotropes, les effets de la tension de vent à la surface du plan d'eau ne s'appliquent que sur la couche superficielle de la colonne d'eau (profondeur d'Ekman). La simulation de ces courants nécessite l'emploi d'un modèle 3D.

Suivant la verticale, les simulations forcées uniquement par le vent montrent des différences notables (Figure I-10). En surface, la direction du courant a tendance à suivre la direction du vent en étant contraint par la topographie. L'intensité du courant de surface généré par le vent varie peu hormis pour les zones situés à l'Ouest de l'île Ouen et au-dessus des canyons où l'intensité du courant diminue. Le champ de courant proche du fond est plus complexe. Entre le récif U et le récif barrière, ainsi que dans les zones d'étranglement provoquées par la présence des îlots, le courant au fond est relativement fort et orienté dans la même direction que le courant de surface. Par régime d'alizé, le vent pousse les masses d'eaux vers le Nord-Ouest ; le modèle montre que le niveau du plan d'eau est inférieur au Nord de l'île Ouen qu'à proximité de Nouméa. Un courant de compensation se développe en sub-surface le long de la côte. Ce courant alimente un tourbillon à l'Ouest de l'île Ouen (Douillet et al., 2001).

Considérant le spectre de taille des sédiments benthiques et leur nature variable, les chercheurs de l'UR Camélia ont fait le choix de modéliser la dynamique des particules fines d'origine terrigène. Ce choix est tout à fait en accord avec les objectifs centraux de l'UR Camélia car l'augmentation des flux entrant de particules terrigènes dans le SLNC est un des effets de l'activité anthropique. La modélisation du transport de particules terrigènes (densité 2.65) a été entreprise (Douillet et al., 2001, Ouillon et al., 2004). L'analyse des sédiments terrigènes de la baie de Dumbéa (O'Callaghan, 1999) a permis d'identifier un mode principal de la distribution granulométrique des particules fines à 7µm. Dans Douillet et al. (2001), les contraintes seuils d'érosion et de dépôt ont été fixées à 0.0017 $N.m^{-2}$ de manière à ce que les zones de dépôts simulées (Figure I-11) concordent avec les zones les plus envasées du lagon (Figure I-6) et que les flux d'érosion s'équilibrent avec les flux de dépôt sur un cycle tidal en condition d'alizé moyen.

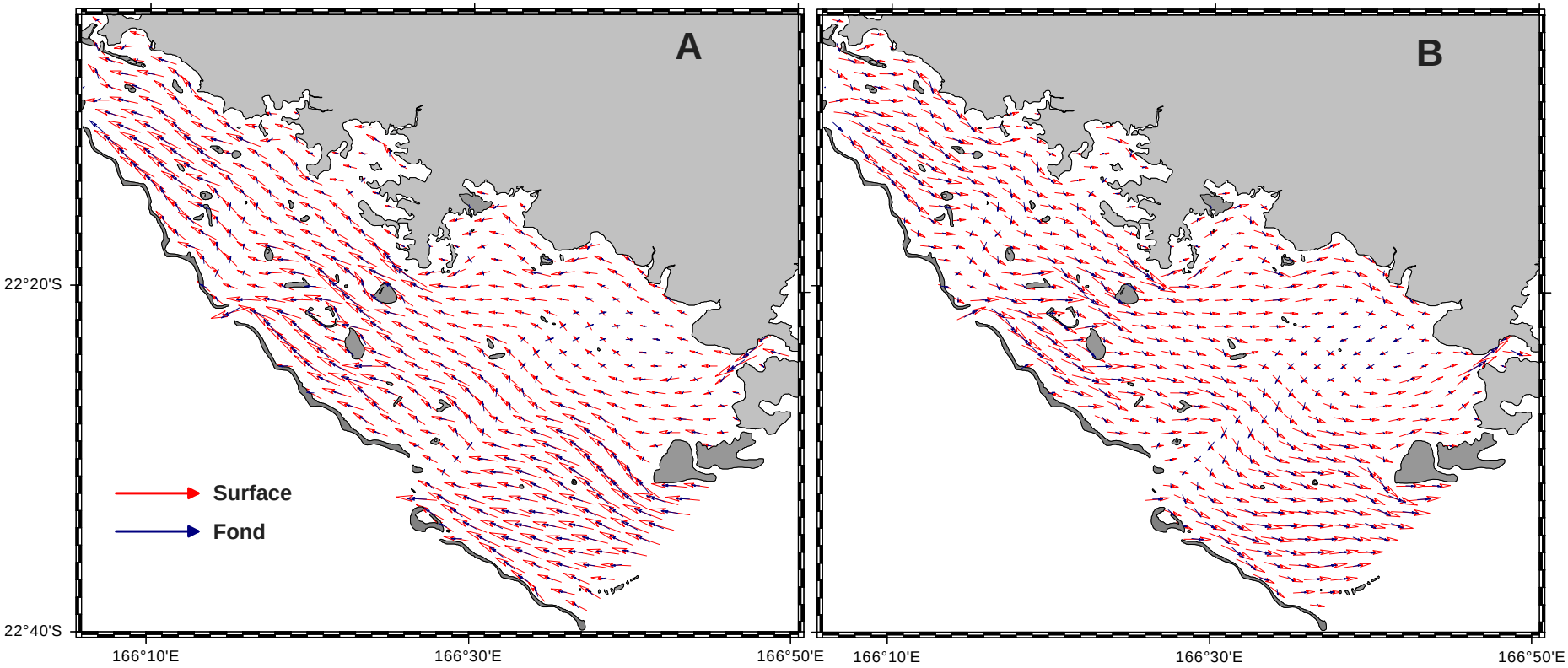

Lagon sud-ouest de Nouvelle-Calédonie		Carte réalisée dans le cadre du partenariat entre ZoNéCo et l'IRD
Courants	50 cm/s →	Sources: modèle hydrodynamique de P. Douillet (IRD-Nouméa)
Projection MTU IGN 72 Echelle : 1/ 500000		

Figure I-10 Courants générés en surface et au fond sur le SLNC par un vent de 8m.s-1. A vent de direction typique Alizé (110° N), B vent d'Ouest (270° N). Données issues du modèle MARS3D implanté sur le SLNC

A partir des résultats de Douillet et al. (2001), des données de turbidité, et d'une cartographie de turbidité tirée d'une image satellite, une zonation des taux d'érosion dans le lagon est apparue nécessaire (Ouillon et al., 2004). Le taux d'érosion a ainsi été ajusté dans certaines zones (Figure I-12) afin que les concentrations simulées de particules en suspension soient en meilleur accord avec des mesures de turbidité effectuées sur le terrain.

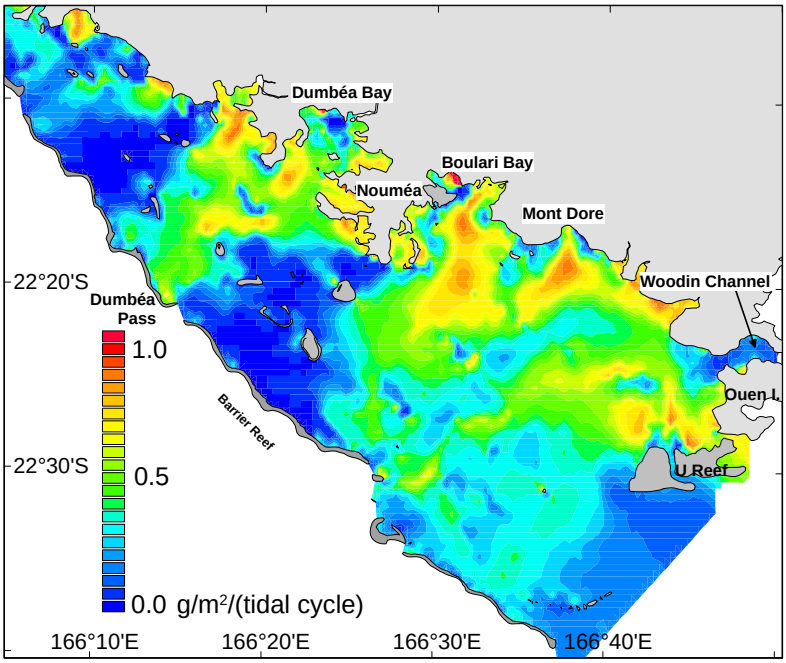

Figure I-11 Localisation et quantité de particules déposées au cours d'un cycle tidale. Simulation numérique avec forçage tidale et tension de vent (8 m.s-1, 110° N) (Douillet et al., 2001)

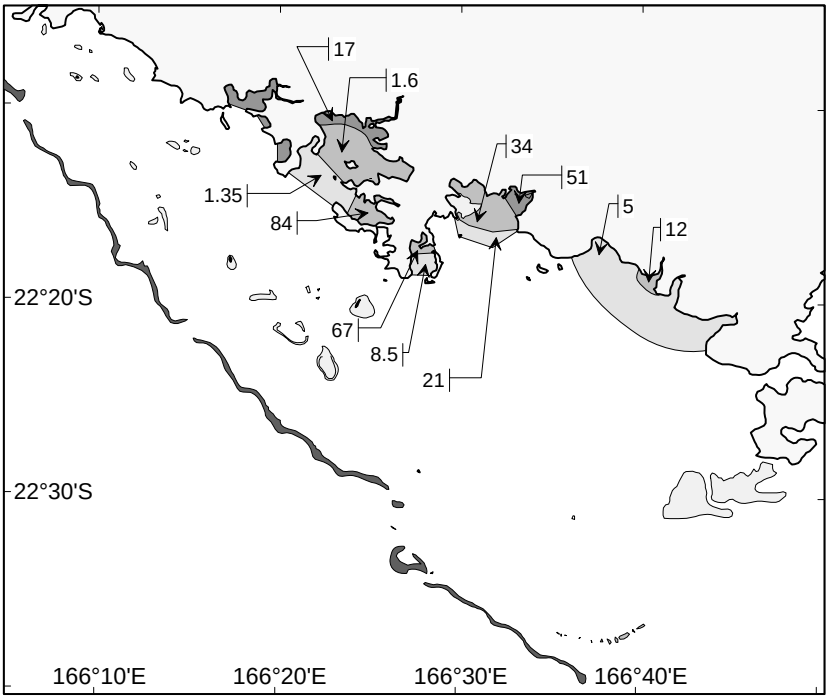

Figure I-12 Zonation du taux d'érosion et valeurs du facteur de proportionnalité appliqué dans la formulation du taux d'érosion (Ouillon et al., 2004)

A la station de mesure A24, située entre le récif U et le récif barrière (Figure II-1), le courant de flot est orienté dans la même direction que le courant généré par un alizé. Ces deux forçages combinés provoquent une importante tension de cisaillement au fond. Au contraire, le courant de jusant s'oppose au courant généré par l'alizé, la conjonction des deux forçages donne lieu à de plus faibles tensions de cisaillement au fond. Le modèle reproduit l'augmentation de la concentration en sédiments liée au flot. Les simulations du modèle de transport ainsi paramétré ont été confrontées à des mesures de turbidité à cette station de mesure sur la base d'une hypothèse d'équivalence entre 1 FTU et une concentration de 1 $mg.L^{-1}$ (Figure I-13).

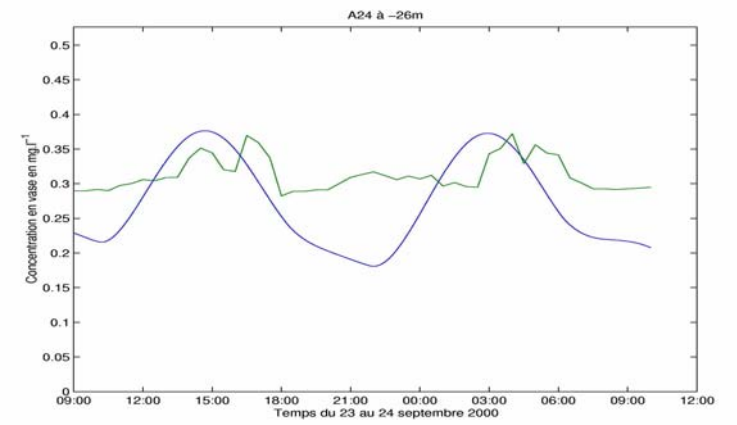

Figure I-13 Comparaison des simulations (bleu) et mesures de turbidité (vert) en station A24 du 23 au 24 septembre 2000 d'après Bouron-Morin (2001)

Entre les périodes de flot, la concentration simulée des particules de 7µm chute alors que la mesure en turbidité tend à se stabiliser à un palier avant de recroître lors du flot suivant.

Malgré une bonne reproduction des pics de concentration de particules en suspension, il existe un biais entre la mesure de turbidité et la quantité de particules en suspension simulée par le modèle de transport particulaire.

I.4 Objectifs et organisation du manuscrit.

L'objectif de cette thèse est d'apporter des éléments permettant d'améliorer notre connaissance du fonctionnement hydro-sédimentaire du lagon et d'affiner la représentativité du modèle hydro-sédimenaire, en s'appuyant sur des mesures, une analyse, et l'implémentation de nouveaux modules dans le modèle numérique.

On s'intéressera tour à tour à différents processus qui participent au transport particulaire. Les équations du transport de particules en suspension synthétisent les différents processus impliqués. C'est autour de ces équations que s'articule ce manuscrit.

L'équation générale de transport de particules rend compte du transport combiné de l'hydrodynamique (advection et diffusion) et de la vitesse de chute des particules. Cette équation est complétée d'une condition limite au fond qui rend compte des échanges entre l'écoulement et le fond résultant des processus de dépôt et d'érosion.

Une description plus détaillée des équations du transport particulaire est proposée en section II.2.3 de ce document de thèse. Les éléments sous accolades des équations présentées ci-après sont les termes sur lesquels sont focalisés chacune des parties de ce manuscrit de thèse.

$$\overbrace{\frac{\partial(C)}{\partial \mathrm{t}}+\frac{\partial(uC)}{\partial \mathrm{x}}+\frac{\partial(vC)}{\partial \mathrm{y}}+\frac{\partial\left(\left(w-\overbrace{w_s}^{\text{VITESSE DE CHUTE}}\right)C\right)}{\partial \mathrm{z}}}^{\text{ADVECTION}}=\overbrace{\frac{\partial\left(F_x^C\right)}{\partial \mathrm{x}}+\frac{\partial\left(F_y^C\right)}{\partial \mathrm{y}}+\frac{\partial\left(F_z^C\right)}{\partial \sigma}}^{\text{DIFFUSION}} \qquad \text{Eq. I-1}$$

$$E_s = k_e.\left(\frac{\overbrace{\tau}^{\text{TENSION DE CISAILLEMENT}}}{\tau_{ce}}-1\right) \quad \text{pour } \tau > \tau_{ce} \; ; \; E_s = 0 \text{ pour } \tau < \tau_{ce} \qquad \text{Eq. I-2}$$

$$D_s = w_s C.\left(1-\frac{\overbrace{\tau}^{\text{TENSION DE CISAILLEMENT}}}{\tau_{cd}}\right) \quad \text{pour } \tau < \tau_{cd} \; ; \; D_s = 0 \text{ pour } \tau > \tau_{cd} \qquad \text{Eq. I-3}$$

La première partie de ce travail concerne l'advection et la dispersion calculée par le modèle hydrodynamique MARS3D. A partir d'outils numériques développés dans le modèle, un travail de synthèse des données hydrodynamiques est effectué afin de les rendre directement utilisables dans d'autres disciplines. Cette première partie porte l'empreinte du contexte pluridisciplinaire de l'Unité de Recherche dans laquelle s'est effectuée cette Thèse.

La seconde partie se concentre sur la tension de cisaillement au fond, responsable de la remise en suspension des particules. Cette seconde partie présente plus spécifiquement la validation de l'implantation du modèle de houle WaveWatchIII sur le SLNC. Cette démarche constitue la première étape en vue de l'intégration de la contribution des vitesses orbitales de houle dans le calcul de la tension de cisaillement au fond.

La troisième partie vise à contribuer à une meilleure caractérisation physique des particules permettant notamment une meilleure paramétrisation de la vitesse de chute des particules.

Le cœur de chacune des parties est présenté sous le format de publication. Ce format synthétique ne permet pas de détailler les principes de fonctionnement des outils utilisés dans ces travaux. Les trois parties présentant les résultats produits au cours de ce travail sont donc précédées d'une partie présentant plus en détail le principe de fonctionnement des outils utilisés.

Chapitre II MATERIEL ET METHODES

II.1 Mesures

II.1.1 Introduction

L'hydrodynamique et le transport particulaire sont des processus qui varient dans le temps et l'espace. Le déploiement d'instruments adéquats sur le terrain est indispensable pour comprendre les processus engagés dans le transport de particules.

Les échelles spatiales et temporelles des études menées pour cette thèse se prêtent particulièrement bien à la mesure. De plus, les moyens mis à disposition pour effectuer ce travail n'ont pas manqué.

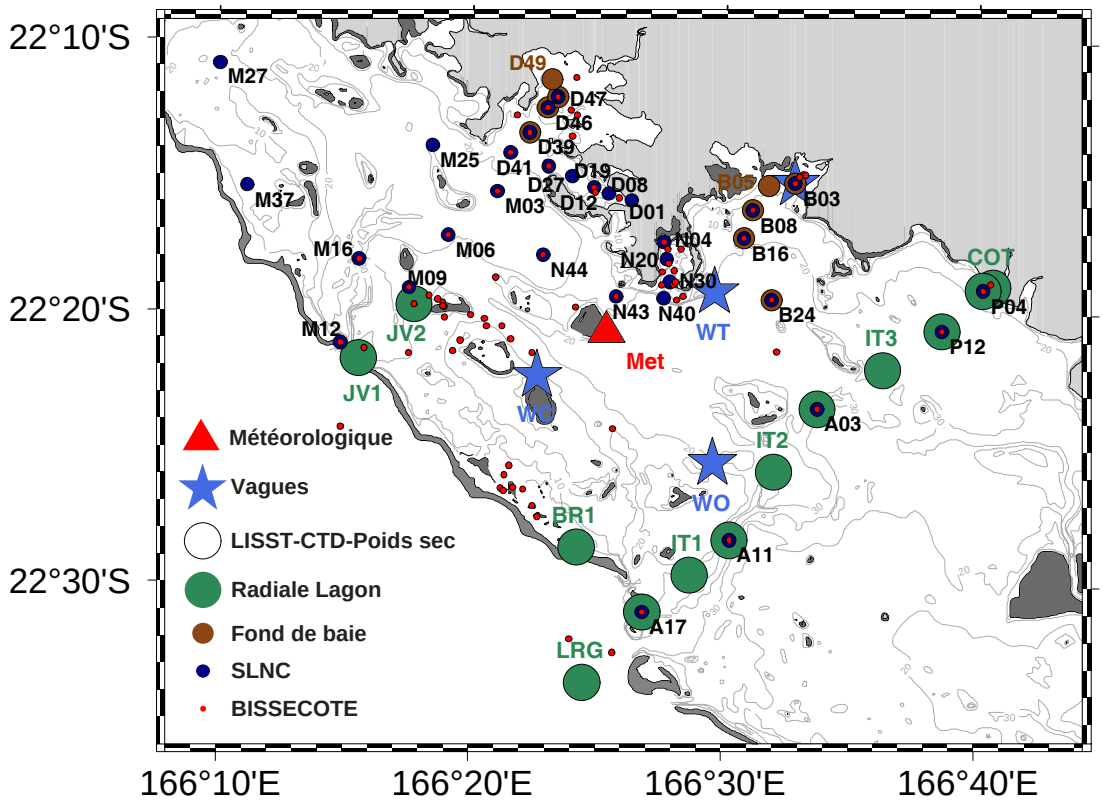

Figure II-1 Distribution géographique de l'ensemble des points de mesures sur le lagon suivant le type de mesure effectué et plan d'échantillonnage des missions en mer.

Pour les besoins de la thèse, plus de 900 profils CTD (sonde mesurant la conductivité, la température, la turbidité et la profondeur) et 500 profils LISST (granulomètre laser *in situ*) ont été effectués, environ 200 concentrations de particules ont été mesurées après filtration, un peu moins de deux mois de mesure ont été collectées avec une sonde WTR9 (houlomètre) ainsi qu'avec un ADV (vélocimètre acoustique doppler). Au final, pas loin de 4000 milles nautiques ont été parcourus (Figure II-1 et Tableau II-1).

Etant donné l'importance des mesures de terrain dans cette thèse et le temps employé à collecter, traiter et organiser les données, une description détaillée des instruments de mesure et des campagnes réalisées est indispensable.

Jours de mesures		Type de campagne	Navire	matériel
17/09/2003	18/09/2003	SLNC	CORIS	CTD
15/10/2003	16/10/2003	SLNC	CORIS	CTD
12/11/2003	13/11/2003	SLNC	CORIS	CTD
10/12/2003	11/12/2003	SLNC	CORIS	CTD
14/01/2004	15/01/2004	SLNC	CORIS	CTD
17/02/2004	18/02/2004	SLNC	CORIS	CTD
17/03/2004	18/03/2004	SLNC	CORIS	CTD
22/03/2004		METEO	PLATE	METEO
14/04/2004	15/04/2004	SLNC	CORIS	CTD
12/05/2004	13/05/2004	SLNC	CORIS	CTD
21/07/2004	22/07/2004	SLNC	CORIS	CTD
18/08/2004	19/08/2004	SLNC	CORIS	CTD
15/09/2004	16/09/2004	SLNC	CORIS	CTD
17/11/2004	18/11/2004	SLNC	CORIS	CTD
20/12/2004	21/12/2004	SLNC	CORIS	CTD
18/01/2005	19/01/2005	SLNC	CORIS	CTD
22/03/2005	23/03/2005	SLNC	CORIS	CTD LISST Poids secs
12/04/2005	13/04/2005	SLNC	CORIS	CTD LISST Poids secs
19/05/2005	20/05/2005	SLNC	CORIS	CTD LISST Poids secs
25/05/2005		METEO	PLATE	Batterie
16/06/2005	17/06/2005	SLNC	CORIS	CTD LISST Poids secs
21/07/2005	22/07/2005	SLNC	CORIS	CTD LISST Poids secs
18/08/2005	19/08/2005	SLNC	CORIS	CTD LISST Poids secs
12/09/2005		Radiale Lagon	CORIS	CTD LISST Poids secs
21/09/2005	22/09/2005	SLNC	CORIS	CTD LISST Poids secs
22/12/2005		SLNC	CORIS	CTD LISST Poids secs
06/01/2006		Radiale Lagon	CORIS	CTD LISST Poids secs
19/01/2006	22/01/2006	Radiales fonds de baies	CORIS	CTD LISST Poids secs
01/02/2006		Radiale Lagon	CORIS	CTD LISST Poids secs
02/02/2006	14/02/2006	BISSECOTE	ALIS	CTD LISST Poids secs
16/02/2006	17/02/2006	SLNC	CORIS	CTD LISST Poids secs
23/03/2006		Radiale Lagon	CORIS	CTD LISST Poids secs
31/03/2006		VAGUES	CORIS	Pose ADV WTR9
14/04/2006		VAGUES	CORIS	Retrait ADV WTR9
19/05/2006		VAGUES	ALDRIC	Pose ADV WTR9
01/06/2006		VAGUES	CORIS	Retrait ADV WTR9
08/06/2006		VAGUES	CORIS	Pose ADV WTR9
11/06/2006		VAGUES	ALDRIC	Retrait ADV WTR9
11/07/2006		VAGUES	ALDRIC	Pose ADV WTR9
06/08/2006		VAGUES	CORIS	Retrait ADV WTR9
08/08/2006		VAGUES	DIODON	Pose ADV WTR9
21/08/2006		VAGUES	CORIS	Retrait ADV WTR9

Tableau II-1 Inventaire des missions de terrain effectués pour cette thèse.

II.1.2 Données de vent

Des mesures de vent sont effectuées en continu à partir de la balise latérale bâbord située à l'extrémité Sud du platier de l'îlot Maître. La mesure du vent en direction (°N) et en intensité ($m.s^{-1}$) se fait à 10m au-dessus de l'eau. Cette station météo enregistre également la température de l'air. Les valeurs enregistrées correspondent à des moyennes sur 10 min. Cette station météo a été mise en place en 1998.

II.1.3 CTD Seabird Seacat 19

La sonde CTD Seacat 19 (**http://www.seabird.com/products/profilers.htm**) mesure la pression, la température, la conductivité, la turbidité, elle est également équipée d'un fluorimètre permettant la détermination *in situ* de la concentration en chlorophylle, et d'un capteur de PAR (*Photosynthetically Active Radiation*) afin de déterminer l'atténuation lumineuse en fonction de la profondeur.

La principale mesure exploitée dans cette thèse est la mesure de turbidité effectuée par un turbidimètre Seapoint. Cette mesure quantifie la rétrodiffusion d'un rayon émis dans le proche infrarouge (870 nm) dans un faible volume, proche de la sonde. L'intensité du signal rétrodiffusé dépend de la quantité de particules en suspension.

Pour l'essentiel, les mesures CTD sont des profils de la surface au fond, dans la limite de 60 m de profondeur (longueur du cordage). La fréquence d'échantillonnage des appareils est de 2 mesures par seconde, la sonde CTD (Figure II-2) est descendue manuellement à vitesse régulière inférieure à 1 $m.s^{-1}$. Le post-traitement des données (obtention de la salinité etc. …) est effectué via les programmes fournis par Seabird (Seaterm et SBE data processing). Les données sont ensuite vérifiées puis intégrées dans une base de données.

Figure II-2 La sonde CTD SBE 19

II.1.4 Concentration massique des matières en suspension

La mesure de la concentration massique de particules en suspension nécessite beaucoup de temps, une faible quantité de données est réalisable par ce moyen.

Des échantillons d'eau de mer sont prélevés avec des bouteilles Niskin à différentes profondeurs. Ces échantillons sont ensuite filtrés (Figure II-3) sur des filtres en polycarbonate perforés à 0.4 µm, préalablement séchés dans une étuve et pesés à vide. En fin de filtration, un rinçage à l'eau distillée est réalisé pour dissoudre d'éventuels cristaux de sel.

Après une nouvelle étape de dessiccation par passage des filtres à l'étuve (température de 60°C, durée de 24h), les filtres chargés en particules sont pesés une seconde fois. Les faibles concentrations rencontrées sur le SLNC nécessitent de filtrer d'importants volumes d'eau afin que la charge particulaire des filtres soit significative. Malgré cette précaution, la charge particulaire des filtres étant faible, il est indispensable d'utiliser une balance de très haute précision. La balance utilisée pour les deux pesées est la Perkin-Elmer AD-4 Autobalance (Figure II-4) qui atteint une précision de 0.001 mg.

Figure II-3 Rampe de filtration: la dépression est contrôlée et se fait par effet Venturi.

Figure II-4 Perkin-Elmer AD-4 Autobalance: précision de 0.001 mg.

II.1.5 LISST 100X

II.1.5.1 Principe de fonctionnement

Le LISST 100X (***L**aser **I**n **S**itu **S**cattering and **T**ransmissometry*) est un granulomètre laser *in situ* développé et commercialisé par Sequoia Scientific Inc. Il fournit une estimation de la concentration volumique (µL/L) des particules en suspension en fonction de leur diamètre (Agrawal et Pottsmith, 2000). La version du LISST utilisé dans cette thèse quantifie les concentrations de particules dont le diamètre est compris entre 1.25 et 250 µm. Ce type d'instrument est novateur. Seuls le LISST et un instrument équivalent, le CILAS (Gentien et al., 1995), développé par l'IFREMER, permettent une mesure *in situ* de la distribution des tailles des particules en suspension.

L'estimation de la concentration volumique donnée par le LISST repose sur la théorie de diffusion de Mie (Van de Hulst, 1957). Lorsqu'un signal lumineux traverse une suspension de particules sphériques le signal lumineux est diffusé. Suivant le rapport du diamètre des

particules sur la longueur d'onde du signal lumineux (d/λ), on distingue deux régimes de diffusion. Lorsque le diamètre des particules est significativement plus petit que la longueur d'onde du signal lumineux (d/λ<<0.1), on considère que le régime de diffusion obéit à la théorie de diffusion de Rayleigh. La théorie de diffusion de Mie s'applique lorsque le diamètre des particules est équivalent ou supérieur à la longueur d'onde du signal lumineux.

A de faibles angles de déviation par rapport à la direction du faisceau lumineux initial, l'intensité lumineuse diffusée est fonction de la taille des particules présentes dans la solution. La nature des particules (indice de réfraction) n'a pas d'effet sur la diffusion à ces faibles angles de déviation. Avec une longueur d'onde de 670 nm et un diamètre de particule supérieur ou égale à 1.25 µm, les conditions nécessaires à l'application de la théorie de Mie pour l'inversion mathématique du signal optique sont réunies. La seule différence entre la théorie et l'application provient de la forme des particules. Les particules en suspension dans l'eau de mer ne sont pas nécessairement sphériques. Les résultats de l'inversion de la mesure optique concernent des particules sphériques de diamètre équivalent. Dans la fourchette des faibles déviations, plus la section caractéristique des particules est faible, plus l'angle de diffraction est important. Le LISST émet un signal lumineux et détecte l'intensité lumineuse répartie selon ces faibles angles de déviation.

Le capteur permettant de détecter l'intensité lumineuse à différents angles de diffusion est une succession concentrique de photodiodes dont le rayon augmente de manière logarithmique (Figure II-5).

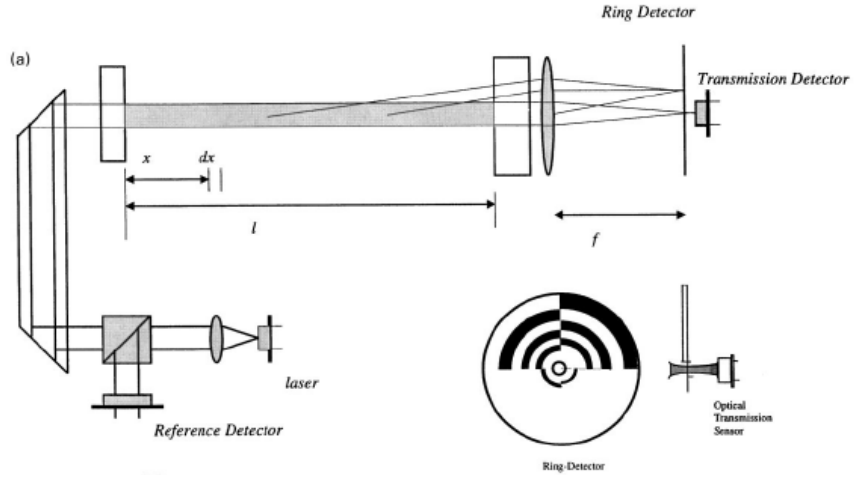

Figure II-5. Géométrie optique du LISST et détails du capteur optique concentrique (Agrawal et Pottsmith, 2000)

L'intensité du signal lumineux $\bar{d}$ captée par chacune des photodiodes est donc fonction de la quantité et de la section optique des particules présentes dans le volume d'échantillonnage.

$\bar{d}$ est corrigée de l'atténuation τ (intensité lumineuse transmise/intensité lumineuse émise) et du signal obtenu pour un échantillon d'eau pure (*zscat*) (Eq. II-1).

$$s = \left[\bar{d}/\tau\right] - zscat \qquad \text{Eq. II-1}$$

où s est l'intensité du signal lumineux normalisée et corrigée, pour chacune des photodiodes. La distribution des tailles de particules $INV(s)$ est ensuite obtenue par inversion mathématique (Hirleman, 1987). Si en théorie l'indice de réfraction influence peu la diffusion, une erreur peut survenir lors de l'inversion, lorsque l'indice de réfraction des particules est très différent de celui choisi pour l'inversion (Agrawal et Pottsmith, 2000). Une fois la distribution surfacique de taille de particules transformée en distribution volumique de taille $INV(s_{vol})$, la concentration volumique dans chacune des classes de taille est obtenue par application d'une constante de conversion $cste_v$.

$$C_{vol} = INV(s_{vol}) \Big/ cste_v \qquad \text{Eq. II-2}$$

$cste_v$ est obtenue expérimentalement en comparant l'intégrale de la distribution de concentration volumique sur l'ensemble des classes de taille à la concentration volumique connue mesurée par le LISST en laboratoire. Ce facteur de conversion est donc un facteur global. Via cet instrument et le post-traitement exposé, le LISST 100X donne une estimation de la concentration volumique des particules dont le diamètre équivalent est compris entre 1.25 et 250 µm. La concentration volumique des particules en suspension est distribuée sur 32 classes de tailles régulièrement espacées suivant une progression logarithmique.

Dans le cadre de cette étude, le LISST a été utilisé en profileur, de la surface au fond. La fréquence d'échantillonnage a été fixée à 1 mesure par seconde. Chaque mesure est la moyenne de 30 mesures effectuées par le LISST en une seconde. Le LISST 100X (Figure II-6) est descendu manuellement à vitesse régulière d'environ 50 $cm.s^{-1}$. La transformation des données issues du LISST en données ascii est effectuée par le programme livré avec l'instrument LISST-SOP version 4.65. Des programmes de traitement et organisation des données ont été élaborés sous Matlab.

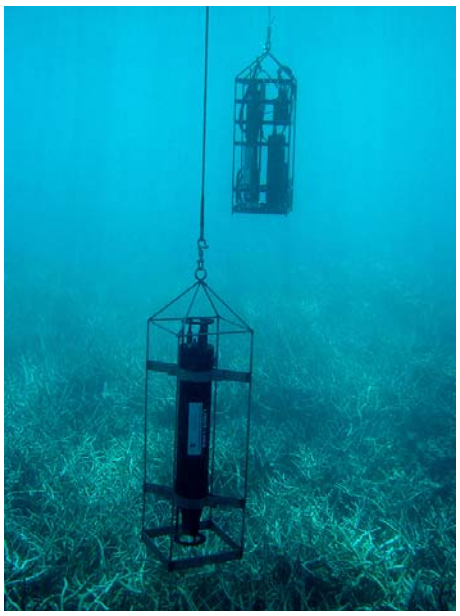

Figure II-6 LISST et CTD en mesure.

II.1.5.2Dispositif de laboratoire

Le LISST est livré avec des accessoires permettant d'effectuer des mesures en laboratoire. Une chambre de mesure équipée d'un agitateur magnétique peut ainsi être fixée sur le parcours du faisceau laser. Un montage reliant un réservoir à la chambre de mesure a été

élaboré (Figure II-7). Selon les besoins, le réservoir peut être un bécher ou une cuve de sonification. La cuve de sonification (Brandson sonifier 250) est employée pour remettre en suspension et désagréger les particules préalablement récoltées sur des filtres en polycarbonate.

Figure II-7 Dispositif de mesure à l'aide du LISST en laboratoire.

II.1.6 WTR9

La sonde Aanderaa WTR9 (*Wave and Tide Recorder 9*)(Figure II-8) est un houlomètre. Elle est équipée d'un capteur de pression et d'un capteur de température. L'enregistrement de la pression se fait à une fréquence de 2 Hz sur des périodes de 512 secondes toutes les 30 minutes. Le traitement des données est réalisé à l'aide de programmes Aanderaa livrés avec la sonde. La température est utilisée dans la conversion de la pression en profondeur et le traitement du signal par décomposition en séries de Fourier est effectué en interne à l'appareil. Le WTR9 fournit des paramètres intégrés de la houle : sa hauteur significative et sa période.

Figure II-8 Le houlomètre Aanderaa WTR9 en opération

II.1.7 ADV

L'ADVOcean (*Acoustic Doppler Velocimeter*) produit par Sontek est une sonde qui mesure en un point (Figure II-9) les trois composantes de vitesse à haute fréquence (maximum 5 Hz). C'est une mesure acoustique basée sur l'effet Doppler. La sonde est équipée d'un compas et d'un système de mesure de l'inclinaison de la sonde afin de pouvoir restituer les mesures dans le repère géographique ENU (Est, North, Up). L'ADVOcean est également équipé d'un capteur de pression.

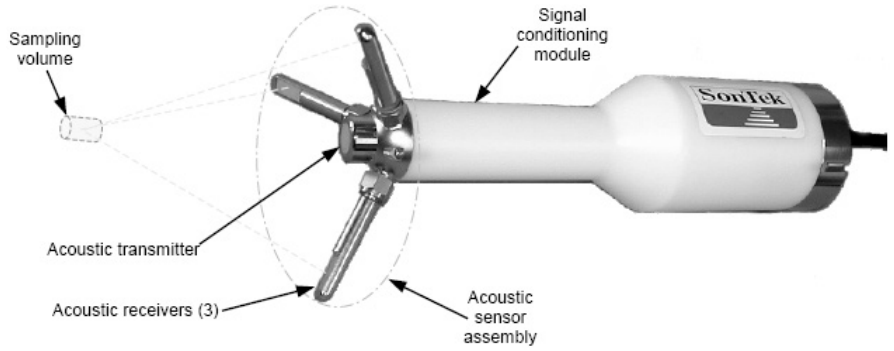

Figure II-9 Localisation du volume de mesure (≈2cm^3) de l'ADVOcean (ADV User Manual, 2001).

Un bâti en aluminium (non magnétique) a été conçu par l'équipe et réalisé par un artisan local pour son déploiement au mouillage (Figure II-10).

Compte tenu de la confidentialité des algorithmes Sontek de traitement du signal qui permettent de déduire les caractéristiques du spectre directionnel de la houle à partir des mesures PUV (Pression et vitesses horizontales U et V), nous avons été contraints de développer nos propres programmes de traitement du signal. Ce travail a été effectué sous Matlab.

Figure II-10 La sonde Sontek ADVOcean en opération

II.2 Modélisation numérique

II.2.1 Introduction

Malgré les progrès faits en instrumentation et en télédétection, il n'est pas réaliste de vouloir obtenir des mesures simultanées sur toute la zone marine de la surface au fond. Il est donc très difficile de s'affranchir de la variabilité temporelle pour mesurer la variabilité spatiale du transport particulaire et vice versa. La modélisation est l'outil d'investigation privilégié permettant d'analyser des données sétalants dans l'espace et le temps.

L'observation et la mesure sont des préalables à toute modélisation que l'on souhaite réaliste. Les mesures permettent d'identifier les processus et d'améliorer leur représentation. Elles permettent de déterminer les processus prépondérants à intégrer dans le modèle.

Les modèles sont des outils de compréhension. Lorsqu'ils sont validés, ils peuvent être employés pour extrapoler les mesures ou analyser la sensibilité du système à différents forçages. Un modèle numérique de transport représente une synthèse de représentations des processus qui y participent. Cet outil peut être utilisé comme support théorique pour la compréhension des processus.

L'utilisation des modèles numériques est en plein essor. Dans le cas d'un modèle validé, il est attrayant de penser qu'il est possible d'effectuer des simulations sur un simple ordinateur portable pour simuler la distribution des particules en suspension. Néanmoins, une telle utilisation des modèles numériques requiert une importante phase de validation et de confrontation à des mesures de terrain.

L'implantation d'un modèle numérique de transport particulaire préexistant dans un contexte différent de celui dans lequel il a été développé, peut requérir d'adopter et/ou de développer de nouveaux modules. Les efforts de recherche concernant la modélisation du transport particulaire portent sur les processus encore mal connus dont l'influence est significative dans un contexte donné (e.g. floculation). L'importance relative des processus participants au transport particulaire peut varier d'un contexte à l'autre.

II.2.2 Principes de fonctionnement d'un modèle numérique hydrodynamique, l'exemple MARS3D.

Le modèle numérique qui a servi de base à ce travail de thèse est le code MARS3D. MARS3D (3D hydrodynamical Model for Applications at Regional Scale) est un modèle numérique hydrodynamique développé par l'IFREMER inspiré par le modèle proposé par Blumberg et Mellor (1987). MARS3D a été le support de nombreuses études (Lazure et Salomon, 1991a,b; Douillet et al., 2001; Plus et al., 2003; Ouillon et al., 2004 ; Huret et al., 2005 ; Andre et al., 2005) qui ont participé à sa validation. Ce modèle a été adapté sur le

SLNC (Clavier et Douillet, 1996 ; Douillet, 1998). Dans cette adaptation, le modèle calcule l'élévation de la surface du plan d'eau et les courants générés par l'action combinée de la marée et du vent. Il calcule également le transport et la diffusion de matières dissoutes (Douillet et al., 2001) ainsi que les trajectoires de particules individuelles (Jouon et al., 2006 cf. section III.2). La simulation numérique des courants requiert plusieurs types d'informations:

- Les lois qui gouvernent le comportement dynamique du fluide (les équations mathématiques du modèle).
- Les lois qui gouvernent le comportement de l'eau aux limites du domaine (les conditions aux limites du modèle).
- La forme du domaine dans lequel évolue l'eau (la bathymétrie).
- Une discrétisation du volume contenu dans le domaine (le maillage).
- Une résolution numérique de l'ensemble des équations en chaque point du maillage.

Un modèle numérique hydrodynamique est un outil mathématique permettant de résoudre les lois physiques de l'hydrodynamique à l'intérieur d'un domaine en fonction des conditions aux limites.

II.2.2.1 Les équations de l'hydrodynamique

Les équations primitives

Les équations qui régissent le comportement d'un fluide sont connues, les équations du mouvement (Kundu, 1990 ; Cushman-Roisin, 1994) d'un fluide dans un repère orthogonal cartésien (Ox,Oy,Oz) s'écrivent comme suit :

$$\frac{\partial u}{\partial t} + u\frac{\partial u}{\partial x} + v\frac{\partial u}{\partial y} + w\frac{\partial u}{\partial z} - fv = -\frac{1}{\rho_0}\frac{\partial p}{\partial x} + \frac{1}{\rho_0}\left(\frac{\partial \tau_{xx}}{\partial x} + \frac{\partial \tau_{xy}}{\partial y} + \frac{\partial \tau_{xz}}{\partial z}\right) \qquad \text{Eq. II-3}$$

$$\frac{\partial v}{\partial t} + u\frac{\partial v}{\partial x} + v\frac{\partial v}{\partial y} + w\frac{\partial v}{\partial z} + fu = -\frac{1}{\rho_0}\frac{\partial p}{\partial y} + \frac{1}{\rho_0}\left(\frac{\partial \tau_{yx}}{\partial x} + \frac{\partial \tau_{yy}}{\partial y} + \frac{\partial \tau_{yz}}{\partial z}\right) \qquad \text{Eq. II-4}$$

t est le temps, u est la composante de la vitesse selon Ox, v est la composante de la vitesse selon Oy, w est la composante de la vitesse selon Oz, f est le paramètre de Coriolis, p est la pression, ρ_0 est la densité de référence. En première approximation et sur la base de mesures de température et de salinité effectuées sur le SLNC (Ouillon et al., 2005), les équations de transport de température et de salinité ne sont pas résolues dans la version de MARS3D implanté sur le SLNC. La densité de l'eau de mer $\rho(x,y,z,t)$ est considérée comme une constante :

$$\rho(x,y,z,t) = \rho_0 \qquad \text{Eq. II-5}$$

Les termes diffusifs seront explicités dans la partie 0.

L'hypothèse de répartition hydrostatique de la pression est employée :

$$\frac{\partial p}{\partial z} = - \rho g \qquad \text{Eq. II-6}$$

où g est l'accélération de la gravité.

L'eau étant un fluide incompressible, et la densité supposée constante, l'équation de continuité s'écrit :

$$\frac{\partial u}{\partial x} + \frac{\partial \mathrm{v}}{\partial y} + \frac{\partial w}{\partial \mathrm{z}} = 0 \qquad \text{Eq. II-7}$$

Le système d'équations Eq. II-3 et Eq. II-4 stipule que l'évolution dans le temps d'une composante de la vitesse en un point dépend de la dérivée de cette composante en amont du courant (advection), de la force de Coriolis, de la transmission sur la verticale de cette composante de la vitesse (diffusion de quantité de mouvement), du gradient de pression suivant l'axe de cette composante, et de la dissipation de cette composante de la vitesse.

Fermeture turbulente

La fermeture turbulente résout les termes de diffusion de quantité de mouvement dans les équations Eq. II-3 et Eq. II-4. La turbulence représente l'effet des processus dont l'échelle temporelle et spatiale n'est pas résolue explicitement par les équations du mouvement (Tartainville, 1998). Les flux diffusifs de quantité de mouvement sont modélisés grâce à une viscosité turbulente.

$$\frac{\tau_{xx}}{\rho_0} = \upsilon_H \frac{\partial u}{\partial x} \quad ; \quad \frac{\tau_{xy}}{\rho_0} = \upsilon_H \frac{\partial u}{\partial y} \quad ; \quad \frac{\tau_{yx}}{\rho_0} = \upsilon_H \frac{\partial v}{\partial x} \quad ; \quad \frac{\tau_{yy}}{\rho_0} = \upsilon_H \frac{\partial v}{\partial y} \qquad \text{Eq. II-8}$$

Plusieurs options existent dans MARS3D pour la résolution de υ_H. La formulation par défaut utilisée dans ce travail exprime la dispersion en fonction de la taille des mailles (Smagorinsky, 1963) :

$$\upsilon_H = f_{visc}\ 0.01\, \Delta y^{1.15} \qquad \text{Eq. II-9}$$

avec : Δy =500m et f_{visc} =3.0 .

Sur l'horizontale, la viscosité turbulente participe à la stabilité du modèle.

La discrétisation verticale est beaucoup plus fine que la discrétisation horizontale. Les fluctuations de vitesses aux échelles de la turbulence ne sont pas calculées directement. La résolution de ces termes se fait par le choix d'un schéma de fermeture turbulente. Le modèle choisi suppose que les flux turbulents verticaux peuvent être modélisés grâce à une viscosité turbulente suivant z.

$$\frac{\tau_{xz}}{\rho_0} = \upsilon_v \frac{\partial u}{\partial z} \quad ; \quad \frac{\tau_{yz}}{\rho_0} = \upsilon_v \frac{\partial v}{\partial z} \qquad \text{Eq. II-10}$$

Il existe de nombreux schémas pour calculer υ_v, le choix de celui-ci doit être fait en fonction des caractéristiques de l'écoulement que l'on cherche à modéliser. MARS3D propose divers schémas, nous exposons par la suite celui qui a été utilisé dans la section III.2, ainsi que les deux modèles de fermeture turbulente qui ont été introduits dans le code dans le cadre de cette thèse.

Modèle de Pacanowski et Philander

La fermeture turbulente proposée par Pacanowski et Philander (1981) est la suivante :

$$\upsilon_v = 10^{-2}\left(\frac{1}{1+5.Ri}\right)^2 + 10^{-4} \qquad \text{Eq. II-11}$$

Ri est le nombre de Richardson :

$$Ri = N^2/\mathrm{M}^2 \quad ; \quad N^2 = \frac{\partial b}{\partial z} \quad ; \quad \mathrm{M}^2 = \left(\frac{\partial \mathrm{u}}{\partial z}\right)^2 + \left(\frac{\partial v}{\partial z}\right)^2 \qquad \text{Eq. II-12}$$

N est appelée la fréquence de Brunt Vaïsala et b est la flottabilité :

$$b = -g(\rho - \rho_0)/\rho_0 \qquad \text{Eq. II-13}$$

La fréquence de Brunt Vaïsälä quantifie la stratification en densité sur la verticale. Cette stratification est synonyme de stabilité de l'écoulement, d'une diminution de la turbulence. Le terme M^2 quantifie le cisaillement suivant la verticale des vitesses horizontales. Ce terme est synonyme de production de turbulence. Le nombre de Richardson est donc un indicateur de la stabilité de l'écoulement, il mesure le rapport des forces stabilisatrices sur les termes de production de turbulence.

Cette fermeture turbulente se réduit à une valeur constante dans le cas d'un écoulement homogène. Des limitations sont imposées à cette fermeture turbulente : υ_v <0.030 m².s^{-1}. Deux autres fermetures turbulentes ont été implémentées dans les options du code MARS3D dans le cadre de cette thèse (modèles q^2-l et q^2-q^2l).

Fermeture turbulente à une équation : q^2-l

La fermeture turbulente q^2-l (Xing et Davies, 1995) repose sur la résolution de q^2, sur le domaine de calcul, et la paramétrisation de l (longueur de mélange) suivant une relation algébrique. q^2 est relié à l'énergie cinétique turbulente E par la relation suivante :

$$q^2 = 2E \qquad \text{Eq. II-14}$$

Les coefficients de turbulence sont reliés à q et l comme suit :

$$\upsilon_v = l.q.S_M \qquad \text{Eq. II-15}$$

où S_M désigne une des fonctions de stabilité de Galperin (1988).

L'équation à résoudre pour la quantité q^2 est la suivante :

$$\frac{\partial q^2}{\partial t} = 2\upsilon_v.M^2 + \beta_0 \frac{\partial}{\partial z}\left(\upsilon_v \frac{\partial q^2}{\partial z}\right) - 2\frac{q^3}{B_1 l} \qquad \text{Eq. II-16}$$

avec $\beta_0 = 0.73$, et $B_1 = 16.6$.

La relation algébrique donnant la longueur de mélange est proposée par Xing et Davies (1996a,b) :

$$l = \frac{1}{\left(\frac{1}{l_1} + \frac{1}{l_2}\right)} \; ; \; l_1 = \kappa(z + h + z_0)\exp\left(\beta_1 \frac{h+z}{D}\right) \; ; \; l_2 = \kappa(\varsigma - z + z_s) \qquad \text{Eq. II-17}$$

où κ est la constante de Von Karman (κ=0.4), β_1 est une valeur empirique comprise entre -2 et +2, z_0 est la rugosité de fond (z_0=0.005 m), z_s est la rugosité de surface (z_s=0.001 m), z est la position du point considéré sur la verticale, au fond $z = -h$ et en surface $z = \zeta$ (l'élévation de surface), et $D = h + \varsigma$ est la hauteur de la colonne d'eau.

l est bornée par la relation de Galperin (1988) qui fait intervenir la fréquence de Brunt Vaïsälä afin de prendre en compte la réduction de la longueur de mélange liée à la stratification.

$$l \le (0.53.q)/N \qquad \text{Eq. II-18}$$

Les fonctions de stabilité de Galperin dépendent également de la stratification locale quantifiée par un nombre sans dimension :

$$G_h = -\frac{l^2}{q^2} N^2 \qquad \text{Eq. II-19}$$

$$S_M = \frac{cst1 - cst2.G_h}{(1 - cst3.G_h)(1 - cst4.G_h)} \qquad \text{Eq. II-20}$$

G_h est l'opposé d'un nombre de Richardson local. Les valeurs des constantes ($cst1$, $cst2$, $cst3$, $cst4$) sont définies dans Lynch et al. (1995).

Fermeture turbulente à deux équations : q²-q²l

La fermeture turbulante q²-q²l (Blumberg et Mellor, 1987) repose sur la résolution de deux équations pronostiques :

$$\frac{\partial q^2}{\partial t} = \upsilon_v.M^2 + \frac{\partial}{\partial z}\left(D_v \frac{\partial q^2}{\partial z}\right) - 2\frac{q^3}{B_1.l} + 2G_h \qquad \text{Eq. II-21}$$

$$\frac{\partial (q^2 l)}{\partial t} = l.E_1.\upsilon_v.M^2 + \frac{\partial}{\partial z}\left(D_v \frac{\partial (q^2 l)}{\partial z}\right) - 2\frac{q^3}{B_1} W + l.E_1.G_h \qquad \text{Eq. II-22}$$

où D_v est la diffusivité turbulente de l'énergie cinétique turbulente donnée par :

$$D_v = l.q.S_q \qquad \text{Eq. II-23}$$

$$S_q = 0.2 \qquad \text{Eq. II-24}$$

où S_q désigne une des fonctions de stabilité de Galperin (1988). E_1 est une constante égale à 1.8, W est une fonction de paroi et dépend de la distance du point aux frontières du domaine (Blumberg et Mellor, 1987).

II.2.2.2 Les conditions aux limites

Les Conditions aux Limites (CL) décrivent le comportement de l'eau aux frontières géographiques (surface, fond, limites latérales ouvertes et fermées). L'adaptation de MARS3D au SLNC répond aux forçages du vent et de la marée par l'intermédiaire des CL.

Les CL de surface sont les suivantes :

$$w = u\frac{\partial \zeta}{\partial x} + v\frac{\partial \zeta}{\partial y} + \frac{\partial \zeta}{\partial t} \qquad \text{Eq. II-25}$$

$$\rho_0 N_z \frac{\partial (u,v)}{\partial z} = (\tau_{sx}, \tau_{sy}) \qquad \text{Eq. II-26}$$

τ_{sx} et τ_{sy} sont les tensions de cisaillement du vent suivant les directions Ox et Oy.

La première CL stipule que la vitesse verticale en surface est fonction de la pente de la surface et de sa vitesse d'élévation. Le forçage du vent est introduit par la seconde CL qui stipule que le mouvement induit par le vent se transmet à la surface par frottement et se transmet suivant la profondeur par diffusion de quantité de mouvement.

Les CL de fond sont les suivantes :

$$w = - \mathrm{u} \frac{\partial h}{\partial x} - \mathrm{v} \frac{\partial h}{\partial y} \qquad \text{Eq. II-27}$$

$$\rho_0 \, \mathrm{N}_z \frac{\partial (\mathrm{u}, \mathrm{v})}{\partial z} = \mathrm{C}_\mathrm{d} \sqrt{\mathrm{u}_\mathrm{b}^2 + \mathrm{v}_\mathrm{b}^2} \, (\mathrm{u}_\mathrm{b}, \mathrm{v}_\mathrm{b}) \qquad \text{Eq. II-28}$$

h est la topographie du fond. C_d est le coefficient de frottement du fond, u_b et v_b sont les vitesses au premier point de calcul près du fond. La formulation du frottement (terme de droite Eq. II-28) est quadratique.

La première CL au fond stipule que la vitesse verticale au voisinage du fond suit les variations de topographie, l'eau ne transperce pas le fond du domaine. La seconde implique que les effets du frottement se transmettent suivant la verticale par diffusion de quantité de mouvement.

Les limites latérales sont de deux types.

Les positions des limites latérales fermées sont définies par les limites entre zone mouillée et zone sèche. La grande difficulté concernant la formulation des conditions aux limites latérales fermées est que ces limites ne sont pas figées. Les zones découvrant aux basses mers font apparaître de nouvelles limites latérales fermées (bancs découvrants) et augmentent l'extension des zones sèches accolées au trait de côte (estran). Malgré le caractère mobile ou inconstant des limites latérales fermées, une description synthétique de la condition aux limites latérales fermée se résume à annuler la composante de vitesse perpendiculaire à la limite fermée.

La CL ouverte en élévation de la surface permet d'imposer le forçage lié à la marée. L'élévation de la surface libre (ζ) est imposée et l'onde de marée se propage à travers le domaine de calcul. Une seconde condition aux limites ouvertes est nécessaire pour fermer le système d'équations. Si l'on considère que les courants sont les mêmes de part et d'autre de la limite, on peut par exemple imposer sur les composantes de vitesse la condition aux limites suivante :

$$\frac{\partial (u, v)}{\partial n} = 0 \qquad \text{Eq. II-29}$$

n étant la direction perpendiculaire à la frontière ouverte considérée.

II.2.2.3Les données bathymétriques

La première caractéristique du domaine à prendre en compte lorsque l'on veut modéliser l'hydrodynamique d'une zone est sa forme. En océanographie côtière, celle-ci est contrainte par la géomorphologie du fond de la zone sur laquelle est implanté le modèle. Pour l'implantation de MARS3D sur le SLNC, la forme de la topographie sous-marine a été obtenue par krigeage des minutes de bathymétrie relevées par le SHOM (Service Hydrographique et Océanographique de la Marine), préalablement numérisées. Les minutes de bathymétrie du SHOM sont référencées en altitude par rapport au niveau des plus basses mers (zéro hydrographique).

Dans le modèle, la hauteur d'eau (D) est définie comme la somme de la profondeur (H) et de l'élévation de surface (ζ).

$$D = \zeta + H \qquad \text{Eq. II-30}$$

L'élévation de surface est la somme du niveau moyen et des variations dues à la marée et au vent. Le niveau moyen que l'on introduit dans le modèle correspond la hauteur d'eau au repos, elle est prise égale au niveau moyen de la mer. A moins d'une décote exceptionnelle liée aux mouvements de l'eau, les hauteurs d'eau dans le modèle et dans la réalité sont toujours légèrement supérieures aux données bathymétriques du SHOM (Figure II-11).

L'élévation de surface (limite haute du volume de contrôle) étant dynamique, l'intersection des surfaces décrivant les limites hautes et basses du volume de contrôle est également dynamique. Cette intersection représente les limites latérales fermées du modèle. Par opposition, les limites latérales ouvertes du modèle sont dictées par les limites d'extension géographiques du modèle.

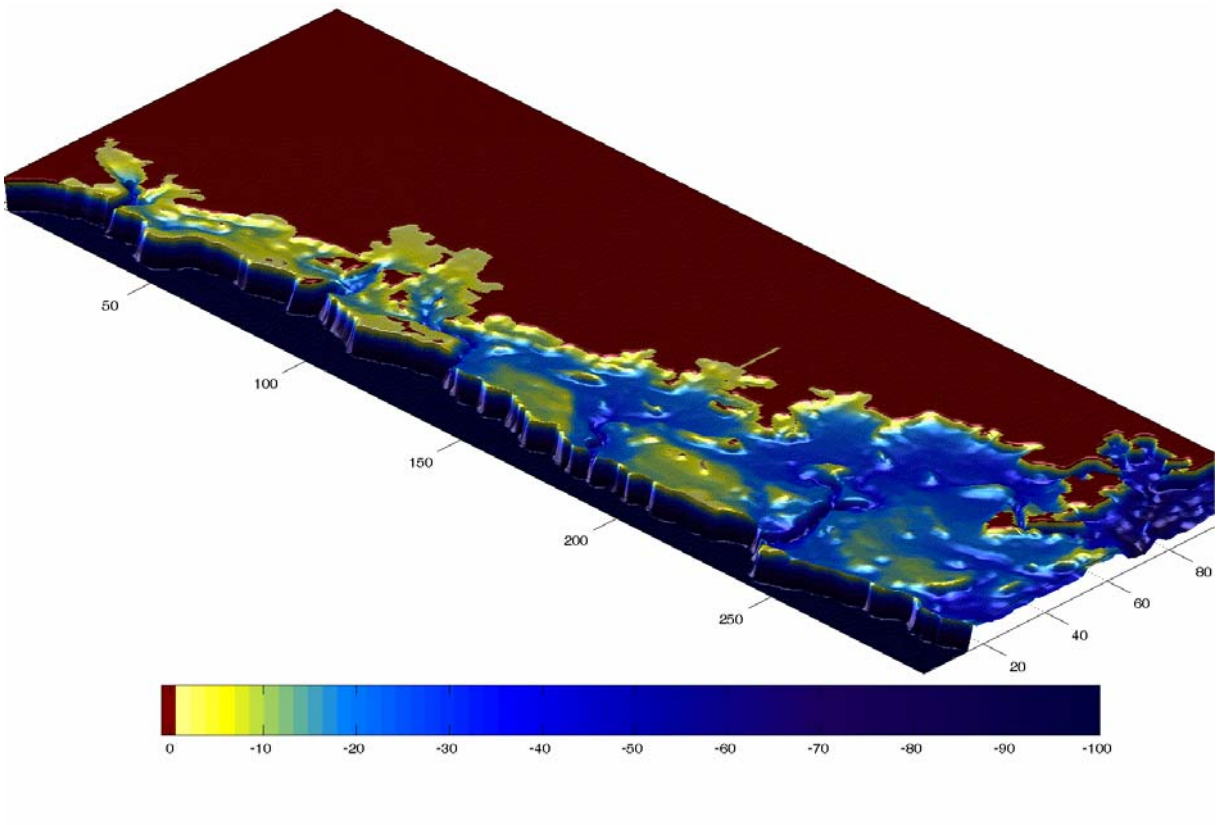

Figure II-11 Bathymétrie du SLNC (m).

II.2.2.4Le maillage

La résolution des équations de l'hydrodynamique se fait de manière discrète sur l'ensemble du domaine modélisé. Il est nécessaire de procéder à la distribution spatiale des points sur lesquels on cherche à résoudre les équations de l'hydrodynamique. Le maillage détermine la résolution spatiale du modèle numérique. Plus il est fin, plus le modèle aura la capacité de simuler les processus de petite échelle. En contrepartie, une meilleure résolution augmente le temps de calcul.

Le modèle Mars3D sur le SLNC est un modèle à mailles carrées de dimensions uniformes sur l'horizontale et à maille à extension variable (niveaux-σ) suivant la direction verticale. Les niveaux-σ (Blumberg and Mellor, 1987; Lazure and Salomon, 1991; Deleersnijder and Beckers, 1992) découpent la colonne d'eau en parts relatives. Plus la colonne d'eau est étendue plus l'extension de chaque niveau σ est importante. Cette répartition des niveaux de calcul permet d'affiner la résolution verticale du modèle dans les petits fonds. L'adoption de niveaux-σ requiert de projeter l'ensemble des équations de l'hydrodynamique dans ce nouveau repère. Par suite, l'indice k désignera le numéro du niveau σ sur lequel on situe un point (ex : 0=fond, 10=surface). La transformation des équations en coordonnées σ dérive de la modification :

$$z \rightarrow \sigma = \frac{z + H}{\zeta + H} \qquad \text{Eq. II-31}$$

ζ est l'élévation de la surface libre, H est la profondeur, z est l'altitude du point considéré au sein de la colonne d'eau.

Dans le système de coordonnées (x , y , σ , t), (u, v) reste la projection horizontale de la vitesse. Les équations primitives (Eq. II-3 et Eq. II-4) projetées dans ce nouveau repère s'écrivent de la manière suivante :

$$\frac{\partial u}{\partial t} + u\frac{\partial u}{\partial x} + v\frac{\partial u}{\partial y} + \tilde{w}\frac{\partial u}{\partial \sigma} - fv = -\frac{1}{\rho_0}\left(\frac{\partial p}{\partial x} + \frac{\partial p}{\partial \sigma}\frac{\partial \sigma}{\partial x}\right) + \frac{1}{\rho_0}\left(\frac{\partial \tau_{xx}}{\partial x} + \frac{\partial \tau_{xy}}{\partial y} + \frac{1}{D}\frac{\partial \tau_{xz}}{\partial \sigma}\right) \quad \text{Eq. II-32}$$

$$\frac{\partial v}{\partial t} + u\frac{\partial v}{\partial x} + v\frac{\partial v}{\partial y} + \tilde{w}\frac{\partial v}{\partial \sigma} + fu = -\frac{1}{\rho_0}\left(\frac{\partial p}{\partial y} + \frac{\partial p}{\partial \sigma}\frac{\partial \sigma}{\partial y}\right) + \frac{1}{\rho_0}\left(\frac{\partial \tau_{yx}}{\partial x} + \frac{\partial \tau_{yy}}{\partial y} + \frac{1}{D}\frac{\partial \tau_{yz}}{\partial \sigma}\right) \quad \text{Eq. II-33}$$

L'équation du gradient de pression hydrostatique devient :

$$\frac{1}{D}\frac{\partial p}{\partial \sigma} = -\rho g \quad \text{Eq. II-34}$$

et l'équation de continuité devient :

$$\frac{\partial \varsigma}{\partial t} + \frac{\partial (Du)}{\partial x} + \frac{\partial (Dv)}{\partial y} + \frac{\partial (D\tilde{w})}{\partial \sigma} = 0 \quad \text{Eq. II-35}$$

Sur l'horizontale la dimension d'une maille pour la version de Mars 3D sur le SLNC est de 500m (Figure II-12). Dans la version de MARS3D adapté au SLNC, il n'existe pas de correspondance directe entre i et la latitude ni entre j et la longitude. A la différence des versions « classiques » de MARS 3D dont l'orientation de grille est W-E et S-N, l'orientation de la grille adoptée sur le SLNC est NNW-SSE. Cette orientation a été choisie en fonction de l'orientation de la côte et du récif pour limiter le nombre de cellules et le coût des calculs matriciels correspondants.

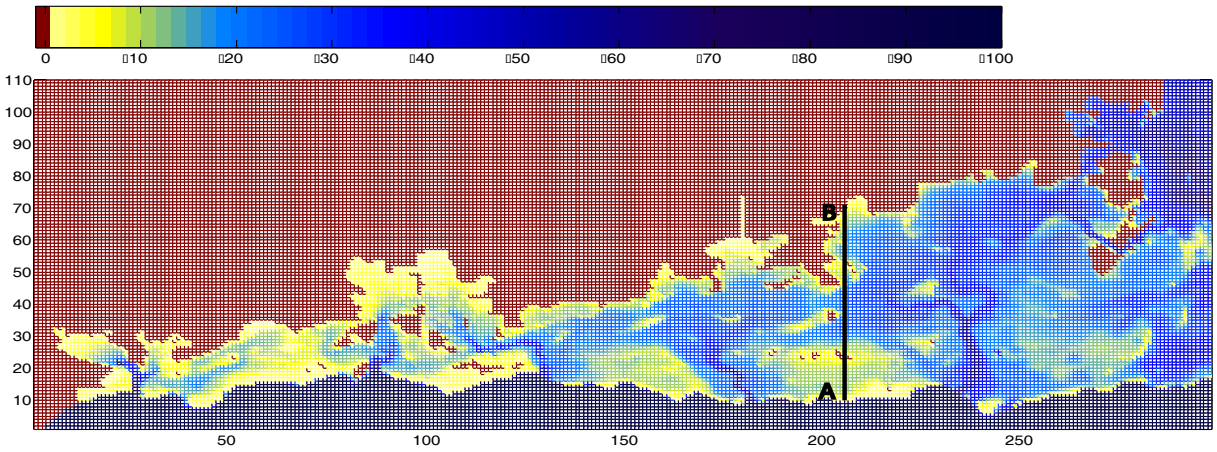

Figure II-12 Maillage horizontal à 500m et données bathymétriques (m) pour MARS3D sur le SLNC

Mars3D sur le SLNC fonctionne avec 10 niveaux-σ. Les niveaux-σ proches de la surface et du fond sont resserrés de manière à avoir une meilleure résolution proche des interfaces eau/fond et eau/surface (Figure II-13).

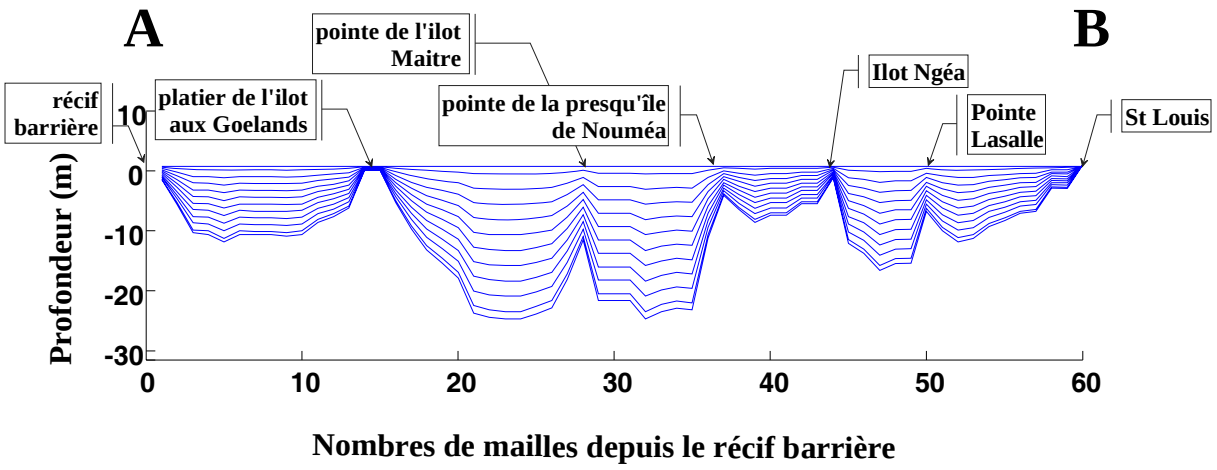

Figure II-13 Extension variable des niveaux sigmas sur la colonne d'eau suivant le transect récif barrière-St Louis présenté en Figure II-12

II.2.2.5 La résolution numérique

La discrétisation spatiale est basée sur la méthode des différences finies. Les paramètres participants à la résolution du modèle sont distribués sur la grille 3D (Figure II-14 et Figure II-15). Cette distribution est faite de telle manière que la discrétisation de chaque terme de chaque équation soit centré sur le point où l'on calcule la variable (u et v pour les équations de mouvement, ζ pour l'équation de continuité, etc…).

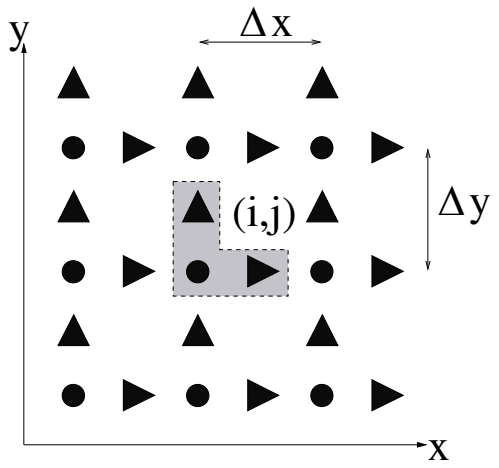

symbole	variables	
	2D	3D
▲	$\bar{v}$, h_v, τby, τsy	v
►	$\bar{u}$, h_x, τx, τbx, τsx	u
●	ζ, ν_H	$\tilde{w}$, ν_V, κ_V

Figure II-14 Distribution horizontale des variables sur la grille d'après Pérenne (2006).

La grille choisie dans Mars 3D est la grille Arakawa-C (Arakawa et Lamb, 1977) sur laquelle a été effectuée quelques modifications (Lazure et Salomon, 1991). Les indices i et j repèrent les positions des points sur la grille. i désigne le numéro de colonne du point considéré, j désigne la ligne (en partant du bas) du point considéré (Figure II-14). Les mêmes indices (i, j) correspondent donc à des coordonnées géographiques différentes selon la variable concernée (+/- dx/2, +/- dy/2). Les modifications apportées à la grille Arakawa-C consistent à prendre en compte la profondeur d'eau (donnée bathymétrique) en deux points distincts sur chaque maille (Figure II-14). Cette modification combinée à une résolution temporelle numérique du type ADI (Leenderstse, 1967), permet de tenir compte des phénomènes d'inondation/exondation de certaines zones du lagon (estrans et bancs découvrants) qui représentent une part non négligeable de la superficie du SLNC.

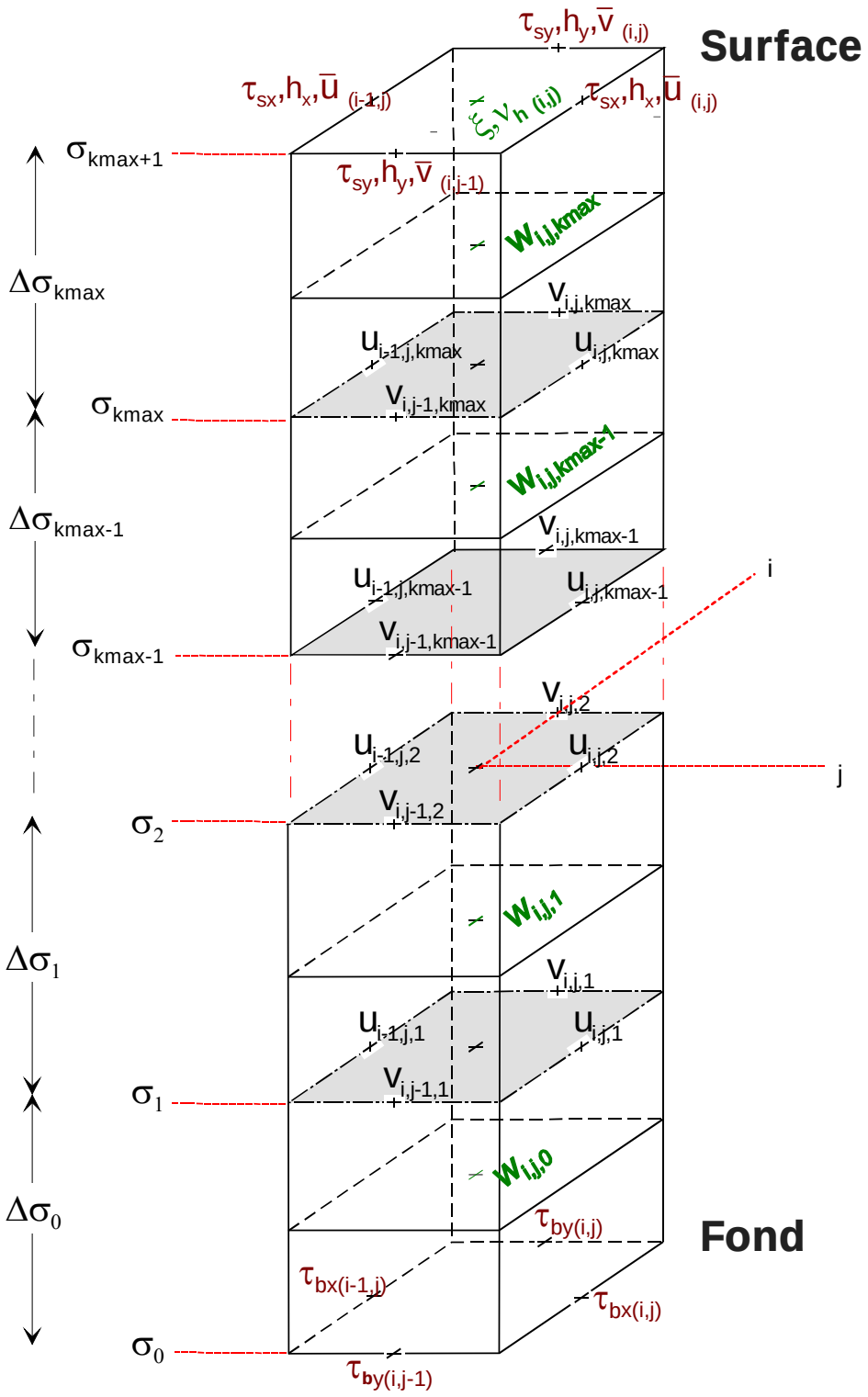

Figure II-15 Distribution 3D des variables sur le maillage

A titre d'exemple, voici une formulation simple, dans une seule dimension (axe Ox) d'un gradient de vitesse suivant la composante u de la vitesse horizontale et d'un gradient d'élévation de la surface libre (pente de la surface). Ces deux gradients sont calculés au lieu de U_i et suivant un schéma centré d'ordre 1 (seuls les plus proches voisins de part et d'autre de U_i sont pris en considération pour le calcul du gradient) :

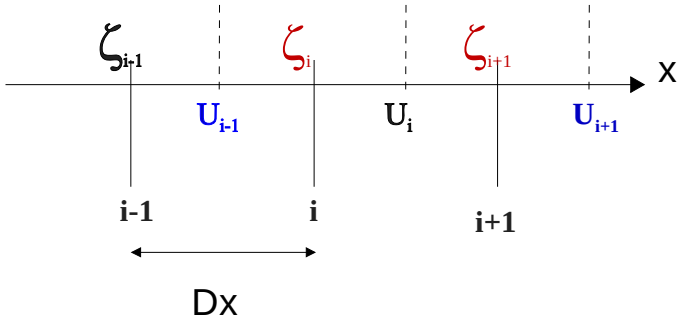

Figure II-16 Projection de la composante u de la vitesse horizontale et de l'élévation de surface sur l'axe 0x

Chaque terme des équations est ainsi discrétisé par la méthode des différences finies. Les calculs de l'élévation et des concentrations en traceurs sont réalisés au centre des mailles tandis que les composantes du courant le sont sur les bords des mailles (Figure II-14, Eq. II-36Eq. II-37). Sur la verticale, les vitesses horizontales et les concentrations sont calculées aux niveaux σ. MARS3D est construit sur une séparation des modes interne et externe (Blumberg et Mellor, 1987). Le mode externe consiste à calculer l'évolution de la surface libre et des courants moyens sur la verticale (2D), le mode interne opère une résolution complète du champ de courants et des traceurs considérés dans les trois dimensions.

$$\left[\frac{\partial U}{\partial x}\right]_{Ui} = \frac{U_{i+1} - U_{i-1}}{2Dx} \qquad \text{Eq. II-36}$$

$$\left[\frac{\partial \zeta}{\partial x}\right]_{Ui} = \frac{\zeta_{i+1} - \zeta_i}{Dx} \qquad \text{Eq. II-37}$$

La résolution des équations 2D se fait suivant un schéma centré. On utilise une méthode ADI (Alternate Direction Implicit, Leendertse, 1967; Leendertse et Gritton, 1971) car elle introduit une part implicite dans le modèle ce qui permet d'utiliser des pas de temps plus grands, comparables à ceux du 3D. Les équations du mouvement sont découplées selon les deux axes horizontaux. A un demi-pas de temps on résout les équations suivant l'axe Ox ligne par ligne, au demi-pas de temps suivant on résout les équations suivant l'axe Oy colonne par colonne. La spécificité du modèle est d'utiliser le même pas de temps pour la résolution des modes interne et externe avec un processus itératif permettant l'ajustement progressif des deux modes. Ceci permet de rendre implicite certains termes d'advection et de frottement sur le fond. Le détail de la méthode de résolution est donné dans Lazure et Dumas (soumis).

Le schéma d'advection des vitesses horizontales du modèle 3D est un schéma centré. L'équation d'advection-diffusion en 3D est résolue à chaque demi-pas de temps. Les dérivées verticales des équations 3D sont calculées suivant un schéma implicite centré dans l'espace.

Le schéma de résolution de l'advection horizontale des scalaires (température, salinité et substances dissoutes) dans les équations 3D est un schéma explicite de type TVD (Total Variance Diminishing). Le schéma TVD utilisé dans cette thèse est une reconstruction

linéaire faisant intervenir le schéma Quick (Leonard, 1979) et le schéma décentré amont (Upstream). Le schéma d'advection du second ordre (Quick) est plus précis que le schéma d'advection d'ordre un (Upstream), mais génère des oscillations dans des configurations à forts gradients. Ces oscillations font augmenter la variation totale du champ advecté. Au contraire, le schéma d'ordre un a tendance à lisser les gradients. Ce lissage va dans le sens d'une diminution de la variation totale du champ advecté. Dans les cas de forts gradients, l'utilisation de la reconstruction linéaire permet d'employer, le schéma d'ordre un lorsque le schéma d'ordre deux génère de la variation. L'adoption occasionnelle du schéma d'ordre un permet ainsi d'utiliser le plus souvent un schéma d'ordre deux tout en garantissant l'absence d'oscillations numériques. L'utilisation de schémas d'ordre supérieur à deux est également possible dans un schéma TVD (Arnoux-Chiavassa, 2003).

Le pas de temps est variable, il est ajusté selon la vitesse du courant horizontal maximum observé de façon à avoir un pas de temps maximal tout en respectant le critère de stabilité Courant-Friedrich-Levy (CFL) du fait du schéma explicite d'advection horizontale.

II.2.3 Modèles de transport

II.2.3.1 Transport de scalaires

Dans son implémentation au SLNC, MARS3D résout l'équation de transport de traceurs passifs ou d'une substance dissoute. L'équation qui régit le transport d'un constituant dissout conservatif (C) est connue.

$$\frac{\partial(DC)}{\partial \mathrm{t}} + \frac{\partial(DuC)}{\partial \mathrm{x}} + \frac{\partial(DvC)}{\partial \mathrm{y}} + \frac{\partial(D\tilde{w}C)}{\partial \sigma} = \frac{\partial(DF_x^C)}{\partial \mathrm{x}} + \frac{\partial(DF_y^C)}{\partial \mathrm{y}} + \frac{\partial(DF_z^C)}{\partial \sigma} + s^C - p^C \qquad \text{Eq. II-38}$$

où F_x^C et F_y^C sont les termes diffusifs horizontaux du scalaire. F_z^C est le terme diffusif verticale du scalaire (Eq. II-39). Il est possible de prendre en compte les effets de puits et/ou de sources de concentration via les termes p^C et s^C.

$$F_x^C = \kappa_H \frac{\partial C}{\partial x} \quad ; \; F_y^C = \kappa_H \frac{\partial C}{\partial y} \quad ; \; F_z^C = \frac{\kappa_v}{D}\frac{\partial C}{\partial \sigma} \qquad \text{Eq. II-39}$$

Comme pour les flux diffusifs de quantité de mouvement, les flux diffusifs du scalaire C (F_x^C, F_y^C, F_z^C) sont modélisés grâce à une viscosité turbulente. Sur l'horizontale, elle est fixée à sa valeur minimum égale à 1.

$$\kappa_H = 1 \qquad \text{Eq. II-40}$$

Selon la fermeture turbulente de Pacanowski et Philander (1981), la diffusivité verticale du scalaire (κ_v) est formulé de la façon suivante :

$$\kappa_v = \upsilon_v\left(\frac{1}{1+5.Ri}\right)+10^{-5} \qquad \text{Eq. II-41}$$

avec une limite imposée : κ_v<0.052 $m^2.s^{-1}$.

Selon les fermetures turbulentes q^2-l et q^2-q^2l, sa formulation est la suivante :

$$\kappa_v = l.q.S_H \qquad \text{Eq. II-42}$$

$$S_H = \frac{cst5}{(1-cst3.G_h)} \qquad \text{Eq. II-43}$$

où S_H désigne une des fonction de stabilité de Galperin (1988) et $cst5$ est définie dans Lynch et al. (1995).

Les conditions aux limites telles que nous les avons formulées pour les travaux exposés en partie III.2 sont :

En surface et au fond, aucune évaporation ou infiltration du traceur dans le substrat :

$$\frac{F_z^C}{D}\frac{\partial C}{\partial \sigma} = 0 \qquad \text{Eq. II-44}$$

A l'extérieur des limites du volume de contrôle, la concentration est fixée en entrée (ex : C=0), le flux est conservé en sortie.

II.2.3.2Particules lagrangiennes de flottabilité nulle

La version de MARS3D adaptée sur le SLNC calcule individuellement les trajectoires de particules individuelles de flottabilité nulle. La position des particules suivies en lagrangien évolue d'après l'équation suivante (Hunter et al., 1993; Tartinville et al., 1997; Visser, 1997; Spagnol et al., 2002):

$$\mathbf{r}(t+\Delta t) = \mathbf{r}(t) + \Delta t\left[U + (6k_h/\Delta t)^{1/2}\mathbf{d}_h + \left[w + (6k_v/\Delta t)^{1/2} d_v + \frac{\partial k_v}{\partial z}\right]\mathbf{e}_z\right] \qquad \text{Eq. II-45}$$

Δt est l'intervalle de temps sur lequel on résout l'équation de transport lagrangienne. La position de chaque traceur est recalculé tous les Δt. U représente ici les deux composantes horizontales de la vitesse. k_h détermine l'importance potentielle de la composante aléatoire du déplacement des particules lagrangiennes. Cette composante aléatoire du déplacement est due aux processus hydrodynamiques non résolus à l'échelle de la maille, k_h est fixé égale à

κ_H (Eq. II-9). k_v est l'homologue de k_h sur la verticale, il est pris égale à κ_v (Eq. II-41). dh et dv sont des facteurs aléatoires adimensionnels distribués entre -1 et +1.

II.2.3.3 Particules en suspension

Équation du transport

Le module de transport de particules en suspension reprend une formulation dont une partie est commune à l'équation de transport de matière dissoute (Eq. II-38).

$$\frac{\partial(DC)}{\partial \mathrm{t}} + \frac{\partial(DuC)}{\partial \mathrm{x}} + \frac{\partial(DvC)}{\partial \mathrm{y}} + \frac{\partial\left(D\left(\tilde{w} - \frac{w_s}{D}\right)C\right)}{\partial \sigma} = \frac{\partial\left(DF_x^C\right)}{\partial \mathrm{x}} + \frac{\partial\left(DF_y^C\right)}{\partial \mathrm{y}} + \frac{\partial\left(DF_z^C\right)}{\partial \sigma} + s^C - p^C \qquad \text{Eq. II-46}$$

Une différence importante avec l'équation de transport d'un scalaire conservatif est la vitesse de chute w_s (m.s^{-1}). Cette vitesse de chute, orientée vers le bas, dépend des caractéristiques physiques des particules transportées. La résolution de l'équation de transport est réalisée au centre des mailles. Pour les particules fines (D < 100 µm), la vitesse de chute est calculée suivant la loi de Stokes :

$$w_s = \frac{1}{18}\frac{(s-1)}{\nu}\,\mathrm{g}\,D_p^2 \qquad \text{Eq. II-47}$$

$$s = \frac{\rho_{particule}}{\rho_{eau}} \qquad \text{Eq. II-48}$$

s est la densité relative des particules, ν est la viscosité cinématique de l'eau (10^{-6} m^2.s^{-1}), et D_p est le diamètre des particules (m).

La CL de surface est la suivante :

$$\frac{F_z^C}{D}\frac{\partial C}{\partial \sigma} - w_s C = 0 \qquad \text{Eq. II-49}$$

Elle exprime que le flux de particules est nul à la surface.

La CL de fond fait intervenir deux termes respectivement source et puit, résultants de l'érosion (E_s) et du dépôt (D_s) de particules.

$$\frac{F_z^C}{D}\frac{\partial C}{\partial \sigma} - w_s C = E_s - D_s \qquad \text{Eq. II-50}$$

Érosion et Dépôt de sédiments fins

Dans le cas du transport de sédiments fins (cohésifs), le dépôt s'exprime suivant la formulation de Krone (1962) :

$$D_s = w_s C.\left(1-\frac{\tau}{\tau_{cd}}\right) \text{ pour } \tau < \tau_{cd} \; ; \; D_s = 0 \text{ pour } \tau > \tau_{cd} \qquad \text{Eq. II-51}$$

où τ est la contrainte de cisaillement et τ_{cd} est la contrainte de cisaillement critique de dépôt. La condition d'érosion est celle proposée par Parthéniades (1962) :

$$E_s = k_e.\left(\frac{\tau}{\tau_{ce}}-1\right) \text{ pour } \tau > \tau_{ce} \; ; \; E_s = 0 \text{ pour } \tau < \tau_{ce} \qquad \text{Eq. II-52}$$

où τ_{ce} est la contrainte de cisaillement critique d'érosion. Les deux contraintes de cisaillement critique de dépôt et d'érosion dépendent, entre autre, des caractéristiques intrinsèques des particules transportées et du substrat.

II.2.4 Le modèle de vagues : WaveWatch III (NOAA)

La version 1.18 de WAVEWATCH III (WWATCH)(Tolman, 1999) que nous avons utilisée est un modèle de vagues de troisième génération développé à la NOAA/NCEP (US National Centers for Environmental Prediction) par Hendrik Tolman. On distingue les générations de modèles suivant le mode de calcul du terme qui décrit les interactions non linéaires entre différentes vagues de fréquences liées. Dans la première génération, on négligeait ou on paramétrait simplement ce terme source. Dans la deuxième, on utilisait une « panoplie » de spectres prédéfinis qui dépendaient de la longueur du fetch. Dans la troisième, on effectue le calcul explicite des interactions non linéaires.

Les équations régissant la génération et la propagation des vagues de vent sont présentées en détail dans Tolman (1989, 1991a, b). Les termes source et puits sont décrits avec précision dans Tolman et Chalikov (1996). Les vagues de vent sont caractérisées par leur énergie F (proportionnelle au carré de la hauteur des vagues) qui dépend de paramètres intrinsèques : le nombre d'onde k, la fréquence (ou pulsation) relative σ observée dans un référentiel qui se déplace à la vitesse moyenne $\vec{U}$ des courants, la fréquence absolue ω observée dans un référentiel fixe et la direction de propagation θ du train de houle. Dans la théorie linéaire des ondes de gravité de surface, pour des variations faibles des courants et de la profondeur (Leblond et Mysak 1978), la relation de dispersion permet de lier les différentes fréquences au nombre d'onde :

$$\sigma = \sqrt{gk\tanh(kd)} = \omega - \vec{k}\vec{U} \qquad \text{Eq. II-53}$$

où d est la profondeur et k le vecteur d'onde d'amplitude k et de direction θ.

Les travaux exposés dans cette thèse ne tiennent pas compte de l'effet du courant sur le champ de vagues. On considère donc que $\vec{U} = 0$ et donc :

$$\sigma = \omega \qquad \text{Eq. II-54}$$

Dans WWATCH, les variations de F dues à la propagation des vagues sur des profondeurs et au sein de courants variables sont décrites au moyen de l'équation de transport (appelée aussi équation de transfert radiatif):

$$\frac{\partial N}{\partial t} + \vec{\nabla}.\left[\left(\vec{c}_g + \vec{U}\right)N\right] + \frac{\partial}{\partial \omega}\left(c_\omega N\right) + \frac{\partial}{\partial \theta}\left(c_\theta N\right) = \frac{S_{wind}}{\sigma} + \frac{S_{ds}}{\sigma} + \frac{S_{nl}}{\sigma} + \frac{S_{bf}}{\sigma} \qquad \text{Eq. II-55}$$

où N = F(x, y, f, θ, t) / σ est le spectre d'action d'onde (ou plus simplement l'action d'onde), $\vec{c}_g$ la vitesse de groupe, c_ω et c_θ les vitesses de propagation dans l'espace spectral (fréquence et direction). Les termes du membre de gauche de l'équation de transfert radiatif représentent les taux de variation locale de la densité d'action, de la propagation, et de la dérive en fréquence et en direction des vagues. Ces variations sont causées par les variations spatio-temporelles de la profondeur et du courant moyens: S_{wind} (positif ou nul) représente la croissance des vagues sous l'action du vent, S_{ds} (négatif ou nul) correspond au moutonnement et à la dissipation turbulente d'énergie en surface, S_{nl} (positif, nul ou négatif) décrit les interactions non-linéaires entre vagues et les transferts d'énergie qui en résultent, et S_{bf} (négatif, ou nul par fonds profonds) représente la dissipation sur le fond, provoquée soit par frottement soit par interactions avec un fond au comportement élastique.

S_{wind} et S_{ds} se réfèrent à des processus de natures différentes, mais peuvent être considérés comme liés puisque de leurs poids relatifs dépendent l'ensemble des caractéristiques de croissance des vagues dans le modèle. Deux options sont disponibles dans WWATCH pour définir ces deux termes, le premier étant basé sur les cycles 1 à 3 du modèle WAM, le second sur Tolman et Chalikov (1996). Les interactions non linéaires vague-vague (S_{nl}) sont modélisées grâce à l'approximation d'interaction discrète de Hasselman et al (1985). S_{bf} est modélisée au moyen de l'expression empirique de JONSWAP (Hasselman et al. 1973).

La formulation des apports et de la dissipation d'énergie par Tolman et Chalikov (1996) (voir également une description complète de cette formulation dans Tolman, 1999) est adaptée aux conditions de fetch limité et a donc été utilisée dans notre étude. « Le terme-source de dissipation est le terme le moins connu de la relation d'équilibre, et est principalement utilisé comme un terme réglable de fermeture » (Tolman et Chalikov, 1996). Dans la version 1.18 que nous utilisons, WWATCH nécessite un réglage spécifique adapté à chaque application pratique pour ce terme (voir section III.).

Les simulations fournissent de nombreux paramètres. La donnée de sortie de WWATCH la plus détaillée est le spectre d'énergie directionnelle F(x, y, f, θ, t). D'autres paramètres intégrés à partir de F(x, y, f, θ, t) sont également disponibles parmi lesquels la hauteur significative, la période moyenne, la longueur d'onde moyenne, ainsi que la direction moyenne des vagues.

L'hypothèse effectuée implicitement pour les équations considérées consiste à dire que le milieu (profondeur et courants) ainsi que le champ de vagues varient sur des échelles de temps et d'espace bien plus grandes que les échelles correspondantes pour une seule vague. De plus, la physique modélisée ne couvre pas les conditions où la propagation des vagues est fortement limitée par la profondeur (conditions de déferlement). Ceci implique que le modèle peut être appliqué sur des échelles spatiales de l'ordre de quelques centaines de mètres à quelques kilomètres, et à l'extérieur de la zone de déferlement. Le maillage utilisé est le même que celui des modèles hydrodynamique et sédimentaire décrit dans Douillet et al (2001).

Chapitre III TEMPS CARACTERISTIQUES DE L'HYDRODYNAMIQUE

III.1 Introduction

La quantité des données produites par un modèle hydrodynamique est souvent colossale et difficilement exploitable en l'état. Dans la version utilisé pour cette étude, chaque paramètre tridimensionnel est retourné par le modèle sous forme d'un tableau de 110*340*10 et ce, à chaque pas de temps sauvegardé. Il est donc nécessaire de synthétiser l'information. La manipulation des sorties de modèles numériques donne naissance à de nouveaux paramètres. L'indice de stratification, inspiré du traitement de données *in situ*, permet ainsi d'étudier le lien qui existe entre stratification et production primaire (Hidalgo-Gonzalez et Alvarez-Borrego, 2001). Inspiré des méthodes de traitement d'images satellites (Cayula et Cornillon, 1992), la détection des fronts hydrologiques peut être effectuée de manière automatique. L'utilisation des algorithmes biomimétiques à colonies de fourmis permet de détecter automatiquement sur des champs de vecteurs de courants issus d'un modèle hydrodynamique les cellules de rétention des masses d'eau (Segond et al., 2004).

Devant le caractère central du modèle hydrodynamique et afin d'en acquérir une bonne maîtrise, le première travail de thèse fut orienté vers le développement d'outils numériques permettant le calcul d'indices synthétiques. Un des objectifs de ce travail a été de synthétiser l'information hydrodynamique produite par MARS3D dans un format qui soit le plus pratique possible pour la compréhension de l'influence de l'hydrodynamique sur les processus biologiques. Cette partie porte donc l'empreinte de la pluridisciplinarité de l'UR Camélia.

Dans une masse d'eau donnée, hormis la dépendance à l'éclairement solaire, l'eutrophisation est régulée par les apports en nutriments et la capacité de ces nutriments à s'accumuler dans ce volume d'eau. Le mélange des masses d'eau qui bénéficient d'apport en nutriments avec des eaux plus oligotrophes est donc un processus limitant de l'eutrophisation. L'eutrophisation est une caractéristique liée à une masse d'eau. Le suivi de l'eutrophisation nécessiterait donc en théorie de suivre l'évolution de la masse d'eau indépendamment de sa localisation. L'évolution du caractère eutrophe de la masse d'eau (processus biologiques mis à part) n'est dictée que par les apports en nutriments et son mélange avec d'autres volumes d'eau aux caractères eutrophes différents. En pratique, il est très difficile de différencier les masses d'eaux les unes des autres, ce type de suivi n'est pas réalisable à travers des mesures. Étant donné que dans de nombreuses configurations, les sources de nutriments sont fixes dans l'espace, la notion d'eutrophisation est généralement associée à une zone. L'évolution du caractère eutrophe d'une zone est donc soumise d'une part à la fluctuation des apports en nutriments, d'autre part à l'advection et au mélange des masses d'eau aux frontières de la zone : le renouvellement.

Le niveau d'eutrophisation des masses d'eau est très hétérogène sur le SLNC. Les masses d'eaux les plus eutrophes sont localisées dans les baies. Le lagon est semi-ouvert, les masses d'eau provenant de l'extérieur du lagon sont oligotrophes. L'efficacité avec laquelle les eaux du large pénètrent dans le lagon et se mélangent aux masses d'eaux eutrophisées est donc un facteur limitant de l'eutrophisation dans les différentes zones du SLNC.

Cette partie consiste à caractériser et quantifier l'efficacité de renouvellement des eaux du lagon. De nombreuses études ont proposé de quantifier le renouvellement par des indices ayant la dimension d'un temps (Abdelrhman, 2005; Andréfouët et al., 2001 ; Bolin et Rodhe, 1973 ; Bujan, 2000 ; Crump et al., 2004 ; Delesalle et Sournia, 1992 ; Delhez et al., 2004ab ; Dettmann, 2001 ; Geyer, 1997 ; Monsen, 2002, Rasmussen et Josefson, 2002 ; Shen et Haas, 2004 ; Tartinville et al., 1997 ; Takeoka, 1984 ; Wang et al, 2004 ; Wolanski et King, 1990, Zimmerman, 1976). Certains des termes employés pour désignés ces temps caractéristiques de l'hydrodynamique (TH) n'ont pas la même signification d'une étude à l'autre. La signification des termes temps de transit, temps de résidence et âge de la masse d'eau adopté dans cette thèse sont explicités par la Figure III-1.

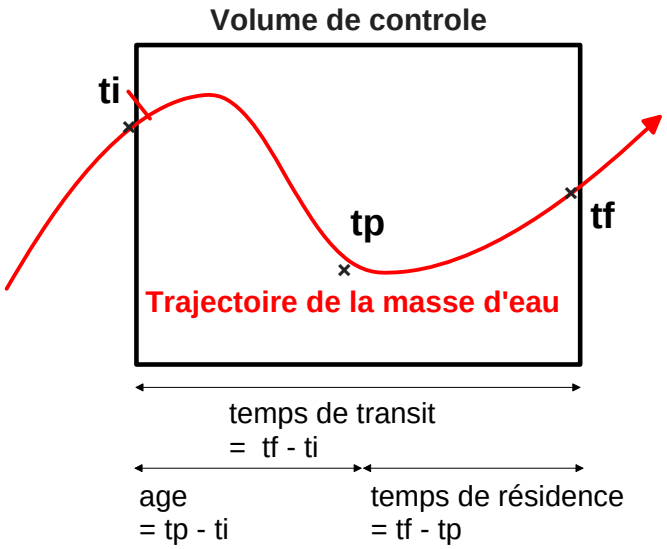

Figure III-1 Définitions de temps de transit, âge et temps de résidence.

Le temps de transit est le temps que passe la masse d'eau dans le volume de contrôle. L'âge de la masse d'eau est le temps que la masse d'eau a passé dans le volume de contrôle depuis son entrée. L'âge de la masse d'eau a trait au passé de la masse d'eau. Le temps de résidence est le temps que va passer la masse d'eau dans le volume de contrôle jusqu'à sa sortie. Le temps de résidence a trait au devenir de la masse d'eau. Ces trois TH font référence à l'advection d'une masse d'eau. Le temps de vidange (flushing time) fait davantage référence au mélange des masses d'eau dans un volume donné. Pour un réservoir entièrement et constamment mélangé à une concentration donnée en substance dissoute quelconque, le temps de vidange est le temps nécessaire pour diminuer la concentration initiale de 64% (de C_0 àC_0/e) par ajout continu d'eau de concentration nulle en cette substance.

Partant de ces définitions, nous proposons d'estimer ces TH à l'aide d'outils numériques implémentés dans le modèle hydrodynamique. Les outils numériques développés sont le transport de traceurs lagrangiens de flottabilité neutre et le transport d'un champ de concentration passif. L'élaboration de TH spatialisés, inspirée des précédentes définitions est ensuite proposée.

III.2 Publication:

Jouon, A., Douillet, P., Ouillon, S., Fraunié, P. (2006) Calculations of hydrodynamic time parameters in a semi-opened coastal zone using a 3D hydrodynamic model. Continental Shelf Research 26, 1395-1415

Available online at www.sciencedirect.com
SCIENCE DIRECT®
Continental Shelf Research 26 (2006) 1395–1415
CONTINENTAL SHELF RESEARCH
www.elsevier.com/locate/csr

Calculations of hydrodynamic time parameters in a semi-opened coastal zone using a 3D hydrodynamic model

Aymeric Jouon[a,*], Pascal Douillet[a], Sylvain Ouillon[a], Philippe Fraunié[b]

[a]UR Camelia, IRD, BP A5, 98848 Noumea cedex, New Caledonia
[b]LSEET-LEPI, Université du Sud Toulon-Var, BP 132, 83957 La Garde, Cedex, France

Received 20 July 2005; received in revised form 9 November 2005; accepted 16 November 2005

Abstract

Hydrodynamic time parameters (HTs) in a semi-opened aquatic ecosystem are synthetic indicators offering the opportunity to bring out the links between its physical functioning and its biology. The generic term "residence time" is frequently used through literature to mention HTs resulting in various calculation methods. This article presents different computing methods relying on the use of a 3D numerical hydrodynamic model and the HTs to which they give access. Several large-scale (water exchange time, average water export time, e-flushing time) and local time parameters (export time, flushing lag, local e-flushing time) are defined. The applications presented are carried out within the south-west lagoon of New Caledonia (SLNC), on three embedded control volumes. The definition of the control volume is more important for the values of local HTs than for their comparative distribution. The comparison of the global hydrodynamic time scales applied to a control volume provides information on the mixing processes inside the control volume.

Keywords: Residence time; Drifters; Flushing; Local e-flushing time; Tracer techniques; Mathematical model; Lagoons; New Caledonia

1. Introduction

The ecology of an aquatic ecosystem is strongly affected by hydrodynamics. The nutrient level, for example, depends on the speed at which the water is renewed, on the size of the retention areas, and generally on the circulation of the water masses. The level of turbulence is also an important factor for biological processes (e.g. the dissemination of larvae). Conversely, and in certain cases, biological activity can affect local hydrodynamics (e.g. the effect on turbulence and bed roughness inferred by the presence of benthic species). In order to obtain a better understanding of the interaction between hydrodynamics and biology, one must first identify the hydrodynamic processes likely to affect the ecology, and propose parameters or indicators for quantifying these processes.

Delesalle and Sournia (1992) adopted this approach and applied it to several coral reef lagoons. They revealed a relationship between phytoplankton biomass and a quantity characteristic of the exchanges between the lagoon and the open ocean which they called "residence time". This quantity is

*Corresponding author. Tel.: +687 26 07 27; fax: +687 26 43 26.
E-mail addresses: jouon@noumea.ird.nc (A. Jouon), douillet@noumea.ird.nc (P. Douillet), ouillon@noumea.ird.nc (S. Ouillon), fraunie@lseet.univ-tln.fr (P. Fraunié).

0278-4343/$ - see front matter © 2006 Elsevier Ltd. All rights reserved.
doi:10.1016/j.csr.2005.11.014

one of the hydrodynamic parameters based on time, which are hereafter called hydrodynamic time parameters (HTs). HTs make it possible to analyse the kinetic of biological reagents or the movements of organisms with respect to the water masses. As an example, Crump et al. (2004) correlated the movement of bacterial populations along the salinity gradient in an estuary with an HT proposed by Vallino and Hopkinson (1998) which they called "residence time"; Pagès and Andréfouët (2001) showed a good correlation between an HT which they named "water renewal time" and dissolved organic matter in 10 lagoons of the Tuamotu Archipelago; Andréfouët et al. (2001) considered the possibility of using this same HT as a criterion for classifying atolls. To underline the strength of the relationship which might exist between certain HTs and biological conditions, Pagès et al. (2001) wrote: "Takapoto Lagoon fits into a gradient of water residence time that controls the overall trophic web organization".

There is a certain amount of ambiguity in the naming of HTs. The term "residence time" relates to computation methods, which may not be the same between one study and another. The resulting parameters have a different physical significance, but are all referred to under the same name—which leads to debate (e.g. Andréfouët et al., 2003; Deleersnijder, 2003). Adding to the confusion, some studies using the same computation method refer to the same HT under different names. With this in mind, we have taken particular care in this article with the naming of the HTs we have calculated. For some of them, we do not use the names most frequently used in other publications. We are careful to point out and justify the names we do use, and mention the other names under which the reader may have encountered them elsewhere.

The aim of this article is to compare different HTs whose formulation makes use of the capabilities of a 3D hydrodynamic model. We do not discuss other computation methods, such as the resolution of an adjoint problem (Delhez et al., 2004a). Tests are carried out in a semi-opened basin, namely the south-west lagoon of New Caledonia (SLNC). Different HTs are calculated in three embedded control volumes so as to assess the sensitivity of each HT to the control volume on which it is calculated. Following a description of the study site (Section 2) and of the 3D model used (Section 3), we present our computation methods for the overall and local HTs (Section 4). Their applications to the embedded domains discussed in Sections 5 and 6 analyses their physical significance and complementarity.

2. The study site

New Caledonia is a tropical island located in the Western Pacific, about 1500 km east of Australia (Fig. 1). It is surrounded by a 23,400 km^2 lagoon. Noumea, the island's main city and home to half of its population, is located on the south-west coast. The lagoon area which surrounds Noumea is known as the SLNC. Its depth averages 17.5 m. It varies in width from 5 km (northern limit) to 40 km (southern limit). It is separated from the open ocean by a barrier reef.

The ongoing integrated study of the SLNC investigates the space–time variability of its physical, chemical, biological and sedimentological parameters. It aims at assessing the impact of human activities (mines, industry, urban expansion, etc.) on marine ecosystems (e.g. Fichez et al., submitted; Fernandez et al., 2006). Concerning the physical dynamics of the lagoon, an analysis of measurements taken over a span of 5 years made it possible to distinguish between seasonal and inter-annual variability in temperature and salinity (Ouillon et al., 2005). A circulation and particle transport numerical model (MARS3D) was adapted to this particular area of the lagoon (Douillet, 1998; Douillet et al., 2001). In this article, the HT computations are performed over the whole of the SLNC as well as on two embedded sub-areas: the "Noumea lagoon" and "Dumbea Bay" (Fig. 2).

3. The 3D hydrodynamic model

The MARS3D hydrodynamic model calculates currents, free surface elevations and concentrations of dissolved substances under the influence of tide, wind and, where appropriate, river inputs. The MARS3D model is made up of two sub-models. A depth-integrated 2D model (Douillet, 1998), which solves the shallow water equations (Blumberg and Mellor, 1987), calculates the water elevation and horizontal velocity at all points. The elevation results of combined action of wind and tidal forcing. The tide is taken into account by forcing the sea surface elevation at the boundaries (Douillet, 1998) in accordance with the results of the algorithms provided by the French Navy's Hydrographic Department (SHOM). The boundary conditions

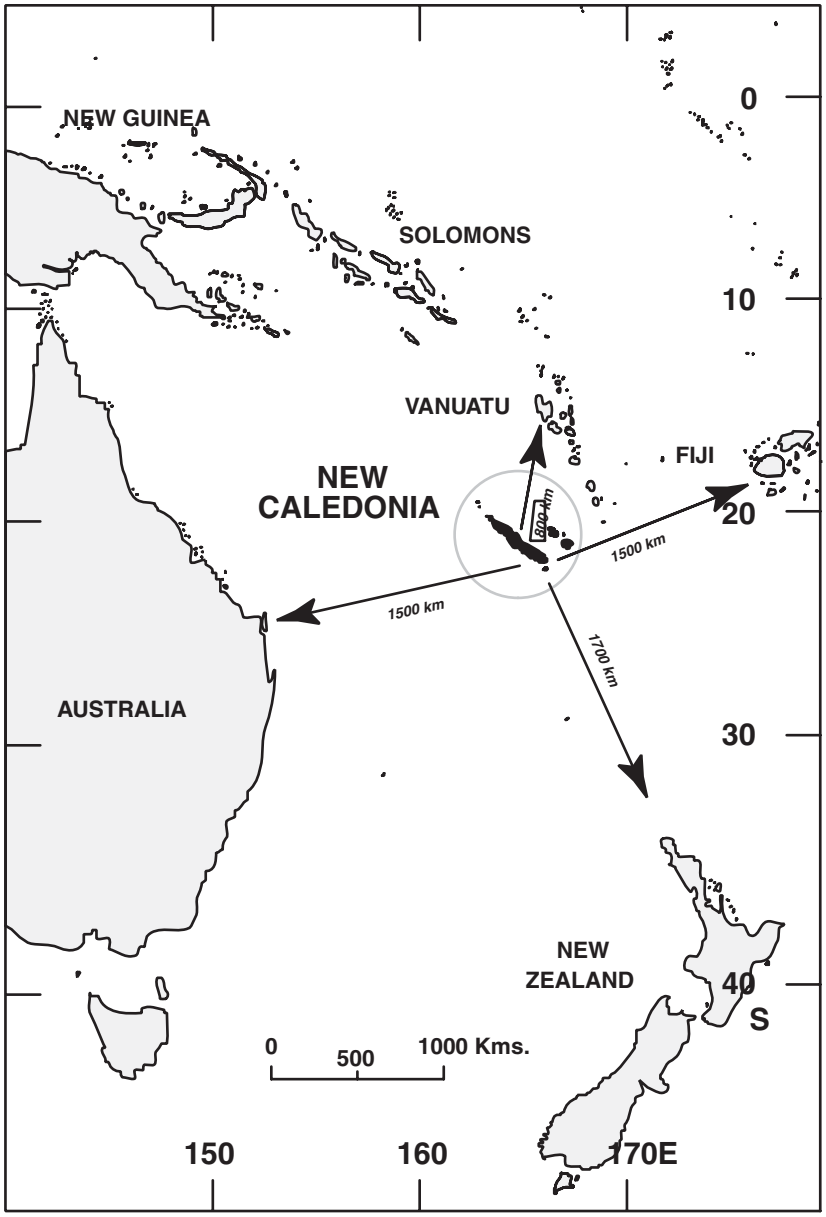

Fig. 1. Location of New Caledonia.

are imposed far away from the domain of study. The elevation is prescribed as a function of time and the normal gradient of velocity is forced to zero at each grid point of the open boundaries.

The results of the 2D model are transferred to a 3D model which uses the same horizontal grid. The vertical axis (depths) is divided in σ-levels (Blumberg and Mellor, 1987; Lazure and Salomon, 1991a; Deleersnijder and Beckers, 1992), which implies changing variables (x, y, z, t) into (x, y, σ, t), where x and y are the horizontal coordinates of the point, z is the depth (m), and σ is defined as

$$\sigma = \frac{z + h}{\zeta + h}, \tag{1}$$

where h is the bottom depth and ζ is the free surface elevation. The 3D computation module solves the Navier–Stokes equations using the Boussinesq approximation and the hydrostatic equilibrium hypothesis. The turbulence model used is of the Pacanowski and Philander (1981) type. The bottom stress is parameterized by means of a quadratic function of the velocity

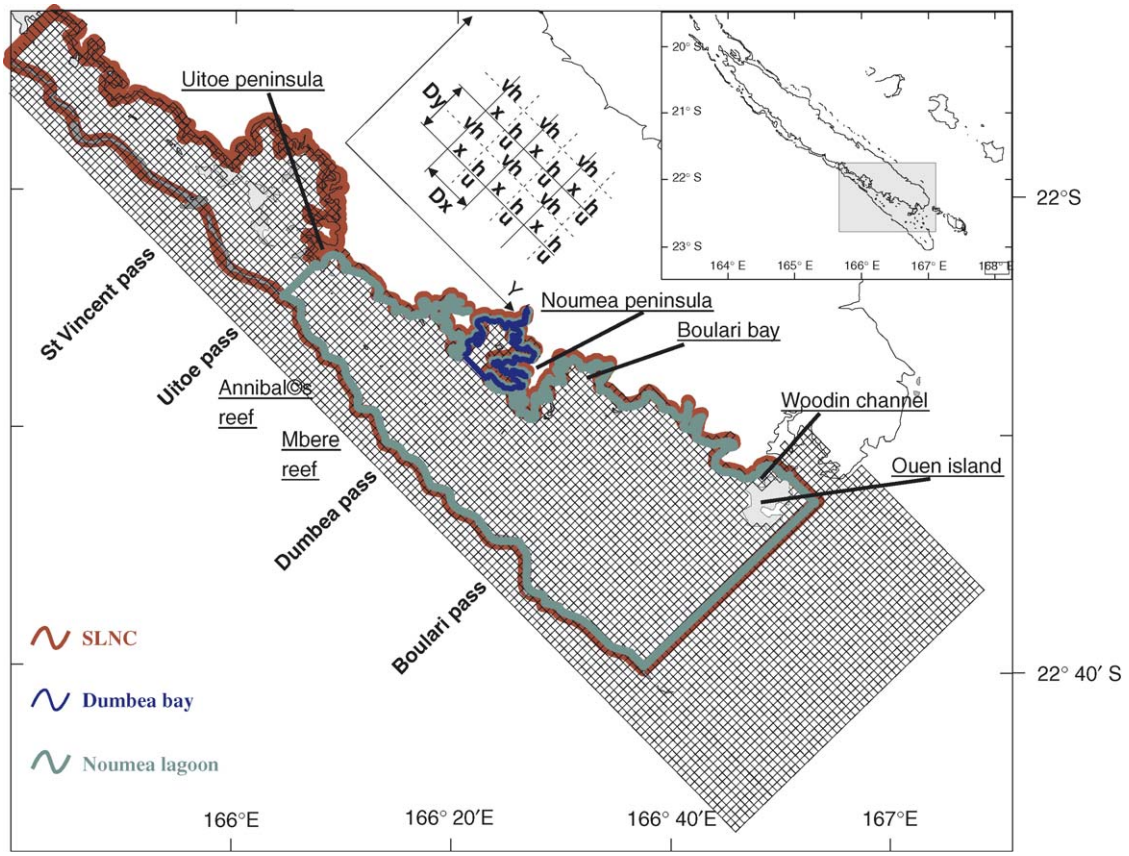

Fig. 2. Computational domain considered in the numerical simulations and the three control volumes used for hydrodynamic time computation.

that is consistent with the existence of a logarithmic layer adjacent to the bottom (Blumberg and Mellor, 1987; Deleersnijder et al., 1992; Douillet, 1998). A wind friction condition is applied at the surface (Douillet et al., 2001). Open boundary conditions are the same than those applied in the 2D model (Neumann type for velocity, Dirichlet for water height). The MARS3D model also solves transport equations of dissolved and particulate matter (Douillet et al., 2001; Ouillon et al., 2004). The heat and salt transport module available in MARS3D are not used in the present study, the simulations here shown do not reproduce the thermo-haline stratification.

Solving is based on the Alternating Direction Implicit (ADI; Leendertse, 1967) method for time discretization, and on finite differences for spatial discretization. For advection, we use a Total Variation Diminishing (TVD) method, less diffusive than the upstream scheme. We use a grid of the modified Arakawa C type (Lazure and Salomon, 1991a). Arakawa C type grid is modified for what concerns water depths which are indicated at the same grid location as velocity components. The automatic handling of emerging tidal flats is the result of the combined use of a test during the ADI procedure and the above-mentioned grid modification. The velocity component which is perpendicular to the obstacle (dried bank) is set to zero and the test conserves the linearity of the equation of motion (Lazure and Salomon, 1991a, b). It makes it possible to process automatically channels, islands, shallows, drying banks and inter-tidal areas, which represent a significant portion of the lagoon area. Lazure and Salomon (1991a), Tartinville et al. (1998) and Plus et al. (2003) have presented examples of the use of this model. In this study, we use a $\Delta x = \Delta y = 500\,\mathrm{m}$ grid spacing (Fig. 2) and 10 σ-levels.

4. HTs: definitions and computation methods

4.1. Water exchange time

For any given domain, the simplest general HT is the ratio between its total volume V and the daily

volume flux Q entering or leaving it:

$$\theta = \frac{\langle V \rangle_t}{\langle Q \rangle_t}. \quad (2)$$

In the literature, the parameter θ is frequently found under a variety of names: "residence time" (Gallagher et al., 1971; Delesalle and Sournia, 1992; Kraines et al., 1998, 1999; Rasmussen and Josefson, 2001; Gómez-Gesteira et al., 2003), "average residence time" (Pagès et al., 2001), "turn over time" (Takeoka, 1984), "flushing time" (Fisher et al., 1979; Geyer et al., 1997, 2000; Monsen et al., 2002; Delhez et al., 2004a), "water exchange rate" (Kraines et al., 2001) or "water renewal time" (Andréfouët et al., 2001).

On a given site, the value of this general HT depends directly on the arbitrary choice of the control volume (Bujan, 2000; Gómez-Gesteira et al., 2003). Space and time variability of the hydrodynamics within the control volume are not considered. This HT represents the length of time required for the entire mass of water to be replaced by input water, provided that all water particles have the same transit time through the control volume (Takeoka, 1984; Vallino and Hopkinson, 1998). To name this HT "renewal time" implies that this condition is met, which is not the case for a site where the hydrodynamics are highly heterogeneous. When large variations in hydrodynamics occur, the significance of this parameter is limited. Considering that this parameter quantifies the exchanges of a given body of water (a bay, a lagoon, etc.) with the surrounding environment, we chose to give it the name "water exchange time". This HT is widely used when studying the relationship between hydrodynamics and biology in a nearly enclosed system (Delesalle and Sournia, 1992) or as a criterion for the classification of coral structures (Andréfouët et al., 2001).

4.2. Water export time

The definition given by Takeoka (1984) for his "residence time" applies well to what we have chosen to call "water export time": "the residence time at a given point in the lagoon is the period of time that a water parcel, initially located at the point considered, needs to leave the lagoon". We feel that the name "water export time" is more explicit. Water export time is a local HT which means it is defined for each grid point.

The most suitable method for estimating the water export time uses a Lagrangian tracer model. Kraines et al. (2001), who introduced the term "export time", applied it to settling particles. In this way, it was not strictly speaking an HT, but a time characteristic of particulate transport. In order to calculate the export time, we apply the same method to water particles. The method consists of following the movement of a non-buoyant particle, initially located at the centre of each grid mesh of the control volume, assuming that the trajectory of such a particle during the simulation is representative of the trajectory of the initial mesh volume. The particles are transported by advection and diffusion during the numerical simulation. Turbulent mixing is included in the particle tracking model by means of a stochastic model. The position vector $\mathbf{r}$ of a Lagrangian particle is given in z-coordinate systems by the following equation (Hunter et al., 1993; Tartinville et al., 1997; Visser, 1997; Spagnol et al., 2002):

$$\mathbf{r}(t+\Delta t) = \mathbf{r}(t) + \Delta t\Big[\mathbf{u} + \left(6k_{\mathrm{h}}/\Delta t\right)^{1/2}\mathbf{d}_{\mathrm{h}} + \left[w + \left(6k_{\mathrm{v}}/\Delta t\right)^{1/2} d_{\mathrm{v}} + \frac{\partial k_v}{\partial z}\right]\mathbf{e}_z\Big], \quad (3)$$

where Δt is the time step, u is the horizontal velocity vector, w is the vertical component of the velocity, k_{h} and k_{v} are the horizontal and vertical eddy diffusivities, respectively, d_{v} and the components of the horizontal vector $\mathbf{d}_{\mathrm{h}}$ are dimensionless numbers randomly distributed between -1 and $+1$, and $\mathbf{e}_z$ is the vertical unit vector.

The time for a particle to exit the control volume from its initial position is the "export time" of this position. Its distribution expresses the hydrodynamic spatial variability. However, the water export time depends also on the choice of the control volume. The number of particles for which a trajectory is calculated depends on the site and on the grid spacing selected.

The spatial average for export time, calculated by weighting each point with the ratio of the volume of the initial grid mesh to the total volume of the system, is given the name of "turnover time" by Deleersnijder et al. (1997), Anonymous (1998), and Andréfouët et al. (2001). We prefer to use the term "average water export time", more consistent with the terminology defined in this article.

4.3. e-flushing time

What we call "e-flushing time" is the HT variously called "flushing time" by Zimmerman

(1976), Thomann and Mueller (1987) and Monsen et al. (2002), "residence time" by Rasmussen and Josefson (2001), Wang et al. (2004) and Shen and Haas (2004), and "e-folding time" by Dettmann (2001) and Delhez et al. (2004a). The term "e-folding time" suggests a partial replacement of the water, but is less descriptive than "flushing time". We feel the name "e-flushing time", which combines the two, is more appropriate. It is based on the definition by Thomann and Mueller (1987): If one considers that a known quantity of a substance is injected in a homogenous water mass at time t_0 at an initial concentration C_0, that no further amount of this substance is added after t_0, that the volume of the water mass and fluxes at its boundaries are constant, the concentration of the substance within the water mass at time t is given by the equation:

$$C(t-t_0) = C_0 e^{-Q/V*(t-t_0)} = C_0 e^{(-(t-t_0)/\theta)}, \quad (4)$$

where Q represents the flux of substance (entering or exiting), V is the volume of the control volume considered, t is the time ($t > t_0$) and θ is the e-flushing time.

The e-flushing time is the time required for the tracer mass initially contained within the whole domain to be reduced by a factor of $1/e$. This is a general parameter, defined for a control volume, and therefore does not take into account the space and time variability of the hydrodynamics.

4.4. Toward a new local hydrodynamic time: flushing lag, local e-flushing time

In this article, we propose adapting the e-flushing time to the local scale in order to be able to define a hydrodynamic time for each grid element. The computation method is as follows: initially, a concentration C_0 of a passive, non-settling tracer is imposed on the whole of the grid within the domain, and given a non-zero value (e.g. $C_0 = 1$). On the grid meshes outside the domain, concentration is held at zero. The evolution of this concentration within the domain under the influence of the hydrodynamics is then calculated. This evolution shows the progression of a front. The moment when concentration within one grid mesh reaches a threshold value C_1 (arbitrarily set as 95% of C_0) is named t_1 and is considered to be the beginning of exponential decrease in concentration within this grid mesh. We call t_1 the "flushing lag". The "local e-flushing time" is then defined within the grid mesh considered based on the decrease in concentration between C_1 and $1/e * C_0$, using an exponential regression of the same type as Eq. (4) that correlates best with the actual concentration decrease within the grid element.

This method generates two local parameters for each grid mesh, the "flushing lag" relating to the time required for water coming from outside the control volume to reach the mesh in significant quantity, and the "local e-flushing time" which defines the time span required after the flushing lag, for water from outside the control volume to occupy approximately 63% ($1 - 1/e \approx 0.632$) of the mesh's volume.

The accuracy of the numerical solving of advection terms, relating to the conservation of the front, and the accuracy of the turbulence model are important for the computation. The local e-flushing time is shorter when using computation methods which correctly preserve fronts, such as monotonicity preserving schemes (TVD type, e.g. Sweby, 1984) than with a classical upstream advection scheme. Finer grid resolution also leads to a better representation of the evolution of the front, especially when near to the coastline.

Introducing such an HT brings out the spatial variability of the hydrodynamics in a domain where currents are highly irregular, which is the case for the SLNC. The HT gradients given by this method can lead to establishing a spatial differentiation of areas within the SLNC, a result which is at least as interesting as the HT values themselves.

The flushing lag relates to the minimum age of the water masses at the studied point (Bolin and Rodhe, 1973; Takeoka, 1984; Deleersnijder et al., 1998; Shen and Haas, 2004; Delhez et al., 2004b), in the sense that it indicates the time required for a water particle coming from outside the SLNC to reach this point. Unlike the flushing lag for which the end time limit is when $C_1 = 0.95\ C_0$, the minimum age would be the period from initial starting time, to the time when the concentration within the grid mesh becomes less than C_0. The minimum age corresponds to the length of time required for water from outside the domain to begin to reach the grid mesh considered. The flushing lag is an integral part of the data which must be taken into account if our HT is to have a physical significance. It also has some similitude with the time lag as defined in Deleersnijder et al. (1998); flushing lag may

be regarded as the spatially variable version of the time lag.

5. Results

The results presented in this article were obtained for the case of a periodic tide (components M2 and S2; see tide analysis in Douillet, 1998) and a constant moderate wind, uniform over the study area, corresponding to normal SE trade wind (110°, $8\,m\,s^{-1}$). This choice has been made on the basis of a statistic analysis of meteorological data (Douillet et al., 2001; Ouillon et al., 2004) bringing out this particular wind regime as the most frequent and long-lasting scenario. Deleersnijder et al. (1998) have demonstrated the strong influence of wind intensity and direction on HTs. Wind is assumed to have a predominant effect on the HTs exposed in the lagoon of New Caledonia; however, the aim of the present study is to explore the meaning of the different HTs and not to detail the sensitivity to the wind velocity and direction. Our approach goes through the comparison of different HT's computation under the same forcing conditions. The results presented hereafter were averaged over several simulations starting at different phases of the tide. The time step used was 100 s. Preliminary calculation tests were performed with a 1000 m grid spacing. The final 500 m grid spacing led to a better representation of the front evolution, especially near to the coastline, but the general trends obtained with both grid sizes were very much alike. A better grid resolution is scheduled with future computer upgrades.

5.1. Water exchange time

The water exchange time was calculated over the entire SLNC. We obtained the incoming flow ($\geqslant 0$) on each boundary grid point, then its resultant over the whole of the SLNC boundaries, and the instantaneous water volume within the domain, from simulations of the MARS3D code. These vary with the state of the tide (Fig. 3). To get around this variability, we averaged incoming volume and flow rate over several daily cycles and several cycles of spring tides/neap tides. Note that the same method can be applied as well to the outgoing flow rate which compensates incoming flow rate over a spring/neap tide.

The result yields a water exchange time of 6.8 days over the whole SLNC. This value is substantially lower than the 11 days estimated for this part of the lagoon given by Rougerie (1986) and Bujan (2000). The difference between Bujan's calculations and ours is twofold: (a) Bujan's study relies on a hydrodynamic model which is only forced by wind, not by tide, which reduces the flux considerably at the domain's boundaries, and (b) there is a small difference in control volume between the two computation methods: Bujan (2000) uses the Noumea Lagoon (see Fig. 2), which is slightly smaller in extent than the SLNC as we defined it.

In order to illustrate the sensitivity of HTs to the choice of control volume, computations were performed on all three embedded domains: the SLNC, the Noumea Lagoon and Dumbea Bay (see Fig. 2). For the Noumea Lagoon, the water exchange time computed is 6.5 days. This is very

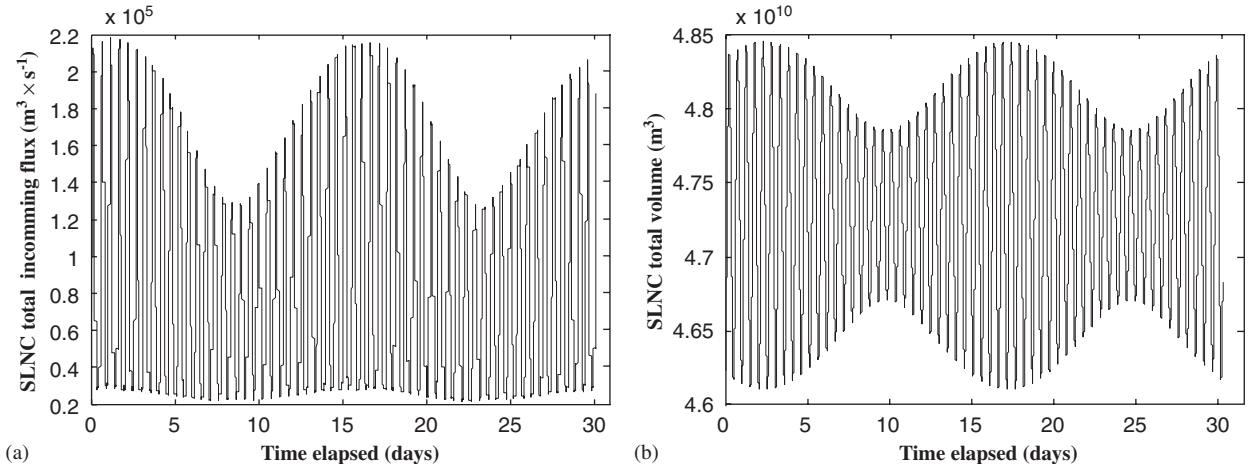

Fig. 3. Parameters used in the water exchange time calculation: (a) incoming water flux, (b) total SLNC volume.

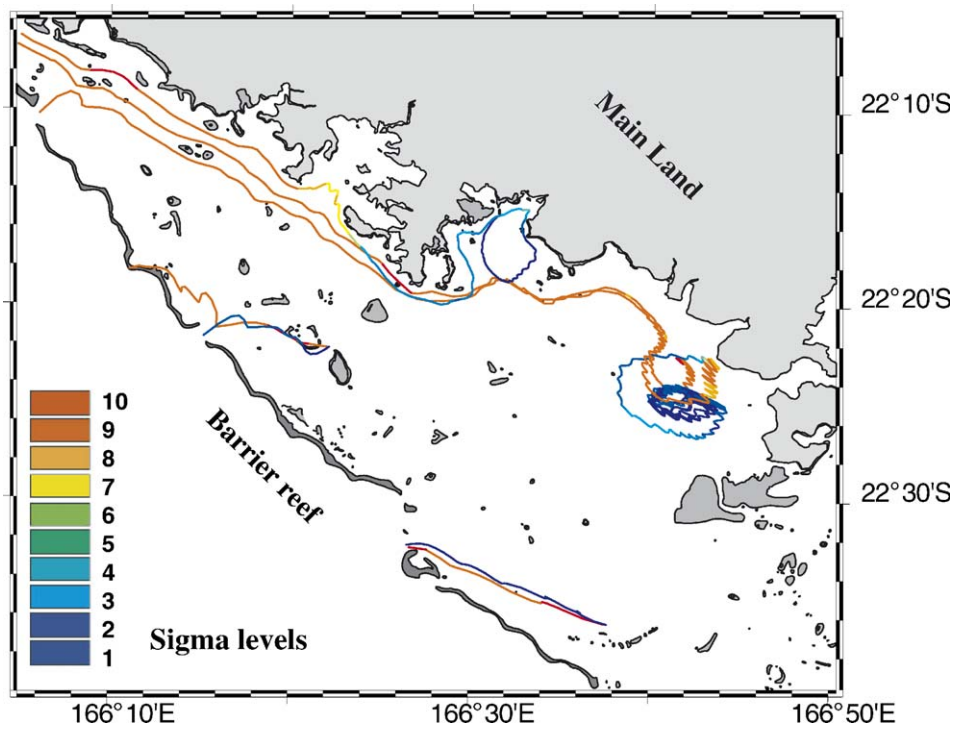

Fig. 4. Example of Lagrangian particle trajectories under forcing conditions: tide and trade winds (110°, 8 m s^{-1}).

close to the value found for the SLNC, as the difference in the volume of water is slight. For Dumbea Bay, calculations yielded a value of 4.0 days. This value, substantially shorter than for the other two domains, corresponds to the exchange time between the bay and outside the bay.

5.2. Water export time

The water export time was calculated on the basis of the release of 110,800 tracers in the SLNC, 87,990 in the Noumea Lagoon and 2390 in Dumbea Bay. Eq. (3) was applied using the vertical eddy diffusion coefficient k_v calculated from the turbulence model, and a coefficient k_h representing spreading due to velocity shear and spreading by turbulent motion. In this study, we applied a value of 0.05 m^2 s^{-1}, the median value of k_h measurements obtained by Riddle and Lewis (2000) in United Kingdom coastal waters. Supplementary simulations performed using a higher horizontal diffusivity (0.3 m^2 s^{-1} for a 500 m grid size following Okubo, 1980) led to a diffusive contribution more important than advection for the transport of individual particles. This value was not retained for k_h in the present study.

The computation of the export time was repeated 12 times, the beginning of calculations being spaced by 1 h intervals over a full tidal cycle. These results were averaged for the export time not to be dependent on the phase of the tide at which the particles are released. As an example, eight particle trajectories are shown in Fig. 4. The distributions of water export time, for the surface layer and for the bottom layer, are shown in Fig. 5a for the SLNC and in Fig. 5b for Dumbea Bay.

In the case of the SLNC, although distribution patterns at surface and bottom generally show a sharp decrease in export time the further one gets from the shore, we noted that distribution depended notably on depth in absolute value and over the gradients. Residence times were generally longer for particles released at the bottom. Areas of short residence time were found near the barrier reef. They are fan-shaped with the apex at a pass through which nearly all particles released within the fan exit the area. We noted a cell of long residence time to the north-west of Ouen Island, located slightly differently at the surface and on the bottom. This corresponds to a gyre described by Douillet et al. (2001).

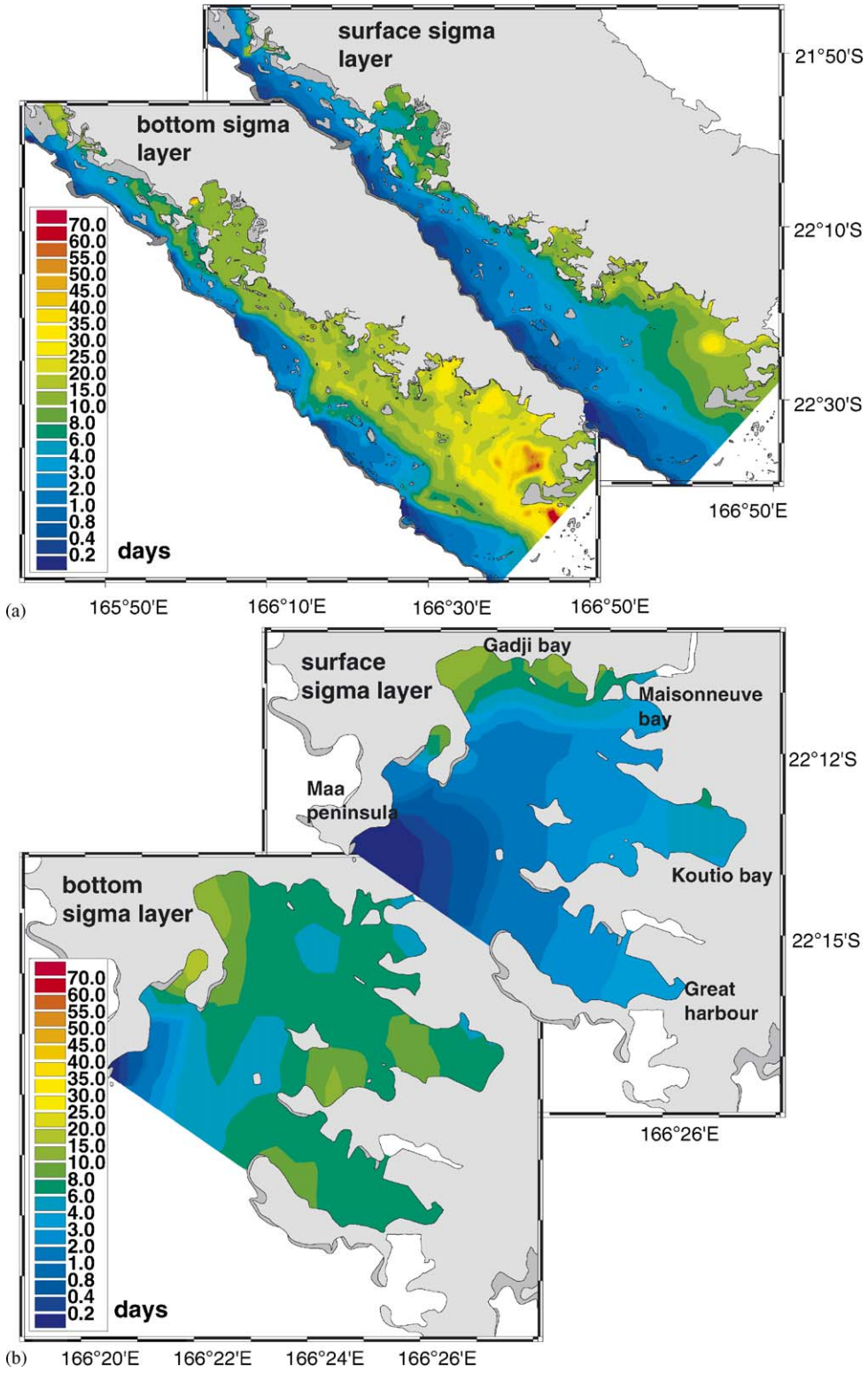

Fig. 5. Water export time calculated for two control volumes: (a) the SLNC, (b) the Dumbea Bay.

At the end of a circulation simulation spanning a 4-month period, nearly 2.5% of the tracer particles from the initial release were still within the SLNC. This is a numerical artefact of the model, which tends to immobilize particles in certain grid mesh at the bottom of the bays, rather than the expression of a physical process.

The distribution of export time in the Noumea Lagoon (not shown here), is not much different than that of the SLNC. This similarity indicates that the bulk of the water masses located within the Noumea Lagoon exits though boundaries shared by the Noumea Lagoon and the SLNC, mostly through the passes. The differences reflect those water masses which leave the Noumea Lagoon through its north-western end (see Fig. 2), thus remaining within the SLNC. For such water masses, the export time is shorter when defined with respect to the Noumea Lagoon than when defined with respect to the SLNC due to the general flow from SE to NW.

Water export times calculated using Dumbea Bay as control volume are distinctly shorter (Fig. 5b) than for the other two domains. The shortest export times are generally found at the surface near the Maa Peninsula, where the majority of currents lead outside the bay. The longest export times are found mostly at the inner end of the coves which make up Dumbea Bay, particularly Gadji Bay which was also noted as the area of maximum export time when studying the whole SLNC (see Fig. 5). The connection between length of export time and volume of the study area is more pronounced in terms of absolute rather than relative values.

The average export times, calculated using export time for each grid mesh weighted for its volume, were 10.8 days for the SLNC, 9.6 days for the Noumea Lagoon and 3.7 days for Dumbea bay, respectively.

5.3. *e-flushing time*

Fig. 6 shows the evolution of average concentration for the SLNC and for Dumbea Bay. For a given domain, the e-flushing time is calculated using the law of exponential decrease based on the successive moments when concentration reaches arbitrarily set thresholds. In this article, we established the regression using a range of thresholds going from 95% to 35% of C_0 in steps of 5%. The 35% threshold corresponds roughly to $1/e$, as the e-flushing time is associated to a decrease in concentration by a factor of $1/e$.

The application of the original method, seeking a relationship of exponential decrease of concentration going through C_0 in $t = 0$ (Eq. (4)) yields 11.4 days for the SLNC ($R^2 = 0.978$), 9.9 days for the Noumea Lagoon ($R^2 = 0.969$) and 6.6 days for Dumbea Bay ($R^2 = 0.930$) (Fig. 6). We also tested an adaptation of the method consisting of not forcing the exponential regression to pass through the point $C = C_0$ in $t = 0$. For each control volume, the regression relationships which resulted show a better correlation with the points yielded by the numerical model. This adapted method yields e-flushing times of 12.5 days ($R^2 = 0.993$), 11.1 days ($R^2 = 0.993$) and 7.6 days ($R^2 = 0.974$) for the SLNC, the Noumea Lagoon and Dumbea Bay, respectively.

5.4. *Flushing lag and local e-flushing time*

5.4.1. *Flushing lag*

The "flushing lag" describes the progression through the control volume of water coming in from outside. The adaptation of the method described by Thomann and Mueller (1987) to the computation of a local HT requires the storage of the time evolution of the concentration for each grid element which produces a vast amount of data beyond our storage capacity. We used instead the sampled times when the concentration in the grid mesh reaches arbitrarily set thresholds for the first time.

Fig. 7 shows the evolution of concentration, and the decomposition of this evolution, leading to the computation of the flushing lag and the local e-flushing time for a grid mesh located within Dumbea Bay, using first the whole SLNC then Dumbea Bay as control volume. The flushing lag is the time during which concentration within this grid mesh remains greater than 95% of C_0.

Fig. 8 shows flushing lag distributions in the SLNC and in Dumbea Bay for the surface σ-level. The distribution pattern varies little between levels, through the whole water column. Areas of short flushing lag indicate closeness with a point of water entry into the volume. For the SLNC, the majority of such water entry points are located in its south-eastern end, between U Reef (an extension of Ouen Island) and the barrier reef. The second largest inflow is through Woodin Channel, between Ouen Island and the mainland. Substantial amounts of

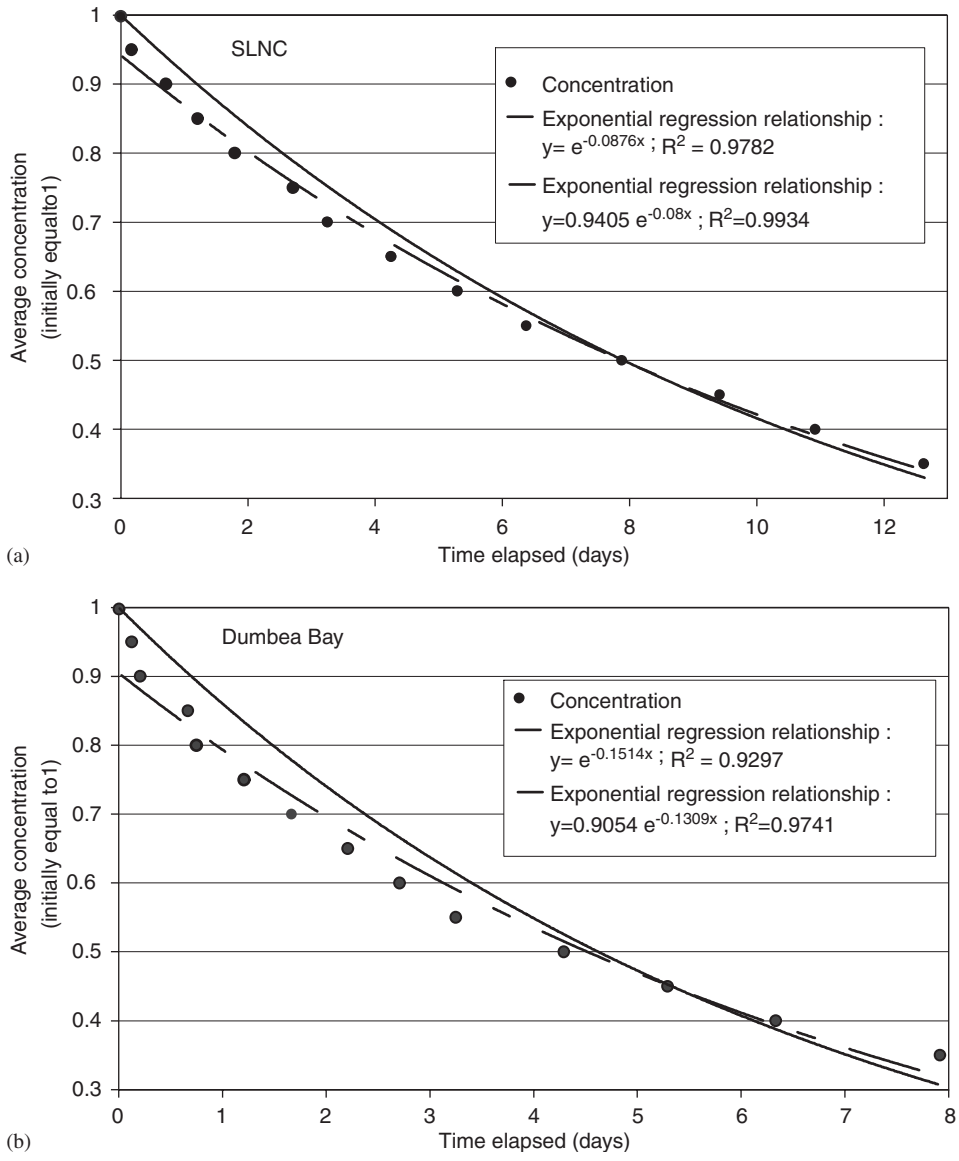

Fig. 6. Evolution of global concentration, used in the computation of e-flushing time for two control volumes: (a) the SLNC, (b) the Dumbea Bay.

water enter also through the passes in the barrier reef. The distribution pattern of short flushing lags in the vicinity of the passes continues, in decreasing sharpness, toward the north-west along the barrier reef. Such cells of short flushing lag have a limited extent in the Noumea Lagoon, whereas they occupy more than half of the area of the lagoon between St. Vincent Pass and the north-west end of the SLNC.

The flushing lag gradient generally trends SSE–NNW. It is the result of the combined effect of the tide-induced and wind-induced circulation (SE–NW) and of water entry through the passes (from the reef toward the mainland). We observed a circular area of long flushing lag (15–20 days) west of Ouen Island. This matches the location of a gyre, described by Douillet (1998) and Douillet et al. (2001), fed by Woodin Channel.

Flushing lags are longer when calculated on the basis of the whole SLNC than when only Dumbea Bay is considered. The time required for a front to arrive at a given point increases with the distance from the open boundary of the control volume (see Fig. 7). Calculation of the flushing lag in Dumbea

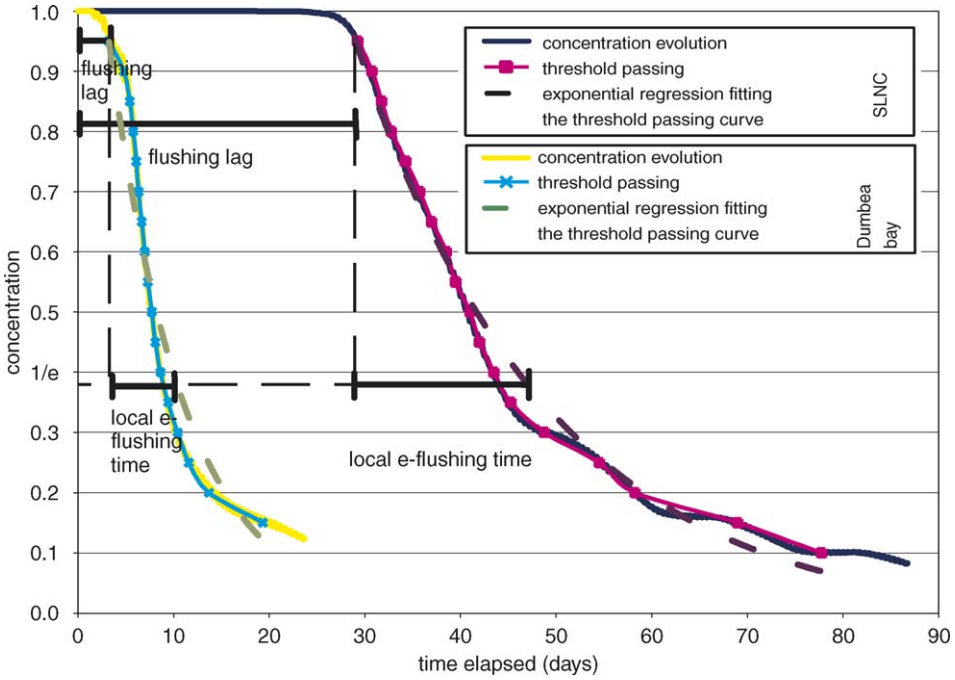

Fig. 7. Example of concentration decrease at a grid point located in the Dumbea Bay (166.35937 W, 22.21741 S) for SLNC and Dumbea Bay as control volume. Flushing lag and local e-flushing time computation.

Bay shows that the progress of water masses from outside of the bay is rapid along the axis of the bay, slower for the coves to leeward (Maisonneuve Cove, Gadji Bay) and even slower for the coves to windward (Grande Rade, Koutio Bay). The flushing lag gradients are very similar whether they are calculated using Dumbea Bay, the Noumea Lagoon or the whole SLNC as a control volume. The sensitivity of the flushing lag to the choice of control volume is more pronounced on the actual values than on the general patterns of spatial distribution.

5.4.2. *Local e-flushing time*

Local e-flushing time fields calculated for the SLNC (Fig. 9a) and for the Noumea Lagoon (not shown here) are similar over their shared areas. The major gradient is oriented from the barrier reef toward the coast. The longest local e-flushing times were observed at the inner ends of bays, with maxima in Noumea Harbour (>2 months), at the centre of the gyre west of Ouen Island (>1 month) and in the north-western part of the SLNC (>1 month). Local e-flushing times were very short within the passes (<1 day), forming structures surrounded and extended along the reef toward the north-west by zones of longer local e-flushing time (>4 days). The spatial extent and e-flushing time variation amplitude of such structures were greater in the north-western part of the SLNC than within the Noumea Lagoon.

Values computed for Dumbea Bay were much shorter when using Dumbea Bay as a control volume than when using the whole SLNC (Fig. 9). Values increase toward the inner ends of the coves which make up the bay. The highest values were found in Noumea's Grande Rade and in the windward part of Koutio Bay. Qualitatively, this distribution is the same whether the control volume is the SLNC or the Dumbea Bay. The sensitivity of the local e-flushing time to the choice of control volume is more pronounced on the actual values than on the general patterns of spatial distribution.

6. Discussion

6.1. *Water exchange time*

The determination of the flux entering the domain is crucial for calculating the water exchange time. We chose to consider the whole of these fluxes. This choice amounts to considering that any water particle entering the control volume participates in

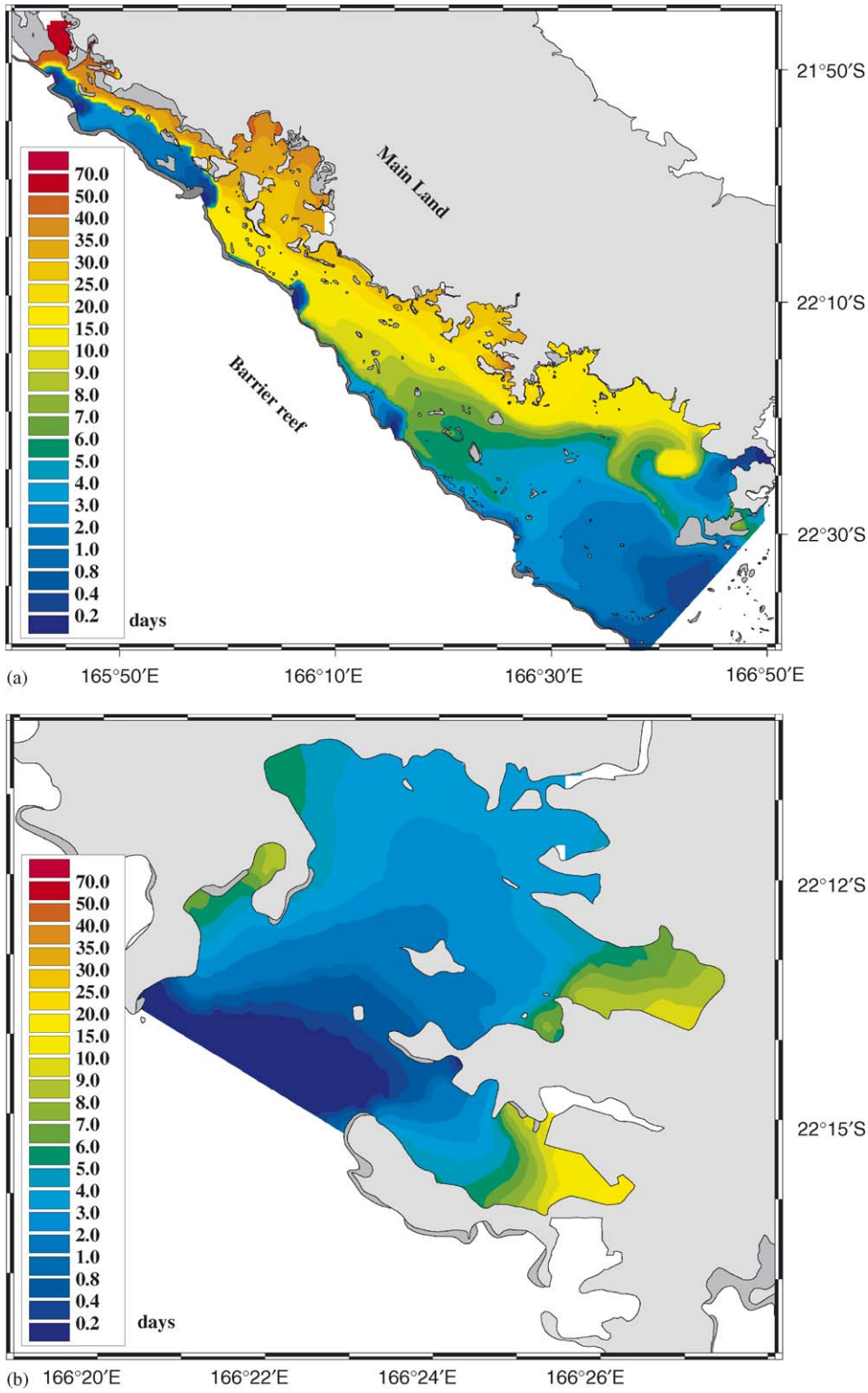

Fig. 8. Flushing lag distribution for two control volumes: (a) the SLNC, (b) the Dumbea Bay.

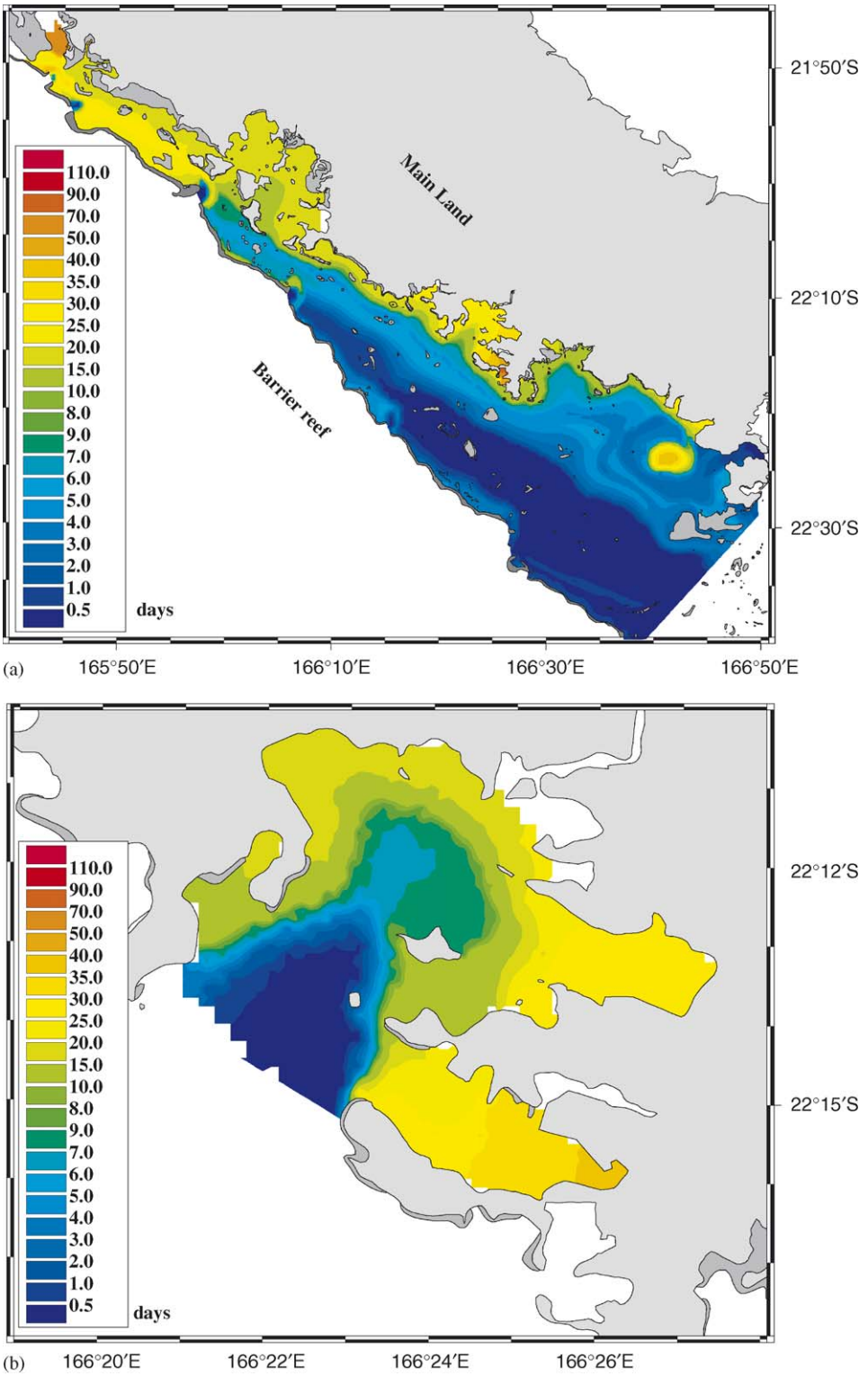

Fig. 9. Local e-flushing time distribution for two control volumes: (a) the SLNC, (b) the Dumbea Bay.

the overall exchange process, yielding a basic parameter for exchange time. Rasmussen and Josefson (2001) and Wang et al. (2004) proceeded differently. In calculating the volume of the water masses entering the control volume, they chose not to take into account the water which enters the domain and exits with the following turn of the tide. Often, this type of approach comes along with simplifying hypothesis on hydrodynamics, and aims at extending the significance of the water exchange time. In the case of a site subject only to tidal forcing, the residual tidal flux makes it possible, for instance, to take into account the repeated entries and exits of water particles within the control volume. The computation of the water exchange time applied to the residual tidal flux yields a water exchange time much longer than using the incoming (or outgoing) flux.

6.2. Water export time

To complement the definition of the water export time given by Eq. (3), it should be possible to take into account the water masses which return into the domain with the tide. Monsen et al. (2002) calls the cumulated duration of the times a water particle spends within the domain "exposure time". As was done for the exchange time, we did not take this effect of the tidal oscillation into account in our computation, for the sake of consistency with the tests for the different HTs, and to adhere more closely to the definition of the water export time proposed by Takeoka (1984). This choice is equivalent to assuming that, on our site, the combined effect of wind and tide during the flow phase of the tide limits the re-entry of water particles which had been carried out during the preceding ebb.

An HT integrated over space does not provide any information of hydrodynamic spatial variability, which is high in our study area. The broad range of export time values calculated for the SLNC (0.2–60 days) gives a good indication of the wide differences in hydrodynamic processes, which would not be apparent using an averaged water export time (here 10.7 days). The water export time is also useful in establishing the direction of dominant fluxes. In simple structures, such as areas where water exits through passes, the dominant flux is orientated along an axis of decreasing values of export time.

6.3. e-flushing time

There are some difficulties in computing the e-flushing time. The existence of a regression coefficient between numerical results and the regression relationship of exponential decrease raises the question of the limits of applicability of this parameter to any domain. In a constantly mixed volume, the concentration decrease is perfectly exponential. It is not, however, in the case of a system where different particles have the same transit time. More generally, when the decrease in average concentration in a given domain is not exponential one can deduce that mixing does not tend toward homogeneity of the water masses. In certain cases, exponential regression may be poorly adapted, and the results lack significance. This is a serious limitation of this method, and of this HT when compared with others which may be calculated without restriction. This consideration leads to the important question when calculating e-flushing time: up to what regression coefficient can one assume that the decrease follows an exponential law?

6.4. Local e-flushing time

Fig. 10 shows the distribution of the regression coefficient obtained between the simulated evolution of concentration in a given grid mesh and an exponential decrease regression relationship (see Eq. (4)). The values for the regression coefficient indicate that this evolution does indeed behave generally in an exponential manner. The regression coefficients calculated for Dumbea Bay are lower when the Bay itself is the control volume (Fig. 10a) than when the whole SLNC is the control volume (Fig. 10b). In this bay, the results vary significantly depending on the control volume chosen (see also Fig. 7).

In the SLNC, the areas which receive water input from the passes show low regression coefficients (e.g. station A in Fig. 10a). The evolution of concentration at station A (Fig. 11a) shows a significant lowering of concentration when water enters the pass, followed by a period during which concentration changes within a narrow range under the influence of the semi-diurnal tide, then followed by a further sharp lowering of concentration linked to water input from south-east. The existence of two plateaux, corresponding to flooding by two different water masses, makes the evolution of the concentration inconsistent

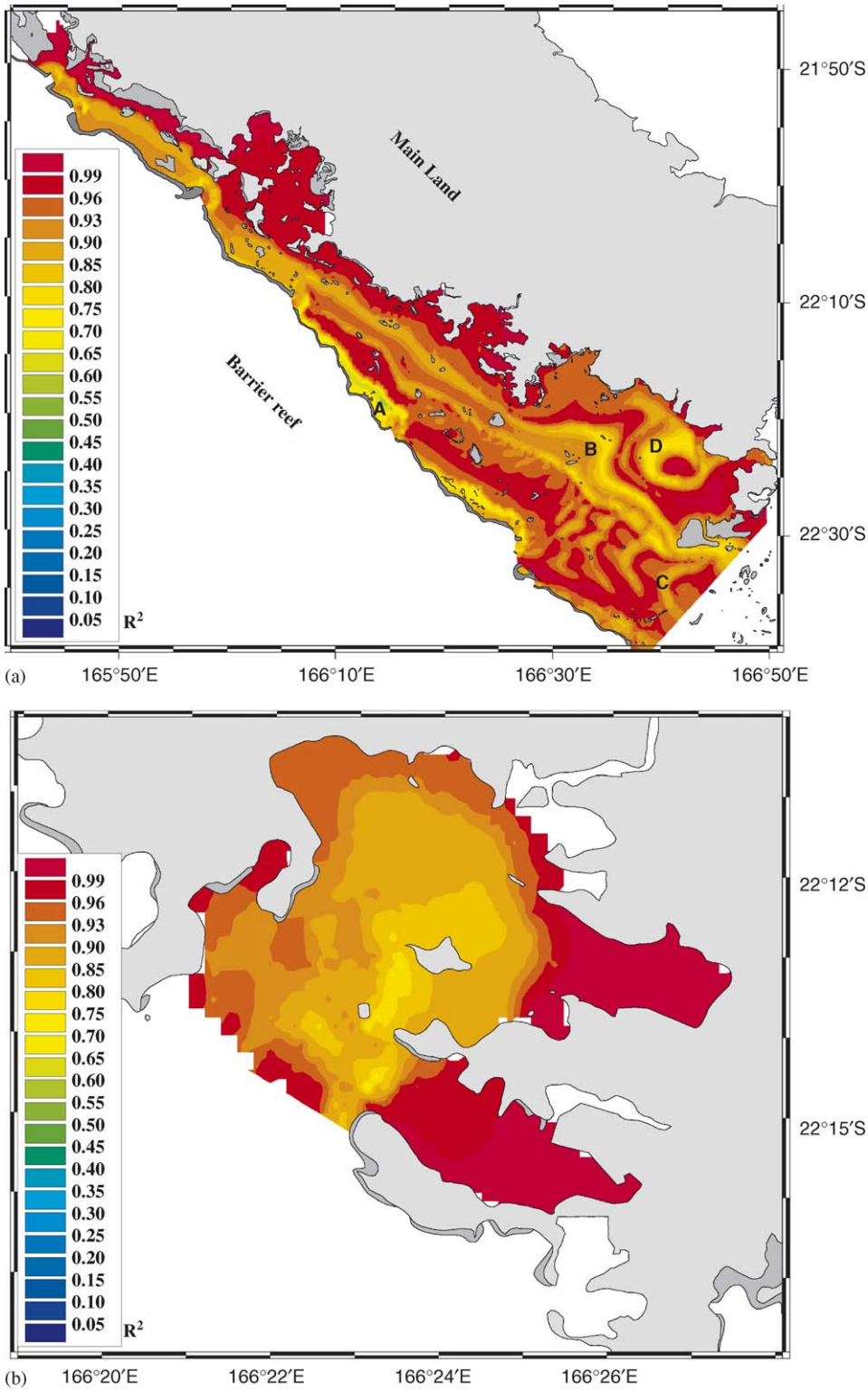

Fig. 10. Regression coefficient between calculated concentration decrease and theoretical exponential concentration decrease for two control volumes: (a) the SLNC, (b) the Dumbea Bay.

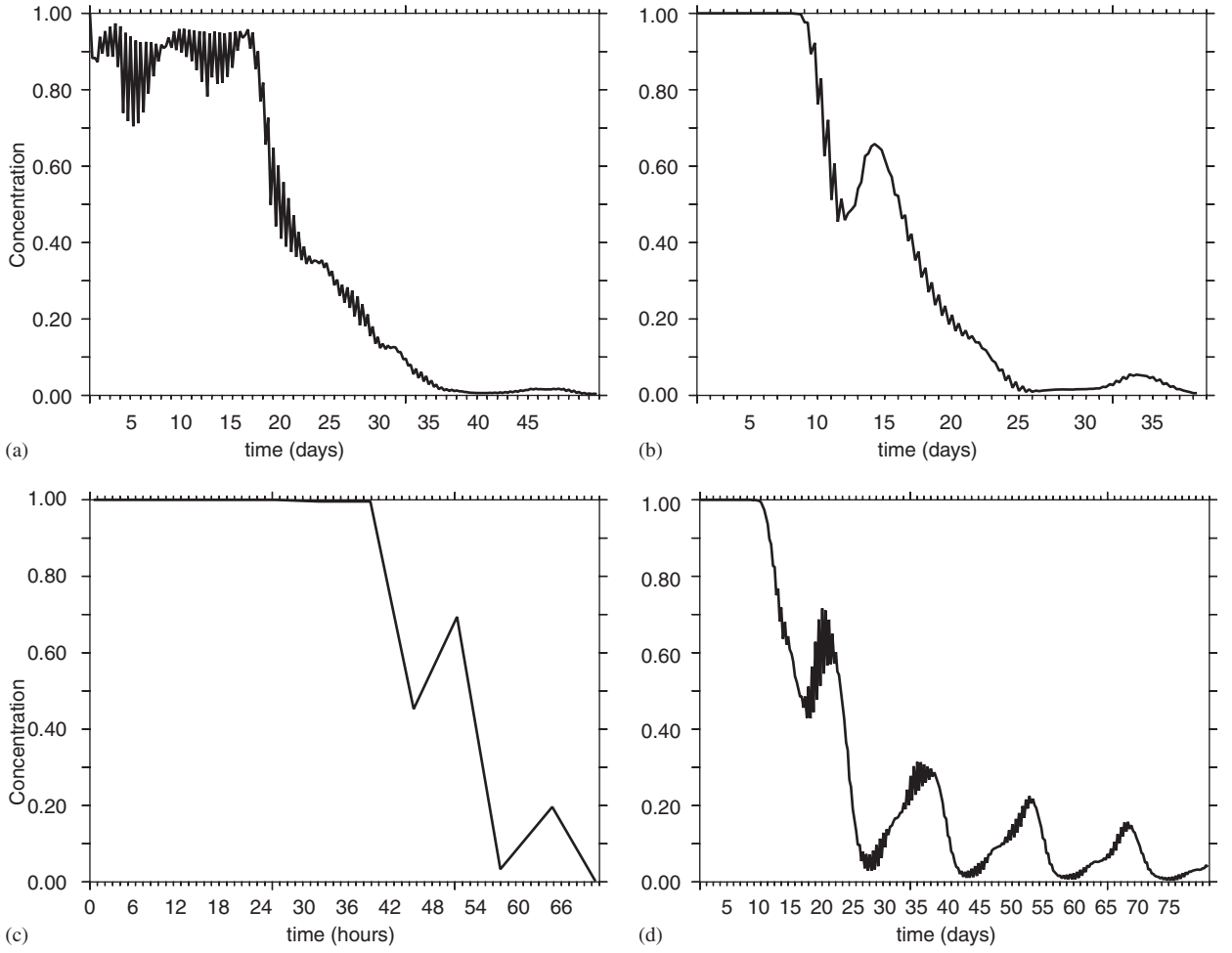

Fig. 11. Concentration evolution at four stations (see locations in Fig 10a).

with an exponential type of behaviour, thus the relatively low regression coefficient. The other areas with a low regression coefficient also have a concentration-vs.-time curve showing plateaux, where decrease no longer behaves in an exponential manner. At station B (Fig. 10a), the poor regression is linked to the entry of two distinct water masses, one from the south-east boundary of the domain, the other from Woodin Channel, arriving at slightly different times. The boundary between these two water masses of different concentration oscillates according to the spring-tide/neap-tide cycle (Fig. 11b). At station C we observe the arrival of a low-concentration tidal front, followed by a rise in concentration as this front recedes with the ebb, until the turn of the tide when concentration begins to drop again (Fig. 11c). The tidal cycle is responsible for these oscillations in concentration. This would not be apparent if one performed the computation using the average of a large number of simulations starting each at a different stage of the tide cycle. At station D the oscillation of the concentration (Fig. 11d) is related to the dynamics of the gyre, and concentration at the centre remains higher than outside for a long time (see Fig. 9a). The plateaux or oscillations in concentration values, which prevent concentration from following a truly exponential decrease, are in all cases linked to the input of two water masses, either originating from two different entries (by the south-east entry and through a passage at station A, by the south-east entry and by the Woodin Channel at station B, or by alternatively waters from inside and outside the gyre at station D), or from the same entry but with different ages (e.g. two entries from the south-east during two consecutive flood tides at station C).

The record of concentration decrease which we use for computing the local e-flushing time consists of the times when concentration drops below pre-set thresholds. Note that using a different method of recording the evolution of concentration within the grid elements would be likely to alter the results slightly. Note also that the regression coefficient of an exponential rule is generally better when one considers all thresholds between $0.95C_0$ and $0.05C_0$, rather than only those between $0.95C_0$ and $0.35C_0$ (i.e. close to $1/e * C_0$).

As we indicated previously, in this article we applied the e-flushing time parameter frequently encountered in other publications (Thomann and Mueller, 1987; Rasmussen and Josefson, 2001; Dettmann, 2001; Monsen et al., 2002; Wang et al., 2004; Shen and Haas, 2004; Delhez et al., 2004a), which we adapted to a local HT. A parameter close to local e-flushing time can be defined in any situation, without postulating a particular mode of concentration decrease, based only on times t_1 and t_2 when concentration reaches arbitrary pre-determined thresholds (for instance 95% and 35% of the initial concentration). t_1 corresponds to the flushing lag, and the difference $(t_2 - t_1)$ is close to the local e-flushing time. The "local residence time" proposed by Abdelrhman (2005) corresponds to the time when concentration at one point reaches a set percentage of the initial concentration. When using 95% of the initial concentration as the threshold, Abdelrhman's "local residence time" is equal to the flushing lag.

6.5. Comparing the general HTs

Each one of the general HTs tested in our study has been called "residence time" in published articles. The differences between them and between the three control volumes used, as illustrated in Fig. 12, make it clear that there is a need to refine the terminology. There does not appear to be any simple relationship between them if one avoids making simplifying assumptions on the hydrodynamics. The average export time of a system can be longer or shorter than its water exchange time. As explained in Section 4, the two HTs do not have the same significance. Considering an idealized system where all particles have the same transit time, the water exchange time corresponds to the time required for all particles to have been replaced. In this configuration, if the incoming flux remains constant, the average export time corresponds to

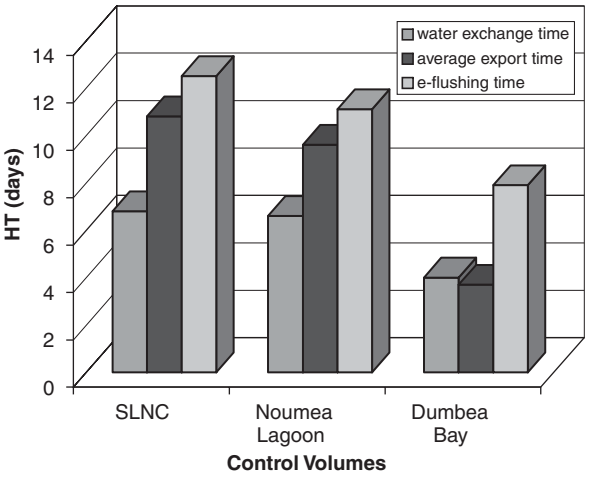

Fig. 12. General hydrodynamic time scales calculated for three different control volumes.

half the water exchange time. Outside of this ideal case, there is no simple relationship between the two parameters. Export time gets further away from half of the water exchange time when the domain includes a short transit area and large retention areas. The increase of the export time compared with half the exchange time reflects a domain with highly heterogeneous hydrodynamics. In contrast with the SLNC and the Noumea Lagoon, the average export time in Dumbea Bay is shorter than the water exchange time. Based on our results, we observe that the difference between the average export time and half of the exchange time increases with the size of the domain considered. Comparing average export time vs. exchange time over two different domains also provides information on the relative effectiveness of the processes of export and exchange.

Let us consider now the similarities between the e-flushing time and the average export time. The e-flushing time is the time required for the average concentration to decrease to $1/e$ times the initial concentration, provided the concentration decrease follows an exponential rule. As we showed previously, concentration decrease in Dumbea Bay does not always follow such a rule (Figs. 7 and 10b), making this parameter poorly adapted to the particular domain. The e-flushing time is the time required to dispose of approximately 63.2% [more precisely $(1 - 1/e) * 100\%$)], of the initial concentration in the domain. The average export time is the time required for half the water initially present to exit the domain. Both these HTs quantify the

time required for a similar percentage of the water present to exit the domain. In the case where concentration decrease is truly exponential, the average export time is the moment θ' such that

$$C(\theta') = C_0 e^{(-\theta'/\theta)} = \tfrac{1}{2}C_0 \quad (5)$$

or

$$\theta' = \ln 2\theta \approx 0.693\theta, \quad (6)$$

where θ is the e-flushing time. For calculating the e-flushing time for the SLNC and for the Noumea Lagoon, concentration decrease is nearly exponential. The average export time and the e-flushing time follow the same trends ($\theta' = 0.596\ \theta$ for the SLNC; $\theta' = 0.667\ \theta$ for the Noumea Lagoon).

6.6. Comparing local HTs

Local HTs can be used to identify areas of particular hydrodynamic regime. Relating the flushing lag and local e-flushing time, while comparing the distribution of the concentration decrease regression coefficient with an exponential decrease, yields further information. The most obvious example of this can be seen in the areas near the passes. The water input through the pass is sufficiently large to affect the flushing lag (decreasing the concentration within grid elements to 95%) and start the count for the local e-flushing time, but is not enough to induce a theoretical exponential decrease for these grid elements. The other concentration thresholds are crossed when water from a more abundant source, in this case from the southeast end of the lagoon, reaches the mesh. More generally, areas where concentration decrease departs substantially from an exponential regression are areas receiving water inputs from more than one source (see Section 6.4). Fig. 10 gives a static illustration of the dynamic, particularly oscillatory, behaviour of the water masses.

Apart from this aspect, the higher the flushing lag, the more diffuse the concentration front. Regression coefficients improve, and local e-flushing times become longer.

Since the flushing lag relates to the minimum age of the water masses within the grid element, and since the export time corresponds to the length of time required for the water present locally to exit the domain, adding these two HTs gives a good estimate of the low value for the transit time.

The results obtained by this study on the three chosen domains show that the relative distribution of local HTs (export time, flushing lag and local e-flushing time) remains the same over all three domains for a given method.

7. Conclusion

Numerical modelling makes it possible to calculate at the same time general and local HTs. The interest of local HTs is most evident in domains where the hydrodynamics are highly heterogeneous, such as the SLNC. The capacity of a 3D hydrodynamic model for yielding data for the entire lagoon makes it possible to do away with simplifications of the hydrodynamic regime such as are often used to estimate HTs. The removal of the need for such simplifications (e.g. perfectly mixed waters within a system, uniform transit time for all particles, uniform velocity) can at times invalidate the theoretical relationships between the HTs found in publications. There is therefore a need for renaming the HTs derived from different calculation methods in order to arrive at a more accurate description than the generic term of ''residence time'', often applied to distinct different parameters.

It is important to point out that the HT values mentioned in this article are directly dependent on the control volume chosen. This choice was easy to make in the case of the SLNC, in spite of its large internal variability, since it represents an entity quite distinct from the surrounding ocean, being naturally bounded by its barrier reef. We also wish to point out that the importance of the choice of domain is less crucial when one is more concerned with relative spatially defined HT values than with the absolute values.

The investigations carried out for this study were more focused on the nature and physical significance of the HTs than on their potential for analysing the biological dynamics of an aquatic ecosystem. Based on the definitions proposed and tested in this article in the case of a periodic forcing standing for mean conditions, it will be possible to perform calculations bearing on real climatological studies. Notably, the solution of the equation for heat transport, not included in the present study, should describe the seasonal stratification of water masses observed in the SLNC during the southern summer (Ouillon et al., 2005), a phenomenon which limits vertical exchanges at the interfaces. Such realistic simulations will yield better differentiated HT distributions between the bottom and the surface than is possible using academic types of

simulations. They may lead to a statistical analysis of HTs through the various areas of the study site. It will then be possible to undertake a comparative analysis of the relationships between HTs and biological parameters or observational data.

Acknowledgements

This work was supported by the New Caledonian "ZoNéCo" program, by the French "Programme National Environnement Côtier" and by NASA Grant NNG04GO90G from "Interdisciplinary Program". The authors thank Eric Deleersnijder and an anonymous reviewer for their valuable comments on this paper.

References

Abdelrhman, M.A., 2005. Simplified modeling of flushing and residence times in 42 embayments in New England, USA, with special attention to Greenwich Bay, Rhode Island. Estuarine Coastal and Shelf Science 62, 339–351.

Andréfouët, S., Pagès, J., Tartinville, B., 2001. Water renewal time for classification of atoll lagoons in the Tuamotu Archipelago (French Polynesia). Coral Reefs 20, 399–408.

Andréfouët, A., Pagès, J., Tartinville, B., 2003. Response to the comment by Deleersnijder on "Water renewal time for classification of atoll lagoons in the Tuamotu Archipelago (French Polynesia)". Coral Reefs 22, 309–310.

Anonymous, 1998. Circulation and mixing in the lagoons. In: Anonymous (Ed.), The Radiological Situation at the Atolls of Mururoa and Fangataufa, Technical Report, vol. 5: Transport of Radioactive Material within the Marine Environment. IAEA, Austria, pp. 5–29.

Blumberg, A.F., Mellor, G.L., 1987. A description of a three-dimensional coastal ocean circulation model. In: Heaps, N.S. (Ed.), Three-dimensional Coastal Ocean Models. AGU, Washington, DC, pp. 1–16.

Bolin, B., Rodhe, H., 1973. A note on the concepts of age distribution and transit time in natural reservoirs. Tellus 25, 58–62.

Bujan, S., 2000. Modélisation biogéochimique du cycle du carbone et de l'azote dans les écosystèmes côtiers tropicaux sous influences terrigènes et anthropiques. Ph.D. Thesis Dissertation, University of Aix-Marseille II, France.

Crump, B.C., Hopkinson, C.S., Sogin, J.E., 2004. Microbial biogeography along an estuarine salinity gradient: combined influences of bacterial growth and residence time. Applied and Environmental Microbiology 70, 1494–1505.

Deleersnijder, E., 2003. Comments on Water renewal time for classification of atoll lagoons in the Tuamotu Archipelago (French Polynesia) by Andréfouët et al. [Coral Reefs 20:399–408]. Coral Reefs 22, 319.

Deleersnijder, E., Beckers, J.M., 1992. On the use of σ-coordinate system in regions of large bathymetric variations. Journal of Marine Systems 3, 381–390.

Deleersnijder, E., Norro, A., Wolanski, E., 1992. A three-dimensional model of the water circulation around an island in shallow water. Continental Shelf Research 12, 891–906.

Deleersnijder, E., Tartinville, B., Rancher, J., 1997. A simple model of the tracer flux from the Mururoa lagoon to the Pacific. Applied Mathematical Letters 10 (5), 13–17.

Deleersnijder, E., Wang, J., Mooers, C.N.K., 1998. A two-compartment model for understanding the simulated three-dimensional circulation in Prince William Sound, Alaska. Continental Shelf Research 18, 279–287.

Delesalle, B., Sournia, A., 1992. Residence time of water and phytoplankton biomass in coral reef lagoons. Continental Shelf Research 12, 939–949.

Delhez, E.J.M., Heemink, A.W., Deleersnijder, E., 2004a. Residence time in a semi-enclosed domain from the solution of an adjoint problem. Estuarine Coastal and Shelf Science 61, 691–702.

Delhez, E.J.M., Lacroix, G., Deleersnijder, E., 2004b. The age as a diagnostic of the dynamics of marine ecosystem models. Ocean Dynamics 54, 221–231.

Dettmann, E.H., 2001. Appendix C Additional information on flushing in estuaries. Nutrient Criteria Guidance Manual—Estuarine and Coastal Marine Waters. US Environment Protection Agency.

Douillet, P., 1998. Tidal dynamics of the south-west lagoon of New Caledonia: observations and 2D numerical modelling. Oceanologica Acta 21, 69–79.

Douillet, P., Ouillon, S., Cordier, E., 2001. A numerical model for fine suspended sediment transport in the southwest lagoon of New Caledonia. Coral Reefs 20, 361–372.

Fernandez, J.M., Ouillon, S., Chevillon, C., Douillet, P., Fichez, R., Le Gendre, R., 2006. A combined modelling and geochemical study of the fate of terrigenous inputs from mixed natural and mining sources in a coral reef lagoon (New Caledonia). Marine Pollution Bulletin 52, 320–331.

Fichez, R., Chifflet, S., Douillet, P., Gérard, P., Ouillon, S., submitted. Biogeochemical typology and temporal variability of lagoon waters in a coral reef ecosystem subject to terrigenous and anthropogenic inputs (New Caledonia). Marine Pollution Bulletin.

Fisher, H.B., List, E.J., Koh, R.C.Y., Imberger, J., Brooks, N.H., 1979. Mixing in Inland and Coastal Waters. Academic Press, New York, NY.

Gallagher, B.S., Shimada, K.M., Gonzalez Jr., F.I., Stroup, E.D., 1971. Tides and currents in fanning atoll lagoon. Pacific Science 25, 191–205.

Geyer, W.R., 1997. Influence of Wind on Dynamics and Flushing of Shallow Estuaries. Estuarine Coastal and Shelf Science 44, 713–722.

Geyer, W.R., Morris, J.T., Pahl, F.G., Jay, D.A., 2000. Interaction between physical processes and ecosystem structure: a comparative approach. In: Hobbie, J.E. (Ed.), Estuarine Science: a Synthetic Approach to Research and Practice. Island Press, Washington, DC, pp. 177–206.

Gómez-Gesteira, M., deCastro, M., Prego, R., 2003. Dependence of the water residence time in Ria of Pontevedra (NW Spain) on the seawater inflow and the river discharge. Estuarine Coastal and Shelf Science 58, 567–573.

Hunter, J.R., Craig, P.D., Phillips, H.E., 1993. On the use of random walk models to with spatially variable diffusivity. Journal of Computational Physics 106, 366–376.

Kraines, S.B., Yanagi, T., Isobe, M., Komiyama, H., 1998. Wind wave driven circulation on the coral reef at Bora Bay, Miyako Island. Coral Reefs 17, 133–143.

Kraines, S.B., Suzuki, A., Yanagi, T., Isobe, M., Guo, X., Komiyama, H., 1999. Rapid water exchange between the lagoon and the open ocean at Majuro Atoll due to wind, waves, and tide. Journal of Geophysical Research 104, 15,634–15,653.

Kraines, S.B., Isobe, M., Komiyama, H., 2001. Seasonnal variations in the exchange of water and water-borne particles at Majuro Atoll, the Republic of the Marshall Island. Coral Reefs 20, 330–340.

Lazure, P., Salomon, J.C., 1991a. Coupled 2-D and 3-D modelling of coastal area. Oceanologica Acta 14, 173–180.

Lazure, P., Salomon, J.C., 1991b. Etude par modèles mathématiques de la circulation marine entre Quiberon et Noirmoutier. Oceanologica Acta 14 (SP), 93–99.

Leendertse, J.J., 1967. Aspects of computational model for long-period water-wave propagation. The Rand Corporation, Santa Monica, CA, Rep RM-5294-PR.

Monsen, N.E., Cloern, J.E., Lucas, L.V., Monismith, S.G., 2002. A comment on the use of flushing time, residence time, and age as transport time scales. Limnology & Oceanography 47, 1545–1553.

Okubo, A., 1980. Diffusion and Ecological Problems: Mathematical Models. Springer, Berlin, Germany.

Ouillon, S., Douillet, P., Andréfouët, S., 2004. Coupling satellite data with in situ measurements and numerical modeling to study fine suspended sediment transport: a study for the lagoon of New Caledonia. Coral Reefs 23, 109–122.

Ouillon, S., Douillet, P., Fichez, R., Panché, J.Y., 2005. Enhancement of Regional Variations in Salinity and Temperature in a coral reef lagoon, New Caledonia. CR Geoscience 337, 1509–1517.

Pacanowski, R.C., Philander, S.G.H., 1981. Parameterization of vertical mixing in numerical models of tropical oceans. Journal of Physical Oceanography 11, 1443–1451.

Pagès, J., Andréfouët, S., Delesalle, B., Prasil, V., 2001. Hydrology and trophic state in Takapoto Atoll lagoon: comparison with other Tuamotu lagoons. Aquatic Living Resources 14 (3), 183–193.

Pagès, J., Andréfouët, S., 2001. A reconnaissance approach for hydrology of atoll lagoons. Coral Reefs 20, 409–414.

Plus, M., Chapelle, A., Lazure, P., Auby, I., Levavasseur, G., Verlaque, M., Belsher, T., Deslous-Paoli, J.-M., Zaldívar, J.-M., Murray, C.N., 2003. Modelling of oxygen and nitrogen cycling as a function of macrophyte community in the Thau lagoon. Continental Shelf Research 23, 1877–1898.

Rasmussen, B., Josefson, A.B., 2001. Consistent estimates for the residence time of micro-tidal estuaries. Estuarine Coastal and Shelf Science 54, 65–73.

Riddle, A.M., Lewis, R.E., 2000. Dispersion experiments in UK coastal waters. Estuarine Coastal Shelf Science 51, 243–254.

Rougerie, F., 1986. Le Lagon Sud Ouest de Nouvelle Calédonie: spécificité hydrologique, dynamique et productivité. ORSTOM, Paris.

Shen, J., Haas, L., 2004. Calculating age and residence time in the tidal York River using three-dimensional model experiments. Estuarine Coastal and Shelf Science 61, 449–461.

Spagnol, S., Wolanski, E., Deleersnijder, E., Brinkman, R., McAllister, F., Cushman-Roisin, B., Hanert, E., 2002. An error frequently made in the evaluation of advective transport in two-dimensionnal Lagrangian models of advection-diffusion in coral reef waters. Marine Ecology Progress Series 235, 299–302.

Sweby, P.K., 1984. High resolution schemes using flux limiters for hyperbolic conservation laws. SIAM Journal of Numerical Analysis 21, 995–1011.

Takeoka, H., 1984. Fundamental concepts of exchange and transport time scales in a coastal sea. Continental Shelf Research 3, 311–326.

Tartinville, B., Deleersnijder, E., Rancher, R., 1997. The water residence time in the Mururoa Atoll Lagoon: sensitivity analysis of a three dimensional model. Coral Reef 16, 193–203.

Tartinville, B., Deleersnijder, E., Lazure, P., Proctor, R., Ruddick, K.G., Uittenbogaard, R.E., 1998. A coastal ocean model intercomparison study for a three-dimensional idealised test case. Applied Mathematical Modelling 22, 165–182.

Thomann, R.V., Mueller, J.A., 1987. Principles of Surface Water Quality Modelling and Control. Harper Collins, New York, NY.

Vallino, J.J., Hopkinson Jr., C.S., 1998. Estimation of dispersion and characteristic mixing times in plum island sound estuary. Estuarine Coastal and Shelf Science 46, 333–350.

Visser, A.W., 1997. Using random walk models to simulate the vertical distribution of particles in a turbulent water column. Marine Ecology Progress Series 158, 275–281.

Wang, C.F., Hsu, M.H., Kuo, A.Y., 2004. Residence time of the Danshuei River estuary, Taiwan. Estuarine Coastal Shelf Science 60, 381–393.

Zimmerman, J.T.F., 1976. Mixing and flushing of tidal embayments in the Western Dutch Wadden Sea, Part I: distribution of salinity and calculation of mixing time scales. Netherlands Journals of Sea Research 10, 149–191.

III.3 Conclusion

La principale motivation de cette étude était de fournir des indicateurs susceptibles d'intéresser nos collègues biologistes et biogéochimistes, à partir des simulations de MARS3D. Les temps hydrodynamiques ont montré de très bonnes corrélations avec plusieurs variables biologiques et biogéochimiques. L'utilisation des TH produit dans Jouon et al. (2006) dans les travaux Mari et al. (2007), Torreton et al. (Sous presse) et Migon et al. (Sous presse) couronne cette première entreprise de succès.

Mari et al. (2007) souligne une dépendance de la réactivité du carbone organique dissout au temps de vidange local (Local e-Flushing Time : LeFT) (Annexe I).

Les ExoPolymères Transparents (TEP) sont formés par coagulation du Carbone Organique Dissout (DOC). Ils contribuent au pool des substances exopolymères (EPS). Cette étude utilise le rapport des quantitées DOC/TEP comme un indice de la réactivité de Matière Organique Dissoute (DOM). Le TH mis en relation avec la réactivité de la DOM est le LeFT (Local e-Flushing Time). L'hypothèse est faite que le LeFT est un indicateur de l'âge du DOC. Le résultat principal de cette étude est que la réactivité de la DOC diminue à mesure que le DOC vieillit.

Le SLNC comporte des zones où le renouvellement des masses d'eau est lent et où la DOM peut s'accumuler, vieillir et perdre en réactivité physico-chimique par dégradation bactérienne. Ces configurations, dans un contexte où la matière organique est continuellement dégradée peuvent mener à la formation de DOM réfractaire à faible reactivité physico chimique. Dans une étude précédente, Mari et al. (2005) montre que la dégradation bactérienne des TEP augmente leur porosité. Cette augmentation de porosité diminue la teneur du TEP en carbone mais pas son volume extérieur. La quantité de carbone contenu dans le TEP est un paramètre essentiel de la mesure de quantité de TEP par spectrophotométrie. La dégradation bactérienne induit une diminution de la mesure de la quantité de TEP par spectrophotométrie mais ne modifie pas la mesure de la quantité de TEP par microscopie. Les différences entre ces modes d'estimation de la quantité de TEP sont utilisées dans cette étude comme des indicateurs de l'état de dégradation du TEP par les bactéries. Or, cet indicateur soutient l'hypothèse d'une importante dégradation bactérienne des TEP dans les zones faiblement renouvelées.

A l'échelle des océans, une diminution notable de la réactivité de la DOM est peu susceptible de se produire en surface car le turn-over de la DOM y est rapide. En revanche, cette diminution de réactivité est susceptible se produire lors du transport de la DOM vers les profondeurs. En faisant l'hypothèse que la quantité relative de TEP et d'autres particules incluses dans les agrégats organiques en suspension est la même que ce qu'elle est dans l'eau de mer, cette étude estime que la proportion de TEP dans les agrégats organiques en

suspension varie de 20% au niveau du récif barrière à 60 % au fond des baies. En faisant l'hypothèse supplémentaire que les autres particules formant les agrégats organiques sont essentiellement des protistes, cette étude estime à 65 % la part volumique de TEP dans les agrégats organiques au fond des baies, et à 3% au niveau du récif barrière. En considérant une échelle de densité des matériaux inclus dans les grands agrégats (de 1.095 à 1.497 $g.cm^{-3}$ Azetsu-Scott et Johnson, 1992) et en considérant que les agrégats ne comportent pas d'eau interstitielle, les agrégats auraient une flottabilité positive au fond des baies alors qu'ils auraient tendance à couler au niveau du récif barrière. Les résultats de cette étude tendent à montrer que l'hydrodynamique participe à l'accumulation de DOM dans les zones côtières à faible renouvellement.

Torreton et al. (sous presse) met en évidence une correspondance entre la distribution du LeFT et la distribution de variables biologiques et chimiques (Annexe II).

Les relations statistiques entre les variables biologiques (la Chlorophylle a, déterminée selon le protocole exposé dans Holm-Hansen (1965) et la production bactérienne déterminée suivant Briand et al. (2004)), la teneur en silice (déterminée suivant le protocole de Grasshoff et al. (1983)) et le LeFT montrent une bonne cohérence de ces paramètres sur l'ensemble des stations échantillonnées sur le SLNC.

Puisque l'enrichissement de la colonne d'eau se fait dans les baies, cette étude dissocie les baies du reste du SLNC (chenal principal) vis-à-vis de la relation entre le LeFT et les variables biologiques et chimiques.

Les relations statistiques sont recalculées sur le chenal principal du SLNC. Parmi les variables chimiques échantillonnées (ammonium suivant Holmes et al. (1999), nitrate et nitrites suivant Raimbault et al. (1990), phosphate et silice suivant Grasshoff et al. (1983)), seule la silice présente une relation significative avec le LeFT. Cette particularité est expliquée par le fait que la silice n'est pas un élément limitant de la production primaire sur le SLNC (Jacquet et al., 2006), elle est donc davantage conservative que les autres variables chimiques échantillonnées. Les variables Chlorophylle a et production bactérienne montrent de très bonnes corrélations avec le LeFT sur le chenal principal.

Les relations statistiques des paramètres biologiques et chimiques avec le LeFT sont plus variables dans les baies. Dans les baies de St-Marie, Dumbéa et Koutio, les concentrations en silicates sont au dessus de la ligne de régression établie pour le chenal principal, car elles bénéficient d'apports des rivières. La Grande rade, qui n'est pas alimentée par des cours d'eau, présente des valeurs cohérentes avec la tendance du chenal principal du SLNC. Dans les baies, la production bactérienne présente de bonnes corrélations avec le LeFT.

Il est souligné que la qualité des relations statistiques est sensible aux écarts des conditions météos (intensité du vent et direction réels) à la configuration adoptée pour le calcul des LeFT (Alizé 8 $m.s^{-1}$).

Cette étude en vient à la conclusion que le SLNC peut-être considéré comme un écosystème mésotrophe vidangé par les eaux oligotrophes de la Mer de Corail.

L'article de Migon et al. (sous presse) montre par ailleurs une bonne corrélation entre le LeFT et les concentrations en métaux dissouts dans le SLNC.

L'UR CAMELIA a implanté le modèle MARS3D dans le Lagon de Suva à Fidji, et dans la lagune de Cienfuegos à Cuba. Les modules de calcul des TH développés dans le cadre de cette thèse, sont en cours d'implémentation sur ces zones d'études. Ils sont également mis à la disposition des utilisateurs du code MARS3D.

L'exercice de synthèse mené dans cette partie peut être adapté à de nombreuses autres problématiques. Non seulement les traceurs lagrangiens et le champ de concentration passif peuvent servir à construire d'autres outils de synthèse, mais on peut aussi en utilisé de plus complexes. Le concept de l'évolution d'un traceur dans une dimension de classes d'âge (Constituent Age Theory) peut s'appliquer à un traceur dissous (Delhez et al, 1999 ; Deleersnijder, 2001 ; Delhez et Deleersnijder, 2002). L'évolution du traceur se fait alors dans le temps *t*, l'espace (x, y, σ) et la classe d'âge τ. L'équation de transport de C(t, x, y, σ, τ) s'exprime de la manière suivante :

$$\frac{\partial(DC)}{\partial t}+\frac{\partial(DuC)}{\partial x}+\frac{\partial(DvC)}{\partial y}+\frac{\partial(D\tilde{w}C)}{\partial \sigma} = \frac{\partial(DF_x^C)}{\partial x}+\frac{\partial(DF_y^C)}{\partial y}+\frac{\partial(DF_z^C)}{\partial \sigma}+s^C-p^C+\frac{\partial(DC)}{\partial \tau} \qquad \text{Eq. III-7}$$

On remarquera que seul le terme $\frac{\partial(DC)}{\partial \tau}$ différencie cette équation de transport de celle d'un constituant dissous (Eq. II-38).

Le traceur évolue dans des classes d'âge τ dont l'extension peut être fixée suivant les besoins. L'âge d'une masse d'eau peut alors être défini comme le temps écoulé depuis un évènement particulier. L'évènement qui initialise l'âge à zéro peut correspondre à l'entrée dans le volume de contrôle par l'embouchure d'un fleuve (Jouon, 2002), ou par une frontière quelconque du volume de contrôle. Cette initialisation peut également correspondre à d'autres évènements. L'utilisation du traceur évoluant dans des classes d'âge permet de suivre des masses d'eau ayant le même critère d'initialisation et une origine temporelle différente. L'application de cet outil numérique, avec pour critère d'initialisation l'entrée dans le SLNC, en différenciant les masses d'eau par leur chemin d'entrée et des forçages réalistes pourrait fournir une répartition moyenne des âges des masses d'eau sur le SLNC.

Le calcul de temps caractéristique de l'hydrodynamique à partir de la simulation de l'évolution d'un champ de concentration de traceur passif a révélée que le mélange sur la verticale était trop important dans nos simulations. Les différences de concentration virtuelle entre la surface et le fond n'étaient pas significatives, alors que Douillet (2001) présente une circulation contrastée entre ces niveaux. Une étape importante du développement de MARS3D sur le SLNC doit être franchie. Cette étape consiste à paramétrer les flux de chaleurs et d'évaporation aux limites du modèle et à introduire une fermeture turbulente qui reproduira correctement la stratification thermo-haline qui se produit sur le SLNC.

Le codage des fermetures turbulentes à une équation (résolution de q^2, paramétrisation de l cf. pg. 49) et deux équations (résolution de q^2 et de q^2l cf. pg. 50) a été effectué pendant cette thèse. Les fermetures turbulentes de Munk et Anderson (1948), de Pacanowski et Philander (1981) et de Lehfeld et Bloss (1988) font toutes les trois intervenir le nombre de Richardson. Les travaux de Cugier et Le Hir (2002) reprennent les résultats de Nunes Vaz et Simpson (1994) qui proposent une formulation à partir de laquelle le choix des constantes paramétriques permet de retomber sur chacune de ces fermetures turbulentes. L'implémentation de cette formulation dans MARS permettrait de tester ces trois fermetures turbulentes. Le forçage de flux de chaleur aux limites de MARS sera obtenu par couplage avec différents modèles. Le couplage du modèle de circulation atmosphérique WRF (**http://wrf-model.org/index.php**) implanté sur la Nouvelle-Calédonie (Luconthe, 2006), avec MARS3D fournira les flux à l'interface air-mer. Le couplage du model ROMS (Shchepetkin et McWilliams, 2005), implanté par l'UR 65 LEGOS sur le Pacifique Sud-Ouest (Couvelard et al., en cours) avec MARS3D, fournira les flux de sel et de température aux limites ouvertes de MARS3D. Les données hydrologiques seront fournies par le service compétent du territoire de Nouvelle-Calédonie. La base de donnée CTD de l'UR CAMELIA sera ensuite d'une grande utilité pour valider le transport de sel et de température dans MARS3D.

Chapitre IV MODELISATION DE LA MER DE VENT SUR LE LAGON SW DE NOUVELLE-CALEDONIE

IV.1 Introduction

La première modélisation du transport de sédiments fins dans le SLNC a montré qu'il existait une différence significative entre la concentration de particules en suspension simulée par le modèle de transport particulaire et la turbidité mesurée, notamment par petits fonds. Bouron Morin (2001) a identifié un signal de turbidité rémanent entre deux pics de turbidités induit par les effets combinés du vent et de la marée en sur une station du SLNC. Les différences entre turbidités mesurées et concentrations simulées peuvent être interprétées comme une insuffisance dans la remise en suspension au sein du modèle. Pour palier ces différences, Ouillon et al. (2004) a introduit une zonation du taux d'érosion conduisant à optimiser les sorties du modèle en regard des mesures.

Le modèle de transport prend en compte la contrainte de cisaillement induite par le courant (Douillet et al., 2001 ; Bouron Morin, 2001 ; Ouillon et al., 2004). Or le courant n'est pas le seul forçage responsable des contraintes de cisaillement qui s'appliquent sur le fond. Bien que le SLNC soit relativement abrité des houles océaniques par le récif barrière, son extension et le régime de vent local permettent le développement d'une mer de vent pouvant atteindre des hauteurs significatives supérieurs à 1.5 m. En eaux peu profondes, c'est-à-dire sur les zones telles que :

$$D < 0.1\, gT^2 \quad \text{ou plus simplement} \quad D < 10Hs \qquad \text{Eq. IV-1}$$

où D est la hauteur d'eau, T la période la houle et H_s sa hauteur significative, il se produit des oscillations des particules d'eau au dessus du fond liées au passage des vagues. Cette oscillation crée une contrainte de cisaillement qui est quadratique en fonction de la vitesse orbitale de la houle au fond :

$$\tau_w = 0.5\, f_w\, \rho_0\, U_b^{\,2} \qquad \text{Eq. IV-2}$$

où τ_w est la contrainte de cisaillement provoquée par la houle, f_w est un facteur de frottement (Jonsson, 1966) et U_b est la vitesse orbitale de la houle au fond. Pour une houle sinusoïdale, la vitesse orbitale U_b au fond s'exprime suivant :

$$U_b = \frac{\pi\, Hs}{T \sinh\left(2\pi D / L\right)} \qquad \text{Eq. IV-3}$$

La contribution de la contrainte de cisaillement liée aux vagues sur la remise en suspension, jusqu'à présent non prise en compte dans le modèle hydro-sédimentaire, est l'une des causes des écarts observés entre concentrations simulées et turbidités mesurées.

Afin d'explorer les effets de la mer de vent sur la remise en suspension des sédiments benthiques, il est nécessaire de mettre en place et de valider un modèle numérique reproduisant la génération et la propagation des vagues de vent sur le SLNC. Cette partie y est consacrée. Des mesures de houle non-directionnelles et directionnelles ont été effectuées grâce au déploiement d'un houlomètre Aanderaa (Wave and Tide Recorder 9) et d'un vélocimètre acoustique Doppler Sontek (ADVOcean). Le choix du modèle de vagues s'est porté sur le modèle WaveWatch III (WWATCH) qui est ouvert au domaine public. D'autres modèles similaires sont également ouverts au domaine public, tels que le modèle explicite WAM-Cycle 4 (Komen et al., 1994) ou le modèle implicite SWAN (Booij et al, 1987 ; Booij et al., 1999 ; Ris et al., 1999). Des applications en domaine côtier de ces modèles ont été effectuées par exemple par Monbaliu et al (1999, 2000) avec WAM, et par Holthuijsen avec SWAN (Holthuijsen et al., 1989). L'adoption de WWATCH a permis de bénéficier des résultats de travaux préliminaires de Bel Madani (2003), et d'une collaboration entre Camélia et Loys Schmied de l'Université du Sud Toulon Var.

La difficulté majeure de ce travail a concerné la mesure de vagues de vent dans un milieu à fetch limité. En effet, ces vagues ont en général une faible hauteur significative (de l'ordre du mètre) et une période relativement courte (quelques secondes). L'instrumentation disponible dans le commerce pour la mesure des vagues est bien adaptée à la mesure de vagues plus haute et plus longue, mais leur déploiement en condition de « petites » vagues et l'analyse des mesures nécessitent de nombreuses précautions pour que l'on puisse comparer données et simulations numériques à des fins de validation. L'article qui suit présente en détail les travaux conduits sur le SLNC, les difficultés de la mesure des vagues en condition de fetch limité, la démarche adoptée, l'analyse des données, et la validation du modèle de vagues.

IV.2 Publication:

Jouon, A., Lefebvre, J.P., Douillet, P., Ouillon, S., Schmied, L., submitted. Wind wave modelling and measurements in a fetch-limited semi-enclosed lagoon. Coastal Engineering

Wind wave modelling and measurements in a fetch-limited semi-enclosed lagoon

Aymeric Jouon, Jean Pierre Lefebvre, Pascal Douillet, Sylvain Ouillon, Loys Schmied.

Abstract

WaveWatch III (WWATCH), a public-domain wave model, is used to simulate the wind wave distribution in the Southwest reef Lagoon of New Caledonia (SLNC). The *in situ* measurements are compared to non-directional statistical wave parameters obtained from Aanderaa WTR9 wavemeter gauge and from pressure data provided by a Sontek ADVOcean. The fetch-limited context in which the measurements were achieved required special attention to the depth at which the probe was deployed. As the cut-off frequency of the wave measuring instrument decreases with depth, the measurement of high frequency waves calls for deployment in shallow water. If this is generally not a problem in opened sites with sufficiently long waves, this point is very crucial in quasi-enclosed basins such as the southwest lagoon of New Caledonia. If this criterion is not meet, the truncation of the wave spectrum may be too important, therefore leading to statistical wave parameters unrepresentative of actual waves. The ADV data analysis was adapted to the fetch limited constrains. WWATCH is used to simulate the generation and propagation of wind waves in the SLNC. As most of the oceanic waves' energy is dissipated over the barrier reef, locally generated wind waves are the essential component of the sea state in the lagoon. In order to validate the wind wave field simulated by WWATCH over the same frequency band as the measurements, filters were applied on the directional wave spectra obtained from the PUV measurements of the ADV in order to avoid non simulated swell component in the measured wave field. WWATCH wave spectra were also bounded in the high frequencies at the ADV cut-off frequency. The wave model is then validated from time-series of measurements in the SLNC under variable forcings.

Keywords

Wave modelling - Shallow water - Fetch-limited – Directional wave spectrum - Lagoon - New Caledonia - WaveWatch

8. Introduction

Since 1996, the South-West Lagoon of New Caledonia (SLNC) has been a reference site for studying the anthropogenic impacts on a coastal coral reef ecosystem. The study of the hydrodynamic functioning of the lagoon stands on *in situ* measurements (Ouillon et al., 2005 ; Bonneton et al., 2007 ; Jouon et al., submitted), remote sensing (Ouillon et al., 2004), as well as on numerical model simulations (Douillet, 1998 ; Douillet et al., 2001 ; Jouon et al., 2006). A fine particle transport model has been coupled to a 3D hydrodynamic model. Its calibration

and validation were first based on comparisons between deposition rates and fine sediment coverage (Douillet et al., 2001), then on turbidity measurements and maps derived from satellite data (Ouillon et al., 2004). Except during floods which are scarce and generally short (a few days per year at maximum), rivers bring little sediment to the lagoon. Re-suspension is thus the main origin of particles in the SLNC (Clavier et al. 1995). In many coastal environments, waves have a major effect on re-suspension of benthic particles (Booth, 2000; Prandle et al., 2000). This study focuses on the wind wave field on the SLNC. The validation of a wave generation and propagation model is undertaken. This wave model provides necessary data to take into account the influence of waves on sediment resuspension over shallow waters (Grant W.D. et Madsen, 1979, Zang et Li, 1997). Furthermore, a validated wave model could be used to simulate the extreme wind seas under storm conditions on the SLNC.

In opened lagoons, ocean waves and wind-waves superimpose. In the SLNC, passes are relatively narrow compared to the enclosing reef extension. Although ocean waves are strongly attenuated by wave breaking and friction over the enclosing reef flat (Bonneton et al., 2007), some of the oceanic waves enter the lagoon through the passes. The local wind intensity coupled to the dimensions of this semi-enclosed basin make it possible for wind to generate waves. A higher limit estimation of sea state characteristics can be assessed following empirical SMB (Sverdrup, Munk, Bretschneider) method (Bretschneider, 1970). For a 10m.s^{-1} trade wind blowing over a 45 km fetch, during at least 5 hours, the SMB method gives a significant wave height of 1.25 m and a 5 s peak spectral period in infinite depth.

The goals of this study were to check the ability of WaveWatch III (WWATCH) to simulate the wind wave field in a coastal fetch-limited environment and to quantify oceanic waves entering the SLNC. For that purpose, we compared *in situ* measurements to wave spectra modelled by WWATCH at different sites and under variable wind forcing conditions.

However, the two approaches did not yield exactly the same data. On one hand, the implementation of WWATCH used in this study did not simulate the transformation of oceanic waves, whose frequencies are low (<0.1 Hz). On the other hand, due to the attenuation of high frequency components with depth, there is an intrinsic limitation of spectra measured in the field at high frequencies. Fortunately, by deploying wave measurement devices near the surface and selecting a proper value of the cut-off frequency, it was possible to access an important part of the wind-generated spectrum. Precautions are taken to compare modelled data to measurements over the shared spectral band.

9. The study site

New Caledonia is a tropical island located in the Western Pacific, about 1500 km east of Australia. It is surrounded by a 23 400 km^2 lagoon. Noumea, the island's main city and home to half of its population, is located on the south-west coast. The lagoon area, which surrounds

Noumea is known as the "South West Lagoon of New Caledonia" (SLNC). Its depth averages 17.5 m and there are many coral reef islands in the SLNC (Figure 1). Its width varies from 5 km (northern limit) to 40 km (southern limit). It is separated from the open ocean by a barrier reef incised by deep and narrow passes. Statistic analysis of meteorological data (Douillet et al., 2001; Ouillon et al., 2005) brought out the South-easterly trade wind regime as the most frequent and long-lasting wind forcing. A second wind regime was also identified (Bujan, 2000), when more variable Westerly winds are predominant during shorter episodes.

The local wind generates wind waves in this semi-enclosed lagoon. Except for episodes of low wind intensity, the wind wave field is fetch limited. On the SLNC, the mean wind waves have generally short periods (of less than 5 s), because they result from the wind action over a fetch of a few tens of kilometres long at maximum.

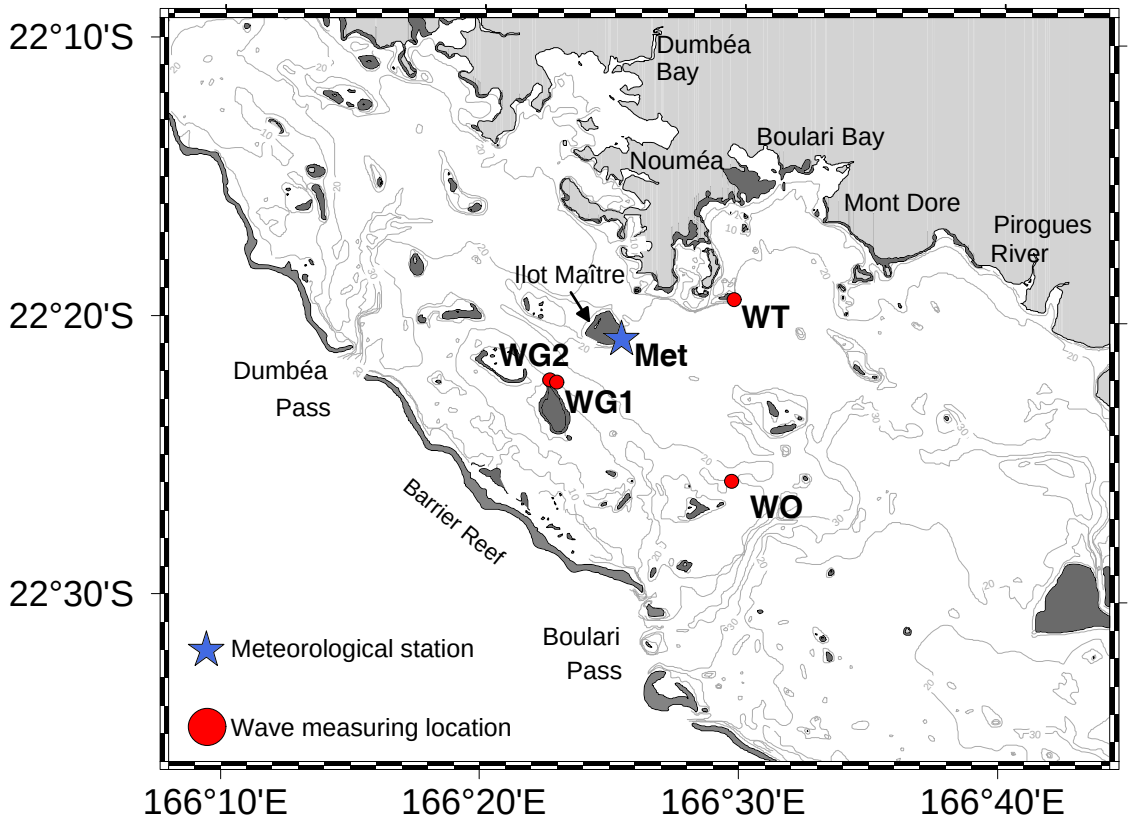

Figure 1 SLNC bathymetry and wave measuring locations

10. Material and Methods

10.1. Field Measurements

Two devices have been used in this study: a wave and tide recorder (WTR9, Aanderaa) and an acoustic Doppler velocimeter (ADVOcean, Sontek). For each measurement session, they were deployed simultaneously at the same locations, mounted on a nonmagnetic structure that assures the sensors to be located 0.5 m over the seabed. Both pressure measurements were achieved every 30 minutes.

10.2. Sampling strategy

Because the wave-induced pressure and velocity components decrease exponentially with depth and are not significant at depths greater than a half wave length, it was not possible to measure the wave parameters by deploying wave gaugemeters at the sea bed at a depth of more than a half wavelength (about 5 m under mean trade wind condition).

This short wave period context required taking special care in choosing the location and depth at which the *in situ* measurement were achieved. In order to get time-series of data with a cut-off frequency as high as possible, the wave gauges were placed close to the surface and at locations where wind waves were likely to have high amplitudes. Both probes were fix-mounted and deployed close to sea-bed to avoid boat collisions during measurement episodes. The shallower waters are located at the head of bays. Due to topographic constrains, the wind intensity and direction are different in the bays than in the outer lagoon. As the wind forcing of the model was measured in the outer part of the lagoon, these shallow areas were not recommended for model validation purposes. Other shallow areas are located around coral islands. The locations of wave gauges deployments were chosen in the windward side (defined for the main trade wind) of small reefs or small islands, within the main track of the lagoon where the waves have the greater fetch. On the windward side of these islands, the reef fall is abrupt and depth increases quickly from approximately 5 to 20 m. Waves were recorded at different sites in the SLNC (Figure 1). Summary of the deployment sessions is given in Table 1.

Name of station	Session	Location (WGS84)	Water Depth (m)
WO	06/03/31-06/04/14	166°29.76' E - 22°25.33' S	3.6
WG1	06/05/19-06/06/01	166°22.79' E - 22°22.17' S	5.5
WG2	06/06/08-06/06/11	166°22.39’ E -22°22.03’ S	6.2
WT	06/08/08-06/08/21	166°29.77’ E - 22°19.04' S	4.7

Table 1 Summary of session and locations of wave recording

10.3. WTR9 Wave parameters estimation

WTR9 samples pressure at the frequency of 2 Hz over 512 s long episodes. The device includes an inboard processing routine that directly estimates the significant height (H_s) and the mean zero crossing period (T_{02}). Prior to deployment, WTR9 required selecting a distance to seabed and a mooring depth amongst fixed intervals for data analysis purpose. WTR9 sets automatically the cut-off frequency (f_c) according to the deployment depth (f_c=0.5 Hz for deployment at 5 m depth).

10.4. ADV Wave parameters estimation

Non-directional parameters

The used ADV Sontek was equipped with a high accuracy resonant pressure transducer (Drück). It yielded time series sampled at 5 Hz of pressure and tri-dimensional components of velocity over 410 s long episodes. In a first step, the pressure time-series collected by ADV were used to determine the wave spectrum and non-directional wave parameters.

The mean water level (MWL) was estimated from each pressure sample burst as the mean pressure corrected by the sensor elevation from the seabed. The wave-induced pressure time-series were deduced from the pressure time-series corrected from the MWL. From a wave-induced pressure data set, we estimated a one sided-PSD (Power Spectrum Density) of pressure ($P_\eta(f)$) using Welch's averaged modified periodogram method of spectral estimation (Welch, 1967). This PSD is related to the power spectrum $S_{xx}(f)$ by:

$$P_{onesided}(f) = \frac{2}{f_s} S_{xx}(f) \quad \text{for} \quad 0 \le f < \frac{f_s}{2}$$

$$P_{onesided}(f) = 0 \qquad \text{otherwise} \qquad \text{eq 1}$$

where f_s represents the sampling frequency. The final estimated PSD results from the averaging of many PSDs estimated on 512 samples segments, which overlap by 25%, and corrected by a Hamming window. The PSD corresponding to the sea surface elevation ($P_\eta(f)$) is deduced by application of the transfer function $H_w(f)$:

$$P_\eta(f) = \frac{P(f)}{H_w(f)^2} \qquad \text{eq 2}$$

with

$$H_w(f) = \rho g \frac{\cosh(k(h+z))}{\cosh(kh)} \qquad \text{eq 3}$$

where h is the water depth and z is the distance from the MWL to the sensor, counted positively upward. For each frequency, the corresponding wave number (k) is computed using the generalized first order dispersion relationship (Leblond et Mysak, 1978) for surface wave and neglecting all ambient currents, as follows:

$$\omega = 2\pi . f = \sqrt{gk \tanh(kh)} \qquad \text{eq 4}$$

where g is the acceleration of gravity.

The PSD corresponding to the elevation of the sea surface is hereafter called wave spectrum. It is used to estimate the significant height (H_s) and the mean zero crossing period (T_{02}) according to the following equations:

$$Hs = 4\sqrt{m_0} \quad \text{eq 5}$$

$$T_{02} = \sqrt{\frac{m_0}{m_2}} \quad \text{eq 6}$$

where the statistical zero and second moments (m_0, m_2) are estimated from the wave spectrum $P_\eta(f)$ bounded by a low frequency (f_l) and the cut-off frequency (f_c) as follows:

$$m_k = \int_{f_l}^{f_c} P_n(f) f^k df \quad \text{eq 7}$$

Directional density power spectrum

The directional density power spectrum was assessed using the wave spectrum $P_\eta(f)$, computed from the ADV pressure time-series and the spreading function $D_\eta(f,\theta)$ derived from the tri-dimensional components of velocity measured by the ADV. We assume that the directional density power spectrum results from two decorrelated functions of the elevation of the sea level, $P_\eta(f)$ and $D_\eta(f,\theta)$, according to:

$$P_\eta(f,\theta) = P_\eta(f).D_\eta(f,\theta) \quad \text{eq 8}$$

Inboard processing of ADV corrects the pitch and roll, and gives the Northward, Eastward and Upward velocity components according to the magnetic direction reference. A supplementary correction must be applied by the user in order to convert the velocity components into the geographical referential (in New-Caledonia and in year 2007, the magnetic declination is 13°N).

The spreading function $D_\eta(f,\theta)$ was computed from the East- and North- wave orbital velocity data. The measurements were scaled so that they had equal standard deviation and zero mean. The spreading function was estimated by use of routines adapted from the ones developed by the Wave Analysis for Fatigue and Oceanography Group (WAFO Group, 2000). At this stage, the optimal cut-off frequency was selected in order to extend the high frequency bound at the most. The one sided auto and cross power spectral densities of velocity were estimated and the corresponding transfer function $G_w(f)$ was applied:

$$G_w(f) = 2\pi f \frac{\cosh(k(h+z))}{\sinh(kh)} \quad \text{eq 9}$$

Extended Maximum Entropy Methods (EMEM) was used to estimate this function (Hashimoto, 1977). The obtained spreading function $D_\eta(f,\theta)$ was normalized in order to fulfil the condition:

$$\int_0^{2\pi} D_\eta(f,\theta)d\theta = 1 \quad \text{eq 10}$$

Some artificial low energy peak may appear out of phase with the main peak, when the latter is of high energy. This drawback is inherent to the method, when second order parameters are estimated. The EMEM iteratively seeked the optimal order for the estimation (Hashimoto, 1977). For our dataset, the optimum order was always comprised between 2 and 3. Nevertheless, the eventual appearance of a weak artificial peak cannot conduct to an ambiguity in the main direction.

10.5. Numerical modelling

WaveWatch III model

The WaveWatch III (WWATCH) public-domain model was implemented to simulate the wave generation and propagation in the SLNC. After sensitivity analysis on WWATCH-simulated H_s, the choice was made that the implementation of WWATCH in the SLNC does not take into account neither the effects of currents on the wave field, nor the variations of surface elevation. The model and the tuning of the model parameters are briefly presented. Simulations of mean tide level and unsteady wind events are presented.

The WWATCH model, a 'state-of-the-art' spectral wave model for deep and intermediate water depths, is a third generation wave model developed by Hendrik Tolman at NOAA/NCEP (US National Center for Environmental Prediction). It is based on previous versions of WWATCH (e.g. Tolman 1989). Version 1.18 of WWATCH (Tolman, 1999) was used in this study.

The governing equations for wind wave propagation and generation are well established (see a review of the basic papers and books in Tolman, 1991b). A detailed description of the model is given in Tolman (1989, 1991a, b) and the source terms are fully presented in Tolman and Chalikov (1996). The physics of the model is discussed here only as far as it is relevant for the discussion of the model tuning and for the simulations.

Wind waves are usually described with an energy or variance density F that depends on wave parameters such as the wave number k, the intrinsic or relative frequency σ (as observed in a frame of reference moving with the mean current $\vec{U}$), the absolute frequency ω (as observed in a fixed frame) and the wave direction θ. In the linear theory of surface gravity waves on slowly varying depths and currents (e.g. Leblond and Mysak 1978), wave number and frequencies are interrelated in the dispersion relation. In this implementation of WWATCH on the SLNC, time variations of depth have been neglected as well as the influence of currents on the wave field ($\vec{U} = \vec{0}\,;\, \sigma = \omega$). The dispersion relation is considered as in eq. 4.

In WWATCH, changes of the variance density F due to propagation over varying depths and currents are described using the action balance equation:

$$\frac{\partial N}{\partial t} + \vec{\nabla}.\left[\left(\vec{C}_g + \vec{U}\right)N\right] + \frac{\partial}{\partial \omega}\left(C_\omega N\right) + \frac{\partial}{\partial \theta}\left(C_\theta N\right) = \frac{S_{wind}}{\sigma} + \frac{S_{ds}}{\sigma} + \frac{S_{nl}}{\sigma} + \frac{S_{bf}}{\sigma} \qquad \text{eq 11}$$

where N = F(x, y; f, θ; t) / σ is the action density spectrum, θ is the direction of propagation of the wave, $\vec{C}_g$ is the group velocity, and C_ω and C_θ are the propagation velocities of frequency and direction, respectively, in spectral space. The left-hand terms of eq 11 represents the local rate of change of wave action density, propagation, and shifting of frequency and direction due to temporal and spatial variations of the mean water depth and the mean current (tides, surges etc.). S_{wind} represents wave growth and decay due to the actions of wind. S_{ds} corresponds to the whitecapping and turbulent dissipation. S_{nl} stands for the nonlinear wave-wave interactions, and S_{bf} represents the bottom friction dissipation. S_{wind} and S_{ds} refers to separate processes, but they may be considered as interrelated, since their balance governs the integral growth characteristics of the wave model. Two source term options are available in WWATCH for these two terms: the first is based on cycles 1 through 3 of the WAM model (WAMDIG 1988), the second, used in this study, is based on Tolman and Chalikov (1996). Nonlinear wave-wave interactions are modelled using the discrete interaction approximation of Hasselman et al (1985) for S_{nl}. S_{bf} is modelled by the empirical JONSWAP expression (Hasselman et al. 1973). The formulation of input and dissipation by Tolman and Chalikov (1996) is mostly used as a tuneable closure term. WWATCH needs specific tuning in each practical application.

The model outputs are the directional wave spectrum and several synthetic parameters retrieved through computations based on the directional wave spectrum.

Wave model implementation in the southwest lagoon of New Caledonia

During the wave recordings, wind was continuously measured at 10 m altitude at one station in the SLNC (see location in Figure 1). In a first attempt, wind is assumed to be homogeneous over the calculation area. Wind data at Ilot Maître were averaged over 30 mn and used as input for the wave model.

The implicit assumption of the considered equations is that the medium (depth and current) as well as the wave field vary on time and space scales that are much larger than the corresponding scales of a single wave. The modelled physics do not cover conditions where the waves are severely depth-limited or in the case of wave reflection. The model can be applied outside the surf zone at spatial scales of several hundreds of meters or several kilometers. The calculations over the SLNC were performed on a Cartesian grid, with a 500 m mesh size in both directions. The grid is the same as those of the hydrodynamics and sediment transport model described in Douillet et al (2001).

The WWATCH output data used in this study is the given directional wave spectrum. Although WWATCH gives the average period and the significant wave height, as the WTR9

used in this study gives T_{02} and H_s, we chose to compute T_{02} from the directional wave spectrum in order to compare the same statistical parameters from measured and simulated data. For better consistency, and to be capable of performing high frequency filter on the WWATCH data, we chose to do the same for H_s.

10.6. Selecting the shared frequency band

In order to evaluate of the ability of WWATCH to simulate wind waves in the SLNC, we chose to bound the modelled spectra up to the cut-off frequency fixed for measurements and the measured spectra down to the lowest modelled frequency in order to filter the swell. The obtained bandwidth corresponds to the wind wave field truncated by cut-off frequency.

Cut-off frequency

The cut-off frequency (f_c) plays an important role in the representation of the wave spectrum given by the probes used in this study. This parameter has no absolute value, but is only an empirically selected parameter. The cut-off frequency is strongly related to the measurement settings by the surface to depth transfer functions (eq. 6 and 8). It is also related to the magnitude of the high frequency components and subsequently to the sensor sensitivity. It is defined as the highest frequency value which corresponds to a component with an acceptable signal to noise ration (SNR).

As stated before, the value of f_c can only take pre-selected values for the WTR9. For deployment conditions on all sites, it corresponded to a cut-off frequency value of 0.5 Hz.

The choice of a too high cut-off frequency produces a rise in the sea surface elevation PSD at frequencies concomitant to cut-off frequency. The value of the cut-off frequency was chosen to coincide the highest value that does not produce such side effects. For comparison matter, we also chose to limit the selection to the frequency scale used by the model:

$$f(i) = 0.11 \times 1.1^{(i-1)} \qquad \text{eq 12}$$

where i corresponds to i^{th} frequency class of WWATCH. Following these guidelines, the cut-off frequency was set to 0.46 Hz for the ADV.

Lowest frequency

Oceanic waves propagating inside the SLNC where identified by their low frequencies (<0.1 Hz). No simulated wind waves reach such low frequencies on the SLNC. In order to evaluate the capacity of WWATCH to simulate wind waves on the SLNC, the filtering of frequencies lower than 0.17 Hz was performed on the measured sea surface elevation DSP. This frequency value is low enough not to interfere with wind waves frequencies and high enough to filter swell.

10.7. Swell contribution to SLNC wave field

Filtering non-simulated wave field components (i.e. swell) also allows quantifying the contribution of these components to the global wave field. It is done by comparing the values of H_s and T_{02} on filtered and non-filtered data. The contribution of filtered wave component to the statistical parameters H_s is computed following the equation:

$$\%Hs_{swell} = \frac{Hs - Hs_{F\,swell}}{Hs} * 100 \qquad \text{eq 13}$$

where *F* stands for filtered data. H_s can be replaced by T_{02} to compute the contribution of the swell to the mean zero crossing period.

10.8. Assessing the ability of WWATCH to simulate wind waves

The agreement between simulations and measurements is assessed through correlation coefficient and linear regression computations over H_s, T_{02} and the mean direction of the wave field (θ_m). The closer the correlation factor is to unity, the better the likelihood between model and measurements. The best least squares fitted line between measurements and simulations yields a regression factor (a) and an offset (b) which can also be interpreted as gain coefficient and an offset coefficient to apply to the WWATCH data to best fit the measurements.

11. Results

11.1. Meteorological conditions during experiments

WO station is the furthest station from the coast (see Fig. 1). During the measurements at WO, wind had globally weak intensity (≤ 5 m.s^{-1}) and variable direction (Fig. 2). Established trade wind (coming from SE with wind speed of approximately 10 m.s-1) occurred from the beginning of measurement episode (31-Mar-2006 12:00) to the end of the same day. The same conditions reappeared on the 03-Apr-2006 during the morning until the evening of 04-Apr-2006 and took place for a longer while from 10-Apr-2006 at noon until the end of measuring episode (12-Apr-2006). These episodes were interposed by long-lived episodes of light wind intensity (≤ 5 m.s^{-1}) with variable direction.

WG stations are located approximately at equal distance between the shore and the barrier reef. Two deployments took place nearly at the same location (see Fig. 1). WG1 deployment was globally characterised by medium intensity trade wind (≤ 10 m.s^{-1}). This predominant condition happened from the beginning of deployment period (19-May-2006 at mid-day) to the morning of 25-May-2006, then reappeared on 27-May-2006 around mid-day and definitely disappeared during the night from 30 to 31-May-2006 (Fig. 3). These episodes were interposed with light winds coming from a westerly direction. Experiment at WG2 was

shorter lived for technical reasons, with consequently more homogeneous wind conditions during the deployment period that can be characterised as established trade winds (≈ 10 $m.s^{-1}$, see Fig. 4).

WT is the closest station to the shore (see Fig. 1). During this deployment session, wind varied slowly following 5 successive stages (Fig. 5). From beginning of the session (08-Aug-2006 at mid day) to 10-Aug-2006 at mid day, wind intensity slowly decreases from 10 $m.s^{-1}$ to near 0 with a direction moving from South to North. From then to the morning of 15-Aug-2006, the direction progressively shifted North-Est through South with medium to low wind speed (between 5 and 10 $m.s^{-1}$). A light trade wind episode occured (up to 17-Aug-2006 at mid day) followed by an established trade wind episode which ended on 18-Aug-2006 in the evening. The deployment session ended with a trade wind episode of variable intensity.

11.2. Comparison of field measurements

In this section, the statistical wave parameters H_s and T_{02} measured by WTR9 and ADV without filtering swell are compared.

On all mooring deployments, H_s and T_{02} from WTR9 show much similarity with those obtained by the use of ADV (Figures 2 to 5). On all mooring deployments, at first sight, curves of H_s from ADV and WTR9 follow the same trend as the wind intensity (Figures 2 to 5). H_s values are slightly higher on ADV data than on WTR9, and T_{02} values are slightly lower on ADV data than on WTR9. The trend of T_{02} is different from that of the wind speed. WG1 and WT show episodes of large differences in T_{02} provided by ADV and WTR9, T_{02} computed from WTR9 data reaching very high values. These episodes corresponded to low H_s phases (Figures 2 to 5).

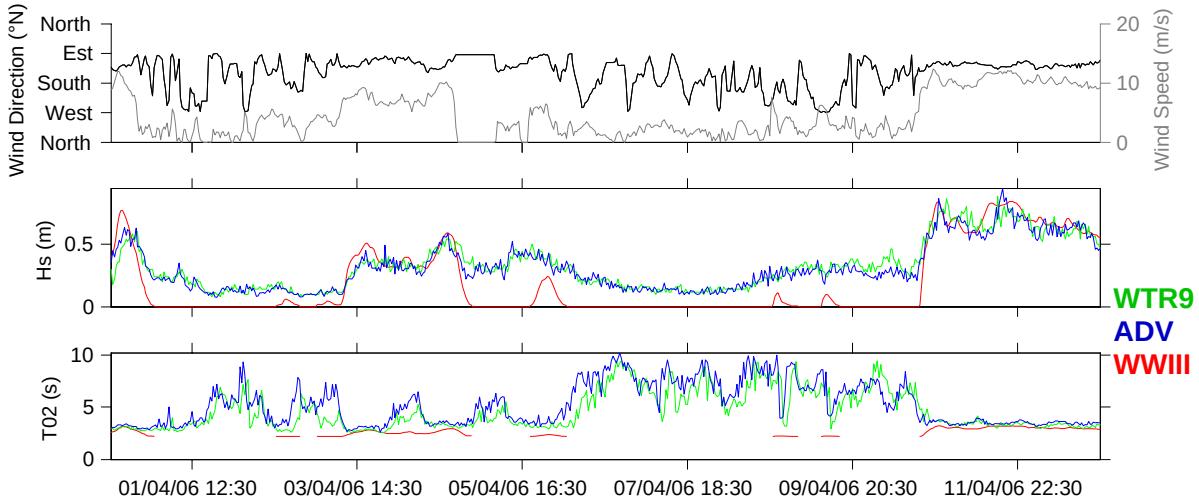

Figure 2 Wind Forcing, H_s and T02 from WTR9, ADV and WWATCH; for WO records.

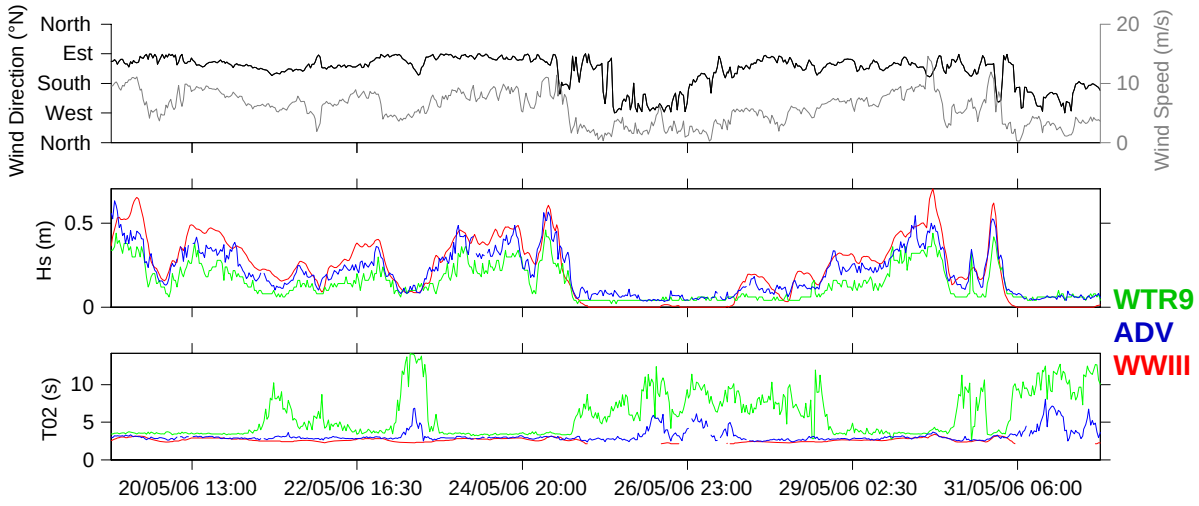

Figure 3 Wind Forcing, H_s and T02 from WTR9, ADV and WWATCH; for WG1 records.

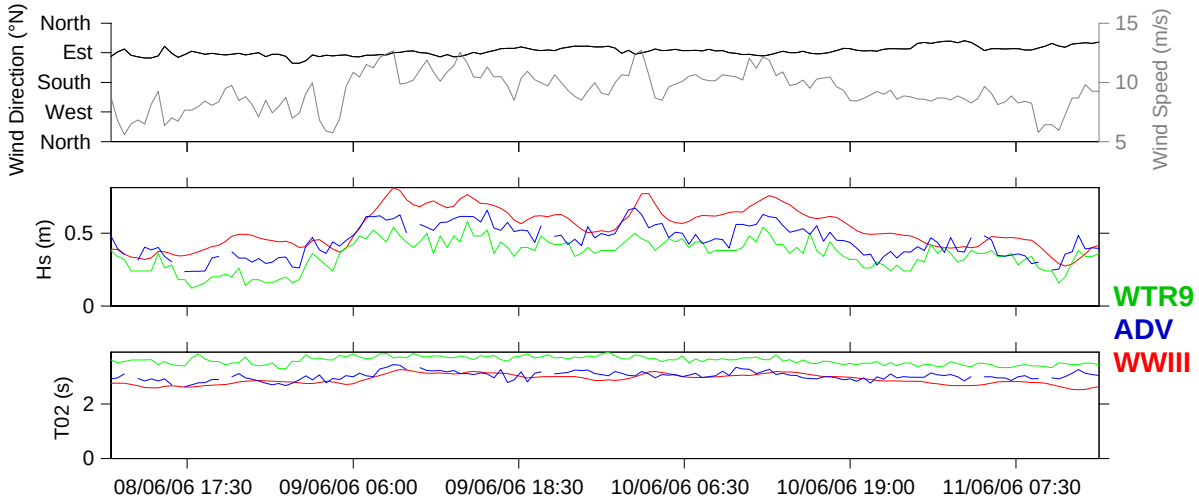

Figure 4 Wind Forcing, H_s and T02 from WTR9, ADV and WWATCH, for WG2 records.

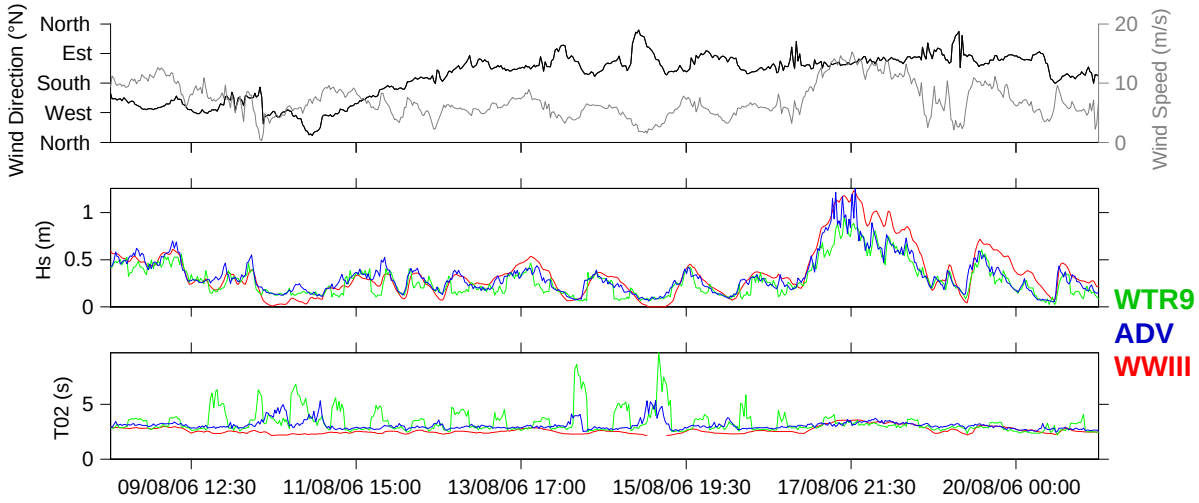

Figure 5 Wind Forcing, H_s and T02 from WTR9, ADV and WWATCH; for WT records.

11.3. H_s and T_{02} measurements and simulations

In agreement with H_s field data, H_s computed from WWATCH follows the same trend as wind intensity (Figures 2 to 5). Values of H_s drop down to zero during episodes of very weak wind intensity. This feature is partly due to our choice of recomputing H_s from the directional wave spectrum given by WWATCH, this output precision is limited by its format (ASCII representing at the most 10^{-3} m^2.s). However, there was no other option giving us the capacity to filter high frequencies of the directional wave spectrum given by WWATCH.

During light wind episodes (<5 m/s), H_s simulated by WWATCH are lower than the measured H_s. This feature is particularly well represented on WO data (Fig. 2). The WO mooring deployment period was coincident to the lowest wind velocities amongst all campaigns. During stronger wind episodes (>5 m/s), H_s calculated using WWATCH were higher than the measured H_s. As WG2 was the most windy campaign, this feature is particularly salient on WG2 data (Fig. 2, Table 2).

The modelled T_{02} values vary little as compared to measurements. Values of T_{02} given by WWATCH are also globally lower than the ones measured. The trend of T_{02} shows similarity with wind speed trend (Figures 2 to 5).

			WTR9			ADV		
			a	b	r	a	b	r
WWATCH	H_s (m)	WO	1.221	-0.144	0.853	1.264	-0.149	0.890
		WG1	1.356	0.057	0.884	1.140	0.004	0.908
		WG2	0.965	0.191	0.736	0.965	0.101	0.792
		WT	1.308	-0.012	0.903	1.178	-0.029	0.909
	T_{02} (s)	WO	-0.097	3.001	-0.306	-0.124	3.160	-0.494
		WG1	-0.066	2.952	-0.663	-0.026	2.688	-0.046
		WG2	0.635	0.619	0.487	0.575	1.165	0.490
		WT	-0.052	2.780	-0.147	0.061	2.422	0.071

Table 2 Parameters of the least square best fitted line between simulated and measured wave parameters and correlation coefficient

The values of the correlation coefficient for H_s are close to unity (Table 2). They are systematically better using ADV data than WTR9 data. At WO, WG1 and WT, the regression factor was greater than unity, WWATCH tended to undershoot the data. At WG2, it was the opposite. Offsets were in every case less than 20 cm and did not reveal any global trend over the deployment sessions.

The correlation for T_{02} were very low, the data did not seem to be co-related. Although it was far from unity, the correlation coefficient of T_{02} at WC2 (the most windy deployment) was better than during the other experiments.

11.4. Swell contribution to wave field on the SLNC

WATCH and ADV data were compared before and after filtering of swell frequencies. When ADV data is filtered from swell, the comparison is made over the same frequency band. The contribution of swell to the wave field (Figure 6) yielded the same results for H_s and T_{02}. The periods during which it is very important coincide with low intensity wind episodes.

On Figure 6, episodes of higher contribution of swell to the wave field corresponding to a decrease in wind intensity have been surrounded by a blue rectangle. During WG1 and WT experiments, the decrease in wind intensity went along with a variation of wind direction. At WT, a dotted line materialises a threshold of wind intensity (approximately 5 $m.s^{-1}$) under which the contribution of swell reaches values around 50%. At WO, the surrounded areas of the graph underline periods where the wind direction was relatively constant and the wind intensity drastically increased; these episodes correspond to lowering of swell contribution to SLNC wave field. At WT, wind came from North-West during the episode surrounded in red. The wind velocity during this stage was higher than the threshold line, and the contribution of swell to the wave height reached around 50%. This can be the consequence of an even more limited fetch in that particular direction at that station. Wind was so weak that swell contribution became important.

WG2 was characterised by a well established trade wind regime. The wave field was well developed and the contribution of oceanic waves to wave height did not exceed 3%.

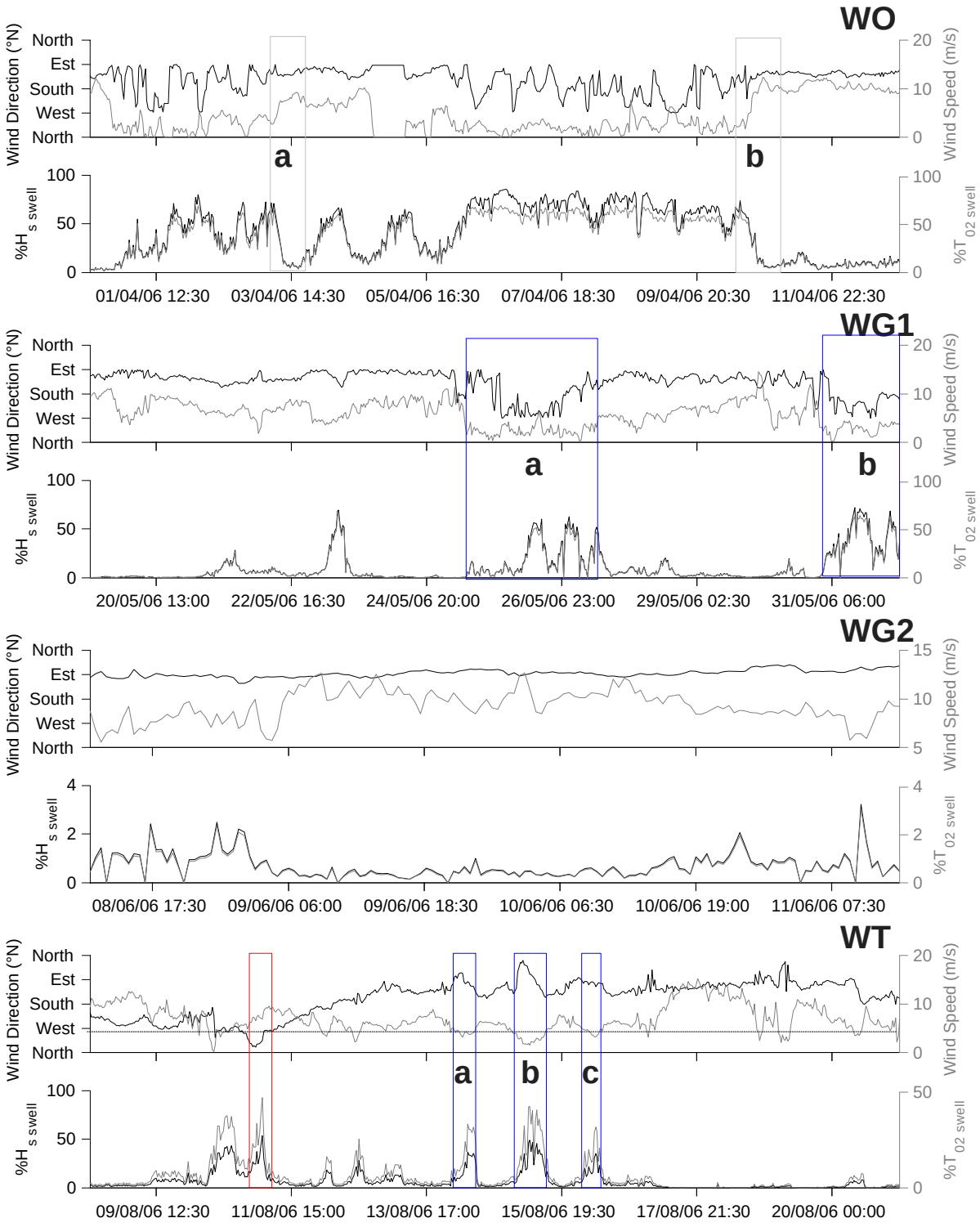

Figure 6 Wind conditions and swell contribution to SLNC wave field for all deployment sessions

11.5. Ability of WWATCH to simulate wind waves

The direction of the computed wind waves follows the wind direction, and the most energetic episodes correspond to high wind speed phases (Figures 7 to 10). The directional-spreading and frequency-spreading values vary in agreement with the wind intensity. The highest directional-spreading and frequency-spreading values obtained by ADV and WWATCH are consistent (Figures 7 to 10). During higher energy events, the directional spreading of waves measured by ADV is wider than that obtained using WWATCH. This feature of the directional spreading is caused by a drawback in the method used during its computation. When EMEM estimates second order parameters, the method creates a secondary artificial wave train in the directional spreading function, that comes from the opposite direction of the sensed wave train.

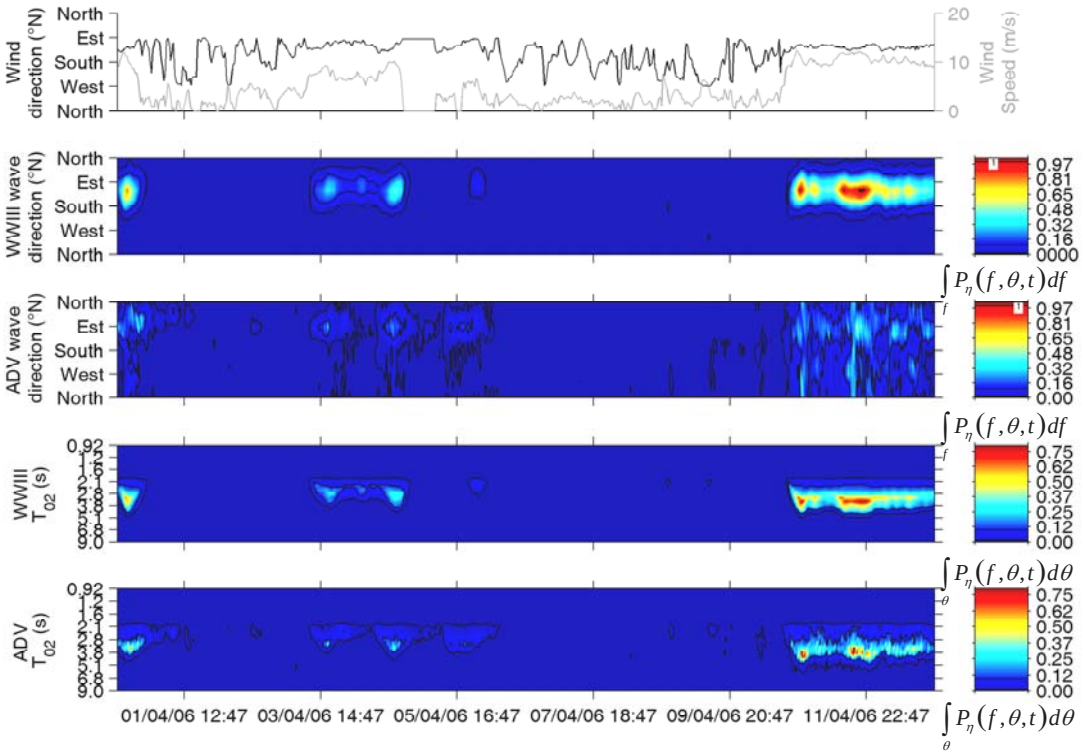

Figure 7 Frequency and direction spreading of WWATCH simulated wind wave field and ADV wave field measurements, for WO records.

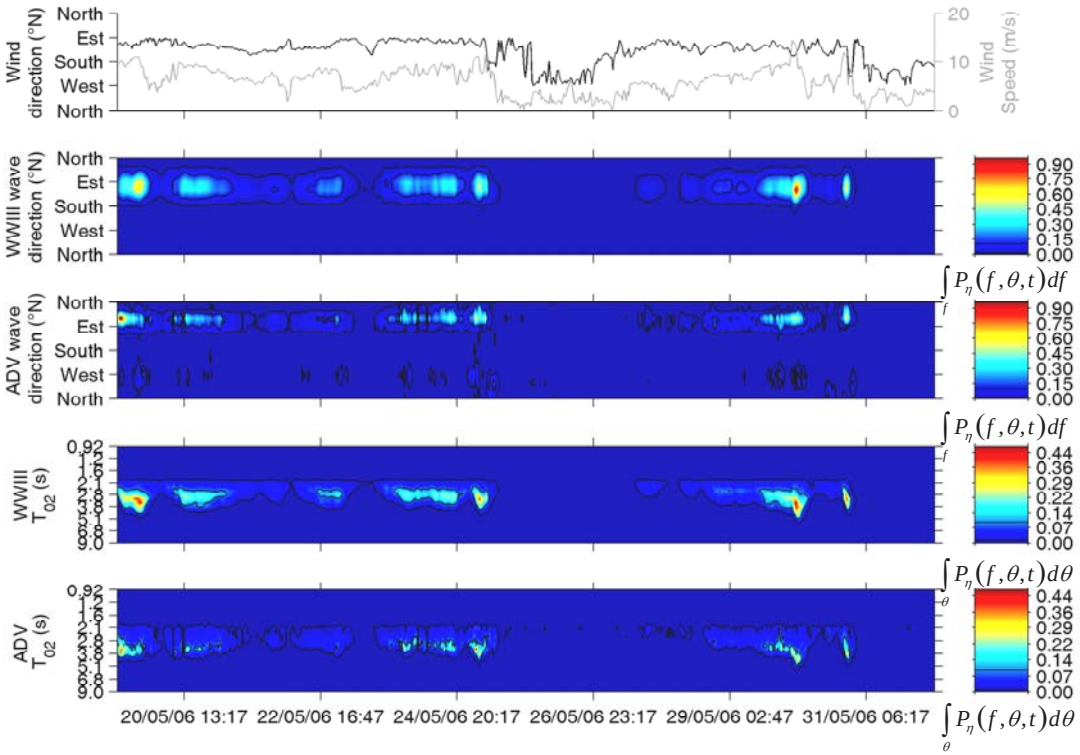

Figure 8 Frequency and direction spreading of WWATCH simulated wind wave field and ADV wave field measurements, for WG1 records.

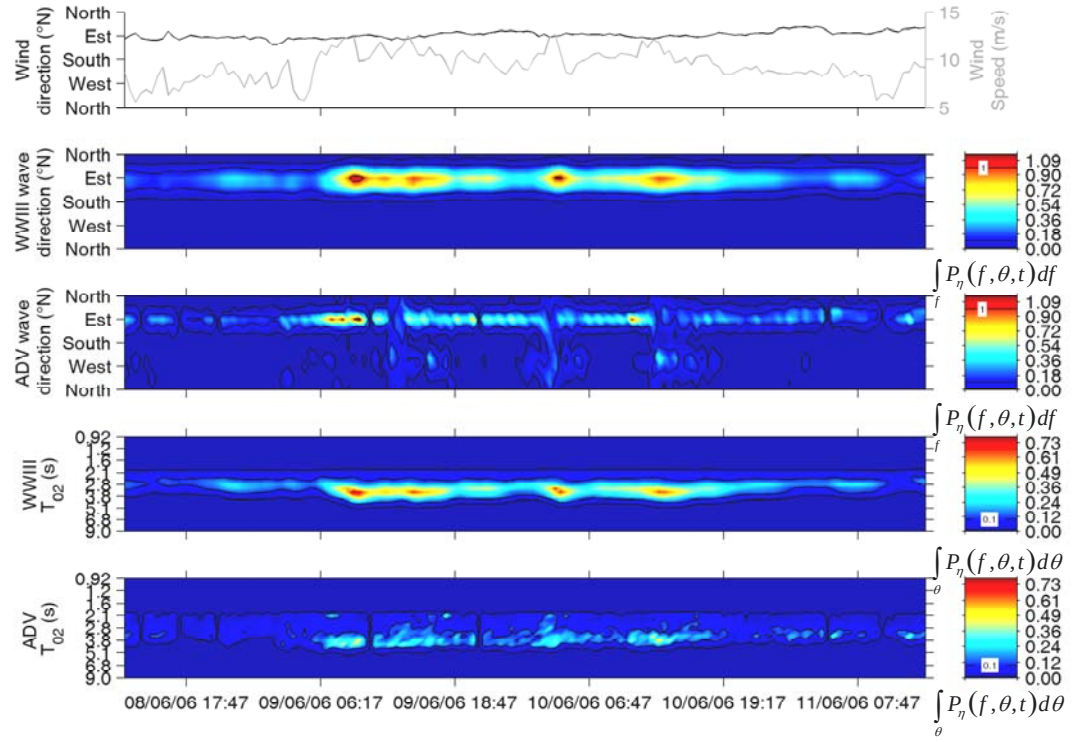

Figure 9 Frequency and direction spreading of WWATCH simulated wind wave field and ADV wave field measurements, for WG2 records.

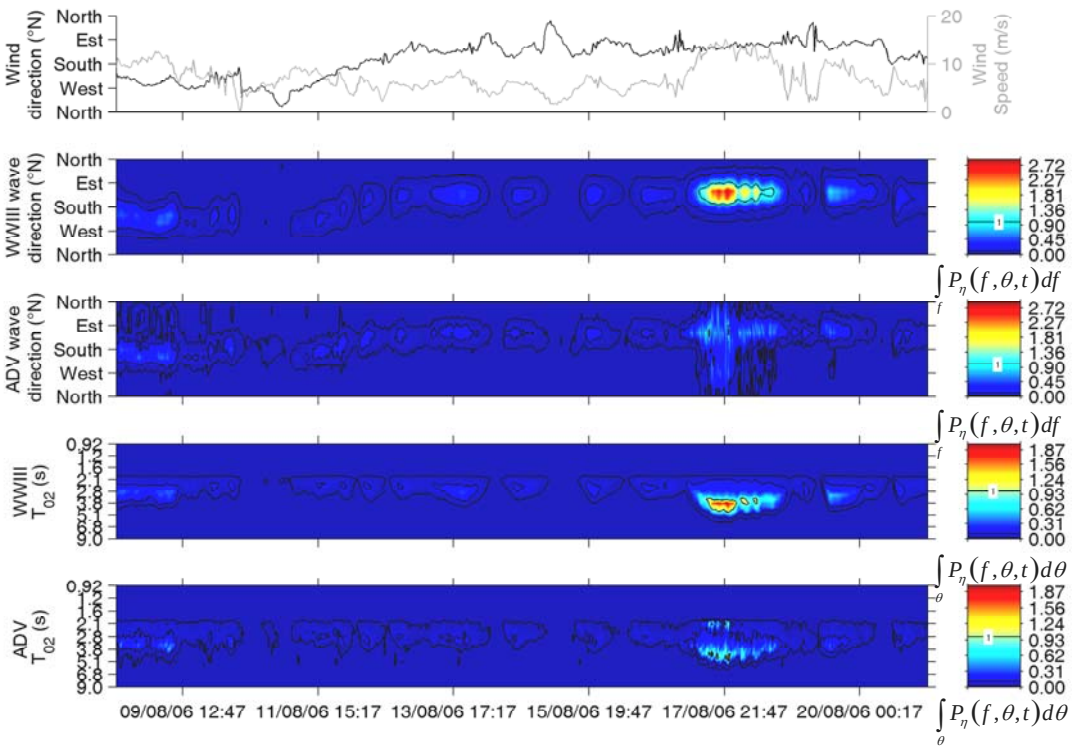

Figure 10 Frequency and direction spreading of WWATCH simulated wind wave field and ADV wave field measurements, for WT records.

The comparison of H_s from WWATCH and H_s from ADV leaded far better correlation coefficients when the swell component was filtered and deduced from the wave measurements (Table 3). In that case, the regression coefficients were closer to unity. The regression factors were higher than unity for WO, WG1 and WT, and lower than unity for WG2 deployment session. The offsets were less than about 10 cm.

The filtering of swell also provided T_{02} from simulations and measurements which are far better correlated than without filtering. WO, WG1 and WT show a regression factor superior to 0.70. The regression factor was also improved at WG2 by filtering swell.

		a	b	r
H_s (m)	WO	1.155	-0.013	0.902
	WC1	1.099	0.022	0.910
	WC2	0.959	0.107	0.793
	WT	1.158	-0.009	0.917
T_{02} (s)	WO	0.801	0.325	0.705
	WC1	0.864	0.225	0.810
	WC2	0.574	1.183	0.511
	WT	1.041	-0.367	0.758
θ_m (°)	WO	0.531	58.085	0.465
	WC1	0.319	85.203	0.420
	WC2	0.029	93.599	0.246
	WT	1.234	-19.168	0.795

Table 3 Parameters of the best fitted linear regression relationship calculated for WWATCH and the swell filtered measurements of ADV

The mean direction of wave field did not yield as good results as the two other statistical wave parameters. The correlation coefficients were far from unity, the correspondence of modelled wave field direction to the measured wave field direction was weak, except for WT. The main explanation for these bad correlation coefficients mainly lies in the range of the wave field direction during the experiments. At WT, wind direction shifted slowly to cover a wide range of angles, and the correlation was better (Fig. 11a). At WG2, where the correlation coefficient is the poorest, wind direction varied little (around a mean 100° average direction), the range of mean wave direction was short, and thus the correlation was low (Fig. 11b).

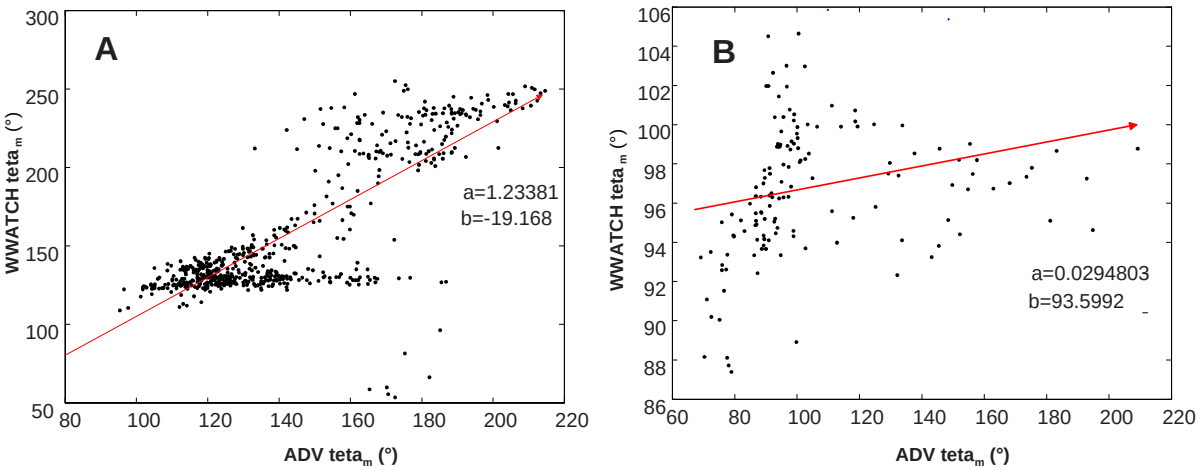

Figure 11 Examples of linear regression performed on mean wave direction between measured and simulated data. A at WT, B at WG2

12. Discussion

Comparing measured and modelled H_s without filtering swell gave fair correlations. T_{02} calculated from field measurements was more variable and did not behave like the wind velocity. High values of T_{02} were reached during low intensity wind events (i.e. wind wave field of low energy). T_{02} computed from WTR9 tended to reach more quickly higher values than from ADV. WTR9 seems to be more sensitive to the swell components and/or less sensitive to high frequency waves, and is thus less suited for wind wave measurements than the ADV.

The analysis of the directional power spectral density brought a lot of new elements to the description of the wave field.

The oceanic swell was identified on the measured PSD of the sea surface elevation. The contribution of swell to the wave field statistical parameters can be high when wind speed is low. The energy carried by swell inside the SLNC is lower than that of wind waves.

Filtering swell in the field data drastically improved correlation between modelled and measured H_s and T_{02}. During low wind episodes, regression factors are over unity, WWATCH tends to slightly underestimate the wind wave field on the SLNC. On the contrary WWATCH tends to overestimate wind waves at WG2 during strong wind episode.

A greater variability of wind direction provided a better regression coefficient between simulated and measured mean wave directions. The wind direction may not have varied enough on the sampling periods for the regression analysis to be well suited to estimate the accuracy of WWATCH to model wave direction. However, the display of wave direction distribution already allowed us to point out some weakness of the used method for the computation of wave direction spreading from ADV measurements. A drawback inherent to the method used in the measured data analysis is put to stake: when second order parameters are estimated, EMEM makes a secondary peak appear on the spreading function. This secondary peak interferes with the mean wave direction.

13. Conclusion

On one side, fetch limited wind waves have high frequencies. On another side, the upper frequency limit to measuring waves, the cut-off frequency, decreases with increasing depth. The wave measurements achieved in this study encompassed special precaution concerning the locations and depths of deployment. Despite these precautions, the cut-off frequency was low enough to interfere with the representation of the wind wave energy spectrum.

The frequency range of the measured data is limited in the high frequencies by the cut-off frequency. This limitation must be taken in account when comparing wave parameters

calculated from field measurements and simulated from wave model. By filtering the wave spectra produced by WWATCH for frequencies higher than the cut-off frequency, this study suggests a method for improving the validation technique of wave model's ability to simulate wind waves in a fetch-limited context. The analysis of the directional wave spectra enabled us to tune the cut-off frequency used in the computations. Morover, the ADV has a higher cut-off frequency than WTR9, thus making the former better suited for fetch limited wind wave measurements than the latter.

The analysis of the directional wave spectra also enabled us to identify the oceanic swell entering the lagoons which was not simulated by the model. After filtration of this component in the data, the quantification of the influence of swell on the SLNC wave field was achieved. This study demonstrates that the influence of swell in the SLNC is limited and that the major component of the wave field on the SLNC and over the sampling periods was the locally generated wind waves. The swell component of the wave field in the SLNC was not simulated in the model in this study. The resolution of swell waves inside the lagoon could be solved by enforcing the oceanic wave characteristics at the limits oceanic boundaries of the computational domain. This analysis suggests also that other components of the wave field, such as induced by wave reflection, could be identified through the analysis of the directional spreading of the wave field.

More precision could be brought in the forcings of the model. The validation of WWATCH was performed at strategic locations were spatial variability of wind field caused by topographic interferences apply the less. The influence of waves on suspended sediment transport is likely to be important near the shore where topographically induced spatial variability of wind is more important. This variability should be better accounted for in future studies when the wind distribution provided by a local atmospheric model (WRF) will force the wave model.

WWATCH showed a good ability to reproduce wind waves in a fetch limited context. This study shows also that considering the only wind waves to simulate the wave field on the SLNC is an acceptable approximation in average wind conditions.

Acknowledgments

This study was supported by IRD (UR CAMELIA), by the french scientific Programme National Environnement Côtier (PNEC) and by the french programme ZoNéCo. The authors are grateful to the divers Jean-Louis Menou, Christophe Peignon, Eric Folcher, and Catherine Geoffray and to Captains Sam Tereua, Miguel Clarque and Napoléon Colombani of R.V. CORIS for their contribution during field data acquisition.

References

Bonneton, P., Lefebvre, J.P., Bretel, P., Ouillon, S., Douillet, P., in press. Tidal modulation of wave-setup and wave-induced currents on the Aboré coral reef, New Caledonia. Journal of Coastal Research in press.

Booth J.G., Miller R.L., McKee B.A., Leathers R.A., 2000. Wind-induced bottom sediment resuspension in a microtidal coastal environment, Cont. Shelf Res. 20, 785-806

Bretschneider, C.L., 1970. Wave Forecasting Relations for Wave Generation. Look Lab/Hawaii, 1, 3.

Douillet P., 1998. Tidal dynamics of the south-west lagoon of New Caledonia: observations and 2D numerical modeling, Oceanol. Acta 21, 69-79.

Douillet P., Ouillon S., Cordier E., 2001. A numerical model for fine suspended sediment transport in the south-west lagoon of New-Caledonia, Coral Reefs, 20, 361-372.

Grant W.D., Madsen O.S., 1979. Combined wave and current interaction with a rough bottom, J. Geoph. Research 84 (C4), 1797-1808.

Hashimoto N., 1997. Analysis of the directional wave spectra from field data. Advances in Coastal and Ocean Eng., 3, 103-143.

Jouon, A., Douillet, P., Ouillon, S., Fraunié, P., 2006. Calculations of hydrodynamic time parameters in a semi-opened coastal zone using a 3D hydrodynamic model. Continental Shelf Research 26, 1395-1415.

Jouon, A., Ouillon, S., Douillet, P., Fernandez, J.M., Mari, X., Lefebvre, J.P., Fraunié, P., (submitted). Importance of biological aggregation revealed by Suspended Particulate Matter concentration, grain size distribution and their variability in a coral reef lagoon. Marine Geology.

Leblond P.H., Mysak L.A., 1978. Waves in the ocean. Elsevier, 602 pp.

Ouillon, S., Douillet, P., Andréfouët, S., 2004. Coupling satellite data with *in situ* measurements and numerical modeling to study fine suspended sediment transport: a study for the lagoon of New Caledonia. Coral Reefs 23, 109-122.

Ouillon, S., Douillet, P., Fichez, R., Panché, J.Y., 2005. Enhancement of regional variations in salinity and temperature in a coral reef lagoon, New Caledonia. CR Geoscience, 337, 1509-1517.

Prandle D., Hargreaves J.C., McManus J.P., R.C. Andrew, Duwe K., Lane A., Mahnke P., Shimwell S., Wolf J., 2000. Tide, wave and suspended sediment modelling on an open coast - Holderness, Coastal Engineering 41 (1-3), 237-267.

Tolman, H.L., 1989. The numerical model WAVEWATCH: a third generation model for the hindcasting of wind waves on tides in shelf seas. Communications on Hydraulic and Geotechnical Engineering, Delft Univ. of Techn., Rep. no. 89-2, 72 pp.

Tolman, H.L., 1991a. Effects of tides and storm surges on North Sea wind waves. J. Phys. Oceanogr., 21, 766- 781.

Tolman, H.L., 1991b. A third-generation model for wind waves on slowly varying, unsteady and inhomogeneous depths and currents. J. Phys. Oceanogr., 21, 782-797

Tolman, H.L., Chalikov, D.V, 1996. Source terms in a third-generation wind-wave model. J. Phys. Oceanogr, 26, 2497-2518.

Tolman, H.L., 1999. User manual and system documentation of WAVEWATCH III version 1.18, NOAA / NWS / NCEP / OMB Technical Note 151, 97 pp. (available at http://polar.wwb.noaa.gov/waves/wavewatch/wavewatch.html)

WAFO Group, 2000. A Matlab toolbox for analysis of random waves and loads. Lund University, Lund Institute of Technology, Centre for Mathematic Sciences, Mathematical Statistics, 112 pp.

WAMDIG, 1988. The WAM model - A third generation ocean wave prediction model. Journal of Physical Oceanography, 18, 1775-1810.

Welch, P.D., 1967. The use of fast Fourier transform for the estimation of power spectra: a method based on time averaging over short, modified periodograms. Trans on Audio and Electroacoustics 15, 70–73

Zhang M.Y., Li Y.S., 1997. The dynamic coupling of a third-generation wave model and a 3D hydrodynamic model through boundary layers, Continental Shelf Research 17 (10), 1141-1170.

IV.3 Conclusion

Les résultats de cette partie ont montré que WWATCH a une très bonne capacité à simuler le champ de houle sur le SLNC. De plus, la mer de vent est apparue comme la composante essentielle de l'état de mer sur le SLNC, pour l'ensemble des périodes de mesure.

WWATCH peut désormais être utilisé sur le SLNC et fournir au code hydrodynamique la contribution des vagues de vent au champ de contraintes sur le fond.

Le facteur de frottement f_w, introduit dans Eq. IV-2, est déterminé de manière empirique. Il dépend du nombre de Reynolds lié aux vagues R_w (Eq. IV-4) et de l'excursion relative des particules A/k_s, où k_s est la rugosité équivalente du fond ($k_s \approx 3d$ où d est le diamètre des particules) et A (Eq. IV-5) la demi excursion des particules au fond.

$$R_w = U_b A/\nu \qquad \text{Eq. IV-4}$$

$$A = \frac{T U_b}{2\pi} \qquad \text{Eq. IV-5}$$

Bel Madani (2003) avait restreint sa revue bibliographique sur les formulations de f_w à des écoulements turbulents rugueux. Or l'alternance de régimes turbulents lisses et turbulents rugueux peut se produire sur un même site (Tessier, 2006), imposant d'utiliser une formulation adaptée et un calcul itératif dans les modèles (e.g. Li et Amos, 2001). Il pourrait être envisagé d'utiliser le paramètre de rugosité du fond mesuré par télédétection acoustique (Chevillon, données non publiées) dans le calcul des contraintes résultant de l'action combinée des vagues (fournis par WWATCH) et des courants (calculés par MARS).

A cause des interactions non linéaires, la contrainte cisaillement au fond résultant des effets combinés de la houle et du courant est plus importante que la somme des effets de chacun de ces forçages. De nombreuses formulations existent pour le calcul de la contrainte mixte courant-vague (Grant et Madsen, 1979 ; Huynh-Thanh et Temperville, 1991 ; Soulsby, 1993). Dans l'optique d'inclure le calcul de la tension de cisaillement mixte dans une modélisation numérique du transport, le choix de cette formulation s'est porté sur DATA2 de Soulsby (1997). Cette formulation de la contrainte mixte offre un bon rapport précision/coût de calcul. La formulation DATA2 est la suivante :

$$\tau_m = \tau_c \left[1 + 1.2 \frac{\tau_w}{\tau_c + \tau_w} \right]^{3.2} \qquad \text{Eq. IV-6}$$

$$\tau_{\max} = \sqrt{\left(\tau_m + \tau_w \cos\theta\right)^2 + \left(\tau_w \sin\theta\right)^2} \qquad \text{Eq. IV-7}$$

où τ_m est la contrainte de cisaillement mixte moyenne, $\tau_{\max}$ est la contrainte de cisaillement mixte maximale qui détermine la mise en suspension des sédiments, et θ est l'angle entre les directions du courant et des vagues.

Si la prise en compte des effets de la houle sur la remise en suspension peut expliquer une part de la différence entre mesures et simulations, celle-ci n'explique pas tout. Notamment, le flux d'érosion fait intervenir, pour une classe de particules donnée, une tension de cisaillement critique au delà de laquelle le sédiment est érodé et un taux d'érosion qui dépendent de la granulométrie, de la nature des matériaux déposés, et de l'état de consolidation du fond. Les particules carbonatées ont de meilleures propriétés cohésives que les particules terrigènes (Tixier, 2003). Or, la zonation du taux d'érosion k_e effectuée dans Ouillon et al. (2004) (Figure I-12) présente des similitudes avec la carte du pourcentage de carbonates contenues dans la fraction fine des sédiments superficiels produite par Chevillon (non publiée) (Figure I-7). En cohérence avec ces travaux, l'étude approfondie de l'érodabilité des sédiments à partir de mesures *in situ* par érodimétrie permettra d'apporter les informations nécessaires à l'amélioration de ces formulations dans le modèle hydro-sédimentaire appliqué au SLNC.

Chapitre V CARACTERISATION DES PARTICULES EN SUSPENSION DANS LE LAGON SW DE NOUVELLE CALEDONIE

V.1 Introduction

Les différences entre les concentrations simulées de particules en suspension et les mesures de turbidité obtenues dans Douillet et al. (2001) peuvent être imputées à de multiples facteurs, dont la paramétrisation du modèle et à la non-équivalence entre turbidité et concentration.

La première tentative pour améliorer la correspondance mesures-simulations s'est attachée à la paramétrisation d'un modèle uni-classe, et plus spécifiquement à la zonation du taux d'érosion k_e (Ouillon et al., 2004). Le modèle simulait alors le transport de particules terrigènes de 7µm, ce diamètre correspondant à un pool majoritaire de fines particules dans le sédiment superficiel (O'Callaghan, 1999). Or, la granulométrie des sédiments du SLNC s'étale sur un spectre de taille continu. Il est possible que des particules ayant un diamètre différent de 7µm soient remises en suspension dans le SLNC, et soient responsable de l'excès de signal de turbidité relativement aux résultats du modèle. Selon cette hypothèse, les résultats de Bouron-Morin (2001) incitent à penser que ces particules ont une vitesse de chute moins importante que les particules de 7µm. Ces particules non définies demeurent en suspension plus longtemps que les particules de 7µm de diamètre (équivalent) et maintiennent un signal de turbidité résiduel entre deux cycles de marée.

Le transport des particules en suspension est conditionné par la vitesse de chute w_s (Eq. II-47) des particules. Il existe de nombreuses formulations de la vitesse de chute (Soulsby, 1997) qui, toutes, nécessitent de connaître deux paramètres physiques caractéristiques de chaque type de particule : leur diamètre et leur densité. Quelles sont les dimensions et les densités des particules en suspension dans le SLNC ?

Les différences entre mesures de turbidité et concentrations simulées peuvent être interprétées comme une inconsistance de la relation qui lie le signal de turbidité à la concentration massique en particules en suspension.

La grande majorité des études de transport particulaire se sont focalisées sur le transport de particules inorganiques terrigènes en milieux à moyenne ou forte concentration (au minimum plusieurs dizaines de mg/l). Les spécificités du contexte lagonaire corallien dans lequel s'effectue cette étude font que les méthodologies généralement adoptées ne sont pas nécessairement applicables. Par exemple, dans les milieux à forte teneur en particules terrigènes, il est communément accepté que la mesure de turbidité est linéairement reliée à la concentration massique des particules dans l'eau. Dans le SLNC, les concentrations en particules terrigènes sont faibles, il est donc nécessaire de vérifier cette approche.

Dans les eaux marines en milieu côtier, il existe une importante variété de natures de particules en suspension (Figure I-1). Des particules, autres que terrigènes, pourraient-elles être à l'origine des différences entre le signal de turbidité et le résultat de la modélisation sur le SLNC ?

Pour répondre aux questions posées, il est nécessaire de ré-explorer les bases sur lesquelles repose la mesure des particules en suspension en milieu corallien et la paramétrisation de la modélisation du transport de particules en suspension dans le SLNC. Pour cela, nous avons mis en oeuvre un granulomètre laser *in situ* LISST 100X qui fut acheté par l'UR Camélia dans le cadre du projet BISSECOTE (ACI Observation de la Terre) en 2004.

V.2 Publication:

Jouon, A., Ouillon, S., Douillet, P., Fernandez, J.M., Mari, X., Lefebvre, J.P., Fraunie, P., submitted. Importance of biological aggregation revealed by Suspended Particulate Matter concentration, grain size distribution and their variability in a coral reef lagoon. Marine Geology.

Importance of biological aggregation revealed by Suspended Particulate Matter concentration, grain size distribution and their variability in a coral reef lagoon

Aymeric Jouon, Sylvain Ouillon, Pascal Douillet, Jean Michel Fernandez, Xavier Mari, Jean Pierre Lefebvre, Philippe Fraunié

Abstract

Optical and gravimetric measurements of suspended particles were performed on a space and time varying sampling scheme in a coral reef lagoon. The amount of particles as well as their size distribution were characterized over space and time. The amount of suspended particles increased from reef to land. A bottom nepheloïd layer formed over the entire lagoon, and was more distinct on the land side of the lagoon. Small particles were more abundant in the nepheloïd layer than in the rest of the water column. While space variability was more important than time variability for the amount of suspended particles, it was the opposite for the particle size distribution. Disaggregating experiments brought evidence that aggregates represented a great part of the particle size distribution on the lagoon. The great efficiency of aggregation combined to low settling velocity upholds the hypothesis of biologically aggregated particles. The spatial display of aggregation efficiency suggested that mucus exuded by corals may play an important role in the aggregation processes. Compared to optical backscattering device or beam attenuation, *in situ* laser diffraction particle sizing was proved to be a relevant optical measure of suspended particulate matter in an aggregate dominated system.

Keywords

Suspended particles, optical backscattering, beam attenuation, particle size distribution, flocs, marine aggregates, variability, coral reef, New Caledonia.

1. Introduction

Anthropogenic pressure is increasing on coastal zones leading to land use intensification and increasing soil erosion. Together with urban and industrial runoffs, river sediment load increases the flux of particles to the coastal zone. For example, land use intensification in Western Australia was estimated to result in four fold increase of sediment delivery to the Great Barrier Reef lagoon (Neil et al., 2002). Despite the global tendency, sediment supply strongly varies from one river catchment to another (Walling and Fang, 2003). In addition to variable inputs, climate change induces sea level variations and temperature and salinity anomalies. Such changes impact coastal ecosystems, and must be quantified. Thus it is necessary to describe each component of these ecosystems in order to gain an understanding

of their present mechanism, and to further monitor their evolution in the context of increasing anthropogenic pressure.

Suspended Particulate Matter (SPM) is a key vector of minerals, organic matter, nutrients and pollutants in aquatic ecosystems. The amount, variability and fate of SPM force many biological processes. High levels of turbidity modify coral reefs development by limiting light penetration and compressing the depth range over which coral can flourish (Hayward, 1982; Rogers, 1990; Hopley, 1994; Hoitink, 2004). Sedimentation also inhibits coral recruitment (Babcock and Davies, 1991; Fabricius et al., 2003). On the other hand, coral abundance impacts on the SPM field characteristics. On Eniwetok Atoll, Johannes (1967) observed a marked increase in the concentration of suspended particulate organic aggregates when oceanic waters crossed the windward coral reef and entered the lagoon. Benson and Muscatine (1974) highlighted the importance of coral mucus within the pool of SPM. By mixing turbid plume water with unfiltered coral reef water, Wolanski et al. (2003) observed a rapid aggregation of particles leading to the formation of large flocs. Wild et al. (2004) reported the occurrence of specific aggregation processes related to the production of mucus by corals, defining coral mucus as “a trap for particles” and as an efficient energy carrier.

Turbidity, dry weight of particles (used to derive the SPM concentration), and carbon concentration are some characteristics of the SPM that are commonly measured. The general composition of particles can be determined by geochemical analyses while the characteristics of single particles (grains) can be assessed through grain size distribution (ie mean, median diameter, and skewness). Some mechanisms governing aggregation and/or disaggregation processes of SPM are revealed through *in situ* particle size distribution. Grain size distribution has usually been measured by laser technology in laboratory, however to avoid aggregates breaking up during sample handling (Gibbs, 1982), and subsequently altering particle size distribution *in situ* measurements are necessary. Recently developed devices based on laser technology such as Cilas and Sequoia LISST instruments have allowed the particle size distribution (PSD) to be recorded *in situ*.

In this paper, a new generation instrument (LISST-100X) was used to study *in situ* SPM amount and PSD in lagoon waters characterized by low quantity of suspended particles (ca. 1 mg.l-1). This study uses a great number (493 LISST and CTD profiles) of *in situ* measurements performed on a time and space spread sampling scheme. The objectives of this study are: (1) to compare *in situ* parameters derived from LISST-100X to those given by other commonly used instruments (such as turbidity and attenuation), (2) to describe time, space and depth variability of SPM and PSD, and (3) to extract information on the properties of aggregates by measuring the grain size distribution after disaggregating large aggregates. We discuss the importance of aggregation processes in a coral reef lagoon.

2. Study area

New Caledonia is a tropical island surrounded by a lagoon of 22,200 km2, located in the Western Pacific 1500 km east of Australia. Over fifty percent of the population reside in Nouméa which is the capital city located on the southwest coast of the island (Fig. 1). The lagoon area surrounding Nouméa is often referred as the "south-west lagoon of New Caledonia" (SLNC). The SLNC is a relatively shallow area (average depth ca.17.5 m), with a width varying from 5 km (northern limit) to 40 km (southern limit). The lagoon is fed by oceanic waters which stream through the passes and shoal over the barrier reef under the impulse of oceanic waves breaking (Bonneton et al., in press).

Nickel mining is the major economic resource of New Caledonia. Over the last century, open-cast mining have increased the load of terrigenous inputs into the lagoon (Fernandez et al., 2006). Hydrologic (Ouillon et al., 2005) and hydrodynamic studies based on the coupling of a 3D numerical model with *in situ* measurements and remotely sensed data (Douillet, 1998; Douillet et al., 2001; Ouillon et al., 2004; Jouon et al., 2006) showed that the reef-land gradient is the major feature of the high spatial variation of physical parameters (temperature, salinity, residence time, turbidity). The spatial variability of benthic cover also roughly coincides to a reef-land gradient of terrigenous and biogenic origin of sediments (Clavier et al., 1995).

Like a considerable number of coral reef systems in the world, the SLNC is influenced by turbid terrestrial runoffs (Spalding et al., 2001). Despite terrestrial runoffs, which affect the nearby shore areas of the SLNC (Fernandez et al., 2006), the concentration of SPM is low. Such low concentrations of SPM require highly sensitive measurements to separate noise from signal. The SPM encompasses particles such as bacteria, phytoplankton, organic detritus, zooplankton, aggregates and inorganic particles. Due to the overall high abundance of inorganic particles in coastal waters, other components of the particle pool are often neglected. However, no specific type of particle has been shown to be more represented than others in the SLNC. Although SPM is assumed to be mostly composed of inorganic particles, further studies are needed to better describe the encountered SPM and thus, give a better understanding of its dynamics and fate.

3. Material and method

3.1. Material

3.1.1. LISST-100X

An *in situ* Laser Scattering and Transmissometry device (LISST-100X; Sequoia Scientific Inc.) was used in this study. The LISST-100X measurements the distribution of particle volume concentration per size range, and the beam attenuation coefficient (c at 670 nm, hereafter denoted c670 and expressed in m-1) over an optical path length (l) of 5 cm. The theoretical sensing range of LISST-100X type B is 1.25 - 250 µm and is subdivided in 32 logarithmically-spaced size classes.

This device uses the laser diffraction technology to measure the size spectrum of particles. At small forward angles, light scattering is determined almost entirely by particle-diffracted light. Fraunhofer's diffraction principle relies on the fact that, in a certain range, the smaller the particle's cross-sectional area, the wider the diffraction angle. If the light wavelength is sufficiently small compared to particle size, which is the case comparing LISST laser wavelength (670 nm) to the particle size range (1.25-250 µm), the intensity of the diffracted light is insensitive to the particle refractive index. The LISST-100X measurements the intensity of light scattered at different angles with 32 concentric ring-type sensors. As mentioned by Traykovski et al. (1999), the size distribution measured by LISST represents the amount of cross-sectional area of particles in each size class. This areal size class distribution multiplied by the median particle size of each class provides the LISST a volumetric size class distribution. After corrections and computations, the software of the LISST-100X provides an experimentally fitted volumetric concentration of suspended particles in each size class. Measurement principles of LISST devices are further explained in Agrawal and Pottsmith (2000).

3.1.2. Optical backscattering sensor (OBS) measurements

Numerous studies have used optical backscattering sensors to assess total SPM concentration through turbidity measurements (e.g. Creed et al., 2001; Fugate and Friedrichs, 2002; Hoitink, 2004; Voulgaris and Meyers, 2004). An OBS device (also called "turbidimeter") emits near-infrared light and measurements the backscattered fraction in a small sampling volume near the sensor. The calibration of backscattered light intensity to the mass concentration of SPM is done experimentally and is usually described by a linear relationship (Hoitink, 2004). OBS sensitivity was shown to be around 1 Formazin Turbidity Unit (FTU) for 1mg.L-1 in coastal waters (Larcombe et al., 1995; Wass et al., 1997; Bunt et al., 1999; Jin et al., 2001). In this study a Seapoint OBS sensor (λ=880 nm) connected to a Seabird SBE19 CTD (conductivity-temperature-depth) probe was used. The Seapoint sensor was factory adjusted for consistent response to Formazin Turbidity Standard measured in (FTU).

Gravimetrically determined mass concentration

Sampling was performed using a 6-L Niskin bottle at 3 m depth and the *in situ* data considered correspond to the average of coincident optical probe data recorded from 1 m above to 1 m below sampling depth. Seawater was filtered in the laboratory on 1-µm polycarbonate pre-weighted filters (Nuclepore) in order to fit the LISST-100X sensing window (i.e., > 1.25 µm). Weight measurements were performed using a Perkin-Elmer AD-4 Autobalance with a precision of 0.001 mg.

Disaggregating process and individual particles

In order to analyse the importance of flocculation processes, the material retained on the filters was resuspended in a solution of 0.01 M Na4P2O7 and sonicated for two minutes in a Brandson Sonifier 250 (Mikkelsen and Pejrup, 2000). A solution containing the primary particles (grains) was then channelled in a closed circuit entrained by a peristaltic pump through the LISST-100X measurement chamber. Water flow rate was constant and high enough to prevent settling, but low enough to avoid the production of bubbles. A magnetic stirrer was also activated in the sampling chamber to prevent particle settlement. Measurements where performed in a clean room to avoid interference with airborne particles.

3.2. Sampling strategy

The data collection consists of LISST-100X profiles in the water column (at 1 Hz-rate) and Seapoint OBS profiles (4 Hz) connected to a Seabird CTD. Only the downcast data were considered in the analysis to avoid potential disturbance in turbidity caused by resuspension of particles when instruments reach the seabed.

The data considered in this study were collected over a series of four surveys (Fig. 1):

1. A 30-hours survey was conducted monthly from March, to September 2005 and in February 2006. This survey covered quasi-synoptically a widespread selection of 31 stations within the SLNC.

2. Transects focusing on open water to coast gradients were performed simultaneously to monthly surveys as well as in December 2005 and March 2006.

3. An attempt to quantify the spatial extent of a turbid plume during a rain event led us to carry out a bay survey during January 2006.

4. The BISSECOTE oceanographic cruise (Ouillon et al., 2006), where sampling strategy was based on substrate variability, took place in February 2006. It provided 158 simultaneous CTD and LISST profiles.

Water was not systematically sampled during these cruises. Filtering and weighting were performed at 137 stations amongst those involving CTD and LISST profiles.

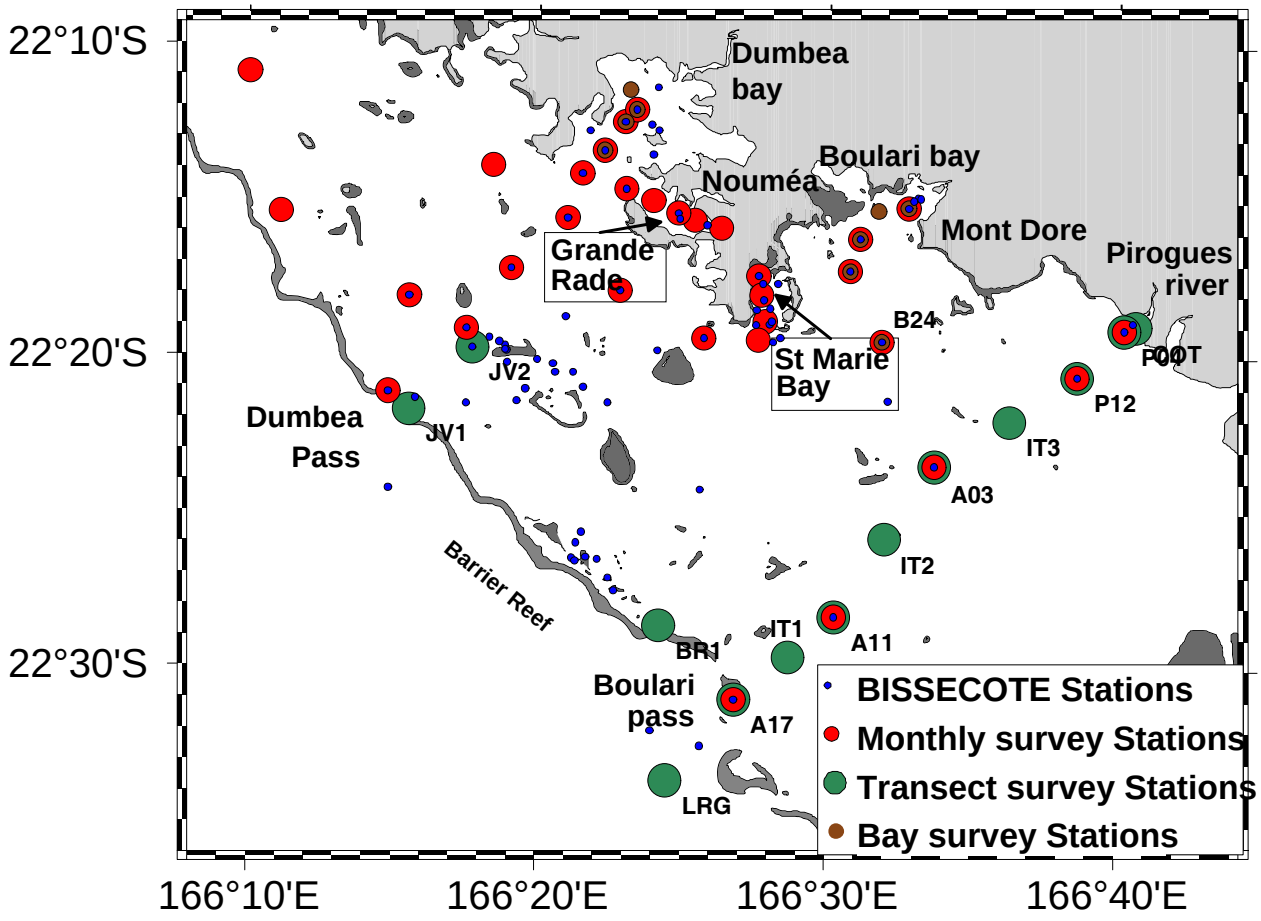

Figure 1Distribution of sampling stations during different surveys within the Southwest Lagoon of New Caledonia (SLNC).

3.3. Data analysis

3.3.1. Suspended Particulate Matter Volume Concentration (SPMVC)

Measurements of volume concentration, beam attenuation at 670nm, turbidity, and gravimetrically measured mass concentration enabled us to compare the effectiveness of these measurements to describe total SPM on the SLNC. LISST-100X measurement of total SPM is the SPM volume concentration (SPMVC, expressed in µL.L-1) given by (Traykovski et al., 1999):

$$SPMVC = \sum_{i} C_{vol,i} \qquad \text{EQ. V-1}$$

where Cvol,i is the volume concentration in the i th LISST size class (i=1, 32).

Despite the smoothing parameter used to compute the particle volume concentration distribution (PVCD) (Traykovski et al., 1999), LISST-100X derived data seemed erratic on extreme classes #1 and #32. This signal behaviour is likely due to the presence of particles smaller and coarser than the measured size range, which affects the estimated size distribution

(Traykovski et al., 1999; Agrawal and Pottsmith, 2000, Mikkelsen and Pejrup, 2000; Fugate and Friedrichs, 2002; Voulgaris and Meyers, 2004). Due to this uncertainty, the first and the last size classes were excluded from the computations.

3.3.2. Particle Volume Concentration Distribution (PVCD)

A particle size distribution (PSD) can be obtained from the number, the cross-sectional, the volume, the mass, or any other criteria applying to the particles. In this study, LISST software provides the volume concentration per size class. The volumetric size class distribution depends on the extension and spacing of each size class as defined in the LISST-100X settings. This could be referred to as the particle size class distribution. If the extent of sensing windows for each size class of LISST-100X was different, the displayed data would also be different. So far, the volumetric size class distribution given by LISST-100X is instrument dependent. A theoretical particle size distribution of volume concentration (PVCD) is a function that yields a value of volume concentration per particle size. A volume concentration distributed on particle size can thus alternatively be expressed per unit volume and per unit bin width as in Mobley (1994) and in Boss et al. (2001a, 2001b).

In order to assess the so-called PVCD, the class extension dependency of data had to be overcome. First, data were normalised by the extent of each sensing class to obtain an instrument independent particle size distribution following:

$$C_{vol}\left(size(i)\right) = \frac{C_{vol,i}}{\max\left(range(i)\right) - \min\left(range(i)\right)} \qquad \text{EQ. V-2}$$

where size (i) is the median diameter of particle size class I and range(i) is the particle size range on which extends the i-th class. The resulting data are expressed in µL.L-1.µm-1. This normalization assumes that the volume concentration for all particle sizes contained in a given class is constant. The modified data are then punctual solutions of the particle volume concentration distribution function (continuous function). The SPMVC can be retrieved through the integration of the continuous volume concentration distribution function over the LISST sensing size range.

Further on, the volume concentrations for each particle size was divided by the SPMVC in order to provide a particle size distribution independent of the global amount of particles, following:

$$C_{vol,rel}\left(size(i)\right) = \frac{C_{vol}\left(size(i)\right)}{SPMVC} \qquad \text{EQ. V-3}$$

Cvol,rel (size(i)) is called hereafter the relative volumetric size distribution as it is normalized on SPMVC. This provides a representation of the data, allowing the comparison

of the volume particle distribution from one size to another within a given distribution as well as from one distribution to another.

3.3.3. Median diameter D_{50}

The median diameter is a synthetic parameter characterizing the PVCD and defined as the diameter of a particle for which the cumulative volumetric distribution reaches 50% of the SPMVC.

3.3.4. Number of particles per size range

A representation of PSD performed on the number of particles per particle size (unit bin width) can be derived from LISST-100X data. The number of particles per size distribution is calculated following:

$$n(size(i)) = C_{vol}(size(i)) \Big/ \left[\frac{4}{3}\pi \left(\frac{size(i)}{2} \right)^3 \right] \qquad \text{EQ. V-4}$$

Its distribution generally fits a logarithmic curve (Mobley, 1994):

$$n(D) = K_1 . D^{-s} \qquad \text{EQ. V-5}$$

where K1 is a constant, D is the diameter of particles and s is the slope of the best fitted linear relationship between log (n(D) and log (D); s is called the Junge parameter. s is a synthetic parameter characterising the particle size distribution. It is a useful parameter for calculations of radiative transfer in the water column and their applications to remote sensing (e.g. Forget et al., 1999). s = 4 generally fits the distribution of biological particles in open ocean waters (Mobley, 1994). The higher s, the more abundant the smaller particles.

3.3.5. Coefficient of variation

From p-values of a given parameter x, its mean value is defined by:

$$\text{mean}(x) = \bar{x} = \frac{1}{p} \sum_{i=1}^{p} x_i \qquad \text{EQ. V-6}$$

and its standard deviation by:

$$\text{stdev}(x) = \left[\frac{1}{n} \sum_{i=1}^{n} (x_i - \bar{x})^2 \right]^{1/2} \qquad \text{EQ. V-7}$$

The ratio of the standard deviation of x on its mean value is called coefficient of variation. Multiplied by 100, the coefficient of variation is expressed as a percentage:

$$Cv = 100\frac{stdev(x)}{\bar{x}} \qquad \text{EQ. V-8}$$

4. Results

4.1. Correlation of measurements of SPM

4.1.1. Optical measurements and mass concentration

Global measurements such as turbidity, c670 and SPMVC were examined as proxies for SPM mass concentration. In the analysis, we considered stations where all of these parameters were measured (N=137) and collected at the same time and depth. For parameters derived from sensor profiles, a mean value was calculated from 1m above to 1m below the depth of sampling. The 137 stations correspond to values in the ranges of 0.2-16 FTU for turbidity, 0.12-6.0 m-1 for c670, 0.48-250.7 µL.L-1 for SPMVC and 0.01-6.48 mg.L-1 for mass concentration.

Linear regression relationships were fitted between optical measurements and gravimetrically-determined mass concentrations (Fig. 2). Turbidity was better correlated to mass concentration (r2=0.747, see Fig. 2c) than c670 (r2=0.667, Fig. 2b) and SPMVC (r2=0.646, Fig. 2a). Although correlation coefficients are acceptable, figures show patches of points with fairly dispersed optical parameters for SPM values around 1 mg.L-1. Several reasons may explain the relatively low regression coefficients.

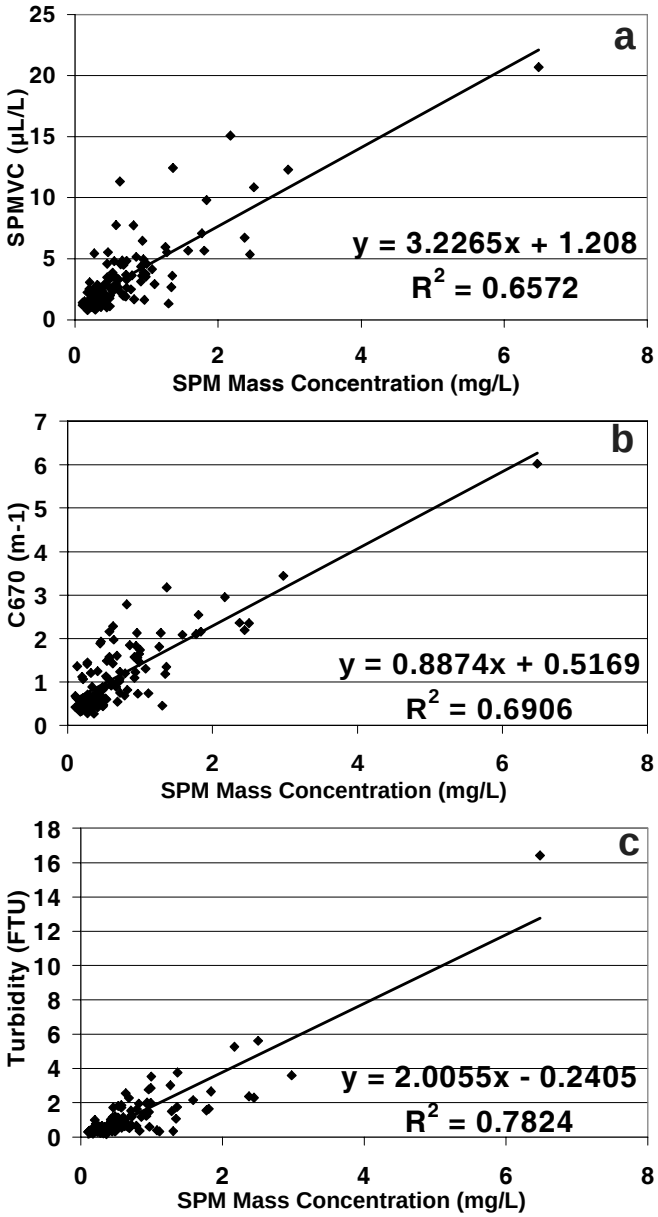

Figure 2 Comparisons between optical parameters and SPM concentrations at 137 stations: (a) total volume concentration vs mass concentration. (b) beam-attenuation at 670 nm vs mass concentration. (c) turbidity vs mass concentration

Despite the uncertainty inherent to the instrument and the sampling process (e.g. potential variability in water composition for measurements taken within a few minutes), we investigated the particle size distribution as a potential source of variability of the response of optical measurements to the SPM mass concentration on the whole sampling scheme.

4.1.2. Measurements per LISST size class versus other parameters

The correlations between turbidity, c670 and mass concentration, and the volume concentration Cvol,i in each LISST-100X size class are shown in Figure 3. The very low values obtained for the outlying size classes support the exclusion of these classes from the calculation of global SPMVC.

Cvol,i in each class showed a higher correlation to mass concentration than to turbidity and c670 for each particle size. Correlation coefficient between Cvol,i and mass concentration was over 0.7 for all size classes except for the minimum size class and for size class #26 (~86 µm) and above. Cvol,i was globally better correlated with turbidity than with c670.

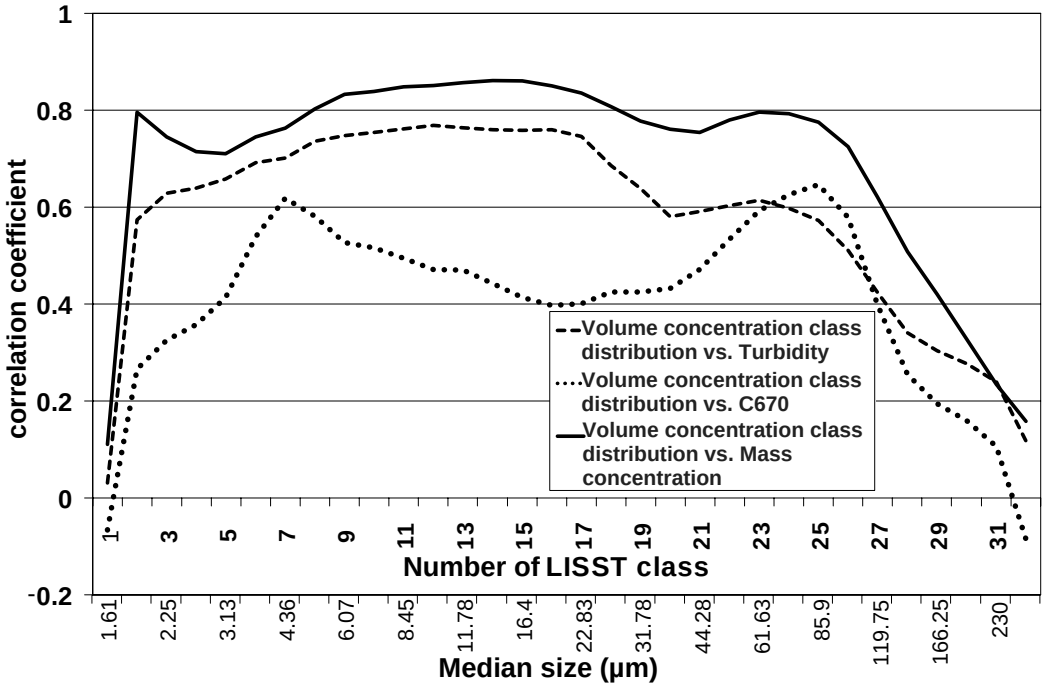

Figure 3 Correlations of turbidity, c670 and mass concentration with SPM volume concentration per LISST size class in the SLNC based on 36043 data.

Interestingly, the correlation between volume concentration and any optical parameter decreased with increasing diameter above class #26. This can be interpreted as a negligible contribution of the coarse particles to turbidity, beam attenuation and mass concentration. This can either be due to the under-representation of these size classes in the SLNC, or that coarser particles backscatter light inefficiently, are light attenuators, and have a very low density.

Figure 3 also demonstrates the strong dependency of turbidity and beam attenuation to the particle sizes. The volume concentration of particles < 3 µm (below class #6) were not as strongly correlated to any optical parameter than particles from size classes #6 to #15. The highest correlations between turbidity and volume concentration were found for classes #6 to #18, i.e. for particles with equivalent diameters between 3 and 23 µm. This result is consistent with the higher sensitivity of OBS to small particles (Bunt et al., 1999; Creed et al., 2001). The highest correlations between c670 and volume concentration were found at two intervals, which extend from classes #6 to #9 (ca. 3 to 5µm) and from #22 to #26 (ca. 40 to 100µm). The first size range to which c670 is more sensitive is in accordance with previously published results: beam attenuation increases with decreasing mean grain size at the same SPM up to 14-fold (Baker and Lavelle, 1984; Boss et al., 2001a, 2001b). Further observations

concerning the second size range showing stronger correlation to the beam attenuation are given in section 5.

4.2. Distribution and variability of SPM volume concentration

4.2.1. Averaged distribution of SPMVC

Mean values of SPMVC were calculated over the water column at stations where monthly measurements were performed. These stations were sampled 8 times to get mean values that were not influenced by the time variability of SPMVC.

Mean SPMVC values were low (< 7.5 µL.L-1 Fig. 4a). A reef-to-land gradient is visible. The volume concentration was highest at the coast-end of the bays, and peaked in a bay strongly impacted by urban inputs, i.e. the bay of Sainte-Marie (see location in Fig. 1). SPMVC was also high in the Dumbea bay (see location in Fig. 1), inside which the bay of Grande Rade is characterized by intense industrial activity. The third zone with relatively high SPMVC was the bay of Boulari, which receives terrestrial inputs from La Coulée River.

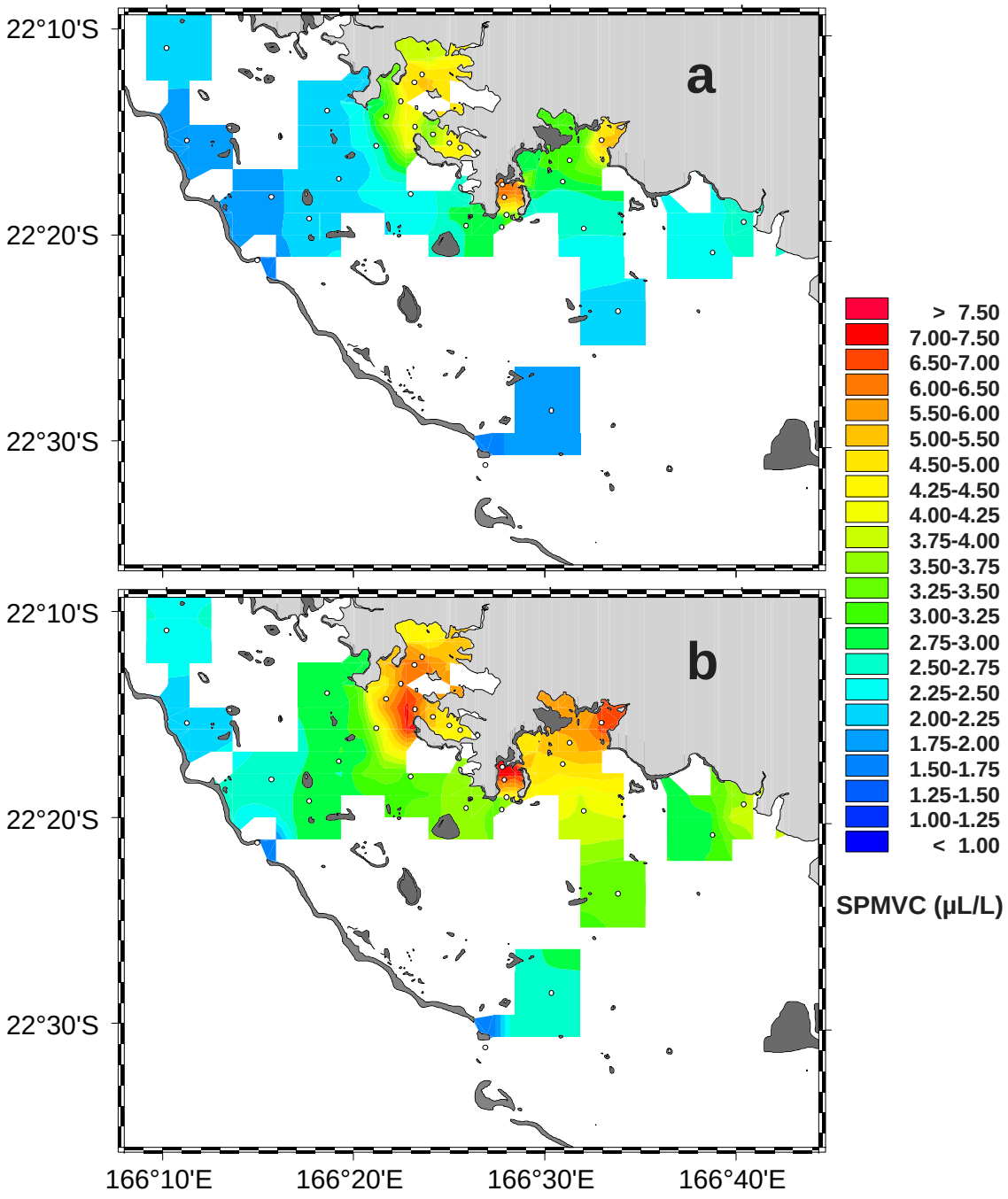

Figure 4Mean SPM volume concentration (in µL.L-1) in the SLNC. Averaging was performed over 8 field campaigns. (a) depth-averaged SPM; (b) mean SPM within 2 m above seabed.

4.2.2. Variation of SPMVC against depth

In order to investigate the influence of depth on the SPMVC field, surface (averaged over 2 meters below surface) and bottom data (2 meters above sea floor) were analysed separately. Only the bottom data showed significant differences with depth-averaged values. SPMVC near the seabed presents a distribution similar to SPMVC averaged over the whole water column but with higher values (Fig. 4b). Depth profiles generally exhibit an increase of SPMVC, turbidity and beam attenuation coefficient in a near-bottom nepheloïd layer of a few

meters thickness (Fig. 5). SPMVC is generally quite homogeneous from the surface to the upper limit of the nepheloïd layer, except when the water column is stratified (Ouillon et al., 2005).

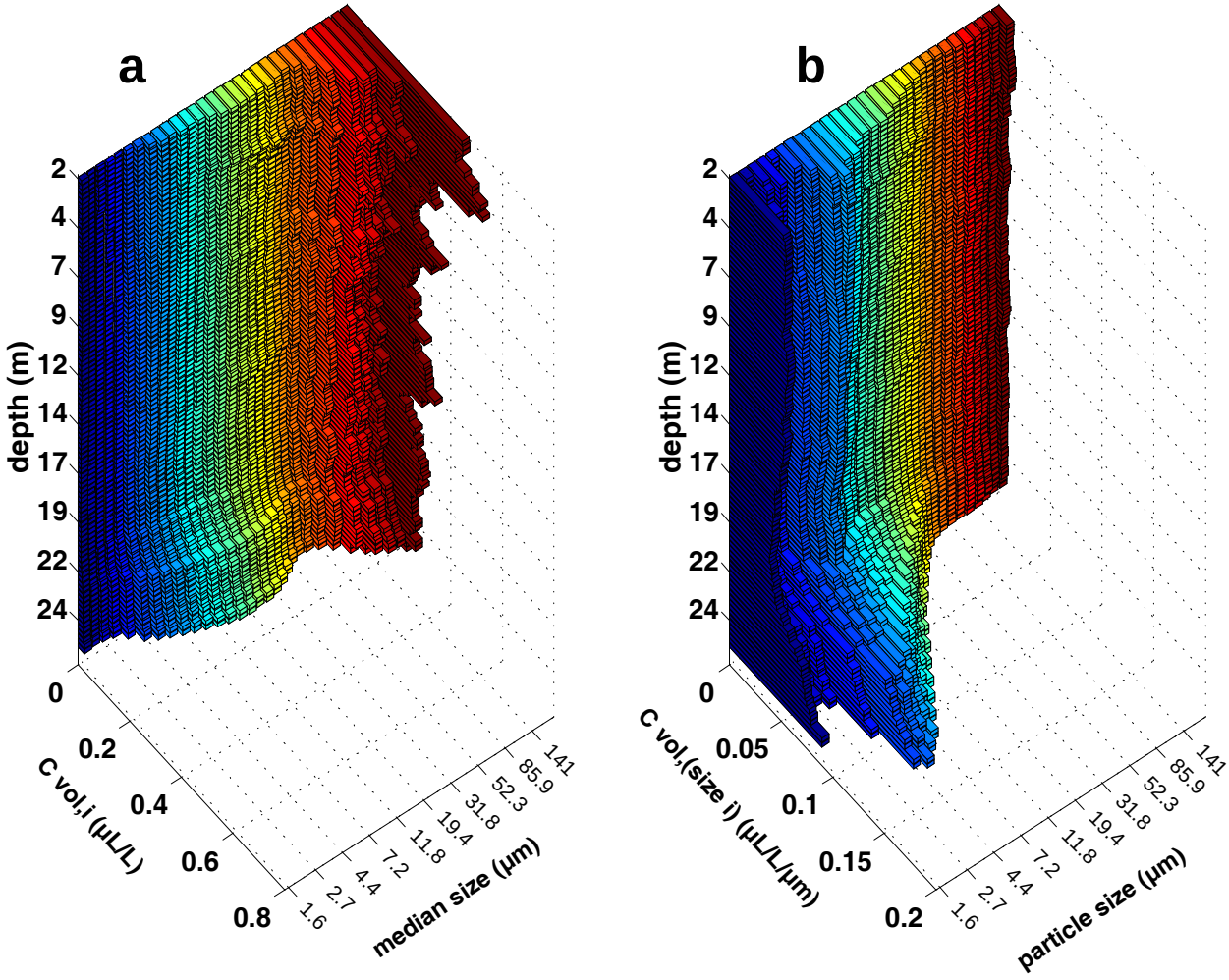

Figure 5 Example of (a) LISST-100X profile and (b) its conversion into particle size distribution profile (Station B24, 01/22/2006, see Fig. 6).

4.2.3. Space and time SPMVC variability

In an attempt to discriminate temporal and spatial variations of SPMVC, the variation coefficients over space and time were calculated. Computations performed over 23 stations all sampled 8 times at monthly intervals. Mean, standard deviation and coefficient of variation were calculated from the spatial (resp. temporal) variations of SPMVC for each cruise (resp. station). The mean coefficient of variation over space is calculated for each field campaign, then averaged on these 8 values, while the mean coefficient of variation over time is calculated for each station, then averaged on these 23 values (Table 1).

CV (SPMVC)	Coefficient of variation over time	Coefficient of variation over space
water column	34 %	68 %
surface	40 %	65 %
bottom	47 %	75 %

Table V-1 Space and time variability of SPMVC at different levels of the water column calculated from 23 stations of the SLNC sampled 8 times.

The variation coefficient of SPMVC over the whole water column is much higher over space (~68%) than it is over time (~34%). The high variability of SPMVC over time and space required a large amount of data to produce a reliable analysis of SPM field characteristics.

The variation coefficient of SPMVC over time fluctuates depending on the section of the water column. It ranged from 34% for the entire water column, to 47 % for the bottom layer were it was generally higher than near the surface (Table 1). Its distribution did not reveal any 2D global gradient within the SLNC, which suggests that the standard variations of SPMVC are a function of SPMVC's mean values.

The coefficient of variation of SPMVC over space was 65% near the surface and 75 %near the bottom. Although the two values were close, the values of coefficient of variation of SPMVC over space calculated over the whole water column were higher to the ones computed for the surface layer.

4.3. In situ particle size distribution

4.3.1. Example of volume concentration distribution

The distribution of SPMVC against particle sizes is characterized by Cvol (size(i)). Distributions of Cvol,i and Cvol (size(i)) at one station from the surface to the bottom are shown in Figure 5. The main variation when Cvol,i and Cvol (size(i)) were compared was that the volume concentration of particles contained in small size classes became more important when the LISST data (Cvol,i) was transformed to PVCD (Cvol (size i)). This change is due to the logarithmic spacing of particle size classes of LISST data. Profiles presented in Figures 5 and 6 are typical of those encountered in the whole SLNC.

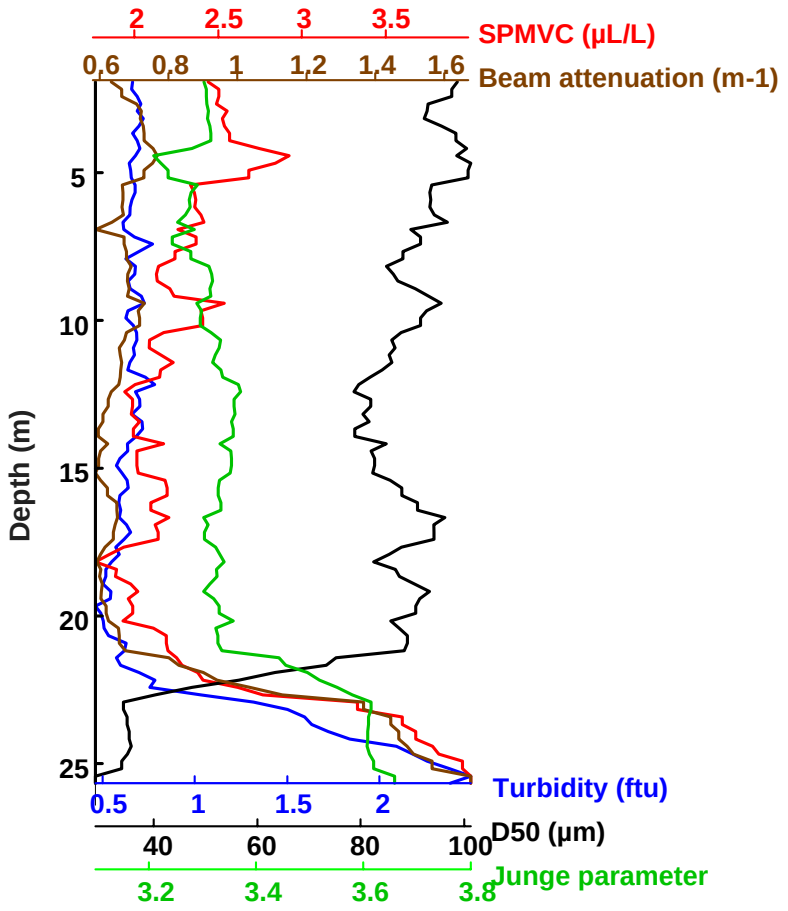

Figure 6 Typical shape of SPMVC, turbidity and c670 profiles within the SLNC. Station B24, 01/22/2006.

4.3.2. PVCD depth dependency

The bottom nepheloïd layer was generally characterized by a decrease in median particle size diameter (D50) and an increase in the Junge parameter value as compared to the upper mixed layer (Fig. 6). The observed shifts of these two synthetic PVCD indices were induced by a more significant fraction of small particles in the nepheloïd layer (Fig. 5b). The upper part of the profiles on Figure 6 shows that the shifts of the Junge parameter curve were opposite of the ones on SPMVC curve. The relative amount of large aggregates increased near the surface. c670 seemed to follow the same pattern as SPMVC and thus varied in opposition to the Junge parameter in the mixed layer.

4.3.3. PVCD space and time variability

The normalized value of Cvol,i , namely Cvol,rel (size i), was averaged over all the measurements performed within the SLNC so as to provide a normalized particle volume concentration distribution representative of the SLNC (Fig. 7). Volume concentration was the highest for particles with a diameter around 6 µm. The lowest volume concentration was obtained for particles within the 1.9-2.6 µm size range. As previously discussed, the high volume concentration recorded for particles of 1.6 µm diameter may be an artefact. Therefore, values obtained in this size range were excluded from the following computations. The curve

describing the mean relative volume concentration distribution decreased from the maximum reached around 6 µm to the highest particle sizes. This decrease was not exactly linear and showed a few stages. A remarkable feature of the curve is the peak observed for particles of size ranging from 60 to 120µm.

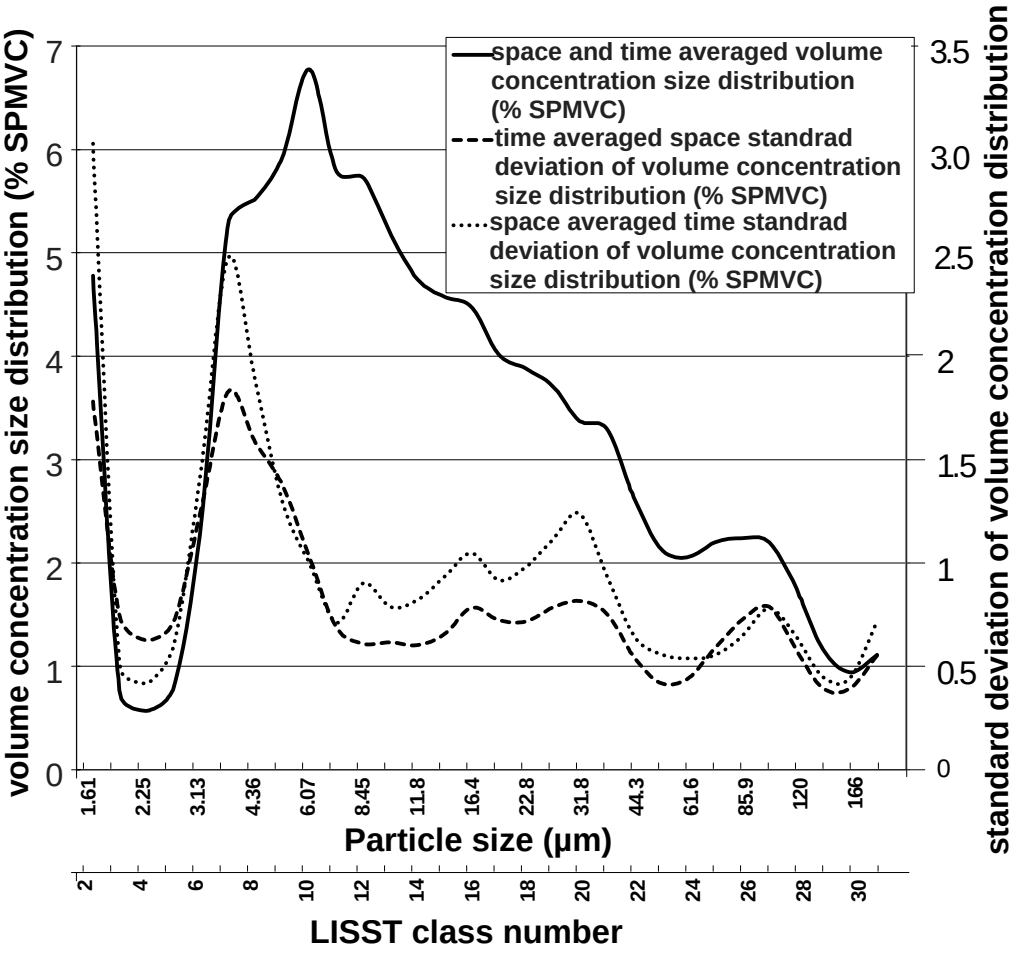

Figure 7 Averaged normalized volume concentration distribution, standard deviation in space and standard deviation in time.

The standard deviation of Cvol,rel (size i) was generally higher on time than on space. The PVCDs were more similar for different stations sampled during the same campaign than those obtained from one station sampled on different campaigns. Both curves of standard deviations show oscillations (Fig. 7). The major peak is reached for particles of 3.7 µm diameter. The standard deviation curves rapidly decreased to a low value for particles of 7 µm. Oscillations of the curves occurred up to the upper end of the distribution. The last oscillation corresponded to the peak described on the space and time averaged normalized PVCD for particles of diameter between 60 and 120µm.

4.3.4. PVCD spatial display

Junge parameters extend from 2.6 to 3.5 (Fig. 8). Globally these values are lower than the theoretical open sea values (Mobley, 1994). Large particles were relatively more abundant in SLNC waters than in the open ocean. The 2D Junge parameter distribution showed a distinct gradient oriented from the reef to the coast. Small particles represented a larger fraction of SPMVC at the head of the bays than near the barrier reef, or the surrounding coral islands. Separating near seabed data from the rest of the profile emphasized the relative prevalence of small particles in the bottom nepheloïd layer (Fig 8b).

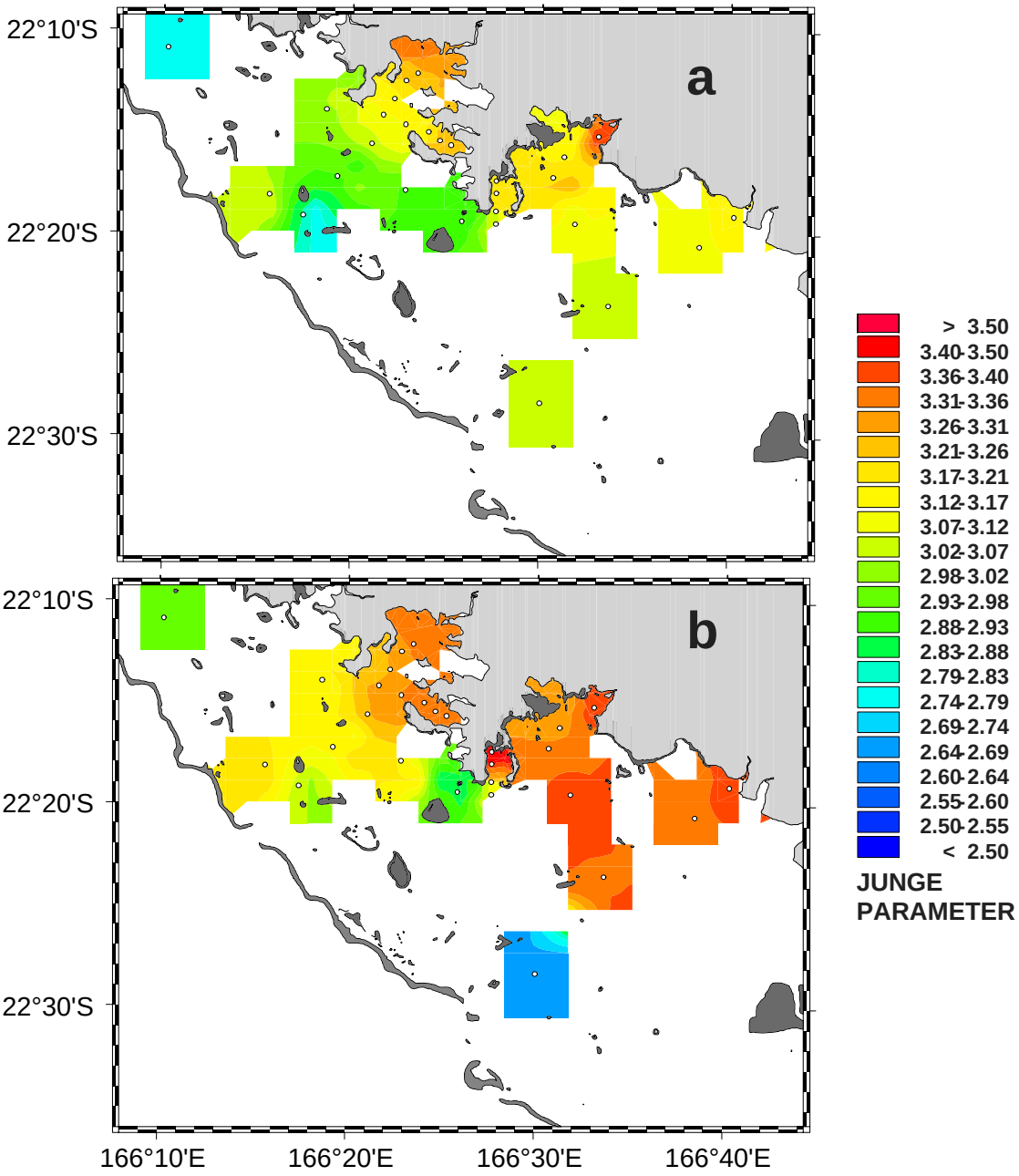

Figure 8 Distribution of the Junge parameter: (a) in the surface layer (averaged from 3m to 5m below the sea surface), (b) in the bottom layer (averaged over 2 m depth).

4.4. Grain volume concentration distribution (disaggregated samples)

4.4.1. Identification of aggregates

Suspended aggregates have been described in various marine environments (Van Leussen, 1994; Mobley, 1994; Gentien et al., 1995; Johannes, 1997; Thornton, 2002; Fabricius et al., 2003; Fugate and Friedrichs, 2003), and are a major constituent of suspended particles (Gibbs and Wolanski, 1992; Droppo, 2001). In order to identify the presence of aggregates, we compared the PVCDs obtained *in situ* (potentially with flocs) to particles sampled at the same stations after disaggregation. Disaggregating experiments were achieved on samples made during a transect survey from Boulari Pass to the Pirogues River mouth, and at two stations sampled on different days (JV1, JV2, see Fig. 1).

Figure 9 shows *in situ* PVCDs (Fig. 9a) and PVCDs of grains (Fig. 9b) at each station. Distribution of disaggregated samples represents the individual particles (grains) that constitute in-situ particles. The comparison of each sampled station of the *in situ* PVCD to the disaggregated PVCD revealed major differences. All disaggregated samples had similar PVCDs, suggesting similar size for the grains constituting the aggregates. *In situ* measurements showed more scattered PVCDs. This demonstrates that aggregation is a major process affecting suspended particles in the SLNC. Individual particles from 1.6 to 3.1 µm appearing in the disaggregated PVCD systematically disappeared in the *in situ* PVCD, suggesting that these particles aggregate. Data suggest that grains do not exceed 60 µm (Fig. 9b). Therefore, the presence of non-negligible volume concentration of particles > 60 µm in field samples can be attributed to aggregated particles.

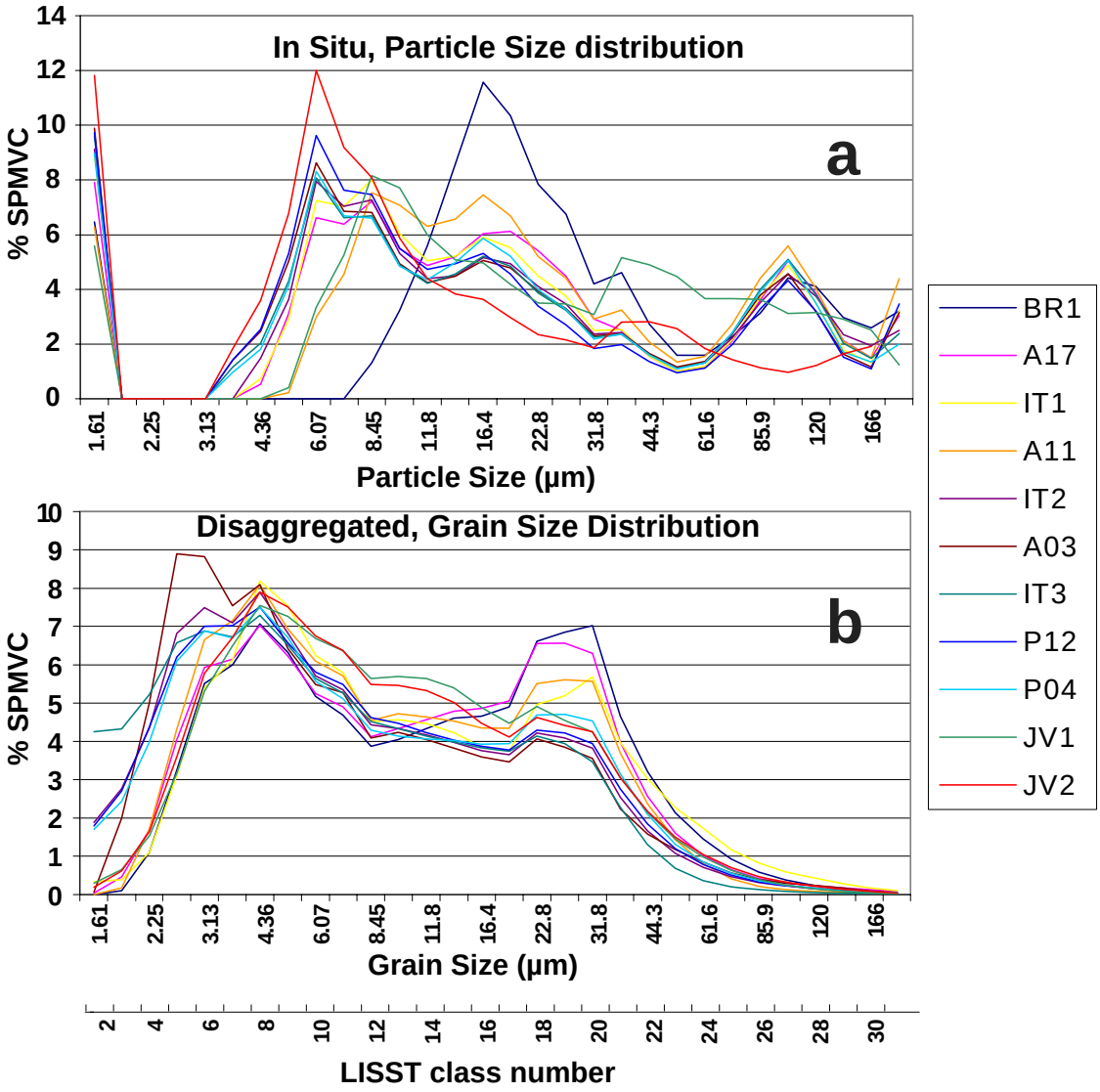

Figure 9 PVCD of (a) *in situ* data and (b) laboratory disaggregated samples at the same stations.

If the experiment was mass conservative, SPMVC of disaggregated samples should be a function of the mass weighted after filtering. Attempts to demonstrate a link between *in situ* measured SPMVC, gravimetrically determined mass concentration and disaggregated sample SPMVC produced no significant results.

4.4.2. Aggregates' contribution to SPMVC

The percentage of SPMVC contained in aggregates > 60 µm always exceeded 38 % on the SLNC (Fig. 10). Higher values of relative abundance of large aggregates (~70%) were found in the surroundings of the barrier reef and coral islands. The percentage of SPMVC contained in aggregates >60 µm on the transect survey stations represented at least 45% of SPMVC (Fig. 11). While the SPMVC increased from the reef to the coast, the percentage of suspended particles in aggregates > 60 µm decreased.

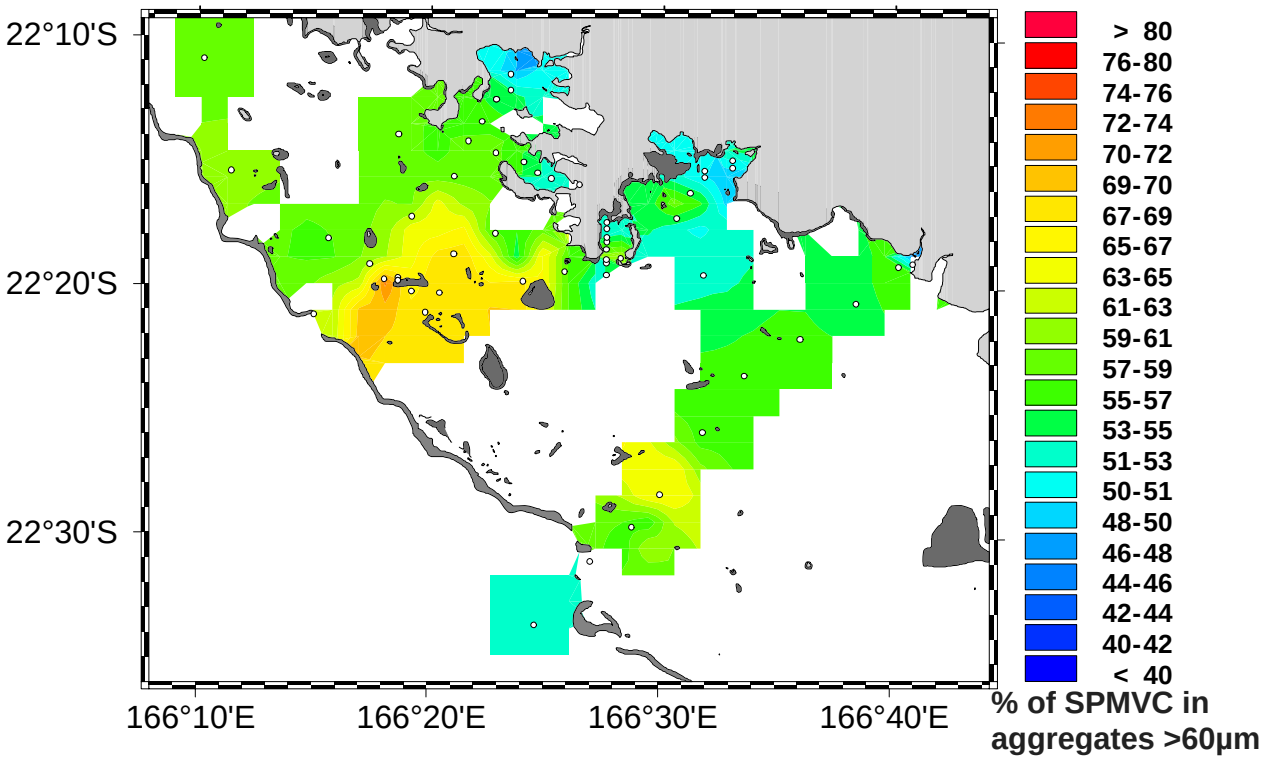

Figure 10 Percentage of SPM volume concentration in aggregates of diameter > 60µm.

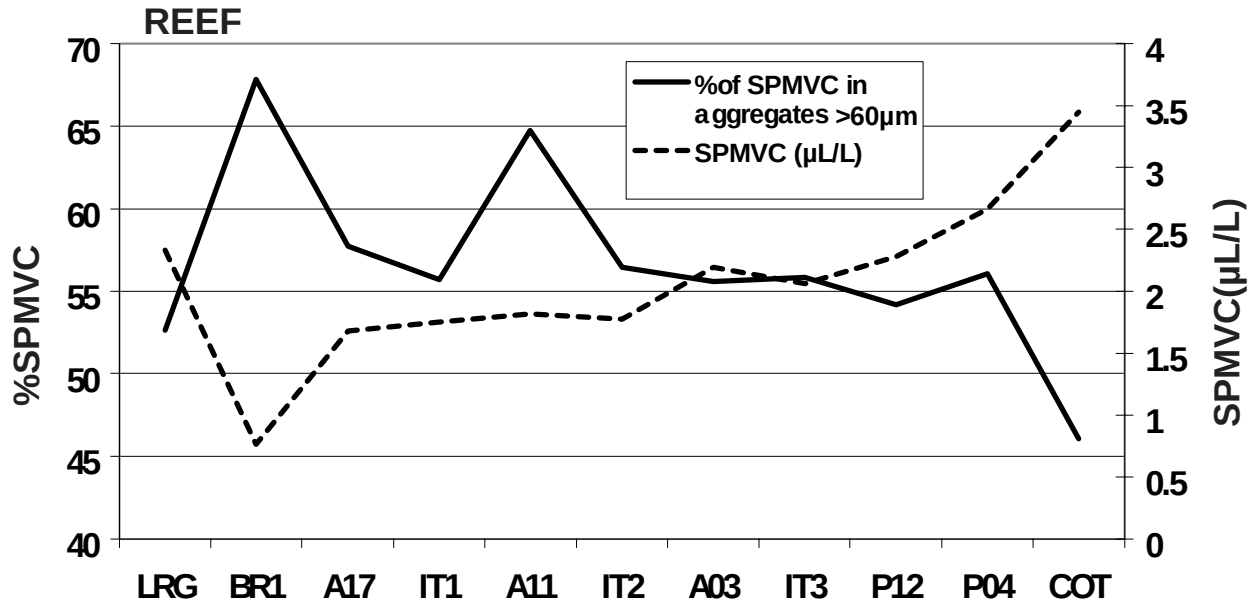

Figure 11 SPMVC and Percentage of SPM volume concentration in aggregates of diameter > 60µm along a coast-large transect.

5. Discussion

5.1. SPMVC

5.1.1. Average distribution of SPMVC

The mean distribution of SPMVC on the SLNC is characterized by two major gradients (Fig. 4). The reef to coast gradient is clearly visible on 2D displays, data from the bottom layer and data from the entire water column. These results strongly support the distributions of turbidity obtained from satellite data, field measurements and modeling exercises conducted in October 2002 (Ouillon et al., 2004).

Within the water depth, all optical measurements showed a net increase of SPM in the bottom nepheloïd layer. The occurrence of this bottom nepheloïd layer appears over the entire SLNC. Furthermore, the occurrence of the bottom nepheloïd layer was more marked in the bays around the Nouméa peninsula, where SPMVC values are higher.

5.1.2. SPMVC variability

Globally the variability of SPMVC is high over space and time (Table 1).

The coefficient of variation gives an indication on the variation of SPMVC relative to the mean value of SPMVC on the portion of the water column at a precise moment (variability coefficient over space) or at a precise location (variability coefficient over time). Variations of SPMVC over space and time are higher in the bottom layer. Comparing the coefficient of variation over time for surface waters vs. bottom waters, and considering that SPMVC reaches higher values at the bottom, the absolute variation of SPMVC is more important at the bottom than at the surface of the SLNC.

5.2. The importance and variability of aggregation processes

The disaggregating experiments showed that *in situ* particles with diameter over 60 µm were aggregates. The particles smaller than 60 µm observed during field measurements were most likely composed of an undetermined fraction of aggregates. Nevertheless, aggregates represent a significant fraction of the SPMVC (40 to 90%) as particles of equivalent diameter over 60 µm are considered to be representative of aggregates. The contribution of these aggregates to the SPMVC can be an indicator of the aggregation process efficiency.

The comparisons of disaggregated PVCDs to *in situ* PVCDs suggest that particles from 1.6 to 3.1 µm systematically aggregate. Higher values of standard deviations over space and time in the PVCD (class #7, see Fig. 7) coincide with the upper size limit of the single particles showing a strong propensity to aggregate (see Fig 9). The highest values of standard deviations also indicate that these particle sizes represent the limit between most abundant (6 µm) and most rare (< 3 µm) sensed particle sizes. Aggregation processes are also directly responsible for the peaks in standard deviation of PVCD over space and time for sizes > 60 µm where all particles are aggregates (Fig. 9a and 9b).

This suggests that an important part of the time and space variability of *in situ* PVCD is due to aggregation processes.

5.3. Quantifying SPM from optical measurements

The overwhelming importance of aggregation processes on the PVCD is responsible for the seemingly low values of correlation between turbidity and mass concentration as well as for the correlation between beam attenuation and mass concentration.

Unlike LISST-100X measurements of SPMVC, turbidity and beam attenuation signals were dependent upon the particle size distribution.

Using the same regression technique as Bunt et al. (1999) and Hoitink (2004), a relatively low regression coefficient of mass concentration versus optical parameters was obtained. This regression coefficient denotes the variability of the association between backscattering signal and mass concentration of SPM on the sampling scheme (through space and time). The comparison of OBS signal to the LISST-100X size class volume concentration shows that turbidity is more sensitive to the smallest particles (between 2 and 22 µm). This result supports previous suggesting a correction of OBS signal to derive SPM concentration by taking into account the median diameter of PSD (Lynch et al., 1994). Aggregation processes increase the mean diameter of SPM and was shown to be responsible for lowering the turbidity signal at an equal mass concentration (Gibbs and Wolanski, 1992). However, mass transported via large size particles and aggregates may not be retrieved in the OBS measurements. This study demonstrated that in the SLNC, a large amount of SPMVC was contained in aggregates of diameter > 60µm. The PSD time standard deviation revealed the important time variability of the state of aggregation. The PSD standard deviation over space, as well as the display of the ratio of SPMVC contained in aggregates over total SPMVC show the importance of space variability of the state of aggregation. The importance and variability of the state of aggregation explains a large amount of the variability generated by the poor regression coefficient between OBS signal and mass concentration. The particle size dependency of OBS signal can lead to errors in quantifying SPM mass concentration.

The highest correlations between beam attenuation at 670 nm and volume concentration were found at two intervals of LISST-100X size classes. The first interval includes particles of 3 to 5 µm, this observation is in agreement with previous observations which pointed out better attenuation efficiency of smaller particles. A second interval of even better correlation between c670 and SPMVC concerns particles in classes #22 to #26 (~40 to 100µm). The dependency of c670 to large particles is also illustrated on Figure 5. These size classes correspond approximately to the smallest particles identified as aggregates. The aggregation process likely intensifies the light attenuation of SPM.

The importance of aggregated particles over the SPMVC and the spatial variability of the state of aggregation may lead to poor results when trying to characterize the SPM field through OBS or beam attenuation measurements. The fact that volume concentration provided by LISST-100X is less dependent on particle size is an advantage over the turbidity and the beam attenuation coefficient measurement. On another hand, the first source of difference between gravimetric measurements and SPMVC relies on particle size range taken in account in the various measurements. For LISST-100X it extends from 1.48 to 213 µm, whereas gravimetric mass concentration concerns particles > 1 µm. Oversized particles for LISST sensing contribute to mass concentration and not to SPMVC.

Potential sources of error include the imprecision of LISST at extreme values and the exclusion of these values from the analysis. Creed et al. (2001) used another version of LISST-100 which sensing window extends from 1.25 to 500 µm. They reported the inability of the instrument to correctly resolve the sediment grain size > 250 µm (which included the top four bins of their LISST's version) and < 5 µm. The lower particle size of 5µm is also indicated as the lowest size to apply the Fraunhofer diffraction technique, as the scattered light patterns are less distinct (Gartner et al., 2001). Furthermore, the contribution of noise to the measurement limits to about 10-12 the number of sizes classes that may be resolved through the 200:1 size range observable by this instrument (Sequoia Scientific Inc., 2001). Each size class measurement is thus not entirely independent from the adjacent size class value. As a result, more than a single size class could be excluded from computations at the boundaries of LISST-100X sensing range.

Another explanation for the low regression coefficient between mass concentration and volume concentration of SPM may be linked to the LISST functioning. The LISST data processing uses a unique and experimentally-determined Volume Conversion Constant. It is used to calculate the volume concentration of particles, from the intensity of diffracted light in every size classes. This Volume conversion constant is determined for each instrument. First studies which used LISST with a single volume conversion constant, proved its accuracy (Traykovski et al., 1999; Agrawal and Pottsmith, 2000), however Gartner et al. (2001) demonstrated that this instrument dependent constant was also class dependent. In the present study, the assumption of a class independency of the volume conversion constant could contribute to the relative low values of the regression coefficient.

The regression coefficient of SPMVC vs. mass concentration provides evidence of the inconsistency of the relation between volume concentration and mass concentration on the sampling scheme. The variability of the density of particles could explain discrepancies between the two parameters. Considering the importance of the volume of aggregated particles over the entire SPMVC, we hypothesize that the variability of sensed particle density is closely related to the variability of aggregation processes over space and time.

Having shown the importance of aggregation processes and its variability on the sampling scheme within the SLNC, it can be argued that the variability of the relationship between mass concentration and SPMVC can be attributed to aggregation processes.

5.4. An insight into Aggregation Process regulation

The aggregation processes are largely responsible for the evolution of the PVCD on the SLNC.

Numerous parameters may influence the aggregation of particles. The size, density and strength of aggregates are dependent on the total amount of sediment in suspension, suspension residence time, flow velocity and turbulence level, salinity, temperature, coatings on particles surfaces, dissolved organic substances, and biological organisms (Voulgaris and Meyers, 2004). The amount of aggregates over total SPM and the size of the aggregates are constantly changing. They arise from a balance between aggregation and disaggregation processes (Chaignon et al., 2002). The time scales of aggregation are short (Gibbs and Wolanski, 1992; Wolanski et al., 2003). The state of aggregation is considered to be in constant equilibrium with the surrounding parameters.

Two fundamental conditions must be fulfilled for aggregation to take place: first, particles must collide and second, they must adhere (Van Leussen, 1994). The frequency of collisions increases when the concentration of suspended particles is high. Working on activated sludge, Chaignon et al. (2002) demonstrated a linear relation between the mass concentration of sludge and the mean aggregate size. The first characteristic of PVCD elucidated in this study concerns the depth dependency of PVCD. The increasing importance of aggregates volume concentration over SPMVC once they leave the bottom nepheloïd layer is somewhat contradictory to the dependency of aggregation processes to the SPM mass concentration. This result is in opposition with the tendency observed in the Mid-Atlantic Bight where the spectral shape of PSD becomes steeper with distance to the bottom (Boss et al., 2001b). The observed rise of SPMVC and lowering of the relative quantity of aggregates over SPMVC on a reef to coast transect also seems paradoxical with the dependency of aggregation processes to the quantity of SPM.

Among collision mechanisms known to promote aggregation (i.e. Brownian motion, turbulence, and differential sedimentation) turbulence is the key hydrodynamic parameter. Conversely high levels of turbulence can break apart aggregates. As a result, the structure of turbulence determines the maximum aggregate size (Alldredge et al. 1990; Van Leussen, 1994; Chaignon et al., 2002). This appears to be in contradiction with higher aggregation efficiency seen around coral reef and coral islands as turbulence is supposed to increase around coral structures. Furthermore, the critical level of turbulence leading to aggregate rupture also depends on the stickiness of the particles, which maintains the grains aggregated. The stickiness of a single particle is determined by two primary mechanisms: electrostatic

forces (Eisma, 1991) and biological activity (Van Leussen, 1997). Electrostatic forces are considered to be the most common interaction responsible for inorganic particle coagulation (Voulgaris and Meyers, 2004).

If we assume that inorganic particles are dominant constituents of SPM, under the conditions of having a much larger volume of water compared to the volume of solid grains in the particles, Mikkelsen and Pejrup (2001) proposed the following relation to determine the mean density of suspended particles:

$$\rho_P \approx \rho_{Pd} + \rho_W \qquad \text{EQ. V-9}$$

where ρ_P is the particle mean density, ρ_W is the water density (ρ_W = 1.02 kg.L-1 is considered in the calculation) and ρ_{Pd} is the density of dry mass per liter of SPM. The linear regression between SPMVC and mass concentration yields a slope coefficient equal to 3.22 µL.mg-1 (see Fig. 2a). The corresponding ρ_{Pd} is thus 0.31 kg.L-1 (= 1 / 3.22). A value of ρ_P =1.33 kg.L-1 is the mean density of particles over the sampling scheme. The low computed value of mean particle density is another evidence of the importance of aggregation processes on the SLNC. However, it should be noted that this method assumes that particles are mostly composed of water and solid grains, it is particularly suited to a context where SPM is dominated by inorganic particles. In a system dominated by mineral particles, aggregation is often associated with an increase in settling velocity (Van Leussen, 1994; Winterwerp, 2002; Gratiot, 2005). On the SLNC, aggregates remain in suspension even after prolonged steady condition which suggests that aggregation may lower settling velocity. This observation discredits the assumption of inorganic particle domination.

The variety of inorganic particles encountered in the SLNC may explain a few results. Among mineral particles found on the SLNC sea floor (Clavier et al., 1995; Fernandez et al., 2006), carbonates are known to have better cohesive properties than terrigenous silicate particles (Tixier, 2003). As mentioned in section 5.2, the occurrence of a bottom nepheloïd layer is more apparent in the bays around Nouméa. The occurrence of this bottom nepheloïd layer with higher Junge parameter values also coincides with higher ratios of terrigenous vs. biogenic particles (i.e., carbonates) in the benthic compartment. As terrigenous particles have lower sticking properties than carbonated particles, the former could partially explain the lower content in aggregates of the benthic nepheloïd layer. Terrigenous particles are more abundant near the shore than on the reef side of the SLNC (Fernandez et al., 2006). These poor sticking properties of terrigenous particles compared to biogenic particles, may contribute to lower the aggregation efficiency on the coastal side compared to the reef side of the SLNC.

The overall high volume of aggregates over SPMVC implies a high efficiency of aggregation processes which depends directly on the stickiness of particles forming the aggregates. This supports the hypothesis that aggregation processes are biologically

dominated as the content in organic matter improves the aggregation efficiency (Gratiot and Manning, 2004). Organic aggregates are 3 to 6 times stickier than flocs made of aluminium oxide (Magara et al., 1976) which could explain the aggregation efficiency encountered in the SLNC. Many studies focusing on biologically aggregated flocs (i.e. organic aggregates) emphasis the importance of ExoPolymeric Substances (EPS) as the main floc forming constituent (Chaignon et al., 2002; Mikkelsen and Keiding, 2002a, 2002b; Thornton, 2002; Tixier, 2003; Wolanski et al., 2003; Sheng et al., 2006). EPS originate from marine life metabolism or cell lyses.

Transparent Exopolymeric Particles (TEP) are formed by coagulation of EPS exuded by phytoplankton, bacteria, and are positively buoyant particles that have been shown to regulate the buoyancy of aggregates (Azetsu-Scott, 2004). TEP may also have an influence on the spatial display of aggregation efficiency. Although TEP concentration decreases with increasing distance to the coast (Fabricius et al., 2003; Mari et al., 2007), Mari et al. (2007) showed that the physico-chemical reactivity of organic matter was largely related to the local residence time, which strongly varies within the SLNC (Jouon et al., 2006). Corals are known to release large amounts of EPS, i.e., up to 4.8 L of mucus per day per square meter of coral reef (Wild et al., 2004). The present study shows that aggregates are more abundant in the surroundings of the barrier reef and around coral islets relatively to SPMVC. This greater efficiency of aggregation processes may be due to the proximity of corals exuding mucus. The abundance of EPS in the surroundings of living corals may enhance overall sticking properties of suspended particles and, thus, raise the critical level of turbulence leading to rupture of aggregates. This theory is verified by the low settling velocity of aggregates observed in the SLNC. Wolanski et al. (2003) also brought to light low settling velocities for aggregates occurring in a reef fringed bay. They argued that these low settling velocities were best explained by the inclusion of TEP in the composition of aggregate. The coral mucus induced flocculation is also a plausible explanation for the conclusions obtained in Hoitink (2004): “Coral reefs create a distinct sedimentary regime in their surroundings, sediments transported towards coral reef environments do not address local turbidity variation”. Biological flocculation processes may lower the light backscattering efficiency of SPM, making SPM less detectable for Optical Backscattering devices.

6. Conclusion

The dependence of the beam attenuation coefficient and the turbidity signal to the particle size distribution has been proved. Both measurements increase with decreasing mean grain size (Baker and Lavelle, 1984; Mikkelsen and Pejrup, 2000; Boss et al. 2001b). For both devices, aggregation processes lead to fluctuations in the signal to mass ratio. Because the state of aggregation may be altered during sample handling, the calibrations of beam attenuation measuring devices and OBS have to be done *in situ*. Even then, the variability of aggregation processes leads to poor consistency between turbidity or c670, and mass

concentration. OBS and c670 measurements may not be suitable to all conditions, in particular in situations where large particles and/or aggregates dominate (Creed et al., 2001). As OBS are less sensitive to large aggregates than to individual grains, disaggregation leads increased turbidity (Mikkelsen and Keiding, 2002b). The influence of disaggregating processes on backscattering signal can lead to the overestimation of re-suspension when it is considered to be the only possible source of turbidity (Ellis et al., 2004).

LISST-100X's measurements have a big advantage over OBS and the beam attenuation coefficient as it is size independent. LISST-100X is therefore capable of sensing the volume concentration of aggregates of sizes included in its sensing range. LISST has proved to be a suitable instrument for measuring SPM *in situ* in a context of aggregate domination. Despite the poor consistency of the relationship between volume concentration and mass concentration, knowing to the importance of aggregates in terms of transport of inorganic particles, pollutants, living cells and other organic components, the characterization of SPM through the use of volume concentration, rather than mass concentration, may be better suited for various issues.

The statistical treatment of LISST-100X particle volume concentration distribution offers an insight to the evolution of the state of aggregation of SPM. Important aggregation efficiency and low settling velocity have been shown to support the hypothesis of biologically dominated aggregation processes on the SLNC. The state of aggregation of SPM is the result of balance between aggregation and disaggregation. These processes are under the influence of numerous forcing parameters (SPMVC, turbulence, nature of elemental particles, EPS). As the time scale of aggregation processes is short, the state of aggregation of SPM depends closely on the variability of its controlling processes. The spatial extent of our study allowed us to identify the increased efficiency of aggregation processes in the surroundings of coral structures thus suggesting that coral mucus induced aggregation could contribute to biological aggregation.

Since aggregation processes have proved to be of major importance in the South-West lagoon of New Caledonia, a future stage of study will be needed to analyze the aggregation/disaggregation processes versus the variability of *in situ* physical and chemical forcings.

Acknowledgments

This work was supported by the New Caledonian ‘‘ZoNeCo’’ program, by the French ‘‘Programme National Environnement Côtier’’ and by the french BISSECOTE program (“ACI Observation de la Terre”). The author warmly thank Jean-Pierre Lamoureux who measured dry weight of particles, Sam Tereua, Napoleon Colombani, Miguel Clarke and the crew of N.O. Alis for their contribution to the field measurements.

References

Agrawal, Y.C., Pottsmith, H.C., 2000. Instrument for particle size and settling velocity observations in sediment transport. Mar. Geol. 16, 89-114.

Alldredge, A.L., Granata, T.C., Golschalk, C.C., Dickey, T.D., 1990. The physical strength of marine snow and its implications for particle disaggregation in the ocean. Limnol. Oceanogr. 35, 1415-1428.

Azetsu-Scott, K., 2004. Ascending marine particles: Significance of transparent exopolymer particles (TEP) in the upper ocean. Limnol. Oceanogr. 49, 741-748.

Babcock, R., Davies, P., 1991. Effects of sedimentation on settlement of *Acropora millepora*. Coral Reefs 9, 205-208.

Baker, E.T., Lavelle, J.W., 1984. The effect of particle size on the light attenuation coefficient of natural suspensions. J. Geophys. Res. 89, 8197-8203.

Benson, A.A., Muscatine, L., 1974. Wax in coral mucus: Energy transfert from coral to fishes. Limnol. Oceanogr. 19, 810-814.

Bonneton, P., Lefebvre, J.P., Bretel, P., Ouillon, S., Douillet, P., (in press). Tidal modulation of wave-setup and wave-induced currents on the Aboré coral reef, New Caledonia. J. Coast. Res.

Boss, E., Pegau, W.S., Gardner, W.D., Zaneveld, J.R.V., Barnard, A.H., Twardowski, M.S., Chang, G.C., Dickey, T.D., 2001b. Spectral particulate attenuation and particle size distribution in the bottom boundary layer of a continental shelf. J. Geophys. Res. 106, 9509-9516.

Boss, E., Twardowski, M.S., Herring, S., 2001a. Shape of the particulate beam attenuation spectrum and its inversion to obtain the shape of the particulate size distribution. Appl. Opt. 40, 4885-4893.

Bunt, J.A.C., Larcombe, P., Jago, C.F., 1999. Quantifying the response of optical backscatter devices and transmissometers to variations in suspended particulate matter. Cont. Shelf Res. 19, 1199-1220.

Chaignon, V., Lartigues, B.S., Samrani, El.A., Mustin, C., 2002. Evolution of size distribution and transfer of mineral particles between flocs in activated sludges : an insight into floc exchange dynamics. Water Res. 36, 676-684.

Clavier, J., Chardy, P., Chevillon, C., 1995. Sedimentation of Particulate Matter in the South-west Lagoon of New Caledonia: Spatial and Temporal Patterns. Estuar. Coast. Shelf Sci. 40, 281-294.

Creed, E.L., Pence, A.M., Rankin, K.L., 2001. Inter-comparison of turbidity and sediment concentration measurements from an ADP, an OBS-3, and a LISST. In Oceans 2001, Proceedings of the MTS/IEEE conference 3, 1750-1754.

Douillet, P., 1998. Tidal dynamics of the south-west lagoon of New Caledonia: observations and 2D numerical modelling. Oceanolo. Acta 21, 69-79.

Douillet, P., Ouillon, S., Cordier, E., 2001. A numerical model for fine suspended sediment transport in the southwest lagoon of New Caledonia. Coral Reefs 20, 361-372.

Droppo, I.G., 2001. Rethinking what constitutes suspended sediments. Hydrol. Process. 15, 1551-1564.

Ellis, K.M., Bowers, D.G., Jones, S.E., 2004. A study of temporal variability in particle size in a high-energy regime. Estuar. Coast. Shelf Sci. 61, 311-315.

Fabricius, K.E., Wild, C., Wolanski, E., Abele, D., 2003. Effects of transparent exopolymer particles and muddy terrigenous sediments on the survival of hard coral recruits. Estuar. Coast. Shelf Sci. 57, 613-621.

Fernandez, J.M., Ouillon, S., Chevillon, C., Douillet, P., Fichez, R., Le Gendre, R., 2006. A combined modelling and geochemical study of the fate of terrigenous inputs from mixed natural and mining sources in a coral reef lagoon (New Caledonia). Mar. Poll. Bulletin 52, 320-331.

Forget, P., Ouillon, S., Lahet, F., Broche, P., 1999. Inversion of reflectance spectra of nonchlorophyllous turbid coastal waters. Rem. Sensing Env. 68, 264-272.

Fugate, D.C., Friedrichs, C.T., 2002. Determining concentration and fall velocity of estuarine particle populations using ADV, OBS and LISST, Cont. Shelf Res. 22, 1867-1888.

Fugate, D.C., Friedrichs, C.T., 2003. Controls on suspended aggregate size in partially mixed estuaries. Estuar. Coast. Shelf Sci. 58, 389-404.

Gartner, J.W., Cheng, R.T., Wang, P.F., Richter, K., 2001. Laboratory and field evaluations of the LISST-100 instrument for suspended particle size distributions, Mar. Geol. 175, 199-219.

Gentien, P., Lunven, M., Lehaître M., Duvent, J.L., 1995. *In-situ* depth profiling of particle sizes. Deep-Sea Res. 42, 1297-1312.

Gibbs, R.J., 1982. Floc stability during Coulter-Counter size analysis. J. Sediment. Petrol. 52, 657-660.

Gibbs, R.J., Wolanski, E., 1992. The effect of flocs on optical backscattering measurements of suspended material concentration. Mar. Geol. 107, 289-291.

Gratiot, N., Manning, A.J., 2004. An experimental investigation of floc characteristics in a diffusive turbulent flow. J. Coast. Res. 41, 105-113.

Gratiot, N., Michallet, H., Mory. M., 2005. On the determination of the settling flux of cohesive sediments in a turbulent fluid. J. Geophys. Res. 110.

Hayward, A.B., 1982. Coral reefs in a clastic sedimentary environment: fossils (Miocene, SW Turkey) and moderns 5recent, Red Sea analogues. Coral Reefs 1, 109-114.

Hoitink, A.J.F., 2004. Tidally-induced clouds of suspended sediment connected to shallow-water coral reefs. Mar. Geol. 208, 13-31.

Hopley, D., 1994. Continental reef systems. In: Carter, R.W.G., Woodroffe, C.D. (Eds.), Coastal Evolution: Late quaternary shoreline Morphodynamics. Cambridge Univ. Press, Cambridge, pp 303-340.

Jin, J.Y., Lee, D.Y., Park, J.S. Park, K.S., Yum, K.D., 2001. Monitoring of suspended sediment concentration using vessels and remote sensing. In: McAnally WH and Mehta AJ (ed) Coastal and Estuarine Fine Sediment Processes. Elsevier, Amsterdam, The Netherlands, pp 287-299.

Johannes, R.E., 1967. Ecology of organic aggregates in the vicinity of a coral reef. Limnol. Oceanogr. 12, 189-195.

Jouon, A., Douillet, P., Ouillon, S., Fraunié, P., 2006. Calculations of hydrodynamic time parameters in a semi-opened coastal zone using a 3D hydrodynamic model. Cont. Shelf Res. 26, 1395-1415.

Larcombe, P., Ridd, P.V., Prytz, A., Wilson, B., 1995. Factors controlling suspended sediment on innershelf coral reefs, Townsville, Australia. Coral Reefs 14, 163-171.

Lynch, J.F., Irish, J.D., Sherwood, C.R., Agrawal, Y.C., 1994. Determining suspended sediment particle size information from acoustical and optical backscatter measurements. Cont. Shelf Res. 14, 1139-1165.

Mari, X., Rochelle-Newall, E., Torréton, J.P., Pringault, O., Jouon, A., Migon, C., 2007. Water residence time: A regulatory factor of the DOM to POM transfer efficiency. Limnol. Oceanogr. 52, 808-819.

Mikkelsen, L.H., Keiding, K., 2002a. Physico-chemical characteristics of full scale sewage sludges with implication to dewatering. Water Res. 36, 2451-2462.

Mikkelsen, L.H., Keiding, K., 2002b. The shear sensitivity of activated sludges: an evaluation of the possibility for a standardised floc strength test. Water Res. 36, 2931-2940.

Mikkelsen, O.A., Pejrup, M., 2000. *In situ* particle size spectra and density of particle aggregates in a dredging plume. Mar. Geol. 170, 443-459.

Mikkelsen, O.A., Pejrup, M., 2001. The use of LISST-100 in-situ laser particle sizer for estimates of floc size, density and settling velocity. Geo-Marine letters 20, 187-195.

Mobley, C.D., 1994. Light and Water Radiative Transfer in Natural Water. Academic Press, San Diego, 592 pp.

Neil, D.T., Orpin, A.R., Ridd, E.V., Yu, B.F., 2002. Sediment yield and impacts from river catchments to the Great Barrier Reef lagoon. Mar. Freshwater Res. 53, 733-752.

Ouillon, S., Douillet, P., Andréfouët, S., 2004. Coupling satellite data with *in situ* measurements and numerical modeling to study fine suspended sediment transport: a study for the lagoon of New Caledonia. Coral Reefs 23, 109-122.

Ouillon, S., Douillet, P., Fichez, R., Panché, J.Y., 2005. Enhancement of regional variations in salinity and temperature in a lagoon, New Caledonia. CR Geoscience 337, 1509-1517.

Ouillon, S., Douillet, P., Jouon, A., Dirberg, G., Dupouy, C., Petrenko, A., Froidefond, J.M., Neveux, J., Lefebvre, J.-P., Andréfouët, S., Muñoz Caravaca, A., Lamoureux, J.P., Fichez, R., 2006. Optical Algorithms for Total Suspended Matter in Coastal Tropical Waters: Preliminary results. Proc. Ocean Optics XVIII, Montréal, Canada, 9-13 oct 2006.

Rogers, C.S., 1990. Responses of coral reefs and reef organisms to sedimentation. Mar. Ecol. Prog. Ser. 62, 185-202.

Sequoia Scientific Inc., 2001. The Size Resolution of the LISST Series of Instruments, Application note L008, 2 p.

Sheng, G.P., Yu, H.Q., Li, X.Y., 2006. Stability of sludge flocs under shear conditions: role of extracellular polymeric substances (EPS). Biotech. Bioeng. 93, 1095-1102.

Spalding, M.D., Ravilous, C.R., Green, E.P., 2001. World Atlas of Coral Reefs University of Carolina Press in association with UNEP World conservation monitering Centre, Berkley, CA.

Thornton, D.C.O., 2002. Diatom aggregation in the sea: mechanism and ecological implications. Eur. J. Phycol. 37, 149-161.

Tixier, N., 2003. Approche des propriétés rhéologiques de suspensions biologiques floculées. Ph.D. Thesis. Univ. de Limoges.

Traykovski, P., Latter, R., Irish, J.D., 1999. A Laboratory Evaluation of the LISST Instrument Using Natural Sediments. Mar. Geol. 159, 355-367.

Van Leussen, W., 1994. Estuarine Macroflocs and their role in fine grained sediment transport. PhD Thesis, University of Utrecht.

Voulgaris, G., Meyers, S.T., 2004. Temporal variability of hydrodynamics, sediment concentration and sediment settling velocity in a tidal creek. Cont. Shelf Res. 24, 1659-1683.

Walling, D.E., Fang, D., 2003. Recent trends in the suspended sediment loads of the world's rivers. Global and Planetary Change 39, 111-126.

Wass, P.D., Marks, S.D., Finch, J.W., Leeks, G.J.L., Ingram, J.K., 1997. Monitoring and preliminary interpretation of in-river turbidity and remote sensing imagery for suspended sediment transport studies in the Humber catchment. Sci Tot Env 194/195, 263-283.

Wild, C., Huettel, M., Klueter, A., Kremb, S.G., Rasheed, M.Y.M., Jorgensen, B.B., 2004. Coral mucus as an energy carrier and particle trap in the reef ecosystem. Nature 428, 66-70.

Winterwerp, J.C., 2002.On the flocculation and settling velocity of estuarine mud. Cont. Shelf Res. 22, 1339-1360.

Wolanski, E., Richmond, R.H., Davis, G., Bonito, V., 2003. Water fine sediment dynamics in a transient river plumes in a small, reef-fringed bay, Guam. Estuar. Coast. Shelf Sci. 56, 1029-1040.

V.3 Autres résultats : tests de sensibilité du granulomètre à l'aide de billes calibrées

Le LISST 100X est un instrument innovant, cette version du LISST a été spécialement conçue pour des mesures de particules en suspension en eaux peu chargées. Quelques tests de sensibilité ont été effectués en laboratoire afin de mieux jauger les capacités du LISST 100X.

Le dispositif expérimental est quasiment identique à celui décrit dans la partie précédente, à la différence près que le sonificateur a été remplacé par un bécher constamment mélangé par un agitateur magnétique. Une quantité donnée de billes est introduite dans le dispositif (Tableau V-2).

Solutions	Vi (µL)	Csol,i (%)	Vsol,i (µL)	Vf (L)	Cf expected (µL/L)	Cf measured (µL/L)
1µm	10.00	10.00	1.00	0.20	5.00	1.18
3µm	30.00	2.69	0.81	0.20	4.04	0.99
6µm	40.00	2.50	1.00	0.20	5.00	2.21
8µm	21.00	5.70	1.20	0.20	5.98	8.29
Powders	Mp (mg)	dsphère (mg.µL-1)	Vsol,i (µL)	Vf (L)	Cf expected (µL/L)	Cf measured (µL/L)
25-32µm	20.00	2.48	8.08	0.30	26.94	13.45
100µm	20.00	2.00	10.00	0.30	33.33	2.80

Tableau V-2 Paramètre initiaux des test de sensibilité menés sur le LISST 100X. Les indices i pour initial, sol pour solide et f pour final.

Les différences entre les concentrations volumiques introduites dans le dispositif et les concentrations volumiques mesurées par le LISST 100X sont considérables (Tableau V-2). Au regard de l'importance de ces différences, il serait surprenant que le LISST 100X (calibré au départ du constructeur) soit à l'origine de ce biais. Nous pensons en revanche que notre dispositif n'est pas conservatif. Malgré l'ensemble des précautions prises, une partie des sphères introduites ne doit pas passer pas dans le volume de détection du LISST. L'adhésion aux parois et le dépôt d'une partie des particules du dispositif (Gartner et al., 2001) pourraient expliquer en partie la perte de signal.

Les distributions des concentrations volumiques sur les classes de taille du LISST ont ensuite été normalisées sur les quantités totales afin d'obtenir la réponse du LISST à chacune des particules calibrées (Figure V-12).

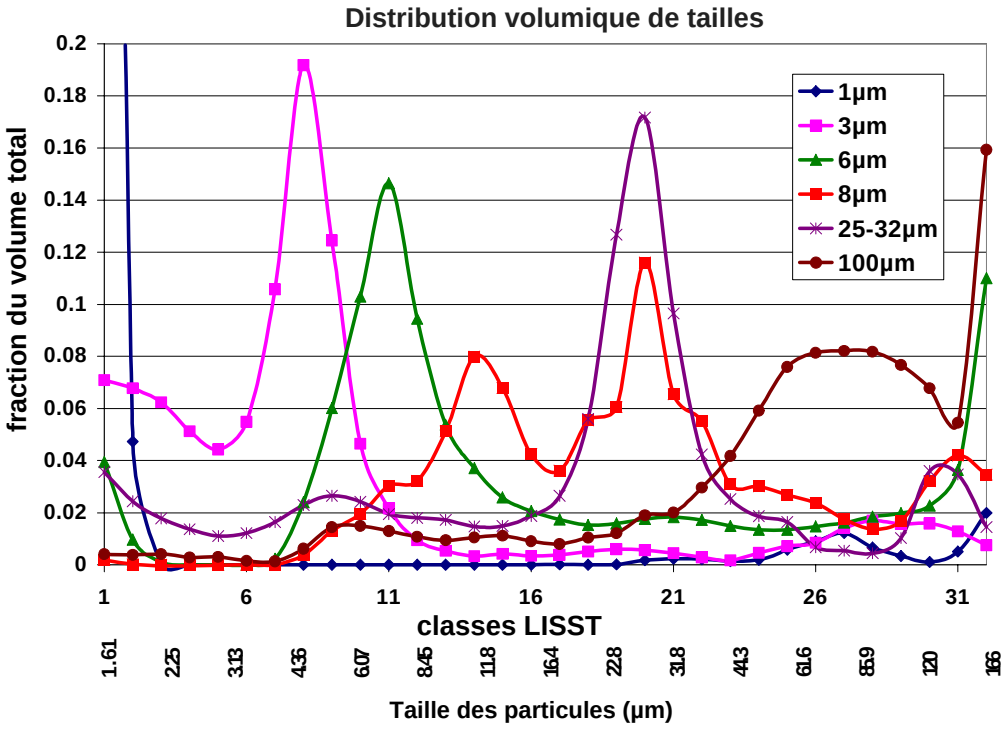

Figure V-12 Distributions granulométriques normalisées des sphères calibrées.

Pour chaque diamètre de sphère, nous avons identifié « les classes cibles » du LISST, dans lesquelles était regroupée une importante partie de distribution granulométrique moyenne normalisée du volume total de la distribution granulométrique relative. Des dilutions successives ont été effectuées sur la solution introduite dans le dispositif. Pour chaque type de sphères, la réponse sur les classes cibles est alors comparée à la réponse globale du LISST 100X.

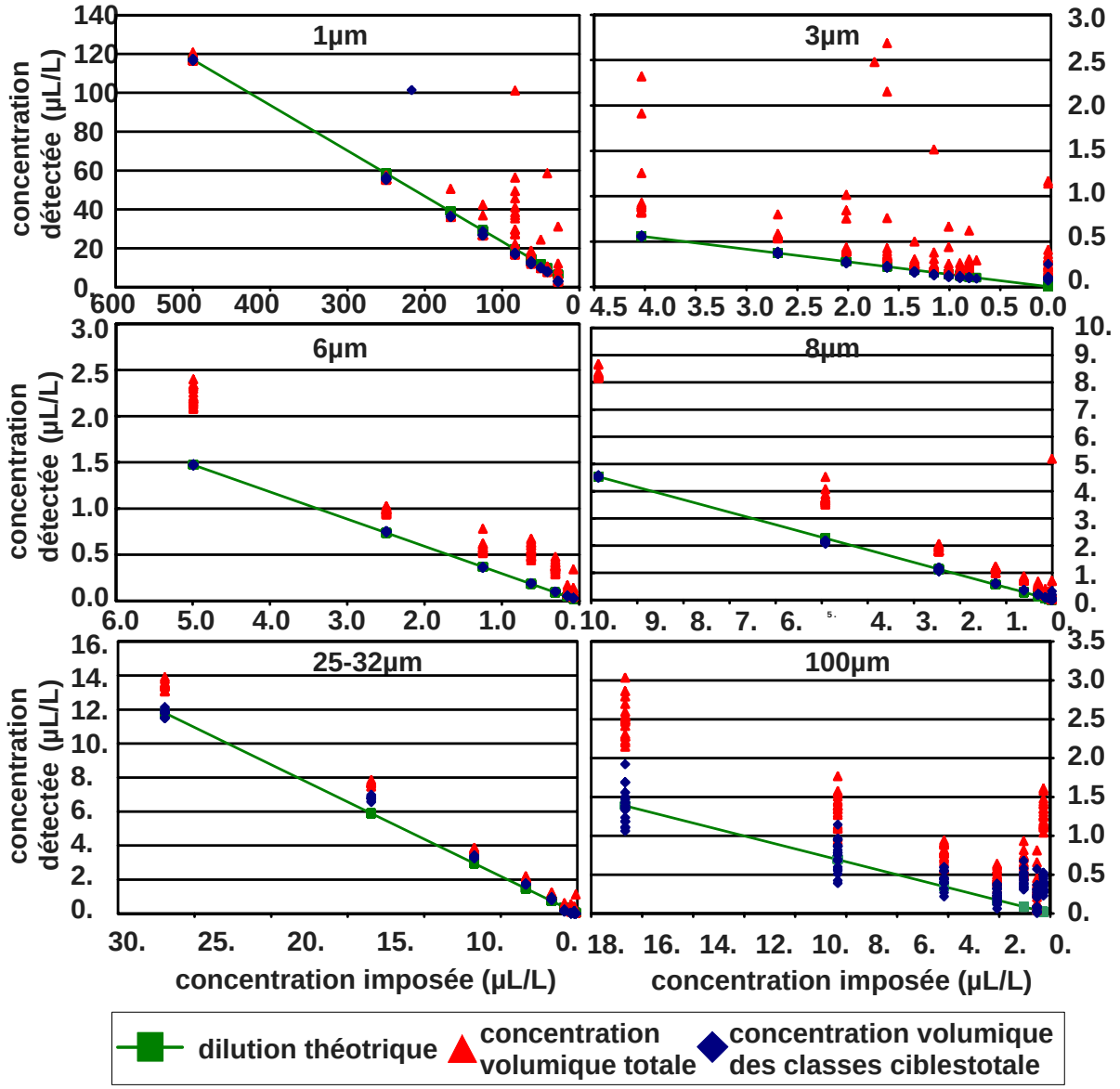

Figure V-13 Relations expérimentales entre concentration imposée, concentration totale mesurée par le LISST et concentration volumique dans une gamme de tailles ciblée mesurée par le LISST.

Pour tous les échantillons de billes calibrées hormis les billes à 100µm, la variabilité du signal à un stade de dilution donné provient des classes de tailles qui n'appartiennent pas aux classes cibles. Ces tests de sensibilité montrent qu'il existe un facteur relativement constant entre la quantité de matériel introduite et la quantité détectée dans les classes cibles. Ce facteur est variable d'un type de bille à l'autre. Si une part de ces biais peut-être imputée aux inexactitudes de manipulation, le fait que ce facteur soit constant nous fait penser qu'une autre partie du biais observé dépend directement de l'appareil. Gartner et al. (2001) affirment que le facteur de conversion qui permet de convertir l'intensité lumineuse détecté en concentration volumique dépend de la classe granulométrique. Ceci n'est pas intégré dans le traitement standard des mesures LISST.

V.4 Conclusion

La mesure de la quantité de MES par des sondes optiques n'est pas triviale. La grande majorité des études visant à caractériser les matières en suspension a été effectuée dans des milieux à moyenne ou forte charge particulaire. Les méthodes appliquées aux études du transport particulaire sont éprouvées dans ces contextes spécifiques. Les résultats exposés dans cette partie montrent que ces méthodes de détection optique « classiques » sont entachées d'erreurs significatives lorsqu'elles sont appliquées dans un environnement lagonaire corallien, qui se caractérise de surcroît par une très faible charge particulaire. Hormis la détermination fastidieuse de la concentration massique d'échantillons par mesure gravimétrique, aucun des moyens de mesure indirecte de la quantité de MES ne permet de déterminer de manière fiable la concentration massique des particules. Il ne semble pas exister de relation simple entre les signaux optiques mesurés et la concentration massique de particules en suspension.

La modélisation du transport particulaire repose sur la résolution de l'équation d'advection-diffusion de la concentration massique des particules en suspension car la masse est le seul paramètre conservatif qui caractérise les particules en suspension. Lors de l'étape de validation d'un modèle de transport particulaire, il est nécessaire de se procurer des données quantifiant la concentration massique des MES. L'avantage du LISST 100X par rapport aux autres sondes utilisées dans ce travail est que son évaluation de la concentration volumique est moins sensible à la dimension des particules mesurées. Malheureusement, le lien qui existe entre la concentration volumique et la concentration massique des particules n'est pas direct dès lors que se produit la floculation ou l'agrégation des particules. L'emploi d'une colonne de filtration dont les filtres correspondraient aux classes de tailles mesurées par le LISST 100X pourrait permettre d'explorer plus en détail le lien entre concentration volumique fournie par le LISST 100X et la concentration volumique.

Malgré la difficulté d'établir un lien entre concentration volumique et concentration massique, le LISST 100X permet d'identifier les classes de tailles des particules en suspension. Même si la régression entre la turbidité et la concentration massique sur le SLNC n'est pas fameuse, la corrélation entre la turbidité et le signal du LISST restreint aux faibles classes de taille est relativement bonne. Une approche « multi-instrumentale » pourrait éventuellement permettre d'accéder à une estimation de la concentration massique qui soit plus fiable que celle de chaque sonde prise à part. La mesure de quantité de matières en suspension par des moyens acoustiques (Tessier, 2006) pourrait également être testée sur le SLNC.

Les résultats de ce travail ont démontré l'importance des processus d'agrégation des particules en suspension sur le SLNC. Ces processus d'agrégation compliquent fortement l'identification de la relation qui existe entre les mesures optiques et la concentration

massique des particules en suspension. L'agrégation des particules a également des effets sur la vitesse de chute des MES. En effet, les paramètres nécessaires au calcul de la vitesse de chute d'un agrégat sont les mêmes que pour le calcul de la vitesse de chute de particules élémentaires (dimension caractéristique et densité, Eq. II-47) à la différence majeure qu'il faut considérer l'agrégat en tant qu'entité. L'état d'agrégation des particules est dynamique. Le calcul de la vitesse de chute d'un agrégat passe par l'estimation de l'état d'agrégation. Des formulations de la vitesse de chute adaptée à la présence d'agrégats existent (Van Leussen, 1994 ; Manning et Dyer, K.R., 1999; Le Hir et al., 2001 ;Winterwerp, 2002). La grande majorité de ces formulations de vitesse de chute a été développée dans des contextes à forte teneur en particules terrigènes. Ces formulations ne peuvent pas être transposées directement aux agrégats formés dans le SLNC. La vitesse de chute des agrégats dans le contexte « classique » est plus importante que celle des particules qui le constituent. A l'inverse, nos observations indiquent que les agrégats ont une faible vitesse de chute.

Quelques travaux visant à identifier les paramètres gouvernant l'état d'agrégation ont été entrepris au cours de cette thèse. Une tentative pour identifier une relation entre le spectre de tailles des particules désagrégées et le spectre de tailles des particules *in situ* a été menée. Le fait que le protocole de mesure de tailles de particules en laboratoire ne soit pas conservatif ajoute de la complexité à cette entreprise. Deux raisons pourraient en être à l'origine. La première est que les particules adhèrent aux parois du circuit. L'utilisation de tuyaux et de récipients ayant une surface plus lisse pourrait être testée. La seconde hypothèse pour laquelle le dispositif n'est pas conservatif pourrait être qu'il est nécessaire de recalculer le coefficient de conversion pour chacune des classes de taille (Gartner et al., 2001). La visualisation au microscope optique ainsi que des analyses au microscope électronique à balayage équipé de sonde EDS ont été initiées dans le cadre de la thèse, ces démarches n'ont pas apportés d'éléments permettant de faire progresser la caractérisation des particules en suspension dans le SLNC.

La compréhension de la dynamique d'agrégation nécessite une étude de la nature des particules transportées. L'adhésivité des agrégats est liée à la composition des particules qui le composent. Des analyses visant à révéler la composition chimique des particules pourraient fournir des résultats pertinents pour avancer dans cette voie.

Enfin, l'influence des paramètres dynamiques sur l'état d'agrégation pourrait être explorée. Une première étude de sensibilité, succincte, de la distribution volumique de taille à l'intensité du courant a été entreprise pendant cette thèse. L'approximation avait été faite que le courant engendré par le vent était négligeable devant le courant de marée pour la détermination de la vitesse instantanée. La distribution volumique de taille avait été mise en relation avec la vitesse d'élévation du plan d'eau obtenue sur le site du SHOM. Cette étude embryonnaire pourrait être poursuivie avec davantage de précisions en prenant comme donnée de courant les sorties du modèle hydrodynamique.

Le regroupement de l'ADV (courants, élévation de surface, vagues, turbulence, et mesure acoustique des MES), du LISST (mesure optique d'atténuation, et distribution de la concentration volumique des particules en suspension en fonction de leur taille) et.de la CTD (turbidité, salinité, température et chlorophylle) sur une station benthique lors d'un suivi temporel sur le SLNC pourrait fournir un jeu de données complet pour prolonger et approfondir cette étude.

Chapitre VI CONCLUSION GENERALE

« What goes around…
Comes around »
(Bob Marley)

En grande majorité, les travaux d'analyse et de modélisation 3D hydro-sédimentaire à sub-méso-échelle concernent des plateaux continentaux ou des milieux estuariens à forte concentration en particules sédimentaires. Les analyses et modèles qui y furent développées ne sont pas transposables sans précautions au lagon calédonien, étant donnés ses particularités qui, de surcroît, demandent des développements spécifiques.

Le SLNC est caractérisé par une importante hétérogénéité spatiale de la circulation. La réflexion menée autour de la signification des différents TH présentés dans la littérature et l'élaboration de TH spatialisés sur le SLNC ont permis de quantifier la variabilité spatiale de l'hydrodynamique en terme de renouvellement des masses d'eau.

Cette démarche, inspirée de la pluridisciplinarité de l'équipe au sein de laquelle s'est effectuée cette thèse, a également permis de participer à des opérations de recherche *a priori* moins proches des sujets traditionnellement abordés en hydrodynamique et en transport particulaire. En comparant des données bio-géochimiques au LeFT (Jouon et al., 2006), Torreton et al. (sous presse) démontrent que le SLNC est un écosystème mésotrophe vidangé par les eaux oligotrophes océaniques. Le choix du volume de contrôle dans le calcul des TH avait été effectué sur des critères géomorphologiques, cette étude démontre *a posteriori* que ce choix avait une cohérence selon des critères biologiques et biochimiques. La conclusion principale de l'article de Mari et al. (2007) établit un lien étroit entre le renouvellement des masses d'eau et la réactivité de la matière organique dissoute. A partir de cette conclusion *a priori* éloignée du transport particulaire, cette étude fait des estimations sur les caractéristiques des agrégats organiques en suspension dans le SLNC. La proportion de TEP dans les agrégats organiques en suspension est estimée à 20% au niveau du récif barrière et à 60 % au fond des baies. La part volumique de TEP dans ces agrégats représente 65 % au fond des baies, et 3% au niveau du récif barrière. Enfin, cette étude formule l'hypothèse que les agrégats organiques ont une flottabilité négative au niveau du récif barrière et positive au fond des baies.

Les TH calculés ont également permis d'affirmer que le mélange vertical était trop important dans la version de MARS3D implémentée sur le SLNC. Ce constat oriente les efforts futurs en modélisation hydrodynamique vers une paramétrisation de la fermeture turbulente plus adaptée au site d'étude, et vers une nécessaire représentation des mélanges thermo-halins.

De manière à améliorer la modélisation du transport particulaire, et notamment le calcul des contraintes de cisaillement au fond responsable de la remise en suspension, le modèle de génération et de propagation de vagues WWATCH III a été implémenté sur le SLNC. Le caractère semi-ouvert et les variations brutales de la bathymétrie dans le SLNC ont motivé un travail de validation de ce modèle couramment employé dans des cas plus génériques. Les spécificités du SLNC ont nécessité l'élaboration d'une méthode de validation adaptée. Cette méthode préconise l'adoption de précautions concernant le déploiment des appareillages de mesures afin d'accéder aux caractéristiques des vagues de hautes fréquences. L'emploi de filtres passe haut et passe bas sur, respectivement, les données mesurées et les résultats de simulation est suggéré pour faire concorder les bandes de fréquences sur lesquelles s'effectue la validation du modèle.

Les résultats de cette étape de validation ont permis de montrer que WWATCH III est adapté à la simulation de vagues de vent dans un contexte de fetch limité, et que la prise en compte de la seule mer de vent suffit à représenter correctement l'état de mer sur le SLNC au premier ordre. L'étude met également en évidence une limitation de la méthode adoptée pour le traitement du signal, puisque la fonction de distribution angulaire de la houle est bruitée.

La caractérisation des particules en suspension a ensuite été entreprise afin d'identifier les raisons potentielles des écarts entre les concentrations simulées et les turbidités mesurées. Cette étude souligne que la variabilité spatiale du volume de particules en suspension est supérieure à sa variabilité temporelle. A l'inverse, les distributions volumiques de tailles de particules sont elles, plus variables dans le temps que dans l'espace. La caractérisation des particules en suspension a également permis de souligner l'importance de la fraction agrégée de particules en suspension. Les agrégats mesurés possèdent des caractéristiques qui semblent différer de celles des flocs formés sous l'effet de la seule agrégation de particules cohésives. Après analyse des données et identification d'un accroissement de l'efficacité d'agrégation aux environs des récifs coralliens, l'hypothèse est formulée que ces agrégats sont en grande partie des agrégats organiques. Cette hypothèse s'accorde avec les conclusions des travaux de Mari et al. (2007) qui estiment que la coagulation de matière organique dissoute représente une part importante du volume des agrégats. La formation des agrégats organiques est différente de la formation des flocs sédimentaires qui se constituent à partir de l'adhésion des particules cohésives.

L'importante proportion de ces agrégats rend difficile l'établissement d'une relation entre le volume de particules et leur masse et remet en question l'analyse des mesures de concentration de particules par transmissométrie et rétrodiffusion optique. Les spécificités du lagon accroissent la difficulté d'estimation de la concentration massique de particules en suspension. La mesure de la concentration de particules sédimentaires en suspension dans le SLNC, et probablement dans les lagons coralliens en général, doit donc tenir compte de la présence de particules annexes et de processus d'agrégation spécifiques.

Pour caractériser plus précisément les particules en suspension dans le SLNC, il serait utile d'effectuer des filtrations en colonnes d'échantillons prélevés simultanément à une mesure à l'aide d'un granulomètre laser *in situ*. A partir des filtres, l'analyse de la nature des matériaux constitutifs des particules suivant les classes de tailles filtrées, et la mesure du spectre de taille des particules désagrégées pourraient fournir des densités des grains constitutifs des particules par classes de taille ainsi qu'une information sur la nature des matériaux constitutifs des agrégats. Le déploiement simultané sur le terrain d'un ADV, d'une CTD, et des mesures de la matière organique dissoute reliées à une estimation de son âge devraient permettre de cerner la plupart des paramètres agissant potentiellement sur les processus d'agrégation.

Les spécificités du SLNC par rapport à des environnements plus fréquemment étudiés nécessitent le développement de méthodes *ad hoc*. La caractérisation des agrégats, notamment organiques, et de leur dynamique s'éloigne des thématiques purement sédimentaires sur lesquelles se sont focalisées la majorité des études de transport particulaire. En effet, contrairement aux particules passives, les agrégats ont la capacité d'apparaître spontanément dans la colonne d'eau (excrétion du mucus par exemple par les coraux). Si l'adaptation des modèles de transport particulaire aux agrégats organiques n'est pas encore envisageable, la démarche proposée conduit néanmoins à un élargissement des thématiques associées au transport particulaire.

REFERENCES BIBLIOGRAPHIQUES

Abdelrhman, M.A., 2005. Simplified modeling of flushing and residence times in 42 embayments in New England, USA, with special attention to Greenwich Bay, Rhode Island. Estuar. Coast. Shelf Sci. 62, 339-351.

Andréfouët, S., Pagès, J., Tartinville, B., 2001. Water renewal time for classification of atoll lagoons in the Tuamotu Archipelago (French Polynesia). Coral Reefs 20, 399-408.

Arakawa, A., Lamb, V.R., 1977. Computational design of the basic dynamical process of the UCLA General Circulation Model In Methods in Computational Physics, 173-265.

Arnoux-Chiavassa, S., Rey, V., Fraunié, P., 2003. Modeling 3D Rhône river plume using a higher order advection scheme. Oceanologica Acta 26, 299-309.

Azetsu-Scott, K., Johnson, B.D., 1992. Measuring physical characteristics of particles: A new method of simultaneous measurement for size, settling velocity and density of constituent matter. Deep-Sea Res. 39, 1057-1066.

Bel Madani, A., 2003. Modélisation du champ de vagues de vent dans le lagon Sud-Ouest de Nouvelle-Calédonie. Rapport de stage Ingénieur ENSEEIHT, 56p.

Bolin, B., Rodhe, H., 1973. A note on the concepts of age distribution and transit time in natural reservoirs. Tellus 25, 58-62.

Booij, N., Holthuijsen, L.H., 1987. Propagation of ocean waves in discrete spectral wave models. J. Comput. Physics 68, 307-326.

Booij, N., Ris, R.C., Holthuijsen, L.H., 1999. A third-generation wave model for coastal regions, Part I, Model description and validation. J. Geoph. Research (C4) 104, 7649-7666.

Bouron Morin, B., 2001. Modélisation sédimentaire dans le lagon Sud-Ouest de Nouvelle-Calédonie. Rapport de stage DEA, Univeristé Pierre et Marie Curie, Paris VI., 37p.

Briand, E., Pringault, O., Jacquet, S., Torréton, J.-P., 2004. The use of oxygen microprobes to measure bacterial respiration for determining bacterioplankton carbon growth efficiency along trophic gradients in a coral reef lagoon. Limnol. Oceanogr. Methods 2, 406-416.

Bruun, P., 1962. Sea-level rise as a cause of shore erosion. Journal of the Waterways and Harbors Division, ASCE, 88, 11-130.

Bryant, DG, Burke, L., McManus, J., Spalding, M., 1998. Reefs at Risk: A Map-based Indicator of Threats to the World's Coral Reefs - World Resources Institute, 56p.

Bujan, S., 2000. Modélisation biogéochimique du cycle du carbone et de l'azote dans les écosystèmes côtiers tropicaux sous influences terrigènes et anthropiques. PhD Thesis dissertation, University of Aix-Marseille II, France, 249p.

Cayula, J.F., Cornillon, P., 1992. Edge detection algorithm for SST Images. J. Atm. Ocean. Tech. 9, 6780.

Chardy, P., Chevillon, C., Clavier, J., 1988. Major benthic communities of the south-west lagoon of New Caledonia. Coral Reefs 7, 69-75.

Chevillotte, V., Douillet, P., Cabioch, G., Lafoyd, Y., Lagabrielle, Y., Maurizot, P., 2005. Évolution géomorphologique de l'avant-pays du Sud-Ouest de la Nouvelle-Calédonie durant les derniers cycles glaciaires. C. R. Geoscience 337, 695–701.

Clavier, J., Chardy, P., Chevillon, C., 1995. Sedimentation of Particulate Matter in the South-west Lagoon of New Caledonia: Spatial and Temporal Patterns. Estuar. Coast. Shelf Sci. 40, 281-294.

Clavier, J., Douillet, P., 1996. Interprétation du fonctionnement écologique d'un lagon corallinen par modélisation hydrodynamique: influences des apports terrigènes. Actes des Journées du Programme Environnement, Vie et Société, Cité des Sciences et de l'industrie, Paris, 15 au 17 janvier 1996, 85-90.

Couvelard, X., Marchesiello, P., Gourdeau, L., Dutrieux, P., (in prep. for Journal of Physical Oceanography). Barotropic Jets induces by Islands in the South West Pacific.

Crump, B.C., Hopkinson, C.S., Sogin, J.E., 2004. Microbial Biogeography along an Estuarine Salinity Gradient: Combined Influences of Bacterial Growth and Residence Time. Appl. Environ. Microb. 70, 1494-1505.

Cugier, P., Le Hir, P., 2002. Development of a 3D Hydrodynamic Model for Coastal Ecosystem Modelling. Application to the Plume of the Seine River (France). Estuar. Coast. Shelf Sci. 55, 673-695.

Cushman-Roisin, B., 1994. Introduction to Geophysical Fluid Dynamics. Prentice-Hall, London.

Debenay, J.P., 1987. Sedimentology in the south-west lagoon of New Caledonia, SW Pacific. J. Coastal Res. 3, 77-91.

Deleersnijder, E., Campin J.-M., Delhez, E.J.M., 2001. The concept of age in marine modelling: I. Theory and preliminary model results. J. Marine Syst. 28(3-4), 229-267.

Delesalle, B., Sournia, A., 1992. Residence time of water and phytoplankton biomass in coral reef lagoons. Cont. Shelf Res. 12, 939-949.

Delhez, E.J.M., Campin, J.-M., Anthony, C., Hirst, A.C., Deleersnijder, E., 1999. Toward a general theory of the age in ocean modelling. Ocean Model. 1(1),17-27.

Delhez, E.J.M., Deleersnijder E., 2001. The concept of age in marine modeling : II - Concentration distribution function in the English Channel and the North Sea. Journal of Marine Systems 31, 279–297.

Delhez, E.J.M., Heemink, A.W., Deleersnijder, E., 2004a. Residence time in a semi-enclosed domain from the solution of an adjoint problem. Estuar. Coast. Shelf Sci. 61, 691-702.

Delhez, E.J.M., Lacroix, G., Deleersnijder, E., 2004b. The age as a diagnostic of the dynamics of marine ecosystem models. Ocean Dynamics 54, 221-231.

Dettmann, E.H., 2001. Appendix C Additional information on flushing in estuaries. Nutrient Criteria guidance Manual – Estuarine and coastal marine waters. U.S. Environment Protection Agency.

Douillet, P., 1998. Tidal dynamics of the south-west lagoon of New Caledonia: observations and 2D numerical modelling. Oceanol. Acta 21, 69-79.

Douillet, P., Ouillon, S., Cordier E., 2001. A numerical model for fine suspended sediment transport in the southwest lagoon of New Caledonia. Coral Reefs 20, 361-372.

Faure, V., 2006. Modélisation couplée physique-biogéochimique tridimensionnelle: étude de l'écosystème pélagique du lagon Sud-Ouest de Nouvelle-Calédonie. Thèse, Université de la Mediterranée, Marseille, 222 p.

Fernandez, J.M., Moreton, B., Fichez, R., Breau, L., Magand, O., Badie, C., 2002. Advantages of combining 210Pb and geochemical signature determinations in sediment record studies: application to coral reef lagoon environments. Environmental Changes and Radioactive Tracers. Proceedings of the 6th South Pacific Environmental Radioactivity Association Conference, Nouméa, New Caledonia, 187-199.

Field, C.B., Behrenfield, M.J., Randerson, J.T., Falkowski, P., 1998. Primary production of the biosphere: integrating terrestrial and oceanic components. Science 281, 237–240.

Galperin, B., Kantha, L.H., Hassid, S., Rosati, A., 1988. A quasi-equilibrium turbulent energy model for geophysical flows. J. Atmos. Sci., 45, 55-62.

Garreau, P., 1993. Hydrodynamics of the North Brittany coast: a synoptic study. Oceanol. Acta 16(5-6), 469-477.

Gentien, P., Lunven, M., Lehaitre, M., Duvent, J.L., 1995. *In situ* depth profiling of particles sizes. Deep-Sea Res. 42(8), 1297-1312.

Geyer, W.R., 1997. Influence of Wind on Dynamics and Flushing of Shallow Estuaries. Estuar. Coast. Shelf Sci. 44, 713-722.

Gouriou, Y., Delcroix, T., 2002. Seasonal and ENSO variations of sea surface salinity and temperature in the South Pacific Convergence zone during 1976-2000. J. Geophy. Res. 107 (C12), 8011.

Grant, W.D., Madsen, O.S., 1979. Combined Wave and Current Interaction with a Rough Bottom. J. Geophy. Res. 84(C4), 1797-1808.

Grasshoff, K., Eherhardt, M., Kremling, K., 1983. Methods of seawaters analysis. Verlag Chemie, Weinheim, RFA, second edition, 419 p.

Hasselmann, K., Barnett, T.P., Bouws, E., Carlson, H., Cartwright, D.E., Enke, K., Ewing, J.A., Gienapp, H., Hasselmann, D.E., Kruseman, P., Meerburg, A., Müller, P., Olbers, D.J., Richter, K., Sell, W., Walden, H., 1973. Measurements of wind-wave growth and swell decay during the Joint North Sea Wave Project (JONSWAP). Ergänzungsheft zur Deutschen Hydrographischen Zeitschrift, Reihe A (8) Nr. 12, 95 pp.

Hasselmann, S., Hasselmann, K., Allender, J.H., Barnett, T.P., 1985. Computations and parameterizations of the nonlinear energy transfer in a gravity-wave spectrum, Part I: A new method for efficient computations of the exact nonlinear transfer integral. J. Phys. Ocean. 15, 1369-1377.

Henin, C., Guillerm, J.M., Chabert, L., 1984. Circulation superficielle autour de la Nouvele-Calédonie. Oceanogr. Trop. 19 (2), 113-126.

Hidalgo-Gonzalez, R.M., Alvarez-Borrego, S., 2001. Chlorophyll profiles and the water column structure in the Gulf of California. Oceanol. acta 24(1), 19-28.

Hirleman, E.D., 1987. Optimal scaling of the inverse Fraunhofer diffraction particle sizing problem: The linear system produced by quadrature. Particle Characterization 4, 128-133.

Hoegh-Guldberg, O., 1999. Climate change, coral bleaching and the future of the world's coral reefs. Mar. Freshwater Res. 50, 839–866.

Holmes, M.R., Aminot, A., Kérouel, R., Hooker, B.A., Peterson, B.J., 1999. A simple and precise method for measuring ammonium in marine and freshwater ecosystems. Can. J. Fish. Aquat. Sci. 56, 1801-1808.

Holm-Hansen, O., Lorenzen, C.J., Holmes, R.W., Strickland, J.D.H., 1965. Fluorimetric determination of chlorophyll. Journal du Conseil Permanent International pour l'Exploration de la Mer 30, 3-15.

Holthuijsen, L.H., Booij, N., Herbers, T.H.C., 1989. Prediction Model for Stationary, Short-crested Waves in Shallow Water with Ambient Currents. Coast. Eng. 13(1), 23-54.

Hughes, T.P., Baird, A.H., Bellwood, D.R., Card, M., Connolly, S.R., Folke, C., Grosberg, R., Hoegh-Guldberg, O., Jackson, J.B.C., Kleypas, J., Lough, J.M., Marshall, P., Nyström, M., Palumbi, S.R., Pandolfi, J.M., Rosen, B., Roughgarden, J., 2003. Climate Change, Human Impacts, and the Resilience of Coral Reefs. Science 301, 929-933.

Huynh-Thanh, S., Temperville, A., 1995. A numerical prediction of bed shear stresses in the wave-current turbulent boundary layer over flat sea beds. Oceanol. Acta 18, 1, 19-27.

Jacquet, S., Delesalle, B., Torréton, J.-P., Blanchot, J., 2006. Responses of the phytoplankton communities to increased anthropogenic influences (Southwestern Lagoon, New Caledonia). Mar. Ecol. Prog. Ser. 320: 65-78.

Jonsson, I.G., 1966. Wave boundary layer and friction factor. Proceedings of the 10 th ICCE, ASCE, 127-148.

Jouon, A., Douillet, P., Ouillon, S., Fraunié, P., 2006. Calculations of hydrodynamic time parameters in a semi-opened coastal zone using a 3D hydrodynamic model. Continental Shelf Research 26, 1395-1415.

Jouon, A., 2002. Outils diagnostiques de la dispersion des eaux du Rhône. Rapport de stage DEA, Université Bretagne Occidentale, 28 p.

Kleypas, J.A., Buddemeier, R.W., Archer, D., Gattuso, J.-P., Langdon, C., Bradley, N.O., 1999. Geochemical Consequences of Increased Atmospheric Carbon Dioxide on Coral Reefs. Science 284(5411), 118-120.

Komen, G.J., Cavaleri, L., Donelan, M., Hasselmann, K., Hasselmann, S., Janssen, P.A.E.M., 1994. Dynamics and Modelling of Ocean Waves. Cambridge University Press, 532 pp.

Krone, R.B., 1962. Flume studies of the transport of sediment in estuarial shoaling processes. Final report, Hydraulic Engineering Laboratory, University of California, Berkeley, C.A., 196 pp.

Kundu, P.K., 1990. Fluid Mechanics. Academic Press, San Diego.

Lazure, P., Dumas, F., (submitted to Ocean Model.). An external-internal mode coupling for a 3D hydrodynamical model for applications at regional scale MARS3D.

Leendertse, J.J., Gritton, E.C., 1971. A water-quality simulation model for well-mixed estuaries and coastal seas. Computation Procedures Vol. 2 of Report R-708-NYC. New York City, Rand Institute, 53pp.

Le Hir, P., Bassoulet, P., Jestin, H., 2001. Application of the continuous modeling concept to simulate high-concentration suspended sediment in a macrotidal estuary. In W. McAnally et A. Mehta (Eds), Coastal and Estuarine Fine Sediment Processes, 229-247.

Lehfeld, R., Bloss, S., 1988. Algebraic turbulence model for stratified tidal flows. In Physical Processes in Estuaries (Donkers, J. & Van Leussen, W., eds). Springer-Verlag, New York, 278-291.

Leonard, B.P., 1979. A stable and accurate convective modelling procedure based on quadratic upstream interpolation. Comp. Methods Appl. Mech. Eng. 19, 59-98.

Li, M.Z., Amos, C.L., 2001. SEDTRANS96 : the upgraded and better calibrated sediment-transport model for continental shelves. Computers and Geoscience 27, 619-645.

Luconthe, C., 2006. Validation d'un modèle d'atmosphère régional forcé par un modèle océanique. Application à la Nouvelle-Calédonie. Rapport Techniciens Supérieurs Exploitation, Ecole Nationale de Météorologie.

Lynch, D.R., Ip, J.T.C., Naimie, C.E., Werner, F.E., 1996. Comprehensive coastal circulation model with application to the Gulf of Maine. Cont. Shelf. Res. 10, 875-906.

Manning, A.J., Dyer, K.R., 1999. A laboratory examination of floc characteristics with regard to turbulent shearing. Marine Geology 160, 147–170

Mari, X., Rassoulzadegan, F., Brussaard, C.P.D., Wassmann, P., 2005. Dynamics of transparent exopolymeric particles (TEP) production by *Phaeocystis globosa* under N- or P-limitation: a controlling factor of the retention/export balance. Harmful Algae 4, 895-914.

Mari, X., Rochelle-Newall, E., Torréton, J.P., Pringault, O., Jouon A., 2007. Water residence time: A regulatory factor of the DOM to POM transfer efficiency. Limnology and Oceanography. 52: 808-819.

Meehl, G.A.,Washington, W.M., Collins, W.D., Arblaster, J.M., Hu, A., Buja, L.E., Strand, W.G., Teng, H., 2005. How Much More Global Warming and Sea Level Rise? Science 307(5716), 1769 – 1772

Migon, C., Ouillon, S., Mari, X., Nicolas, E., (in press). Geochemical and hydrodynamic constrains on the distribution of trace metals concentrations in the lagoon of Noumea, New Caledonia. Est. Cont. Shelf Res.

Monbaliu, J., Hargreaves, J.C., Carretero, J.-C., Gerritsen, H., Flather, R., 1999. Wave modelling in the PROMISE project. Coastal Eng. 37, 379-407.

Monbaliu, J., Padilla-Hernandez, R., Hargreaves, J.C., Carretero, Albiach, J.-C., Luo, W., Sclavo, M., Günther, H., 2000. The spectral wave model WAM adapted for applications with high spatial resolution. Coastal Eng. 41, 41-62.

Monsen, N.E., Cloern, J.E., Lucas, L.V., Monismith, S.G., 2002. A comment on the use of flushing time, residence time, and age as transport time scales. Limnol. Oceanogr. 47, 1545-1553.

Munk, W.H., Anderson, E.R., 1948. Notes on the theory of the thermocline. Journal of Marine Research 7, 276-295.

Nicet, J.B., Delcroix, T., 2000. ENSO-related precipitation changes in New-Caledonia, Southwestern Tropical Pacific : 1969-1998, Mon. Weather Rev. 128, 3001-3006.

Nunes Vaz, R.A., Simpson, J.H., 1994. Turbulence closure modelling of estuarine stratification. Journal of Geophysical research 99 C8, 143-160.

O'Callaghan, J., 1999. The oceanography and sedimentology of a coastal embayment: Dumbea bay, Noumea, New Caledonia. BSc. Thesis, James Cook University, 139p.

Ouillon, S., Douillet, P., Andréfouët, S., 2004. Coupling satellite data with *in situ* measurements and numerical modeling to study fine suspended sediment transport: a study for the lagoon of New Caledonia. Coral Reefs 23, 109-122.

Ouillon, S., Douillet, P., Fichez, R., Panché, J.Y., 2005. Enhancement of regional variations in salinity and temperature in a lagoon, New Caledonia. CR Geoscience 337, 1509-1517.

Pacanowski, R.C., Philander, R.G.H., 1981. Parameterization of vertical mixing in numerical models of tropical oceans. J. Phys. Oceanogr. 11, 1443-1451.

Pandolfi, J.M., Bradbury, R.H., Sala,E., Hughes,T.P., Bjorndal, K.A., Cooke, R.G., McArdle, D., McClenachan, L., Newman, M.J.H., Paredes, G., Warner, R.R., Jackson, J.B.C., 2003. Global Trajectories of the Long-Term Decline of Coral Reef. Science 301, 955-958.

Partheniades, E., 1962. A study of erosion and deposition of cohesive soils in salt water. Thèse de doctorat, University of California, Berkeley, 182 pp.

Pérenne, N., 2006. MARS a Model for Applications at Regional Scale. HOCER Documentation Scientifique V0.1., 51 p.

Raimbault, P., Slawyk, G., Coste, B., Fry, JC., 1990. Feasibility of measuring an automated colorimetric procedure for the determination of seawater nitrate in the 0 to 100 nM range: examples from field and culture. Mar. Biol. 104, 347-351.

Rasmussen, B., Josefson, A.B., 2002. Consistent Estimates for the Residence Time of Micro-tidal Estuaries. Est. Coast.Shelf Sci. 54, 65-73.

Ris, R.C., Holthuijsen, L.H., Booij, N., 1999. A third-generation wave model for coastal regions, Part II: Verification. J. Geoph. Res. 104(C4), 7667-7681.

Rougerie, F., 1985. The New-Caledonian south-West lagoon: Circulation, hydrological specificity and productivity. Proceedings of the 5th International Coral Reef Congress, Tahiti, Vol. 6.

Rougerie, F., 1986. Le lagon sud-ouest de la Nouvelle-Calédonie:spécificité hydrologique et productivité. Paris : ORSTOM. Etudes et thèses, 231pp.

Salomon, J.-C., Guéguéniat, P., Orbi, A., Baron, Y., 1988. A lagrangian model for long term tidally induced transport and mixing. Verification by artificial radionuclide concentration. In: Radionuclides: a tool for oceanography, J.-C Guary, P. Gueguiniat, R.S. Pentreath, eds. Elsevier Applied Science, 384-395.

Segond, M., Mahler, S., Robilliard, D., Fonlupt, C., Planque, B., Lazure, P., 2004 An Algorithm for Detection of Retentive Structures in Coastal Waters. Lecture Notes in Computer Science Artificial Evolution, 166-176.

Shchepetkin, A.F., McWilliams, J.C., 2005. The regional oceanic modeling system (ROMS): a split-explicit, free-surface, topography-following-coordinate oceanic model. Ocean Model. 9, 347–404.

Shen, J., Haas, L., 2004. Calculating age and residence time in the tidal York River using three-dimensional model experiments. Est. Coast. Shelf Sci. 61, 449-461.

Skogen, M.D., Moll., A., 2005. Importance of Ocean circulation in ecological modelling: An example from the North Sea. J. Mar. Syst., 57(3-4), 289-300.

Smagorinsky, J., 1963. General circulation experiments with the primitive equations – I. The basic experiment. Mon. Weather Rev. 91, 99-165.

Soulsby, R., 1997. Dynamics of marine sands. Thomas Telford, ed., 272 pp.

Soulsby, R.L., Hamm, L., Klopman, G., Myrhaug, D., Simons, R.R., Thomas, G.P., 1993. Wave-current interaction within and outside the bottom boundary layer. Coastal Eng. 21, 41-69.

Stern, N., 2006. The Economics of Climate Change The Stern Review Cabinet Office - HM Treasury.

Stramski, D., Boss, E., Bogucki D., Voss, K.J., 2004. The role of seawater constituents in ligth backscattering in the ocean. Progr. Oceanogr. 61, 27-66.

Takeoka, H., 1984. Fundamental concepts of exchange and transport time scales in a coastal sea. Cont. Shelf Res. 3, 311-326.

Tartainville, B., 1998. Modélisation tri-dimensionnelle de la circulation dans le lagon de l'atoll de Mururoa, Polynésie Française. Thèse, Université Catholique de Louvain, 184 p.

Tartinville, B., Deleersnijder, E., Rancher, R., 1997. The water residence time in the Mururoa Atoll Lagoon: sensitivity analysis of a three dimensional model. Coral Reefs 16, 193-203.

Tessier, C., 2006. Caractérisation et dynamique des turbidités en zone côtière : Exemple de la région marine Bretagne Sud. Thèse, Université Bordeaux I, 389p.

Testau, J.L., Conand, F., 1983. Estimation des surfaces des différentes zones du lagon de Nouvelle-Calédonie. Publ. ORSTOM, Nouméa, Nouvelle-Calédonie.

The Royal Society, 2005. Ocean acidification due to increasing atmospheric carbon dioxide, Policy document 12/05.

Tixier, N., 2003. Approche des propriétés rhéologiques de suspensions biologiques floculées. Thèse. Université de Limoges.

Tolman, H.L., 1989. The numerical model WAVEWATCH: a third generation model for the hindcasting of wind waves on tides in shelf seas. Communications on Hydraulic and Geotechnical Engineering, Delft Univ. of Techn., Rep. no. 89-2, 72 pp.

Tolman, H.L., 1991a. Effects of tides and storm surges on North Sea wind waves. J. Phys. Oceanogr. 21, 766- 781.

Tolman, H.L., 1991b. A third-generation model for wind waves on slowly varying, unsteady and inhomogeneous depths and currents. J. Phys. Oceanogr. 21, 782-797.

Tolman, H.L., 1999. User manual and system documentation of WAVEWATCH III version 1.18, NOAA / NWS / NCEP / OMB Technical Note 151, 97 pp. (available at http://polar.wwb.noaa.gov/waves/wavewatch/wavewatch.html).

Tolman, H.L., Chalikov, D.V., 1996. Source terms in a third-generation wind-wave model. J. Phys. Oceanogr. 26, 2497-2518.

Torréton J.P., Rochelle-Newall, E., Jouon, A., Faure, V., Jacquet, S., Douillet, P.(in press). Correspondence between the distribution of hydrodynamic time parameters and the distribution of biological and chemical variables in a semi-enclosed coral reef lagoon. Estuarine, Coastal and Shelf Science.

Van de Hulst, H.C., 1957. Light Scattering by Small Particles. John Wiley & Sons, eds., New York, 470 p.

Van Leussen, W., 1994. Estuarine Macroflocs and their role in fine grained sediment transport. PhD Thesis, University of Utrecht., 488p.

Vecsei, A., 2004. A new estimate of global reefal carbonate production including the fore-reefs. Global Planet. Change 43, 1-18.

Wang, C.F., Hsu, M.H., Kuo, A.Y., 2004. Residence time of the Danshuei River estuary, Taiwan. Est. Coast. Shelf Sci. 60, 381-393.

Wigley, T.M.L., Raper, S.C.B., 1987. Thermal expansion of sea water associated with global warming. Nature 330, 127-131.

Wilkinson, C.R., 1996. Global change and coral reefs: impacts on reefs, economies and human cultures. Global Change Biol. 2(6), 547.

Wolanski, E.J., King, B., 1990. Flushing of Bowden Reef lagoon, Great Barrier Reef. Est. Coast. Shelf Sci. 31, 789-804.

Winterwerp, J.C., 2002.On the flocculation and settling velocity of estuarine mud. Cont. Shelf Res. 22, 1339-1360.

Xing J., Davies, A.M., 1995. Application of three dimensional turbulence energy models to the determination of tidal mixing and currents in a shallow sea. Prog. Oceanog. 35, 153 – 205.

Xing J., Davies, A.M., 1996a. Application of a range of turbulence energy models to the determination of M_4 tidal current profiles. Conti. Shelf Res. 16(4), 517-547.

Xing J., Davies, A.M., 1996b. The Influence of Mixing Length Formulation and Stratification upon Tidal Currents in Shallow Seas. Estuar. Coast. Shelf Sci. 42(4), 417-456.

Zimmerman, J.T.F., 1976. Mixing and flushing of tidal embayments in the Western Dutch Wadden Sea, Part I: distribution of salinity and calculation of mixing time scales. Netherlands Journals of Sea Research 10, 149-191 Douglas, B.C., 1991. Global sea level rise. J. Geophysical Res. 96(C4), 6981-6992.

AUTRES REFERENCES

Internet

Internet 1 http://www.unesco.org/csi/wise/wise6f.htm

Internet 2 http://www.spc.int/demog/fr/index.html

Internet 3 http://nouvellecaledonie.rfo.fr/article12.html

Internet 4 http://www.info.lnc.nc/nickel/20050705.LNC0153.html?0350

Internet 5 http://archive.xstrata.com/falconbridge/www.falconbridge.com/french/growth/growth_initiatives/nickel/koniambo.htm

Internet 6 http://www.goronickel.nc/pages/impacts/emplois.htm

Internet 7 http://www.zoneco.nc/

Internet 8 http://www.ird.fr/

Internet 9 http://www.ird.fr/sais/cgi/Ar?unite=R103

Internet 10 http://www.seabird.com/products/profilers.htm

Internet 11 http://wrf-model.org/index.php

Films

Film 1 DVD « Juan de Nova, l'île de corail », 2004 Tec-Tec Production, ARTE, FR5, IRD.

Film 2 « BULA, ou la caractérisation des eaux d'un lagon », 2004 Canal IRD Production, images et réalisation : Jean-Michel Boré, Narration : Isabelle Périn, durée : 4'34" visible sur http://www.canal.ird.fr/sommaires/missions_cp.htm

LISTE DES FIGURES

LISTE DES TABLEAUX

ANNEXE I

Mari, X., Rochelle-Newall, E., Torréton, J.P., Pringault, O., Jouon A., 2007. Water residence time: A regulatory factor of the DOM to POM transfer efficiency. Limnology and Oceanography. 52: 808-819.

Limnol. Oceanogr., 52(2), 2007, 808–819

Water residence time: A regulatory factor of the DOM to POM transfer efficiency

Xavier Mari, Emma Rochelle-Newall, Jean-Pascal Torréton, Olivier Pringault, and Aymeric Jouon
IRD, UR 103, Noumea Center, BP A5, NC-98848 Noumea, New Caledonia

Christophe Migon
Observatoire Océanologique de Villefranche-sur-Mer, Laboratoire d'Océanographie de Villefranche-sur-Mer, UMR 7093, La Darse, B.P. 8, F-06238 Villefranche-sur-Mer Cedex, France

Abstract

The pools of dissolved (DOM) and particulate organic matter (POM) and of transparent exopolymeric particles (TEP) were studied along two sampling gradients in the lagoon of New Caledonia in relation to the residence time of the water masses. The efficiency of the transfer of material from the dissolved to the particulate phase via TEP formation, indicating the physicochemical reactivity of organic matter, was investigated. DOM, POM, and TEP concentration increased along the sampling gradients, but their relative proportions varied. The contribution of the TEP pool to POM increased from 20% to 60%, from the most oligotrophic stations to the more anthropogenically affected bays. According to the low density of TEP and to the observed variations of the proportion of TEP compared with more conventional and solid particles, the aggregates formed inside the bays would be either neutrally or positively buoyant, whereas in the vicinity of the coral barrier, they would be negatively buoyant. As a result, the downward export of organic matter inside the bays might be greatly reduced, thereby prolonging the residence time of organic matter in the water column. The efficiency of the DOM/TEP transformation and the TEP turnover rate dropped drastically when the residence time increased from 0 to 50 d, suggesting that the reactivity of organic matter is reduced as it ages. The very high residence time of the water mass inside the bays, constrained by the hydrodynamic circulation inside the lagoon, favors the installation of a feedback system in which organic matter is not exported and is continuously degraded, leading to the formation of refractory DOM with a low physicochemical reactivity. In contrast, organic matter produced in areas in which water mass has a low residence time (i.e., near the coral barrier) is rapidly exported because of its high physicochemical reactivity.

A large fraction (~30%) of the dissolved organic matter (DOM) released by phytoplankton is of high molecular weight (HMW; Carlson et al. 1985; Benner et al. 1992; Amon and Benner 1994), and about half of this HMW-DOM fraction is constituted by highly reactive polysaccharides (Benner et al. 1992). Transparent exopolymeric particles (TEP) are formed by coagulation of DOM (Zhou et al. 1998; Mari 1999; Passow 2000), particularly the more reactive fraction (i.e., HMW-DOM; Zhou et al. 1998). Furthermore, it has been suggested that TEP exist along a size continuum from molecules of >1 kDa (HMW-DOM) to particles of hundreds of microns and that the definition of this pool of organic matter should be extended to include both size fractions to form a single reservoir of TEP (Mari et al. 2001).

The transfer of organic matter from the dissolved to the particulate phases via the TEP pathway is driven by collision mechanisms followed by adhesion. Although collisions are mostly controlled by external constraints, such as TEP concentration and turbulence, adhesion is driven by the intrinsic sticking properties of TEP precursors. The sticking properties of TEP and, to a larger extent, the surface-active properties of polysaccharides constituting the HMW-DOM fraction are linked to their chemical composition. The high fraction of polysaccharides with sulfate half-ester groups in the HMW-DOM fraction explains the strong propensity of these polysaccharides to form cationic bridges (Kloareg and Quatrano 1988) and hydrogen bonds (Chin et al. 1998). These highly surface-active polysaccharides are known to be the source of TEP (Zhou et al. 1998). However, because the chemical composition of the exudates released by phytoplankton varies as a function of species and physiological status (Aluwihare and Repeta 1999), the primary composition of TEP and, thus, the sticking properties might also vary as a function of the same factors. Another process that could alter the composition, and thus the reactivity of TEP, is bacterial degradation. TEP are always colonized by bacteria (Alldredge et al. 1993; Passow and Alldredge 1994; Mari and Kiørboe 1996) and, thus, could exhibit very high bacterial activities, such as that observed within marine snow aggregates (Muller-Niklas et al. 1994). This process could lead to the dissolution of aggregates (Smith et al. 1992), to a modification of the composition of the attached bacterial assemblages (Moeseneder et al. 2001), and to a modification of its chemical composition by selectively removing bioreactive components (Aluwihare

Acknowledgments

We thank the crew of the R/V *Coris* for their assistance during sampling and P. Gérard for providing the nutrient data. We are grateful to S. Ouillon and P. Douillet for helpful discussions on the hydrodynamic parameters. Thanks are due to E. A. Canuel and two anonymous reviewers for constructive comments on the manuscript.

This research was supported by the French National Research Agency (ANR-ECCO program) and by the French Research Institute for Development (IRD).

and Repeta 1999; Amon et al. 2001) leading to the production of recalcitrant DOM (Ogawa et al. 2001). Because of their central role in carbon cycling, DOM and TEP exert a significant effect on the vertical flux of elements in the ocean and on their burial to the deep ocean (Engel et al. 2004). However, the influence of polysaccharide aggregation is closely linked to the reactivity of TEP and DOM, which can vary in response to its age and stage of degradation. Other than remineralization, a major determinant of DOM export is by water mass transport In cases in which input rates of DOM match hydrodynamically driven removal rates, DOM will be controlled to a greater extent by physical rather than by biogeochemical processes. However, if input and removal of DOM because of low water mass renewal rates (i.e., long residence times) is imbalanced, the DOM pool will be largely controlled by degradation processes. In other words, long residence time should lead to prolonged bacterial degradation of DOM. Because of topographic constraints, flows are often restricted in estuarine and coastal zones, leading to increased residence times. Although the residence time of a water mass potentially controls the biogeochemistry of coastal and estuarine areas, the relationship between hydrodynamics and DOM reactivity has long been neglected.

In this study, we investigated the reactivity of DOM and its tendency to form TEP by monitoring both pools of organic matter along two sampling gradients in a lagoon in New Caledonia. To link the reactivity of DOM with its age and stage of degradation, variations of the DOM versus TEP equilibrium were correlated with the residence time of the water mass.

Materials and methods

The study site—The southwest lagoon of New Caledonia is an enclosed, relatively shallow site (~20 m) surrounded by oligotrophic oceanic water. In contrast to the oligotrophy observed near the coral barrier, the nearshore environment is subject to terrestrial inputs and to both industrial and urban effluents in the bays around the city of Noumea. This results in well-defined gradients of eutrophication that last throughout the year (Jacquet et al. 2006). Eutrophication in Sainte-Marie Bay (east of Noumea) is mostly due to wastewater outfalls from the Sainte-Marie area (i.e., urban origin). Eutrophication in Grande Rade Bay (west of Noumea) is mainly of industrial origin from the close proximity of a large nickel smelt. In addition to the continuous input of inorganic nutrients and organic matter in the bays, the permanence of this structure is strengthened by a gradient of water mass residence time.

Residence time of the water masses—The parameter used to describe the residence time of the water mass is the local e-flushing time (LeFT, d). The replacement efficiency of water masses can be revealed in the study area by the computation of LeFT. The LeFT is a synthetic parameter that indicates the time required for a tracer mass contained within the station (control volume) to be reduced by a factor 1/e (Jouon et al. 2006) by waters coming from outside the lagoon. The shorter the LeFT, the faster the water masses at the location will be replaced. In contrast, at longer LeFT, water masses are replaced more slowly, leading to higher residence times. The annual average of LeFT at the different stations was calculated from a hydrodynamic model adapted to the studied area taking into account topographic constraints, average wind condition in the lagoon, and tidal cycle (Jouon et al. 2006). This modeling exercise provides estimates of the renewal rates of the water masses in the lagoon (i.e., LeFT), which can be regarded as mean values because the initial parameters used in the model are annual averages of wind conditions. During the sampling period, wind conditions were similar to those used as input parameters in the hydrodynamic model (i.e., well-established trade winds of about 8–10 m s^{-1}); thus, the annual average of LeFT is applicable to the sampling campaigns.

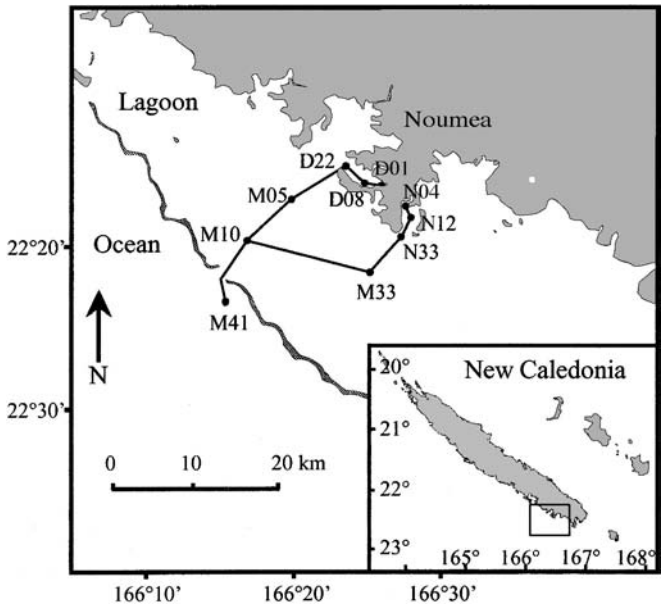

Fig. 1. Map of the study area with position of the sampling stations. The stations D and N are localized in the bays of Grande Rade and of Sainte Marie, respectively.

Sampling—Seawater samples were collected during four sampling occasions in November 2004 with a Teflon pump at 5 m depth for 10 stations. These stations covered two gradients that started in two distinct eutrophied bays (Sainte Marie and Grande Rade) around the city of Noumea and extended to the exterior of the barrier reef (Fig. 1). The sites were divided into six groups (i.e., open ocean, near barrier, middle of the lagoon, mouth of the bays, middle of the bays, and head of the bays). CTD casts were used on each sampling occasion to determine the presence of vertical stratification. After sampling, seawater samples were kept in 30-liter polycarbonate bottles out of direct sunlight until returned to the laboratory within 1–2 h. Each transit was studied twice over a 2-week period, and all stations along each transit were sampled within 1 h.

Pigments and nutrients—Unfiltered replicate 40-mL samples were immediately frozen pending nitrate + nitrite

(NO_x), and phosphate (PO_4^{3-}) analyses. Silicate was determined on one 60-mL subsample, which was immediately frozen after sampling. Nitrate and nitrite concentrations were determined according to Raimbault et al. (1990) on a Bran+Luebbe Autoanalyzer III with an average coefficient of variation (C.V.) of 3% (eutrophic) to 8% (oligotrophic) between replicates. Phosphate and total silicate (dissolved and colloidal) concentrations were determined according to Grasshoff et al. (1983). Phosphate concentrations were determined on a Bran+Luebbe Autoanalyzer III with an average C.V. of 6% to 11% between replicates. The N : P molar ratios (μmol L^{-1} : μmol L^{-1}) were calculated as the sum of dissolved nitrite, nitrate, and ammonia concentrations divided by phosphate concentrations. Chlorophyll *a* (Chl *a*) was determined fluorometrically from duplicate 200-mL subsamples filtered onto 25-mm Whatman GF/F filters.

Nutrient measurements were conducted on unfiltered samples to avoid contamination during filtration. This procedure is similar to the method used for DOC measurements in oligotrophic waters. A test conducted with filtered and unfiltered samples collected in the middle of the lagoon and in the bay of Sainte Marie showed that NO_x and PO_4^{3-} concentrations were not significantly different in the lagoon (*t*-test, $p > 0.05$) whether the samples were filtered or not, whereas they were significantly different (*t*-test, $p < 0.05$) with the samples from the bay. For the bay samples, the concentration of NO_x increased slightly when the samples were filtered (i.e., from 0.855 ± 0.011 to 0.924 ± 0.043 μmol L^{-1} for the unfiltered and the filtered samples, respectively). On the contrary, the concentration of PO_4^{3-} decreased very slightly when the samples were filtered (i.e., from 0.267 ± 0.003 to 0.247 ± 0.011 μmol L^{-1} for the unfiltered and the filtered samples, respectively). This test shows that filtration increases variability, which suggests that filtration rather than freezing alters nutrient concentrations in oligotrophic waters.

Microscopic TEP determination—TEP were stained with Alcian blue (Alldredge et al. 1993) and TEP size spectra were determined from 5- and 10-mL subsamples filtered onto 0.2-μm polycarbonate filters after transfer of the particles retained onto a microscope slide (Passow and Alldredge 1994). TEP size spectra were determined for each slide by counting and sizing TEP at two successive magnifications (×250 and ×400) with a compound light microscope. Ten images were taken per slide and for each magnification. The equivalent spherical diameter of each TEP (d_p, μm) was calculated by measuring its cross-sectional area with an image analysis system (ImagePro Plus, MediaCybernetics), and counts were combined and classified into 20 logarithmic size classes (Mari and Burd 1998). TEP size distributions were described by a power relation of the type $dN/d(d_p) = k d_p^{\delta}$, where dN is the number of particles per unit volume in the size range d_p to $[d_p + d(d_p)]$. The spectral slope, δ, describes the size distribution and was estimated from regressions of $\log[dN/d(d_p)]$ versus $\log(d_p)$. The TEP volume concentration was calculated from the TEP size spectra assuming a spherical volume for each particle.

Colorimetric TEP determination—The semiquantitative colorimetric TEP method, developed by Passow and Alldredge (1995), allows the determination of TEP concentration ($TEP_{spectro}$; xanthan equivalents per liter) by measuring the total amount of Alcian blue adsorbed to all particles, including TEP, that contain carboxylated and sulfated polysaccharides. Two aliquots (100 and 200 mL) of each sample were filtered through 0.4-μm pore size polycarbonate filters at low and constant vacuum pressure (<150 mbar). Particles retained on filters were stained with 500 μL of Alcian blue solution. After staining, filters were rinsed with Milli-Q water and were frozen for later analysis. Filters were transferred to 20-mL polyethylene scintillation vials with 6 mL of H_2SO_4 and were soaked for >2 h. During this period, the vials were agitated to ensure TEP dissolution. The amount of dye bound to particles was determined by measuring adsorption at 787 nm (wavelength of adsorption maximum of Alcian blue) with a spectrophotometer (Perkin-Elmer, Lambda 20). Blanks were taken between each sample with 5 mL of distilled water.

TEP carbon concentration—Estimates of TEP carbon concentration (TEP-C) were calculated two ways. First, by combining TEP size spectra with the relationship giving the carbon content of a given TEP particle according to its size (Mari 1999). Thus, TEP carbon concentration ($TEP\text{-}C_{micro}$, μg C L^{-1}) is given by $TEP\text{-}C_{micro} = 0.25 \times 10^{-6} \sum_i n_i r_i^{2.55}$; where n_i and r_i are, respectively, the concentration of particles and the equivalent spherical radius of the TEP particle in size class *i*. Second, TEP carbon concentration ($TEP\text{-}C_{spectro}$, μg C L^{-1}) was calculated from colorimetric determinations (Engel and Passow 2001) as follows: $TEP\text{-}C_{spectro} = 0.75 TEP_{spectro}/V$, where $TEP_{spectro}$ is the TEP concentration (μg xanthan equivalent L^{-1}) and V is the volume filtered (mL).

Dissolved organic carbon, nitrogen, and phosphorus determination—Dissolved organic carbon (DOC) analyses were performed on 10-mL subsamples collected in precombusted (450°C, overnight) 10-mL glass ampoules, preserved with 12 μL of 85% phosphoric acid (H_3PO_4), and flame sealed. Samples were stored in the dark until analysis. DOC concentration was measured on a Shimadzu TOC VCPH analyzer with potassium phthalate calibration standards over the measurement range 0–250 μmol C L^{-1}. Certified reference materials (Hansell Laboratory, University of Miami, Florida) were also used to assess the performance of the instrument on and between measurement days. The machine blank was between 5 and 10 μmol C L^{-1} for the measurement days. Total organic nitrogen (TON) and phosphorous (TOP) were determined from unfiltered replicate 120-mL samples immediately frozen until analysis. After mineralization of organic material by wet oxidation (Raimbault et al. 1999), phosphate and nitrate were measured as described above. Dissolved organic nitrogen (DON) and phosphorous

(DOP) were computed by subtracting corresponding dissolved inorganic and particulate organic nutrients from TON or TOP. The C : N : P molar ratios were obtained in terms of DOC : DON : DOP from the bulk dissolved fraction.

Particulate organic carbon, nitrogen, and phosphorus determination—Particulate organic carbon (POC) and particulate nitrogen (PN) were measured from 2.5-L subsamples (one for each sampling station) immediately filtered onto 25-mm Whatman GF/F filters precombusted at 550°C for 2 h. After filtration, the filters were dried at 60°C for 24 h and then frozen for later analysis. Analyses were carried out with a LECO-900 CHN analyzer calibrated with ethylenediaminetetraacetic acid standards. For the determination of organic carbon, carbonates were removed with 100-μL of 2 mol L^{-1} HCl and renewed until there was no longer any effervescence. Acidified samples were kept in a drying oven (60–70°C) for 24 h. Detection limits were 40 and 10 μg for carbon and nitrogen, respectively. Particulate organic phosphorus (POP) was measured by an autoanalyzer from 500-mL subsamples (one for each sampling station) filtered on GF/F Whatman filters (Mullin and Riley 1955). The C : N : P molar ratios were obtained in terms of POC : PN : POP from the bulk particulate fraction.

Particulate and dissolved primary production—Particulate and dissolved primary production (PP and DPP, respectively) were measured according to $NaH^{14}CO_3$ (Marañón et al. 2005). Duplicate 63-mL water samples were inoculated with either 0.22, 0.44, or 0.66 MBq of ^{14}C, depending on the anticipated trophic status of the sample, and incubated in a flowing seawater incubation system. Neutral density screening was used to provide a gradient of irradiance. After 4 h of incubation, samples were carefully filtered at low vacuum pressure onto 0.4-μm polycarbonate filters (Whatman Cyclopore). After acidification and drying, 5 mL of scintillation cocktail (Ultima Gold, Packard Instruments) was added. The amount of ^{14}C incorporated into the particulate phase (PP) was calculated with the use of an inorganic carbon concentration of 25,700 μg C L^{-1} (Marañón et al. 2004). For the DPP measurement, 5 mL of filtrate was collected, acidified with 100 μL of 5 mol L^{-1} HCl, and left for 12 h on a horizontal agitator table. A test before the incubations showed that the volume of acid and agitation time was sufficient to remove all the inorganic ^{14}C remaining in the filtrate. After acidification, 15 mL of scintillation cocktail (Ultima Gold XR, Packard Instruments) was added, and the samples were counted. The values of PP and DPP were transformed into water column integrated rates by the trapezoidal method (Marañón et al. 2004), taking in account the water column light distribution of the sample site and the actual irradiation received by the samples.

Reactivity of DOM—Because TEP are produced by coagulation of precursors of colloidal size, the TEP pool takes its roots in the dissolved phase. Because TEP are formed from DOC via coagulation of dissolved and colloidal polysaccharides, the TEP-C : DOC ratio can be used to estimate the fraction of reactive DOC that could enter into coagulation mechanisms. In addition, considering that the carbon content of a given TEP particle is a conservative property and assuming that TEP stainability depends on its solid volume and, thus, its carbon content, both approaches used to estimate TEP-C (microscopic and colorimetric) should give similar results. Discrepancy between the results obtained from the two methods could result if (1) Alcian blue is retained by particles other than TEP or (2) TEP stainability varies (e.g., because of bacterial degradation or modification of TEP composition) (Mari et al. 2005). Therefore, the ratio between TEP-C concentrations estimated spectrophotometrically (TEP-$C_{spectro}$, μmol L^{-1}) and microscopically (TEP-C_{micro}, μmol L^{-1}) was used to indicate an alteration of TEP composition and structure.

Results

Physical characteristics, nutrients, and pigments—The physical characteristics were relatively conservative along the two transects (Table 1). Temperature and salinity averaged (mean ± SD) 24.3 ± 0.7°C and 36.0 ± 0.2, respectively, and no vertical stratification was observed (data not shown). The somewhat higher salinity in Grande Rade and Sainte Marie Bays relative to the open ocean sites is probably linked to longer residence times in the bays, providing more time for evaporation to take place.

Nutrient concentrations increased continuously from the open ocean to the head of the bays (Table 1). Maximum concentrations (mean ± SD) of inorganic nitrogen (0.29 ± 0.06 μmol L^{-1}) and phosphorus (0.10 ± 0.00 μmol L^{-1}) were recorded in the head of Sainte Marie Bay (station N04). Maximum concentrations of silicates (7.87 ± 2.58 μmol L^{-1}) were measured at the head of Grande Rade Bay (station D01). Both transects were characterized by an inorganic nitrogen limitation (N : P $<$ 5; Table 1). The distribution of pigments largely follows that of nutrients, with maximum concentrations in the head of the bays (1.68 ± 0.63 μg Chl *a* L^{-1} and 0.21 ± 0.10 μg phaeopigments L^{-1}; mean ± SD) that rapidly decrease to reach a minimum outside the bays (Table 1).

The estimated LeFT at the different stations varies from 0 to ~50 days for the open ocean and the head of the Grande Rade Bay stations, respectively (Table 1). One of the two studied bays (Grande Rade Bay) is semienclosed, and the water mass renews very slowly (LeFT $>$ 30 d) compared with the other stations. The LeFT is $>$10 d inside the two bays and varies between 0 and 10 d at the studied stations in the middle of the lagoon. By definition, the LeFT of the water mass outside the lagoon (station M41) is set to zero (initial parameter of the model).

Elemental composition of DOM and particulate organic matter—The DOM and particulate organic matter (POM) pools had an average C : N : P stoichiometry (mean ± SD) of 425 (±129) : 32 (±8) : 1 and of 70 (±30) : 10 (±4) : 1, respectively (Fig. 2). The average C : P, N : P, and C : N for both the dissolved and the particulate phase varied between

Table 1. Environmental characteristics at the sampling stations: temperature, salinity, dissolved inorganic nitrogen (DIN), dissolved inorganic phosphorus (DIP), DIN : DIP ratio, silicate, Chl *a*, phaeopigments, and local e-flushing time (LeFT, as calculated from Jouon et al. 2006). Each value corresponds to the average (±SD) of four measurements taken for each group of stations.

Trophic groups	Stations	Temperature (°C)	Salinity	DIN (μmol L^{-1})	DIP (μmol L^{-1})	DIN : DIP	Silicate (μmol L^{-1})	Chl *a* (μg L^{-1})	Phaeopigments (μg L^{-1})	LeFT (d)
Head of the bays	D01	25.1±0.3	36.1±0.0	0.21±0.02	0.08±0.02	2.67	7.87±2.58	1.64±0.25	0.17±0.01	46.9
	N04	24.5±0.3	36.1±0.1	0.29±0.06	0.10±0.04	3.38	3.74±0.19	1.72±1.06	0.25±0.15	17.1
Middle of the bays	D08	25.3±0.2	36.1±0.0	0.15±0.04	0.05±0.03	3.81	5.05±0.24	0.88±0.05	0.07±0.01	40.8
	N12	24.6±0.1	36.2±0.0	0.19±0.07	0.06±0.02	3.18	3.42±0.42	1.12±0.33	0.18±0.03	12.9
Mouth of the bays	D22	24.8±0.2	36.1±0.0	0.09±0.02	0.03±0.01	2.98	3.13±0.87	0.47±0.06	0.06±0.01	31.0
	N33	24.6±0.0	36.1±0.0	0.09±0.01	0.02±0.02	5.33	3.02±0.44	0.38±0.05	0.06±0.01	12.4
Middle of the lagoon	M05	24.3±0.2	35.8±0.0	0.05±0.00	0.02±0.00	2.12	2.71±0.60	0.31±0.04	0.04±0.02	5.6
	M33	24.0±0.0	35.8±0.0	0.06±0.00	0.01±0.01	5.56	2.10±0.24	0.30±0.00	0.03±0.00	0.5
Near barrier	M10	23.9±0.2	35.8±0.0	0.06±0.01	0.02±0.01	3.14	2.32±0.84	0.31±0.05	0.04±0.02	0.4
Open ocean	M41	23.3±0.3	35.7±0.0	0.05±0.01	0.04±0.03	3.07	1.85±0.36	0.19±0.09	0.06±0.04	0.0

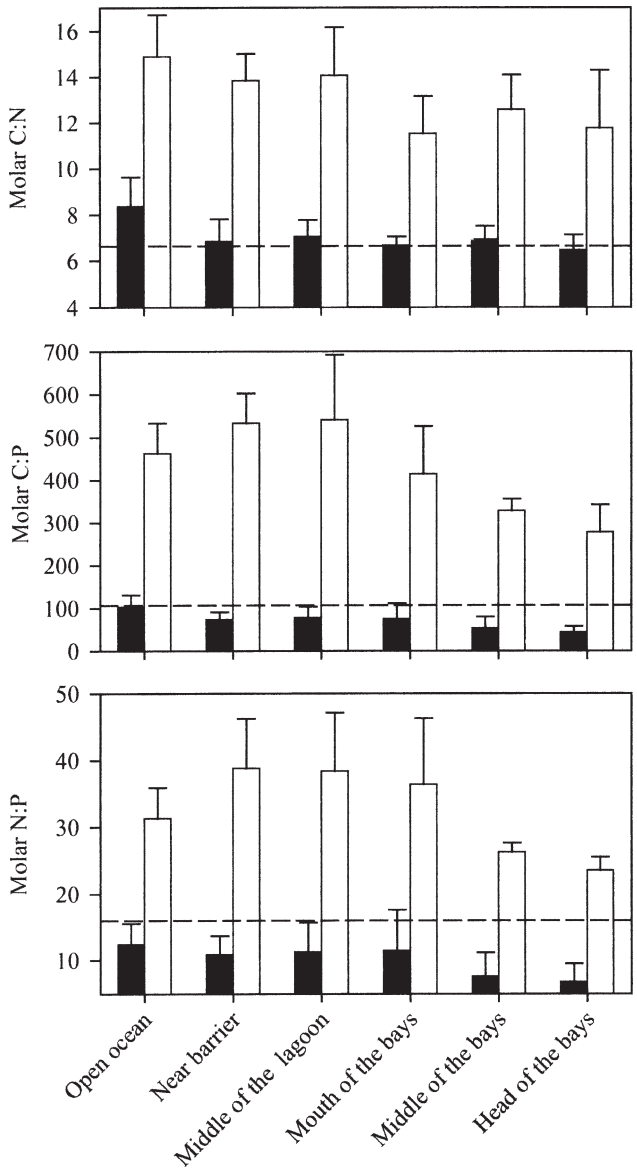

Fig. 2. Variations of C : N : P ratios in the dissolved (open bars) and particulate (filled bars) organic matter along the transects. The dashed lines represent the Redfield C : N : P ratios of 106 : 16 : 1. Each value corresponds to the average (±SD) of four measurements taken for each group of stations.

sampling sites and decreased slightly toward the bays. Although the measured C : N : P ratios for bulk DOM deviated considerably from the Redfield ratio (i.e., the C : N and C : P of DOM were 110% and 330% higher than the Redfield ratio), POM stoichiometry was similar to Redfield. This suggests that although the production of biomass is N-limited for all stations, the biomass produced does not exhibit a N deficit. On the contrary, the organic matter fixed during photosynthesis and directly channeled to the dissolved phase exhibits strong deficits in both nitrogen and phosphorus.

Distribution and dynamics of organic matter pools—TEP occurred at all sampling occasions (Fig. 3). TEP volume

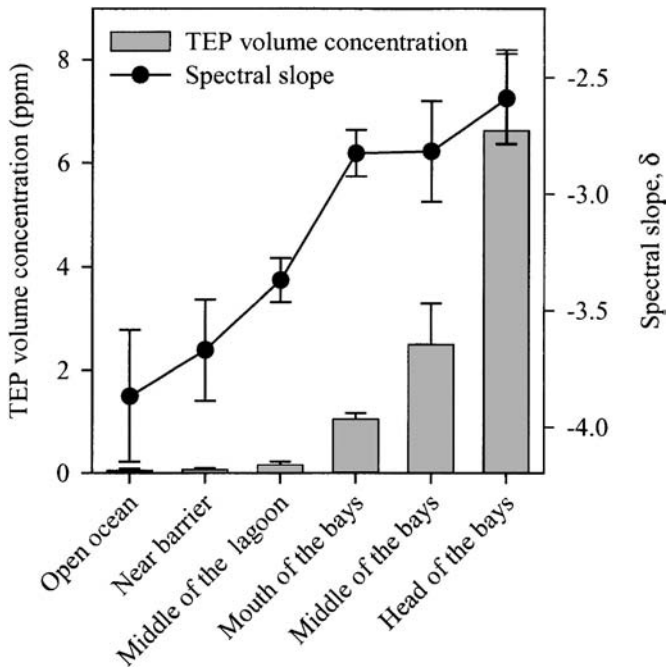

Fig. 3. Variations of TEP volume concentration and of TEP spectral slopes, δ, along the sampling gradient. Each value corresponds to the average (±SD) of four measurements taken for each group of stations.

concentrations varied between 0.05 ± 0.03 and 6.62 ± 1.56 ppm (mean ± SD) and increased from the coral barrier toward the head of the bays. As indicated by the increase of the TEP spectral slope, δ, the observed increase in TEP volume concentration likely results from an increase of the large TEP fraction.

The carbon trend (mean ± SD) within the different pools of organic matter increased along the offshore gradient, from 0.5 ± 0.1 to 3.9 ± 0.3 μmol L^{-1}, from 2.8 ± 1.4 to 7.9 ± 3.5 μmol L^{-1}, and from 63.1 ± 3.1 to 74.7 ± 6.1 μmol L^{-1} for TEP, POC, and DOC, respectively (Fig. 4). TEP-C concentration was positively correlated to both DOC (DOC = 3.9TEP-C + 58, $r^2 = 0.85$, $p < 0.05$, $n = 10$) and POC concentrations (POC = 1.54TEP-C + 1.65, $r^2 = 0.84$, $p < 0.05$, $n = 10$), and POC concentration was positively correlated to DOC concentration (POC = 2.2TEP-C + 56, $r^2 = 0.80$, $p < 0.05$, $n = 10$). Because TEP are formed from DOC, the y-intercept of the regression line of DOC versus TEP-C represents the minimum DOC concentration required to sustain TEP production (i.e., TEP are only formed when the critical DOC concentration of ~60 μmol L^{-1} is reached). The above relationships were used to determine the relative fraction of each pool of organic matter along the gradient. The pools of TEP-C and of POC represented, respectively, ~1% and 4% of DOC at the open ocean station and increased up to ~5% and 10% in the head of the bays. The

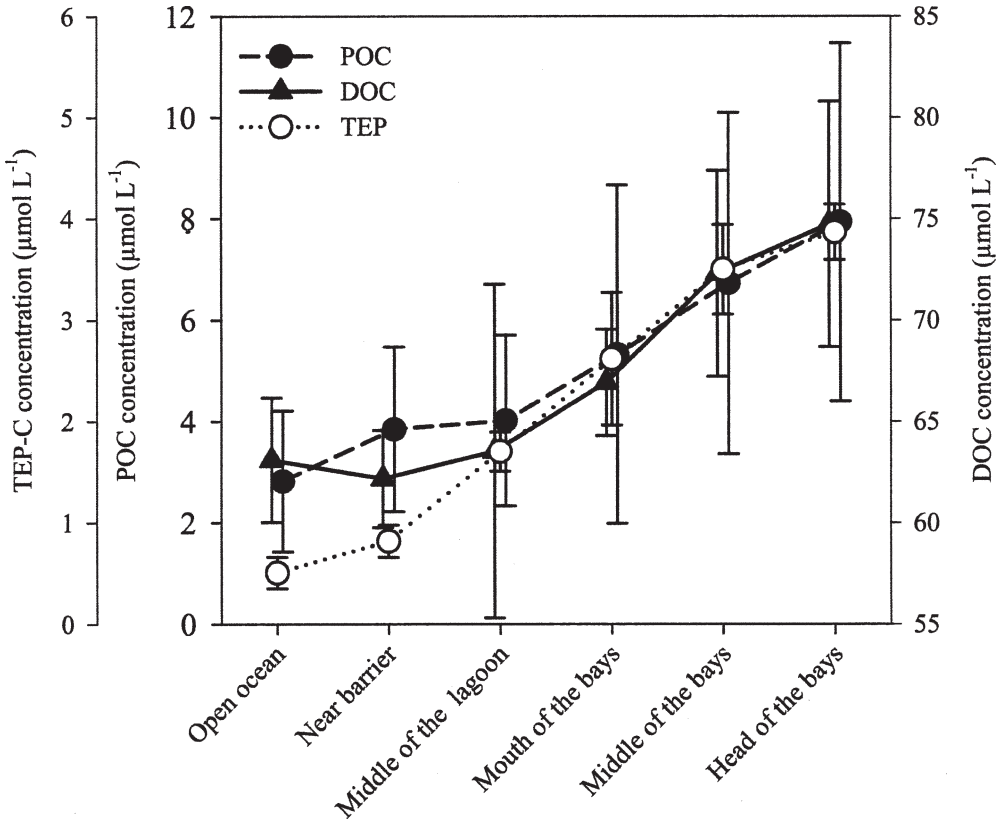

Fig. 4. Variations of TEP-carbon, POC, and DOC concentrations along the sampling gradient. Each value corresponds to the average (±SD) of four measurements taken for each group of stations.

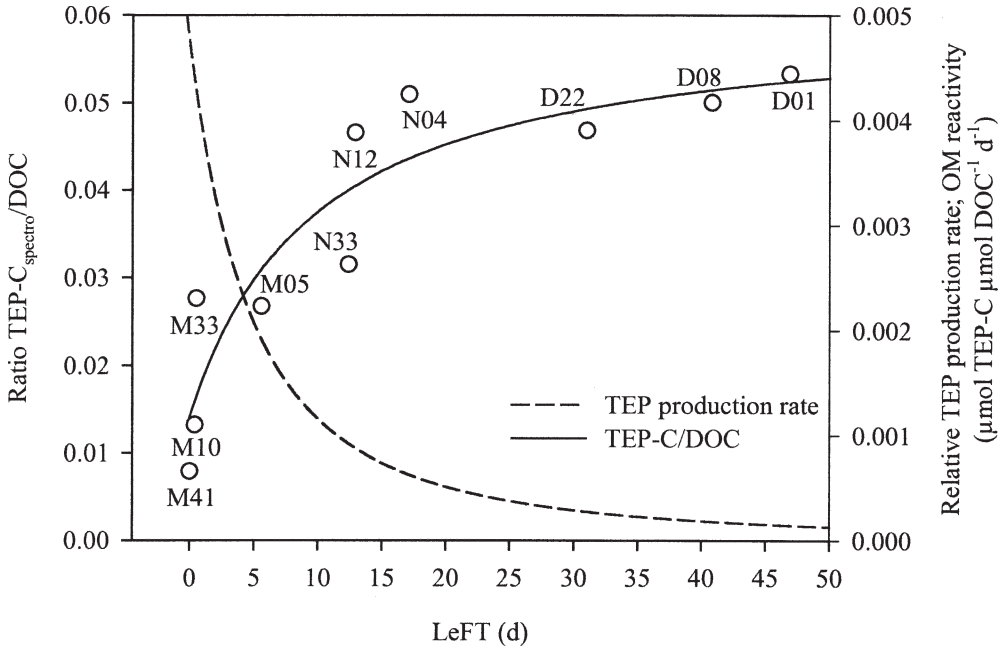

Fig. 5. DOC reactivity as estimated by the TEP-C : DOC ratio (solid line) and TEP production rate (dashed line, estimated as the derivative of the hyperbolic fitting of TEP-C : DOC ratio vs. LeFT) as a function of LeFT. The hyperbolic regression line (solid line) was fitted to the data.

contribution of TEP to POC was low at the most oligotrophic stations (18%) and reached a plateau in the lagoon and in the bays at about 60%.

Organic matter reactivity—The TEP-C : DOC ratio, used to estimate the fraction of reactive DOC entering into coagulation mechanisms and fuelling the TEP pool, was plotted against the LeFT to estimate DOC reactivity as a function of the residence time of the water mass. The variations of the TEP-C : DOC ratio as a function of the LeFT was best described by a hyperbolic relation (Fig. 5). The TEP-C : DOC ratio increased when the LeFT increased (i.e., the formation of TEP-C from DOC becomes less efficient as residence time increases). The reactivity of DOM can be evaluated by calculating the derivative of the ratio TEP-C : DOC versus LeFT, which gives the relative production rate of TEP-C from DOC per day (Fig. 5). This exercise shows that DOM reactivity decreases rapidly as the residence time of the water mass increases, to reach its minimum in the head of the semienclosed bay of Grande Rade. The variations of the TEP-$C_{spectro}$: TEP-C_{micro} ratio support this view (Fig. 6). The observed decrease of the TEP-$C_{spectro}$: TEP-C_{micro} ratio as a function of the residence time of the water mass indicates that TEP stainability is reduced when the LeFT increases; such a diminution being most likely because of the long-term degradation of organic material. TEP turnover rates were calculated as a function of the LeFT from (1) the concentrations of TEP-C and of DOC extrapolated from TEP-C and DOC versus LeFT regression lines and (2) from the relative production rates of TEP-C from DOC per day. The estimated TEP turnover rate drops from 0.3 to 0.0 d^{-1} when the residence time of the water mass increases (i.e., when the LeFT increases from 0 to 50 d), and such turnover rates require a minimum primary production of dissolved organic carbon (DPP) of 0.20 to 0.02 μmol L^{-1} d^{-1} (Fig. 7). The theoretical minimum DPP required to sustain the calculated TEP turnover rate was estimated from (1) TEP-C and DOC versus LeFT

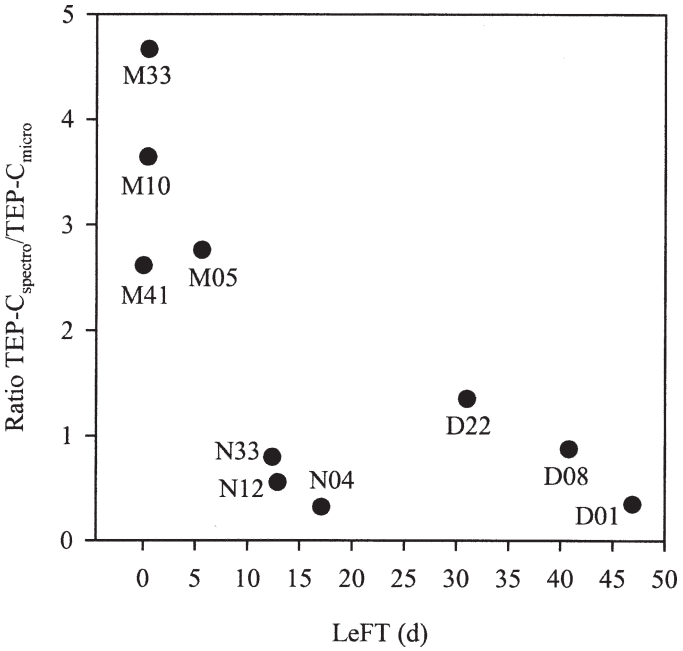

Fig. 6. Relationship between TEP-C concentrations estimated from the colorimetric and the microscopic methods as a function of LeFT.

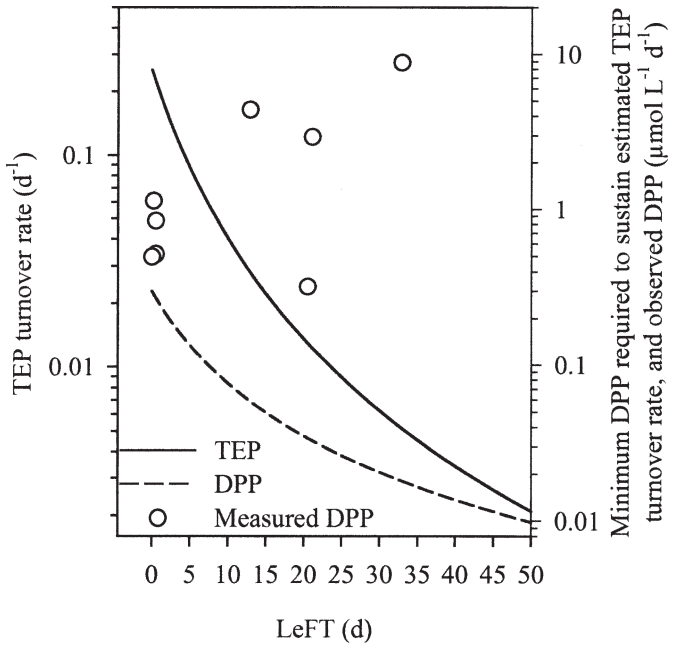

Fig. 7. TEP turnover rate (solid line) and minimum dissolved primary production (DPP; dashed line) required to sustain the estimated TEP turnover rates as a function of LeFT and compared with measured DPP (open circles). DPP are integrated values on the water column.

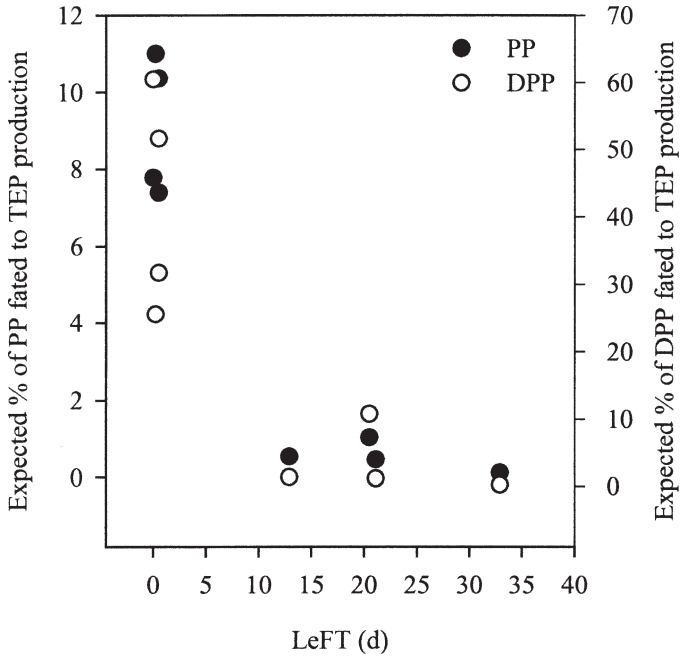

Fig. 8. Estimated fraction of dissolved and total primary production fated to TEP production as a function of LeFT.

regression lines and the (2) calculated TEP turnover rates. Over the range of primary production of DOC and POC measured in the lagoon for water mass with different LeFT, the fraction of DPP going into TEP production decreased from 42.4 ± 16.5% (LeFT < 10 d) to 3.4 ± 4.9% (LeFT > 10 d), which represented a diminution from 9.1 ± 1.8% to 0.5 ± 0.4% of the total PP (Fig. 8).

Discussion

Characteristics of the sampling gradient—The two transects were characterized by a well-established nutrient gradient, as already reported by Jacquet et al. (2006). The concentration gradients of nitrogen and phosphorus reflect the dominance of nutrient inputs from an urban origin in Sainte Marie Bay and the dominance of nutrient inputs from an industrial origin in Grande Rade Bay. The temporal variability of nutrient concentrations along the transects is believed to be controlled by sources external to the lagoon (atmospheric input, surrounding oceanic waters, land drainage). Insofar as oceanic waters exhibit low nutrient concentrations, the land-based input is much more likely to affect nutrient concentration levels, as revealed by the gradient of silicates from the head of the bays to the barrier. The similarities observed between lagoonal (except middle and head of the bays) and oceanic waters could be due to substantial water exchange through the passes. However, water exchange between oceanic and lagoonal waters greatly depends on the hydrodynamic circulation, which is controlled by topographic constraints, wind condition, and tidal cycle. In semienclosed bays, such as the bay of Grande Rade, water exchange with lagoonal water and, to a larger extent with oceanic water, is a very slow process. Therefore, the land-based input of nutrients in such bays might mostly fuel a local production and can be recycled several times before being exported to more oligotrophic waters.

DOC production variability—Previous studies have demonstrated that the percentage of extracellular release (PER) ranges from 5% to 30% of total carbon fixed (Baines and Pace 1991; Biddanda and Benner 1997; Marañón et al. 2005). We observed an average PER of 27 ± 14% (minimum 10%, maximum 43%), and no specific trend was observed along the sampling gradient similar to the recent results of Moran et al. (2004). In contrast, the percentage of DOC production ending in TEP ranged from 3% to 40% in nutrient-rich and oligotrophic waters, respectively. This suggests that although the relative rate of production of DOC does not vary in a consistent manner with nutrient concentrations, the fate of that DOC does depend on the nutrient conditions. Why this might be is undoubtedly related to the physicochemical properties of the DOM precursor material for TEP.

One caveat needs to be kept in mind in the interpretation of these data. The primary production measurements were not made contemporaneously with the other measurements; however, it is improbable that there existed a large difference in trophic status between the two sampling periods that differed only by a few weeks (Jacquet et al. 2006).

Effects of the residence time on DOC reactivity—In this study, we used the efficiency of the DOC/TEP transformation as an index of the physicochemical reactivity of DOM. Our results strongly suggest that reactivity is

lowered when DOC ages because of prolonged retention (i.e., at long residence times). The peculiar hydrodynamic circulation inside the lagoon and especially in semienclosed bays allows the accumulation and aging of DOM, as well as the subsequent loss of physicochemical reactivity caused by bacterial degradation processes. Such a feedback system in which organic matter is continuously degraded could lead to the formation of refractory DOM with low physicochemical reactivity. The observed discrepancy between estimates of TEP-C obtained from the microscopic and spectrophotometric methods shows that TEP retain less Alcian blue in the bays than in water masses characterized by low LeFT, supporting the hypothesis that the observed decrease of organic matter reactivity is caused by prolonged bacterial degradation. Such a reduction in TEP stainability because of increasing porosity leads to an overestimation of the TEP-C concentration by the microscopic method, the latter only relying on the apparent structure of the particles and not on their carbon content. This mechanism of increasing porosity of TEP has already been described at the end of *Phaeocystis* blooms (Mari et al. 2005), during which high bacterial degradation and low TEP production occur. Although a reduction of DOC reactivity is not likely to occur in the surface layer of open ocean sites because DOC turnover is high (Hopkinson and Vallino 2005), it could well occur on a vertical scale as DOC ages during its transport to the deep ocean.

One of the alternative reasons for the presence of DOM with different reactivities in the bay heads could be because of the proximity of potential terrestrial and riverine influences. However, the effects of terrestrial and riverine inputs on the two bays studied are probably minimal. Indeed, riverine influences are extremely weak relative to the oceanic influences in this environment, as is easily seen in the lack of a significant salinity gradient even at the bay heads. Nevertheless, a small degree of terrestrial or riverine influence of DOM characteristics cannot be completely ruled out because we did observe an increase in long-wavelength absorption of CDOM in the samples (data not shown). This can be interpreted as evidence of a terrestrial component in the DOM pool. However, as pointed out by Rochelle-Newall et al. (2004), increases in long-wave absorption of CDOM cannot always be interpreted as being indicative of the presence of terrestrial DOM because diagenetically altered DOM can also exhibit the same signature. Therefore, given the low riverine and terrestrial influences on these two sites, it is improbable that a large proportion of the DOM present is of terrestrial origin. Thus, the DOM present in the bays is probably derived from another source.

Other mechanisms could potentially lead to a reduction of the transfer efficiency from DOM to POM. The chemical composition of exopolymers released by phytoplankton (Aluwihare and Repeta 1999) or bacterioplankton (Stoderegger and Herndl 1998) varies as a function of species and physiological status. Because the chemical composition of exopolymers determines their physicochemical properties, one might expect a modification of DOM reactivity depending on its source. Therefore, variations in bacterio- and phytoplankton community composition along the gradients (Jacquet et al. 2006) could also play a role in the observed variations of DOM reactivity. Finally, because metals bind to exopolymers, these elements might affect their surface charge distribution and their conformation, which in turn, would most likely alter their sticking properties and their tendency to coagulate. Therefore, the transfer efficiency of DOM to POM in the bays around Noumea might also be modified because of the high metal concentrations resulting from industrial pollution.

Potential consequences for vertical flux of POM—It has been shown that TEP density ranged from 0.70 to 0.84 g cm^{-3} and, thus, was lower than that of seawater or that of more conventional particles (Azetsu-Scott and Passow 2004). As a result, the relative proportions of TEP, solid particles (i.e., non-TEP particles) and interstitial water within an aggregate, as well as their respective densities, govern its vertical transport velocity and direction (upward or downward; Azetsu-Scott and Passow 2004). Assume for a moment that the relative proportions of TEP and solid particles within aggregates relate to their relative proportions in seawater. Because the contribution of TEP to the bulk POC decreased from 60% to ~20%, from the head of the bays to the open ocean, the contribution of TEP within organic aggregates might also decrease in the same proportions along the studied transects. Therefore, one could hypothesize that an aggregate from the head of the studied bays we studied should be composed of 60% TEP-C and 40% non–TEP-C, whereas it should be composed of <20% TEP-C in the vicinity of the coral barrier. Assuming that the non-TEP fraction of the POC is mainly composed of protist plankton, the volume occupied by non-TEP particles can be estimated from the non–TEP-C as $[C] = 0.760\,V^{0.819}$, where [C] (pg C) is the carbon concentration of the non-TEP fraction of POC and V (μm^3) is the volume occupied (Menden-Deuer and Lessard 2000). According to the above assumptions, the non-TEP fraction would occupy from 1.7 to 3.4 ppm compared with 0.1 to 6.6 ppm for the TEP fraction, respectively, from the open ocean to the head of the bays. This means that aggregates occurring in the head of the bays could consist of ~65% TEP and 35% non-TEP in terms of volume, whereas TEP volume content inside aggregates occurring in the vicinity of the coral barrier could drop down to 3%. Over the range of measured densities for solid matter of large aggregates (i.e., from 1.095 to 1.497 g cm^{-3}; Azetsu-Scott and Johnson 1992) and assuming that aggregates contain no interstitial water, aggregates occurring inside the bays would encompass a range from neutrally to positively buoyant, and they would become negatively buoyant in the vicinity of the coral barrier (Fig. 9). A consequence would be a rapid sinking of aggregates and an efficient downward export of organic matter near the coral reef. On the contrary, the downward export of organic matter inside the bays could simply come to a stop, and even reverse (i.e., upward flux of matter), thereby prolonging the residence time of organic matter in the water column. These two opposing pathways probably play an important role in regulating the export versus recycling balance in areas structured by strong hydrodynamic constraints.

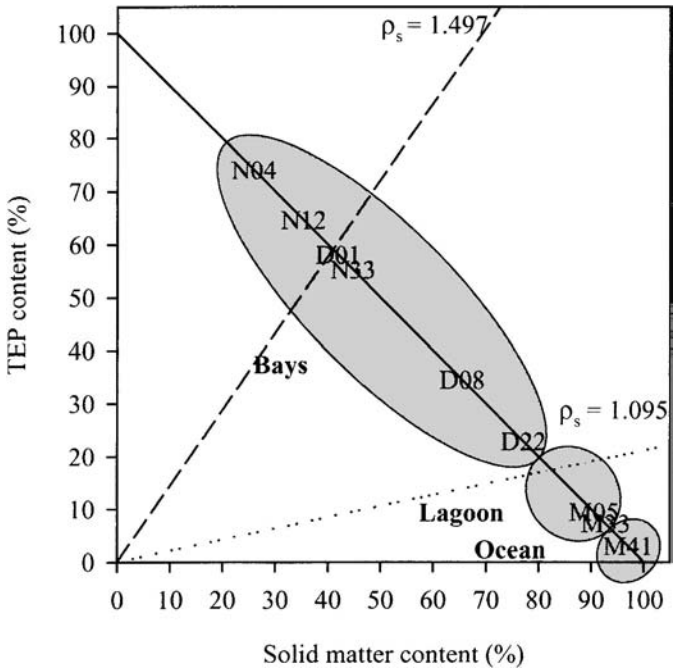

Fig. 9. Model depicting the density of aggregates as a function of the TEP and solid particle volume fractions in aggregates and of the solid particle density (ρ_s) (from Azetsu-Scott and Passow 2004). The two density lines indicate the relationships between the volume fractions of TEP and of solid particles for neutrally buoyant aggregates, as calculated for the upper (ρ_s = 1.497 g cm^{-3}; dashed line) and lower (ρ_s = 1.095 g cm^{-3}; dotted line) limits of measured solid particle densities inside large aggregates. The solid line describes aggregates for which there is no interstitial water (i.e., aggregates only composed of TEP and solid particles). The estimated densities of aggregates occurring at the different sampling stations are represented. Aggregates with a density occurring in the domain constrained above a specific density line for solid matter will be positively buoyant, whereas below this line, aggregates will be negatively buoyant. Aggregates occurring in the bays of Grande Rade and Sainte Marie should be from neutrally to positively buoyant, assuming a density for the solid matter of ρ_s = 1.095 g cm^{-3}. Inversely, aggregates occurring from the middle of the lagoon to the open ocean should sink. The value for station M10 is the same as for station M41.

Implication for DOM cycling in the coastal zone—The decreasing reactivity of DOM during aging of the water masses could corroborate the observed accumulation of DOM in the coastal zone. DOC accumulation has been reported in various areas in the coastal zone (e.g., Zweifel et al. 1995), and it has been shown that the fraction of DOC that accumulated was mainly composed of polysaccharides (e.g., Biersmith and Benner 1998). Various explanations have been proposed to account for the observed accumulation in the coastal zone, such as a malfunctioning microbial loop caused by nutrient limitation (Thingstad et al. 1997). The present data give a new insight into this issue and might help complete the puzzle, because the accumulation of DOM caused by positively buoyant TEP in poorly renewed water masses might also lead to the buildup of a large C-rich (and N- and P-poor) pool of organic matter. Interestingly, the occurrence of giant mucus particles in the northern Adriatic Sea (Herndl 1992) might be the result of very low renewal rate of the water masses (Grilli et al. 2005). Hence, the excess DOM produced would somehow be trapped in areas in which the residence time of the water masses is high, promoting degradation of the labile fraction and a loss of reactivity. Thus, the accumulation of DOM in the coastal zone would be constrained by both the biological activity and hydrodynamics. This scheme is contradictory to the present paradigm that DOM occurring in the coastal zone is highly labile and reactive because it is produced locally from DPP fuelled by terrestrial nutrient inputs. As a result, in coastal ecosystems characterized by low renewal rates of water, the pathway for DOM would be unbalanced from export to local remineralization.

The results of this work highlight the relevance of knowing the chemical composition of DOM along residence time gradients to determine whether specific biomolecules in DOM vary accordingly along the same pattern as described along depth gradients. Depth profile studies have demonstrated that total hydrolysable neutral sugars, amino acids, and amino sugars decrease from the surface to deep waters, from >200 to <50 nmol L^{-1}, from >200 to <160 nmol L^{-1}, and from >40 to <10 nmol L^{-1}, respectively (Benner 2002). Shifts in the relative proportion of biomolecules can be used as an indicator of the degree of alteration of DOM (Dauwe et al. 1999). Clearly, data on the concentrations and distributions of biomolecules along residence time gradients are needed to further investigate the link between the renewal rate of water masses and the transfer efficiency from DOM to POM. The study of the mechanisms leading to a diminution of the bioreactivity of DOM along horizontal gradients of residence time might help us understand the mechanisms by which refractory DOM is formed with increasing depth.

References

Alldredge, A. L., U. Passow, and B. E. Logan. 1993. The abundance and significance of a class of large, transparent organic particles in the ocean. Deep-Sea Res. I **40:** 1131–1140.

Aluwihare, L. I., and D. J. Repeta. 1999. A comparison of the chemical characteristics of oceanic DOM and extracellular DOM produced by marine algae. Mar. Ecol. Prog. Ser. **186:** 105–117.

Amon, R. M. W., and R. Benner. 1994. Rapid cycling of high–molecular-weight dissolved organic matter in the ocean. Nature **369:** 549–552.

———, H.-P. Fitznar, and R. Benner. 2001. Linkages among the bioreactivity, chemical composition, and diagenetic state of marine dissolved organic matter. Limnol. Oceanogr. **46:** 287–297.

Azetsu-Scott, K., and B. D. Johnson. 1992. Measuring physical characteristics of particles: A new method of simultaneous measurement for size, settling velocity and density of constituent matter. Deep-Sea Res. **39:** 1057–1066.

———, and U. Passow. 2004. Ascending marine particles: Significance of transparent exopolymer particles (TEP) in the upper ocean. Limnol. Oceanogr. **49:** 741–748.

Baines, S. B., and M. L. Pace. 1991. The production of dissolved organic matter by phytoplankton and its importance to bacteria: Patterns across marine and freshwater systems. Limnol. Oceanogr. **36:** 1078–1090.

Benner, R. 2002. Chemical composition and reactivity, p. 59–90. *In* D. A. Hansell and G. A. Carlson [eds.], Biochemistry of marine dissolved organic matter. Academic Press.

———, J. D. Pakulsky, M. McCarthy, J. I. Hedges, and P. G. Hatcher. 1992. Bulk chemical characteristics of dissolved organic matter in the ocean. Science **255:** 1561–1564.

Biddanda, B., and R. Benner. 1997. Carbon, nitrogen, and carbohydrate fluxes during the production of particulate and dissolved organic matter by marine phytoplankton. Limnol. Oceanogr. **42:** 506–518.

Biersmith, A., and R. Benner. 1998. Carbohydrates in phytoplankton and freshly-produced dissolved organic matter. Mar. Chem. **63:** 131–144.

Carlson, C. A., M. L. Brann, T. H. Mague, and L. Mayer. 1985. Molecular weight distribution of dissolved organic matter in seawater determined by ultrafiltration: A reexamination. Mar. Chem. **16:** 155–171.

Chin, W., M. W. Orellana, and P. Verdugo. 1998. Spontaneous assembly of marine dissolved organic matter into polymer gels. Nature **391:** 568–570.

Dauwe, B., J. J. Middelburg, P. M. J. Herman, and C. H. R. Heip. 1999. Linking diagenetic alteration of amino acids and bulk organic matter reactivity. Limnol. Oceanogr. **44:** 1809–1814.

Engel, A., and U. Passow. 2001. Carbon and nitrogen content of transparent exopolymer particles (TEP) in relation to their Alcian blue adsorption. Mar. Ecol. Prog. Ser. **219:** 1–10.

———, S. Thoms, U. Riebesell, E. Rochelle-Newall, and I. Zondervan. 2004. Polysaccharide aggregation as a potential sink of marine dissolved organic carbon. Nature **428:** 929–932.

Grasshoff, K., M. Eherhardt, and K. Kremling. 1983. Methods of seawaters analysis, 2nd ed. Verlag Chemie.

Grilli, F., E. Paschini, R. Precali, A. Russo, and N. Supic. 2005. Circulation and horizontal fluxes in the northern Adriatic Sea in the period June 1999–July 2002. Part I: Geostrophic circulation and current measurement. Sci. Total Environ. **353:** 57–67.

Herndl, G. J. 1992. Marine snow in the northern Adriatic Sea: Possible causes and consequences for a shallow ecosystem. Mar. Microb, Food Webs **6:** 149–172.

Hopkinson, C. S. Jr., and J. J. Vallino. 2005. Efficient export of carbon to the deep ocean through dissolved organic matter. Nature **433:** 142–145.

Jacquet, S., B. Delesalle, J.-P. Torréton, and J. Blanchot. 2006. Responses of the phytoplankton communities to increased anthropogenic influences (Southwestern Lagoon, New Caledonia). Mar. Ecol. Prog. Ser. **320:** 65–78.

Jouon, A., P. Douillet, S. Ouillon, and P. Fraunié. 2006. Calculations of hydrodynamic time parameters in a semi-opened coastal zone using a 3D hydrodynamic model. Cont. Shelf Res. **26:** 1395–1415.

Kloareg, B., and R. S. Quatrano. 1988. Structure of cell walls of marine algae and ecophysiological functions of the matrix polysaccharides. Oceanogr. Mar. Biol. Annu. Rev. **26:** 259–315.

Marañón, E., P. Cermeño, E. Fernández, J. Rodríguez, and L. Zabala. 2004. Significance and mechanisms of photosynthetic production of dissolved organic carbon in a coastal eutrophic ecosystem. Limnol. Oceanogr. **49:** 1652–1666.

———, ———, and V. Perez. 2005. Continuity in the photosynthetic production of dissolved organic carbon from eutrophic to oligotrophic waters. Mar. Ecol. Prog. Ser. **299:** 7–17.

Mari, X. 1999. Carbon content and C : N ratio of transparent exopolymeric particles (TEP) produced by bubbling exudates of diatoms. Mar. Ecol. Prog. Ser. **183:** 59–71.

———, S. Beauvais, R. Lemée, and M. L. Pedrotti. 2001. Non-Redfield C : N ratio of transparent exopolymeric particles in the northwestern Mediterranean Sea. Limnol. Oceanogr. **46:** 1831–1836.

———, and A. Burd. 1998. Seasonal size spectra of transparent exopolymeric particles (TEP) in a coastal sea and comparison with those predicted using coagulation theory. Mar. Ecol. Prog. Ser. **163:** 63–76.

———, and T. Kiørboe. 1996. Abundance, size distribution and bacterial colonization of transparent exopolymeric particles (TEP) during spring in the Kattegat. J. Plankton Res. **18:** 969–986.

———, F. Rassoulzadegan, C. P. D. Brussaard, and P. Wassmann. 2005. Dynamics of transparent exopolymeric particles (TEP) production by *Phaeocystis globosa* under N- or P-limitation: A controlling factor of the retention/export balance. Harmful Algae **4:** 895–914.

Menden-Deuer, S., and E. J. Lessard. 2000. Carbon to volume relationships for dinoflagellates, diatoms, and other protist plankton. Limnol. Oceanogr. **45:** 569–579.

Moeseneder, M. M., C. Winter, and G. J. Herndl. 2001. Horizontal and vertical complexity of attached and free-living bacteria of the eastern Mediterranean Sea, determined by 16S rDNA and 16S rRNA fingerprints. Limnol. Oceanogr. **46:** 95–107.

Moran, X. A. G., E. Fernandez, and V. Perez. 2004. Size-fractionated primary production, bacterial production and net community production in subtropical and tropical domains of the oligotrophic NE Atlantic in autumn. Mar. Ecol. Prog. Ser. **274:** 17–29.

Muller-Niklas, G., S. Schuster, E. Kaltenbock, and G. J. Herndl. 1994. Organic content and bacterial metabolism in amorphous aggregations of the northern Adriatic Sea. Limnol. Oceanogr. **39:** 58–68.

Mullin, J. B., and J. P. Riley. 1955. The spectrophotometric determination of silicate-silicon in natural waters with special reference to sea water. Anal. Chim. Acta **12:** 162–170.

Ogawa, H., Y. Amagai, I. Koike, K. Kaiser, and R. Benner. 2001. Production of refractory dissolved organic matter by bacteria. Science **292:** 917–920.

Passow, U. 2000. Formation of transparent exopolymer particles, TEP, from dissolved precursor material. Mar. Ecol. Prog. Ser. **192:** 1–11.

———, and A. L. Alldredge. 1994. Distribution, size and bacterial colonization of transparent exopolymer particles (TEP) in the ocean. Mar. Ecol. Prog. Ser. **113:** 185–198.

———, and ———. 1995. A dye-binding assay for the spectrophotometric measurement of transparent exopolymeric particles (TEP). Limnol. Oceanogr. **40:** 1326–1335.

Raimbault, P., F. Diaz, W. Pouvesle, and B. Boudjellal. 1999. Simultaneous determination of particulate organic carbon, nitrogen and phosphorus collected on filters, using a semi-automatic wet-oxidation method. Mar. Ecol. Prog. Ser. **180:** 289–295.

———, G. Slawyk, B. Coste, and J. C. Fry. 1990. Feasibility of measuring an automated colorimetric procedure for the determination of seawater nitrate in the 0 to 100 nM range: Examples from field and culture. Mar. Biol. **104:** 347–351.

Rochelle-Newall, E., and others. 2004. Chromophoric dissolved organic matter in experimental mesocosms maintained under different pCO_2 levels. Mar. Ecol. Prog. Ser. **272:** 25–31.

Smith, D. C., M. Simon, A. L. Alldredge, and F. Azam. 1992. Intense hydrolytic enzyme activity on marine aggregates and implications for rapid particle dissolution. Nature **359:** 139–141.

Stoderegger, K., and G. J. Herndl. 1998. Production and release of bacterial capsular material and its subsequent utilization by marine bacterioplankton. Limnol. Oceanogr. **43:** 877–884.

Thingstad, T. F., Å. Hagström, and F. Rassoulzadegan. 1997. Accumulation of degradable DOC in surface waters: Is it caused by a malfunctioning microbial loop? Limnol. Oceanogr. **42:** 398–404.

Zhou, J., K. Mopper, and U. Passow. 1998. The role of surface-active carbohydrates in the formation of transparent exopolymer particles by bubble adsorption of seawater. Limnol. Oceanogr. **43:** 1860–1871.

Zweifel, U. L., J. Wikner, Å. Hagström, E. Lundberg, and B. Norrman. 1995. Dynamics of dissolved organic carbon in a coastal ecosystem. Limnol. Oceanogr. **40:** 299–305.

Received: 6 February 2006
Amended: 26 October 2006
Accepted: 27 October 2006

ANNEXE II

Torréton J.P., Rochelle-Newall, E., Jouon, A., Faure, V., Jacquet, S., Douillet, P.(in press). Correspondence between the distribution of hydrodynamic time parameters and the distribution of biological and chemical variables in a semi-enclosed coral reef lagoon. Estuarine, Coastal and Shelf Science.

Correspondence between the distribution of hydrodynamic time parameters and the distribution of biological and chemical variables in a semi-enclosed coral reef lagoon

Jean-Pascal Torréton, Emma Rochelle-Newall, Aymeric Jouon, Vincent Faure, Séverine Jacquet, Pascal Douillet

Abstract

Hydrodynamic modeling can be used to spatially characterize water renewal rates in coastal ecosystems. Using a hydrodynamic model implemented over the semi-enclosed Southwest coral lagoon of New Caledonia, a recent study computed the flushing lag as the minimum time required for a particle coming from outside the lagoon (open ocean) to reach a specific station (Jouon *et al.*, 2006). Local e-flushing time was calculated as the time requested to reach a local grid mesh concentration of 1/e from the precedent step. Here we present an attempt to connect physical forcing to biogeochemical functioning of this coastal ecosystem. An array of stations, located in the lagoonal channel as well as in several bays under anthropogenic influence, was sampled during 3 cruises. We then tested the statistical relationships between the distribution of flushing indices and those of biological and chemical variables. Among the variables tested, silicate, chlorophyll *a* and bacterial biomass production present the highest correlations with flushing indices. Correlations are higher with local e-flushing times than with flushing lags or the sum of these two indices. In the bays, these variables often deviate from the relationships determined in the main lagoon channel. In the 3 bays receiving significant riverine inputs, silicate is well above the regression line, whereas data from the bay receiving almost insignificant freshwater inputs generally fit the lagoon channel regressions. Moreover, in the 3 bays receiving important urban and industrial effluents, chlorophyll *a* and bacterial production of biomass generally display values exceeding the lagoon channel regression trends whereas in the bay under moderate anthropogenic influence values follow the regressions obtained in the lagoon channel. The South West lagoon of New Caledonia can hence be viewed as a coastal mesotrophic ecosystem that is flushed by oligotrophic oceanic waters which subsequently replace the lagoonal waters with water considerably impoverished in resources for microbial growth. This flushing was high enough during the periods of study to influence the distribution of phytoplankton biomass, bacterial production of biomass and silicate concentrations in the lagoon channel as well as in some of the bay areas.

Keywords:

hydrodynamics, flushing time, plankton, secondary production, nutrients, coastal lagoon, Pacific, New Caledonia

Introduction

As pointed out by Monsen *et al.* (2002), in aquatic systems, planktonic biomass and nutrients are carried in a fluid medium and it is therefore essential to understand the hydrodynamic processes that transport water and its constituents. Since Vollenweider (1976)'s work showing the link between the biogeochemical processing of phosphorus in lakes and the residence time of waters, several studies on estuaries have shown relationships between variable water retention or flushing indices and the distribution of phytoplankton blooms (Doering *et al.*, 1994; Lucas *et al.*, 1999), phytoplankton community composition (Ferreira *et al.*, 2005), bacterioplankton abundance (Painchaud *et al.*, 1996) and community composition (Crump *et al.*, 2004).

In coral reef areas, Andrews & Muller (1983) proposed that in a lagoonal patch reef of the Great Barrier Reef, a part of the variance of nutrient concentrations could be explained by tidal movements. Moreover, using literature values from several coral reef lagoons, Delesalle & Sournia (1992) revealed a negative relationship between phytoplankton biomass and estimates of exchange rates between these lagoons and the open ocean. In the Tuamotu Archipelago (French Polynesia), the size of the aperture connecting atoll lagoons to the ocean was shown to be one of the key parameters defining nutrient regime (Dufour *et al*., 2001) and trophic status (Torréton *et al*., 2002).

These studies reporting the link between potential flushing of semi-enclosed atolls and the biological or chemical properties of those atolls demonstrate the importance of water circulation in determining the distribution of chemical and biological variables in coral reef environments. However, none of these studies focused on this link at local scales, *i.e.* none have attempted to relate flushing rates and the distribution of biogeochemical variables on an array of stations within the same water body.

Nutrient concentrations and plankton biomass and activities are higher in the South West lagoon of New Caledonia than in the surrounding ocean and are not uniformly distributed (Bourguet *et al.*, 2003; Briand *et al.*, 2004; Jacquet *et al.*, 2006). Apart from local eutrophication in the bays near Noumea City, differences are also observed in the main lagoon channel. The southern part, which is closer to oceanic inputs flushing the lagoon, usually had lower nutrient concentrations and plankton biomass and activity than in the northern part (Jacquet *et al.*, 2006).

A recent paper focused on computations of hydrodynamic time parameters in the South West lagoon of New Caledonia using a 3D hydrodynamic model (Jouon *et al.*, 2006). In an attempt to connect physical forcing to biogeochemical functioning of the SW lagoon of New Caledonia, the aim of this study was to test the statistical relationships between the distribution of flushing indices determined on an array of stations in the SW lagoon of New Caledonia (Jouon *et al.*, 2006) and the distribution of biological and chemical variables acquired during 3 oceanographic campaigns in the same lagoon.

Material and methods

Study site.

New Caledonia is surrounded by a 23,400 km² lagoon. Noumea City (home to ~60 % of the total population of New Caledonia) is located on the south-west coast. The surrounding lagoonal area is known as the South West Lagoon of New Caledonia. It has an average depth of 17.5 m and varies in width from 5 km (northern limit) to 40 km (southern limit). It is separated from the open ocean by a barrier reef, bisected by 3 main passes (Fig. 1). Around Nouméa City, four bays were sampled. The Sainte-Marie Bay receives urban waste waters from the Sainte-Marie area. The Grande Rade and Koutio Bay also receive urban effluent, as well as industrial effluents originating from the nickel smelt. In contrast, the Dumbéa Bay is under the terrigenous influence from the Dumbéa River and receives neither urban sewage nor industrial effluents.

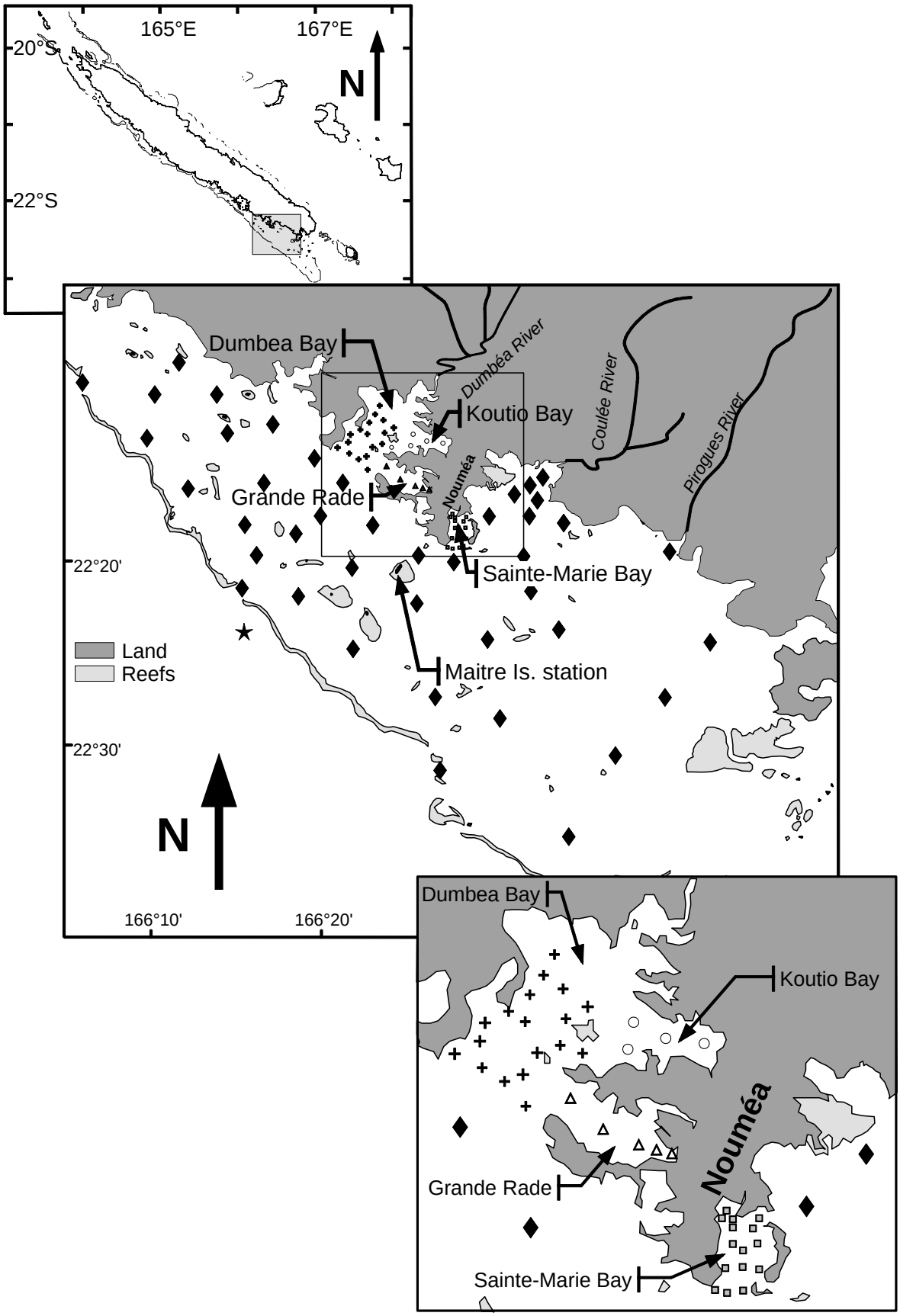

Figure VI-1 The South West lagoon of New Caledonia and the sampling sites. Large grey symbols represent lagoon channel stations. Small dark symbols figure bay stations. Black star represents oceanic station. The weather station at Maitre Is. is indicated.

Hydrodynamics.

The flushing lag (in days) indicates the minimum time required for a particle entering the southwest lagoon of New Caledonia (open ocean) to reach the station in question. More precisely, assuming that lagoon water presents a concentration of a passive tracer of 1 and that incoming waters from outside of the lagoon present a concentration of 0, the flushing lag represents the time required to decrease the local grid mesh concentration by 5% (Jouon *et al.,* 2006). This value is selected to minimize the importance of computation errors. Local e-flushing time represents the time needed to attain a local grid mesh concentration of 1/e from the precedent step where numerical drogues present a concentration of 0.95. Both flushing lag and local e-flushing time at the different stations were computed from MARS3D, a hydrodynamic model implemented over the study area. The accuracy of the time scales is guaranteed by the validation of the advection dispersion of dissolved tracers in the model (Lazure & Salomon, 1991a, 1991b; Douillet et *al.*, 2001; Plus et *al.*, 2003; Ouillon et *al.*, 2004). The computation methods used are the same as those of other readily used computation methods (Thomann & Mueller, 1987; Delhez *et al.*, 2004) which inherently take into account the significance of the time scales used (Jouon et *al.*, 2006).

This model was adapted to compute the free surface elevation, the 3D currents, the transport of suspended particulate matter (Douillet 1998; Douillet *et al.*, 2001; Ouillon *et al.*, 2004) and the hydrodynamic time parameters (Jouon *et al.*, 2006) under tide and wind forcing in the Southwest lagoon of New Caledonia. MARS3D is a finite difference model in σ–coordinates. The computation grid is of the Arakawa C type modified as described in Lazure & Salomon (1991a). The horizontal grid spacing is 500 m. 10 σ–levels (Blumberg & Mellor, 1987) are used to discretise the vertical dimension. The top and bottom boundary conditions are “slip conditions” (Blumberg & Mellor, 1987; Deleersnijder *et al.*, 1992) with wind friction at the top of the surface σ–level and friction on the bottom of the deepest σ–level. The turbulence model used is of the Pacanowsky & Philander (1981) type. The advection scheme is a Total Variation Diminishing (TVD) scheme (*e.g.* Sweby, 1984).

Sampling.

Lagoon water was collected during three campaigns performed in September 2000 (cold season; 91 stations), June 2003 (cold season; 79 stations) and October 2004 (dry season; 83 stations) using the R/V’s Alis and Louis Hénin. Conductivity, temperature, *in vivo* fluorescence and turbidity profiles were simultaneously recorded using a SeaBird SBE 19 profiler and Seapoint Fluorometer and Turbidity Meter, respectively. Water samples were collected at 3 m depth and were immediately processed on board.

Chlorophyll a and nutrients.

Chlorophyll *a* (Chl.*a*) was analyzed fluorometrically on methanol extracts (Holm-Hansen *et al.,* 1965) following filtration onto Whatman GF/F filters of replicate 300 ml samples. Ammonium was fluorometrically determined on a Turner TD-700 immediately after collection on 3 unfiltered 40 ml replicates, using the *o*-phtaldialdehyde method (Holmes *et al.,* 1999). Unfiltered replicate samples (40 ml each) were immediately frozen until nitrate + nitrite (NO_3+NO_2), phosphate (PO_4) and silicate analyses. Nitrates were reduced to nitrites and NO_3+NO_2 concentrations were determined according to Raimbault *et al.* (1990) on a Bran+Luebbe Autoanalyzer III. Phosphates and silicates (dissolved and colloidal) were determined according to Grasshoff *et al.* (1983) on the same autoanalyzer.

Bacterial abundance and production.

Water samples (1.5 ml) for bacterial enumeration were preserved with 7.5 µl glutaraldehyde (Sigma Grade II) and stored in liquid nitrogen. Heterotrophic bacteria were enumerated on a FACScan flow cytometer (Becton Dickinson) equipped with an air-cooled laser providing 15 mW at 488 nm and with a standard filter setup after SYBR green coloration (Mari *et al.,* 1997). Bacterial production of biomass was determined from thymidine incorporation as in Briand et *al. (*2004). The biomass production rates were computed using the average of empirically determined conversion factors ($2.9x10^{18}$cells.mol^{-1} of thymidine, unpublished data) and 12.4 fgC cell^{-1} (Fukuda *et al.,* 1998).

Results

Meteorological conditions

During the three oceanographic cruises, wind was recorded on Maître Island in the middle of the southwest lagoon of New Caledonia (see location on Fig. 1 and wind data on Fig. 2). In September 2000, wind intensity and direction remained relatively constant (mean trade wind, 110°, 8 m s^{-1}) prior to as well as during the cruise. In June 2003, wind intensity varied more than during the preceding campaign with an average of 5 m s^{-1} and more elevated values at the beginning and at the end of the cruise. Wind direction remained that of mean trade wind (110°) during most of the cruise. In October 2004, wind had generally the same direction (110°), however its intensity varied widely with higher values a few days before and during the beginning of the cruise (average±SD 10.2±2.8 m s^{-1}) and lower values (5.1±3.3 m s^{-1}) during the latter part of the cruise. This last part of the cruise was also characterised by large diel variations in wind intensity. On average, wind velocity was 7.2 m s^{-1} during this campaign.

In summary, although wind intensity and direction varied slightly around the mean trade wind (110°, 8 m s^{-1}), the deviations persisted for only short periods. The mean trade wind was thus relevant to force the numerical simulations providing the hydrodynamic time parameters

that were then compared to the biological and chemical parameters measured during the cruises.

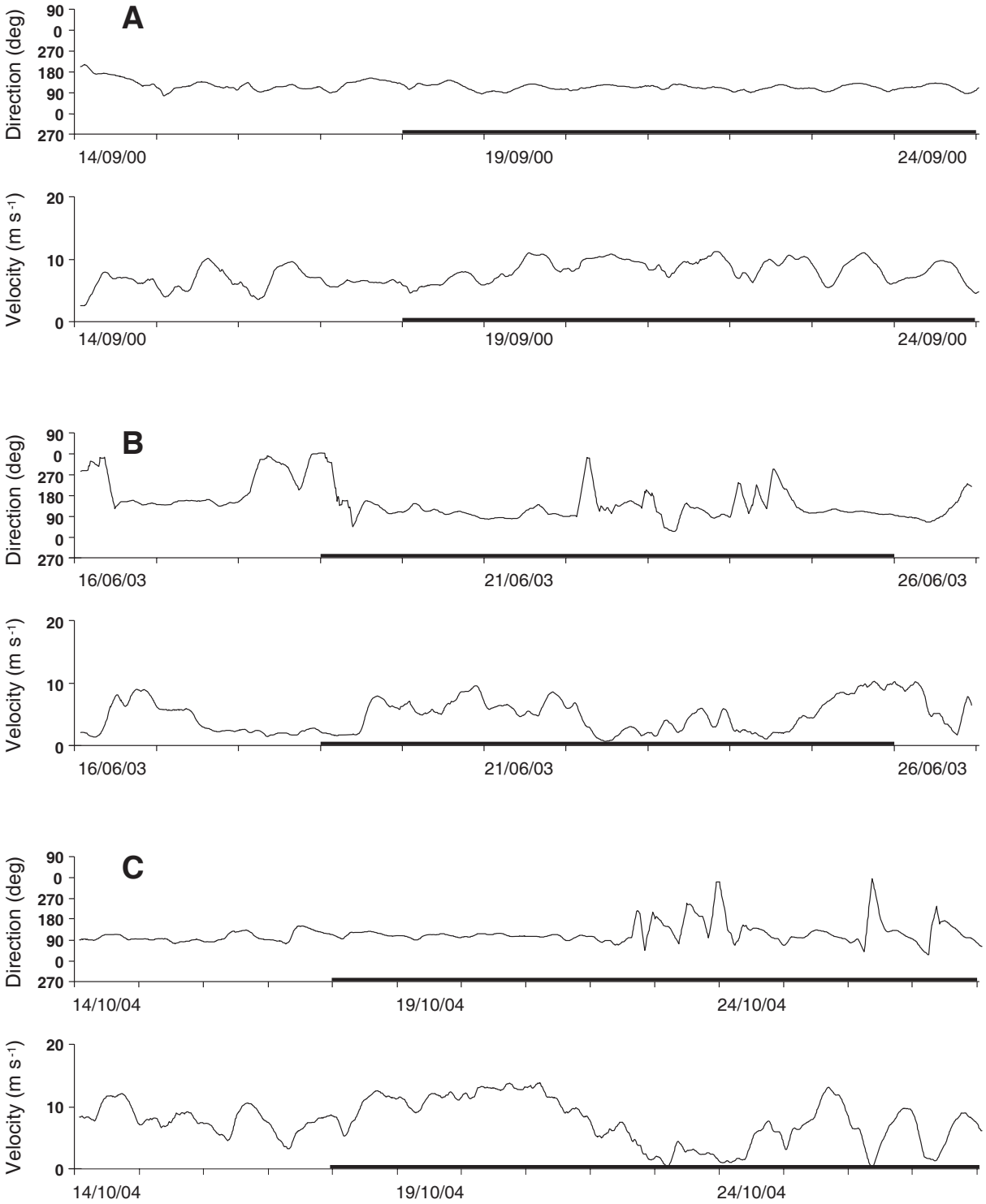

Figure I-2 Wind measurements during and before the 3 oceanographic cruises in (A) September 2000, (B) June 2003, and (C) October 2004. Cruises dates are indicated by wider bars.

Flushing indices.

The estimated flushing lags of the water masses at the sampling stations vary from ~0.1 day for the southernmost sector of the lagoon up to 48 days at the head of the Grande Rade under the combined influences of a typical periodic tide (components M2 and S2; see tide analysis in Douillet, 1998) and a uniform SE trade wind (110°) of 8 m s^{-1}. Under the same forcing conditions, the local e-flushing times at the sampling stations vary from a few minutes for the southernmost sector of the lagoon up to 47 days at the head of the Grande Rade (Fig. 3).

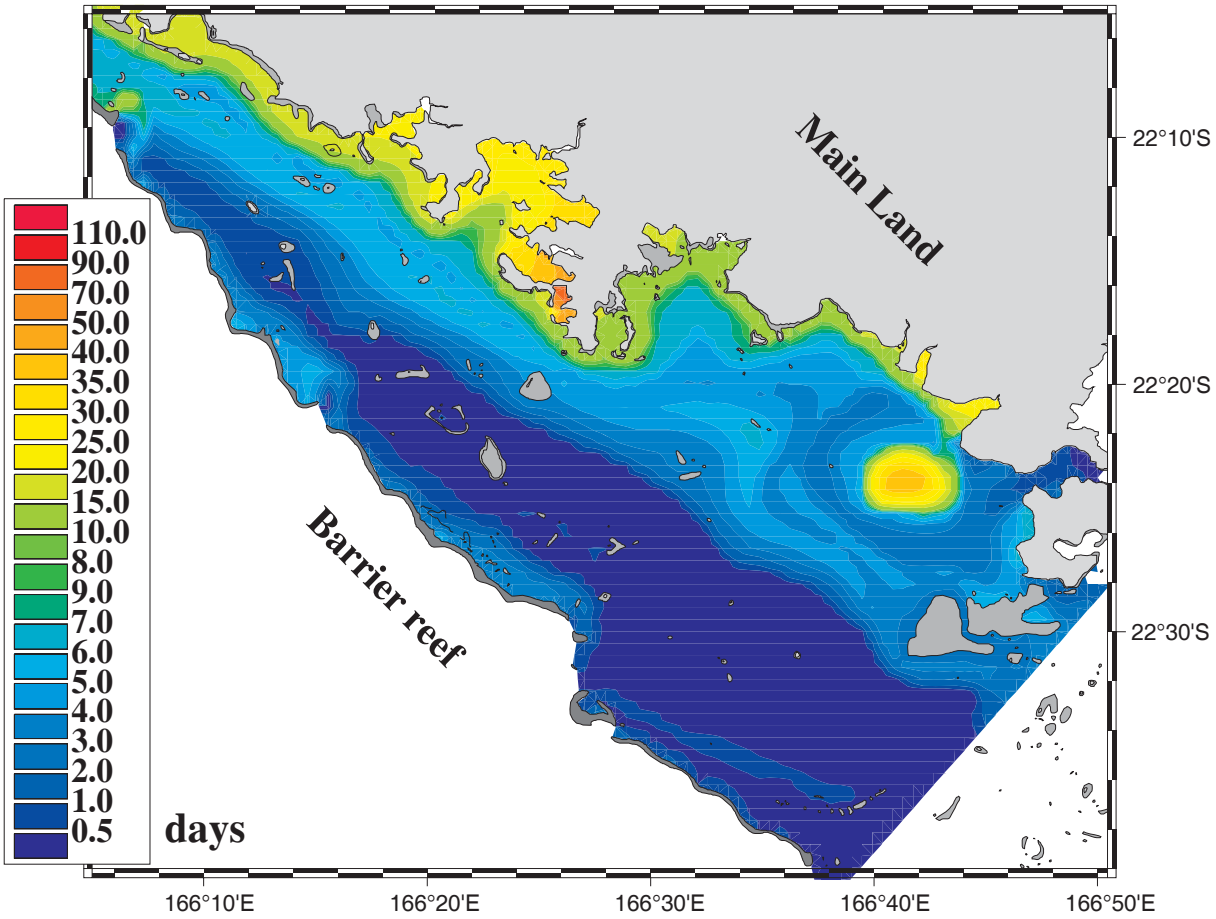

Figure I-3 Local e-flushing times determined under medium tide and 110° and 8 m s-1 Trade Winds in the SW lagoon of New Caledonia.

Physico-chemical characteristics and nutrients.

The physico-chemical characteristics varied little among stations. Salinity averaged 35.21 (range 34.69-35.36), 35.32 (range 34.19-35.57) and 35.90 (range 35.54-36.31) in September 2000, June 2003 and October 2004, respectively. Temperature averaged 22.9°C (range 22.2-23.4), 22.7°C (range 22.1-23.5) and 23.3°C (range 22.5-25.0) in September 2000, June 2003 and October 2004, respectively.

Dissolved inorganic nitrogen (DIN) concentrations varied widely among stations and averaged 0.10 µM (range 0.01-2.85), 0.12 µM (range 0.01-1.27), and 0.16 µM (range 0.01-6.17) during the 3 campaigns. Maximum values were recorded at the heads of the bays subject

to urban and industrial effluents whereas minimum values occurred in the main lagoon channel. Dissolved inorganic phosphorus concentrations generally followed the same distribution as DIN and averaged 0.09 µM (range 0.03-0.57), 0.04 µM (range 0.00-0.45), and 0.06 µM (range 0.00-0.66) during the 3 campaigns.

Phytoplankton biomass and bacterial production of biomass.

Chlorophyll *a* (Chl.*a*) values varied widely among stations and averaged 0.42 µg l^{-1} (range 0.13-1.98), 0.52 µg l^{-1} (range 0.13-3.64), and 0.47 µg l^{-1} (range 0.11-3.54) during the 3 campaigns. Bacterial abundance varied far less spatially with 0.76 $x10^6$ ml^{-1} (range 0.43-1.46), 0.70 $x10^6$ ml^{-1} (range 0.37-0.98), and 0.47 $x10^6$ ml^{-1} (range 0.24-1.18) during the 3 campaigns. Bacterial production of biomass displayed considerable variation between stations with whole campaign averages of 0.26 µgC $l^{-1}h^{-1}$ (range 0.02-1.64), 0.27 µgC $l^{-1}h^{-1}$ (range 0.02-2.02), and 0.37 µgC $l^{-1}h^{-1}$ (range 0.08-2.86) in September 2000, June 2003 and October 2004, respectively. In general, Chl.*a*, bacterial abundance and bacterial production (BP) values were distributed similarly to nutrient concentrations, *i.e.* values were maximal at the heads of the bays receiving urban and industrial effluents, and decreased down to lagoon channel values at the mouth of the bays. However, BP varied more between stations (36 to 114-fold) than phytoplankton biomass (16 to 31-fold), and bacterial abundance (3 to 5-fold) did.

Relationships between biological variables and local e-flushing times in the lagoon channel

Statistical relationships were generally significant between biological and chemical variables and local e-flushing time when all sampling sites were considered (Table 1). However, as most enrichment in the lagoon originates from the heads of the bays, where local e-flushing times are considerably higher than in the main lagoon channel, there could be an artificial increase in the significance of statistical relationships. We therefore determined the statistical linear relationships between biological and chemical variables and local e-flushing time only in lagoon channel stations (Table 2). In the bays the distribution of biological and chemical variables *vs.* local e-flushing time can be compared to the linear relationships in the channel in Figure 4.

		September 2000			June 2003			October 2004		
		r	P	n	r	P	n	r	P	n
Chl.*a*	Channel	0.42	***	46	0.34	**	48	0.27	*	49
	Sainte-Marie Bay	0.56	**	15	0.55	*	10	0.84	***	10
	Grande Rade	0.89	**	5	0.85	*	5	0.63		5
	Koutio Bay	0.74		4	0.63		4	0.71		4
	Dumbea Bay	0.67	***	18	0.55	**	15	0.56	**	15
	Channel & Dumbea	0.70	****	64	0.51	****	63	0.47	****	64
	All stations	0.49	****	88	0.41	****	82	0.40	****	83
BP	Channel	0.32	**	46	0.29	**	47	0.44	***	50
	Sainte-Marie Bay	0.68	**	10	0.12		9	0.79	***	10
	Grande Rade	0.92	**	5	0.41		5	0.57		5
	Koutio Bay	0.45		4	0.70		4	0.70		4
	Dumbea Bay	0.35		17	0.11		15	0.38		15
	Channel & Dumbea	0.52	****	63	0.41	****	62	0.73	****	64
	All stations	0.48	****	82	0.65	****	80	0.64	****	84
Si	Channel	0.58	****	49	0.33	**	41	0.34	**	50
	Sainte-Marie Bay	0.32		15	0.44		10	0.66	**	10
	Grande Rade	0.87	*	5	0.60		5	0.62		5
	Koutio Bay	0.95	*	4	0.99	**	4	0.82		4
	Dumbea Bay	0.54	**	18	0.04		15	0.54	**	15
	Channel & Grande Rade	0.79	****	54	0.80	****	53	0.70	****	55
	All stations	0.59	****	91	0.69	****	75	0.57	****	84

Table I-1 Significance of the linear relationships between biological or chemical variables and local e-flushing times in different areas of the SW lagoon channel of New Caledonia. Chl.a: Chlorophyll a; BP: Bacterial Production; Si: Silicate concentrations. r: correlation coefficient; P: significance level; n: number of points *: P<0.10; **: P<0.05; ***: P<0.01; ****: P<0.0001; otherwise not significant

Chemical variables showed generally non significant relationships with local e-flushing time in the main lagoon channel (not shown). Silicate was the only nutrient displaying significant relationships with flushing indices over the 3 cruises (Table 2). This is probably due to the fact that silicate (Si) is not a limiting nutrient for primary production (Jacquet *et al.*, 2006). Indeed, as the Si:DIN ratio is always much higher than 1, we can therefore expect the turnover time of silicate to be low compared to other nutrients.

Among biological variables, Chl.*a* and BP generally displayed highly significant correlations with local e-flushing times in lagoon channel stations (Fig. 4, Table 2). For example, during the September 2000 cruise, the southernmost part of the lagoon displayed a bacterial production rate of (average±SE) 0.07±0.01 µgC $l^{-1}h^{-1}$, with local e-flushing times corresponding to 0.021±0.016 day. BP was slightly higher (0.15±0.04 µgC $l^{-1}h^{-1}$) in the lagoon channel facing Nouméa City (6 stations, Fig. 1) with local e-flushing times corresponding to 0.81±0.20 day. Finally, BP in the northern part was nearly 3-fold higher than in the southernmost stations with 0.19±0.02 µgC $l^{-1}h^{-1}$ for local e-flushing times averaging 5.2±1.7 days. BP in the oceanic waters that flush the lagoon was 3.5-fold lower than in the Southern lagoon with on average 0.0019±0.002 µgC $l^{-1}h^{-1}$ (unpublished data).

Cruise	Variable	slope±SE	Intercept±SE	R	p	n
Sept. 00	Chl.*a*	0.010±0.001	0.160±0.010	0.412	0.004	46
Sept. 00	BP	0.011±0.002	0.043±0.012	0.318	0.031	46
Sept. 00	Si	0.106±0.013	1.092±0.094	0.576	0.000	49
June 03	Chl.*a*	0.021±0.003	0.195±0.018	0.344	0.015	48
June 03	BP	0.015±0.002	0.091±0.012	0.287	0.050	47
June 03	Si	0.275±0.042	2.438±0.236	0.330	0.035	48
Oct. 04	Chl.*a*				NS	49
Oct. 04	BP	0.013±0.002	0.079±0.013	0.439	0.001	50
Oct. 04	Si	0.079±0.011	1.292±0.078	0.341	0.015	50

Table I-2 Model II linear relationships between biological and chemical variables and local e-flushing times (days) in the SW lagoon channel of New Caledonia. Si: Silicate (µM); Chl.a: Chlorophyll a (µg l-1); BP: bacterial production (µgC l-1h-1). Relationships between biological variables and local e-flushing times in the bays.

In Sainte-Marie, Dumbea and Koutio Bays, silicate displayed values above the lagoon channel regression lines (Fig 4). The only exception occurred in June 03, when atypically elevated values were observed in the lagoon channel. Conversely, in the Grande Rade, silicate concentration generally fitted well with the lagoon channel relationships. Chl.*a* and BP values exhibited similar distributions versus local e-flushing times, with Dumbea Bay values sitting along the lagoon channel regression lines and Sainte-Marie Bay and Koutio Bay values falling well above the regression line (Fig. 4).

Scatter plots of biological or chemical variables as a function of flushing lags or as a function of the sum of flushing lags and local e-flushing times followed similar trends in the channel, with comparable or slightly lower significance levels. In the bays, deviations from these trends were also similar to those observed with local e-flushing times.

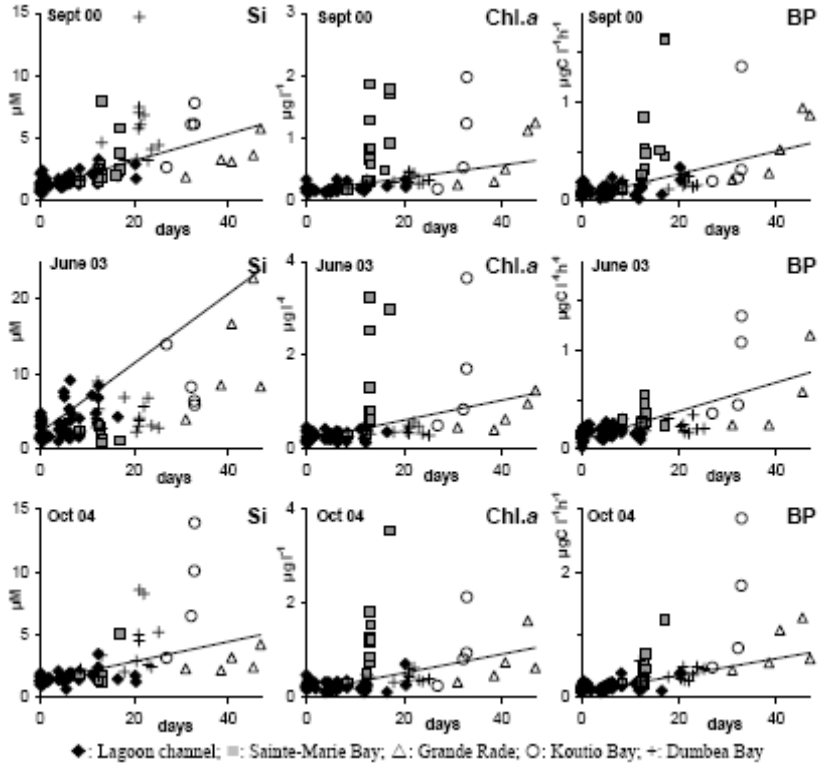

Figure I-4 Scatter plot of silicate, chlorophyll a and bacterioplankton production vs. local e-flushing times in the SW lagoon of New Caledonia. Symbols are the same as in Fig. 1. Solid lines indicate model II linear relationships only including lagoon channel data. Although not significant, regression of Chl.a *vs.* local e-flushing times in Oct. 04 is shown for comparison.

Discussion

Underlying assumptions for the link between local e-flushing times and spatial distributions of nutrients and biological variables

Technically, local e-flushing time is the time required for the concentration (initially set to 1 throughout the whole control volume) in a grid cell to drop down to 1/e x 0.95 from the moment it has reached 0.95. The concentration in each grid cell decreases as more water coming from outside the control volume reaches the mentioned grid cell. Local e-flushing time is meant to quantify the replacement process of water in a grid cell. The choice of the advection scheme and size of grid space discretisation as well as horizontal and vertical parameterisations of turbulence are of crucial importance for the results of the Hydrodynamic Time parameters (HTs) computations. These various choices will influence the conservation of the front formed between the incoming 0 concentration water and the 1 concentration water initially inside the control volume. The better the front is conserved, the shorter the local e-flushing time will tend to be, with all other parameters being equal elsewhere. However, these

choices do not have a major influence on the relative distribution of local e-flushing time, nor on the relationship between e-flushing time and biological or chemical variables as is the main focus of this study.

The version of MARS 3D used in the present study does not solve the heat transport equations and thus the simulation does not reproduce stratification. The lack of stratification amplifies the impact of vertical turbulence. This results in an evolution of the concentration front that is similar in the bottom and surface sigma-layers of the model, leading to identical computed HTs in these two layers of the simulated area.

Representativeness of 3 m deep samples compared to the whole water column.

HTs are therefore considered to be representative of the whole water column (Jouon *et al.*, 2006), however, biological and nutrient data were collected from 3-m deep samples during the 3 cruises. Whether or not the 3-m deep samples can be considered as representative of the whole water column can be assessed by comparing chlorophyll *in vivo* fluorescence at 3 m to water column average. On average, 3-m deep samples were 87% (±3%; 95% confidence limits) of water column means with no significant differences between the cruises. If we assume that the vertical distribution of nutrients and other biological variables in this generally well mixed water column follows the same distribution as phytoplankton, then it can be considered that the 3-m deep samples give a reasonable approximation of the whole water column.

Relationships between nutrient concentrations or biological variables and local e-flushing times in the lagoon channel

Several attempts have been made to relate biological or chemical properties of different water bodies to flushing rates (Delesalle & Sournia 1992; Dufour et al., 2001; Torréton et al., 2002). Most of these studies, especially in coral reef areas, performed these correlations on the scale of the entire water body. One important aspect of this work is that we determined these relationships on local scales, i.e. on a vast array of stations within the same water body.

Linking biological or chemical variables to flushing by oceanic waters implicitly assumes that these variables are continuously supplied at a similar rate over the area considered. It can be argued that these assumptions may not be correct for chemical or biological variables of a terrestrial or riverine origin, such as silicate. However, in this system, Si values decrease sharply with distance from the river mouth and quickly reach values very similar to lagoon channel averages (Fig. 5). This suggests that, at least during the periods examined, flushing by oceanic waters was high enough, relative to freshwater inputs, to verify this assumption.

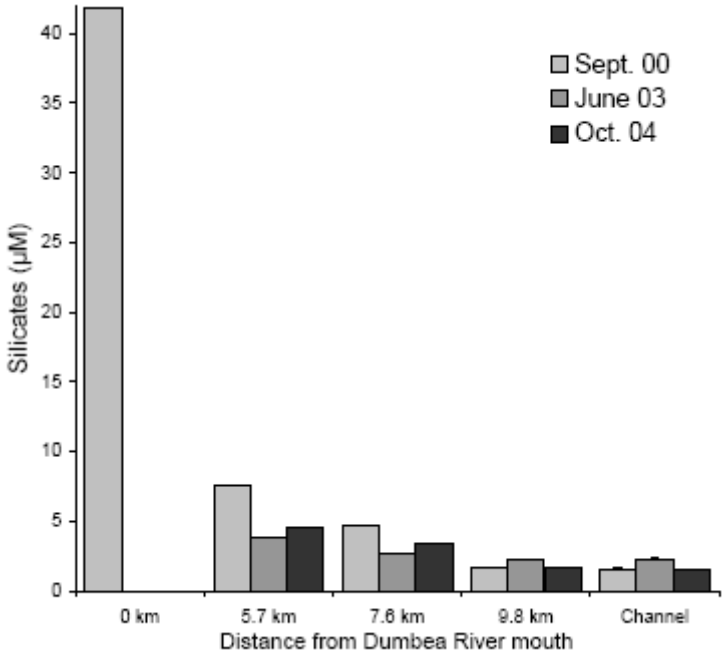

Figure I-5 Silicate concentrations (µM) along a coast-lagoon transect in Dumbea bay during the 3 cruises. 'Channel' denotes average values in the lagoon channel. Bars figure standard errors of the mean for lagoon channel stations.

Similarly, resources (nutrients and organic carbon) for phytoplankton and bacterioplankton growth are supplied at higher rates in the bays receiving important urban and industrial effluents (Grande Rade, Sainte-Marie Bay). However, as with the distribution of silicate, Chl.a and BP both decrease drastically along coast-lagoon channel transects and values at the mouth of the bays are generally very similar to lagoon channel averages (Fig. 6). This again suggests that, over the 3 campaigns, flushing with oceanic waters was important enough compared to organic and inorganic anthropogenic inputs to make this assumption sustainable.

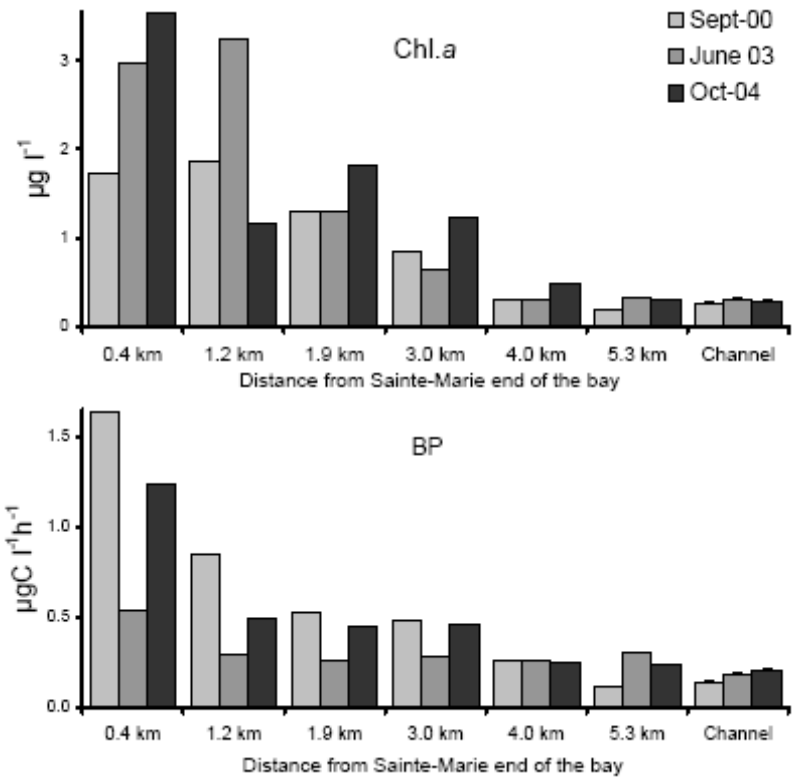

Figure I-6 Chlorophyll a (µg l-1) and bacterial production (µgC l-1h-1) along a coast-lagoon transect in Sainte-Marie Bay during the 3 cruises. 'Channel' denotes average values in the lagoon channel. Bars figure standard errors of the mean for lagoon channel stations.

Relationships between nutrient concentrations or biological variables and local e-flushing times in the bays

In this study silicate concentrations display significant relationships with local e-flushing times in the main lagoon channel. Sainte-Marie Bay, Dumbea Bay and Koutio Bay, characterized by significant freshwater inputs, display Si values well above the regression line of Si vs. local e-flushing times for the main lagoon channel (Fig 4). The only exception is the June 03 cruise where atypically elevated Si values were observed in the lagoon channel. However, as these silicate measurements were determined on only one sample, sample contamination cannot be ruled out. In contrast to the other bays, Si concentrations in the Grande Rade, characterized by almost insignificant freshwater inputs, generally fit well within the main lagoon channel relationship. Moreover, when the two sites are combined, the correlation coefficients are higher than if the relationships are examined separately (Table 1).

Bacterial abundance (BA) presents almost no significant relationship with e-flushing times (not shown). This could be due to the severe top-down pressure (i.e. grazing) generally exerted on BA. Whereas BA varied by only 3 fold at the most during each cruise, BP varied by a factor of 100, yielding a pattern similar to that reported by White et al. (1991) who commented that BA generally varies by 2 orders of magnitude less than BP. Phytoplankton biomass, as assessed by Chl.a concentrations varied more extensively (16 to 31-fold) among

stations than bacterial biomass during the 3 cruises. The cross channel gradients also varied as much as the bay-to-channel gradients, showing decreasing trends persisting at all seasons (Jacquet et al., 2006). Additionally, bacterial abundance is generally determined with a lower precision (10% on average, not shown) than BP or Chl.a (3% on average, not shown).

In contrast to BA, bacterial production of biomass presents significant relationships with local e-flushing times. BP may be considered as a sensitive index of resources available for microbial growth (Ducklow, 1990) and values differ widely within the lagoon environment. Thus while the actual concentrations of nutrients are not well correlated with local e-flushing times, the impact of those nutrients on BP is well correlated. Moreover, in the bays, the scatter plots of bacterial production rates vs. e-flushing times deviated from the relationships in the lagoon channel in a different way than silicate concentrations vs. e-flushing times did. Indeed, Grande Rade, Sainte-Marie Bay and Koutio Bay, which are characterized by important urban and industrial effluents, generally display values well above the regression trends (Fig. 4). Conversely, Dumbea Bay stations present BP values that fit well with the regression lines. The difference between the Si and BP relationships for the Grande Rade is probably due to two factors: heterotrophic bacteria do not require Si, and Grande Rade is not subject to riverine influences. Similarly, the difference in relationship between the lagoon channel and the Dumbea Bay for BP and Si is also due to the fact that while the Dumbea River is an important source of Si to the system, it is relatively poor, in comparison to the other bays, in terms of bioavailable resources for bacteria. Moreover, those sites with both important riverine influences as well as high concentrations of available resources for bacterial growth (Sainte-Marie Bay and Koutio Bay) show the same distributions for Si and BP relative to the lagoon channel transect (i.e. higher than the regression line).

Analogous patterns can be observed for Chl.a distributions across the lagoon channel, while in the bays, deviations from the lagoon channel regressions lines are comparable to those observed for BP.

The South West lagoon of New Caledonia can be viewed as a coastal mesotrophic ecosystem flushed by oligotrophic oceanic waters that replace lagoon waters with water considerably impoverished in resources for microbial growth. This flushing was high enough during the periods of study to shape the distribution of phytoplankton biomass, bacterial production of biomass and silicate concentrations in the lagoon channel as well as in some of the bay areas.

Limits

Hydrodynamic timescales are sensitive to hydrodynamic forcing conditions. Tartinville et al. (1997), Geyer (1997) and Deleersnijder et al. (1998) have demonstrated that hydrodynamic timescales can be rather sensitive to wind stress. In this lagoon, hydrodynamic timescales are

computed assuming the wind to be constant for periods of time up to 90 days, an assumption that is unlikely to occur in this system.

Constant wind is of course a simplification and local e-flushing time has to be considered as a time and space varying quantity. However, taking a constant wind frees us from the sensitivity of local e-flushing time to the time variation of the wind field. In addition to this, the averaging of results over 12 different runs starting at each hour of a tidal cycle further frees us from the sensitivity of local e-flushing time to the phase of the tide at which the simulation is started. These two strategies remove the time varying property of computed local e-flushing time. Undoubtedly, the development of an inverse model (Delhez et al., 2004) would have been the best way to undertake HTs computation conserving the time varying aspect of the HTs. However, without having to develop an inverse model, one could have an idea of the effect of the variation of wind conditions on the local e-flushing time distribution by conducting a sensitivity analysis on wind variation effects.

It is important to recognise that although local e-flushing time does explain some of the variance in the biological and chemical parameters, it does not explain all. For example, in Table 1 we show that local e-flushing time sometimes only explains around 16% of the variability on the whole SW lagoon. However, given that the biological and chemical parameters used are generally considered non-conservative parameters, this is perhaps not surprising and further highlights the importance of large scale physical processes on controlling biological and chemical parameters. Alternatively, it can be argued that a more simple method of estimating these relationships would be to use mixing diagrams (Rochelle-Newall & Fisher, 2002). However, one of the caveats of using mixing diagrams is the need to have correctly defined, non-varying endmembers, at least on the time scale of the measurement (Cifuentes et al., 1990). In the SW lagoon, although we have a clearly identifiable, effectively constant oceanic endmember, this is not the case for the coastal endmember where we have several coastal sources that are relatively heterogeneous both spatially and temporally. Moreover, the lack of significant salinity gradient in this system means that another index would need to be used, such as distance from the coast. We therefore tested the correlations between chemical and biological parameters and distance. We found that while the correlations between the parameters and distance were generally significant for the bays viewed separately, this was not the case for the lagoon channel (data not shown). This lack of correlation in the lagoon channel is due to the fact that while local e-flushing time is approximately linear with distance inside each bay, there is no correlation between distance and local e-flushing time neither in the lagoon channel, nor between local e-flushing time and distance when the entire dataset is considered. Thus, in summary, although local e-flushing time does not describe all of the variance of the parameters, it does provide a relatively robust way to predict the distribution of biological and chemical variables, at least in this system.

Conclusion

This study demonstrates the pertinence of using flushing indices determined from hydrodynamic modelling to explain the distribution of planktonic and chemical variables at the scale of the SW lagoon of New Caledonia. Our flushing indices were calculated for dominant meteorological conditions (i.e. 110° trade winds averaging 8 ms^{-1} and average tides). Wind and tide driven circulation of water is undoubtedly of critical importance for the rate and distribution of planktonic processes in this coastal ecosystem. It is also probable that flushing will also exert a significant influence on short term temporal variations of planktonic processes. Indeed, an annual survey at two stations in the SW lagoon showed that short term (1 – 2 weeks) variations of bacterioplankton and phytoplankton biomass and production are of the same order of magnitude as seasonal variations (unpublished data). The next step will be to assess local variations of flushing lags over this annual cycle in order to determine their importance in constraining biological processes in this ecosystem characterized by moderate seasonal variations of physical variables.

Acknowledgements:

This work was supported by the Institut Français de Recherche pour le Développement (IRD), grants from the Programme National Environnement Côtier (PNEC) and a grant from the ZoNéCo program. We express our gratitude to the crews of the IRD RV Alis and the New Caledonia RV Louis Hénin for their efficient help during sample collection.

References

Andrews, J.C., Muller, H., 1983. Space-time variability of nutrients in a lagoonal patch reef. Limnology and Oceanography 28, 215-227.

Bourguet, N., Torréton, J-P., Galy, O., Arondel, V., Goutx, M., 2003. Specific and sensitive radiometric assay for microbial lipase activities in marine water samples: application to samples from the lagoon of Nouméa. Applied & Environmental Microbiology 69, 7395-7400.

Blumberg, A.F., Mellor, G.L., 1987. A description of a three-dimensional coastal ocean circulation model. In: Heaps, N.S. (Ed.), Three-dimensional coastal ocean models. AGU, Washington, DC, pp. 1-16.

Briand, E., Pringault, O., Jacquet, S., Torréton, J.-P., 2004. The use of oxygen microprobes to measure bacterial respiration for determining bacterioplankton carbon growth efficiency along trophic gradients in a coral reef lagoon. Limnology and Oceanography: Methods 2, 406-416.

Cifuentes, L.A., Schemel, L.E., Sharp, J.H., 1990. Qualitative and numerical analyses of the mixing effects of river inflow variations on mixing diagrams in estuaries. Estuarine, Coastal Shelf Science. 30, 411-417.

Crump, B.C., Hopkinson, C.S., Sogin, J.E., 2004. Microbial Biogeography along an Estuarine Salinity Gradient: Combined Influences of Bacterial Growth and Residence Time. Applied and Environmental Microbiology 70, 1494-1505.

Deleersnijder, E., Norro, A., Wolanski, E., 1992. A three-dimensional model of the water circulation around an island in shallow water. Continental Shelf Research 12, 891-906.

Deleersnijder, E., Wang, J., Mooers, C.N.K., 1998. A two-compartment model for understanding the simulated three-dimensional circulation in Prince William Sound, Alaska. Continental Shelf Research 18, 279-287.

Delesalle, B., Sournia, A., 1992. Residence time of water and phytoplankton biomass in coral reef lagoons. Continental Shelf Research 12, 939-949.

Delhez, E.J.M., Heemink, A.W., Deleersnijder, E., 2004. Residence time in a semi-enclosed domain from the solution of an adjoint problem. Estuarine Coastal and Shelf Science 61, 691-702.

Doering, P.H., Oviatt, C. A., McKenna, J.H., Reed L. W., 1994. Mixing behavior of dissolved organic-carbon and its potential biological significance in the Pawcatuck River estuary. Estuaries 17, 521-536.

Douillet, P., 1998. Tidal dynamics of the south-west lagoon of New Caledonia: observations and 2D numerical modelling. Oceanologica Acta 21, 69-79.

Douillet, P., Ouillon, S., Cordier E., 2001. A numerical model for fine suspended sediment transport in the southwest lagoon of New Caledonia. Coral Reefs 20, 361-372.

Ducklow, H.W., 1990. The biomass, production and fate of bacteria in coral reefs. Coral reefs, Z Dubinsky (Ed.). Elsevier, Amsterdam, p 265-289.

Dufour, P., Andréfouët, S., Charpy, L., Garcia, N., 2001. Atoll morphometry controls lagoon nutrient regime. Limnology and Oceanography 46, 456-461.

Ferreira, J.G., Wolff, W.J., Simas, T.C., Bricker, S.B., 2005. Does biodiversity of estuarine phytoplankton depend on hydrology? Ecological Modelling, 187, 513-523.

Fukuda, R., Ogawa, H., Nagata, T., Koike, I., 1998. Direct determination of carbon and nitrogen contents of natural bacterial assemblages in marine environments. Applied and Environmental Microbiology 64, 3352-3358.

Geyer, W.R., 1997. Influence of wind on dynamics and flushing of shallow estuaries. Estuarine Coastal and Shelf Science 44, 713-722.

Grasshoff, K., Eherhardt, M., Kremling, K., 1983. Methods of seawaters analysis. Verlag Chemie, Weinheim, RFA, second edition. 419 p.

Holmes, M.R., Aminot, A., Kérouel, R., Hooker, B.A., Peterson, B.J., 1999. A simple and precise method for measuring ammonium in marine and freshwater ecosystems. Canadian Journal of Fisheries and Aquatic Sciences 56, 1801-1808.

Holm-Hansen, O., Lorenzen, C.J., Holmes, R.W., Strickland, J.D.H., 1965. Fluorimetric determination of chlorophyll. Journal du Conseil Permanent International pour l'Exploration de la Mer 30, 3-15.

Jacquet, S., Delesalle, B., Torréton, J-P., Blanchot, J. (2006) Response of phytoplankton communities to increased anthropogenic influences (southwestern lagoon, New Caledonia). Marine Ecology-Progress Series 320, 65-78

Jouon, A., Douillet, P., Ouillon, S., Fraunié, P. (2006) Calculations of hydrodynamic time parameters in a semi-opened coastal zone using a 3D hydrodynamic model. Continental Shelf Research 26, 1395-1415

Lazure, P., Salomon, J.C., 1991a. Coupled 2-D and 3-D modelling of coastal area. Oceanologica Acta 14, 173-180.

Lazure, P., Salomon, J.C., 1991b. Etude par modèles mathématiques de la circulation marine entre Quiberon et Noirmoutier. Oceanologica Acta 14 (SP), 93-99.

Lucas, L.V., Koseff, J.R., Cloern, J.E., Monismith, S.G., Thompson, J.K., 1999. Processes governing phytoplankton blooms in estuaries. I: The local production-loss balance. Marine Ecology-Progress Series 187, 17-30.

Marie, D., Partensky, F., Jacquet, S., Vaulot, D., 1997. Enumeration and cell cycle analysis of natural populations of marine picoplankton by flow cytometry using the nucleic acid stain SYBR Green I. Applied and Environmental Microbiology 63, 186-193.

Monsen, N. E., Cloern, J. E., Lucas, L. V., Monismith S. G., 2002. A comment on the use of flushing time, residence time, and age as transport time scales. Limnology and Oceanography 47, 1545-1553.

Ouillon, S., Douillet, P., Andréfouët, S., 2004. Coupling satellite data with *in situ* measurements and numerical modeling to study fine suspended sediment transport: a study for the lagoon of New Caledonia. Coral Reefs 23, 109-122.

Painchaud, J., Lefaivre, D., Therriault, J. C., Legendre, L., 1996. Bacterial dynamics in the upper St. Lawrence estuary. Limnology and Oceanography 41, 1610-1618.

Plus, M., Chapelle, A., Lazure, P., Auby, I., Levavasseur, G., Verlaque, M., Belsher, T., Deslous-Paoli, J.-M., Zaldívar, J.-M., Murray C.N., 2003. Modelling of oxygen and nitrogen cycling as a function of macrophyte community in the Thau lagoon. Continental Shelf Research 23, 1877-1898.

Raimbault, P., Slawyk, G., Coste, B., Fry, JC., 1990. Feasibility of measuring an automated colorimetric procedure for the determination of seawater nitrate in the 0 to 100 nM range: examples from field and culture. Marine Biology 104, 347-351.

Rochelle-Newall E.J., Fisher T.R. 2002. Chromophoric dissolved organic matter and dissolved organic carbon in Chesapeake Bay. Marine Chemistry 77, 23-41.

Sweby P.K., 1984. High resolution schemes using flux limiters for hyperbolic conservation laws. SIAM Journal of Numerical Analysis 21, 995-1011.

Tartinville, B., Deleersnijder, E., Rancher, R., 1997. The water residence time in the Mururoa Atoll Lagoon: sensitivity analysis of a three dimensional model. Coral Reef 16, 193-203.

Thomann, R.V., Mueller, J.A., 1987. Principles of surface water quality modelling and control. Harper Collins, New York, NY.

Torréton, J.-P., Pagès, J., Talbot, V., 2002. Relationship between bacterioplankton and phytoplankton biomass, production and turnover rate in Tuamotu atoll lagoons. Aquatic Microbial Ecology 28, 267-277.

Vollenweider, R.A., 1976. Advances in defining critical loading levels for phosphorus in lake eutrophication. Memorie dell'Istituto Italiano di Idrobiologia 33, 53-83.

White, PA., Kalff, J., Rasmussen, J.B., Gasol, J.M., 1991. The effect of temperature and algal biomass on bacterial production and specific growth rate in freshwater and marine habitats. Microbial Ecology 21, 99-118.

LISTE DES PUBLICATIONS ET SEMINAIRES

Jouon, A., Douillet, P., Ouillon, S., Fraunié, P., 2006. Calculations of hydrodynamic time parameters in a semi-opened coastal zone using a 3D hydrodynamic model. Continental Shelf Research 26, 1395-1415.

Mari, X., Rochelle-Newall, E., Torréton, J.P., Pringault, O., Jouon A., 2007. Water residence time: A regulatory factor of the DOM to POM transfer efficiency. Limnology and Oceanography. 52: 808-819.

Torréton J.P., Rochelle-Newall, E., Jouon, A., Faure, V., Jacquet, S., Douillet, P., in press. Correspondence between the distribution of hydrodynamic time parameters and the distribution of biological and chemical variables in a semi-enclosed coral reef lagoon. Estuarine, Coastal and Shelf Science.

Jouon, A., Ouillon, S., Douillet, P., Fernandez, J.M., Mari, X., Lefebvre, J.P., Fraunié, P., submitted. Importance of biological aggregation revealed by Suspended Particulate Matter concentration, grain size distribution and their variability in a coral reef lagoon. Marine Geology.

Jouon, A., Lefebvre, J.P., Douillet, P., Ouillon, S., Schmied, L., submitted. Wind wave modelling and measurements in a fetch-limited semi-enclosed lagoon. Coastal Engineering

Jouon, A., Douillet, P., Ouillon, S., Flushing time and residence time in coral reef lagoons: application to the southwest lagoon of New Caledonia. Poster, International Coral Reef Symposium 2004, Okinawa.

Ouillon, S., Douillet, P., Schmied, L., Andréfouët, S., Chevillon, C., Jouon, A., Fichez, R., An integrated study of fine suspended sediment transport in a coral reef lagoon, New-Caledonia. Poster, International Coral Reef Symposium 2004, Okinawa.

Douillet P., Schmied, L., Jouon, A., Bel Madani, A., Ouillon, S., Comparison between numerical simulation of wind-wave distribution and wavemeter gauge measurements in a semi-enclosed lagoon. Poster, International Coral Reef Symposium 2004, Okinawa.

Aymeric Jouon, Sylvain Ouillon, Pascal Douillet, Etude hydrodynamique and particle transport in a coral reef lagoon, Séminaire, Barcelone, septembre 2004.

Ouillon, S., Douillet, P., Jouon, A., Etude intégrée de l'hydrodynamique et du transport particulaire dans le lagon de Nouvelle-Calédonie, Séminaire, LEGOS, Toulouse, 13 mai 2005.

226

Jouon, A., Douillet, P., Ouillon, S., Évaluation des échelles de temps de l'hydrodynamique, Séminaire, Université du littoral, Calais, 29 novembre 2005.

Jouon, A., Ouillon, S., Douillet, P., Hydrodynamique et transport particulaire en milieux lagonaires, Séminaire, DGO, Bordeaux I, 7 décembre 2005.

Douillet, P., Ouillon, S., Jouon, A, Hydrodynamique et transport particulaire dans le lagon sud-ouest de Nouvelle-Calédonie : État des connaissances et outils disponibles juin, Séminaire, IRD, Nouméa, juin 2005.

Ouillon, S., Douillet, P., Lefebvre, J.P., Jouon, A., Lefevre, J., Lamoureux, J.P., Circulation des masses d'eau et transport de Matières en Suspension dans le lagon de Nouméa, Séminaire, IRD, Nouméa, janvier 2006.

Ouillon, S., Douillet, P., Lefebvre, J.P., Fernandez, J.M., Chevillon, C., Lefevre, J., Jouon, A., Hydrodynamics and transport of suspended particulate matter in the southwest lagoon of New Caledonia, Atelier prospectif de collaboration IRD-Viêt Nam, Institute of Marine Environment and Resources, Haïphong city, Vietnam, avril 2007.

Ouillon, S., Douillet, P., Lefebvre, J.P., Jouon, A, Fernandez, J.M., Efficacité et limites des paramètres d'érosion dans un modèle de transport en suspension à partir de données de turbidité, Atelier ATI PNEC Erodabilité des sédiments naturels, Ifremer Nantes, mai 2007.

227